DISCLAIMER

This report was prepared as an account of work sponsored by an agency of the United States Government. Neither the United States Government nor any agency thereof, nor any of their employees, makes any warranty, express or implied, or assumes any legal liability or responsibility for the accuracy, completeness, or usefulness of any information, apparatus, product, or process disclosed, or represents that its use would not infringe privately owned rights. Reference herein to any specific commercial product, process, or service by trade name, trademark, manufacturer, or otherwise does not necessarily constitute or imply its endorsement, recommendation, or favoring by the United States Government or any agency thereof. The views and opinions of authors expressed herein do not necessarily state or reflect those of the United States Government or any agency thereof. Reference herein to any social initiative (including but not limited to Diversity, Equity, and Inclusion (DEI); Community Benefits Plans (CBP); Justice 40; etc.) is made by the Author independent of any current requirement by the United States Government and does not constitute or imply endorsement, recommendation, or support by the United States Government or any agency thereof.

Final Technical Report

DAISY: A Rapid Approach to Evaluating Marine Energy Converter Sound

DE-EE0007823

Dr. Brian Polagye
University of Washington

Project Partners

- MarineSitu, Inc.
- Pacific Northwest National Laboratory

Report Contributors

- Christopher Bassett
- Gemma Calandra
- Corey Crisp
- Lindsey Jones
- Paul Murphy
- Jessica Noe

Acknowledgements

This material is based upon work supported by the U.S. Department of Energy's Office of Energy Efficiency and Renewable Energy (EERE) under the Water Power Technologies Office award number DE-EE0007823.

DAISY development and testing benefited from significant support outside the core project team. The authors wish to acknowledge helpful contributions from the following individuals and institutions. Pat Cross facilitated financial support for WETS deployments outside this project's scope general use of DAISYs at WETS to meet permitting requirements. Jim Thomson (University of Washington) and Levi Kilcher (National Renewable Energy Laboratory) provided the ADVs used to characterize relative velocity and helped us interpret the measurement results. Shima Abadi (University of Washington) provided helpful guidance on localization algorithm implementation. Finally, DAISY development was supported by numerous researchers at Pacific Northwest National Laboratory including Emma Cotter, Joe Haxel, Garrett Staines, and last, but not least, John Vavrinec.

Disclaimer

Executive Summary

This project's objective was to improve the quality of acoustic information about marine energy converters that could be collected from groups of drifting hydrophones, while reducing the costs of deployment and data analysis. This was achieved through technology development addressing four focus areas: (1) minimizing flow-noise and self-noise, (2) integrating metadata streams into a single data acquisition system, (3) developing post-processing routines to facilitate rapid data review, and (4) enabling objective identification of marine energy converter sound against a backdrop of ambient noise using time-delay-of-arrival localization.

Drifting Acoustic Instrumentation SYstems (DAISYs) consist of a surface expression to monitor position via GPS, a hydrophone recording package at depth, and a compliant suspension system connecting the two. In energetic waves and currents, there are two mechanisms that degrade the fidelity of acoustic measurements: "self-noise" and "flow-noise". Self-noise is propagating sound produced by an element of the instrumentation system (e.g., metal-on-metal contact for shackles connecting the hydrophone package to the compliant suspension system). Suppressing this is primarily a matter of identifying potential self-noise sources and deploying engineering solutions that mitigate them (e.g., potting shackles in sound-dampening urethane). Flow-noise is non-propagating sound of hydrodynamic origin that is produced by acoustic pressure fluctuations around the hydrophone. This is analogous to the "wind in your ears" that one hears when riding a bicycle but is inaudible to a stationary observer nearby. For a drifting hydrophone, flow-noise arises from either relative motion between the hydrophone and surrounding water that causes turbulent eddies to be shed by the hydrophone element or turbulence advected over the hydrophone. For DAISYs in currents, this problem is partially solved when hydrophones drift with the dominant flow, but some residual relative velocity can remain. For DAISYs in waves, the main issue is that the surface expression is forced by the wave field and its motion transferred to the hydrophone package at depth, generating relative motion. In both cases, engineering solutions were identified to suppress relative motion: for currents, a flow-shield creating a quiescent pocket around the hydrophone and, for waves, a mass-spring-damper suspension system analogous to a sonobuoy[1]. These modifications allow DAISYs to collect data without appreciable flow noise down to frequencies of 10's of Hz, which are at the lower end of the auditory perception thresholds for marine mammals.

Once data are collected, analysis and interpretation are facilitated by semi-automated software to review and compare audio recordings, along with associated metadata streams (e.g., hydrophone depth, spatial position). Software routines developed in MATLAB allow individual DAISY recordings to be simultaneously visualized as spectrograms (acoustic intensity as a function of frequency and time) and listened to as sound. This allows users to build an intuitive understanding of repeated visual elements in a spectrogram (e.g., a high-intensity sound with primary frequency around 1 kHz and duration of < 1 s is the clank of a chain link in a wave energy converter mooring). By identifying differences in the time-of-arrival for the same acoustic event across multiple DAISYs, it is possible to estimate the event's origin and positively attribute sound to a specific source.

An initial DAISY variant – a hydrophone rigidly coupled to the hull of a spar buoy wave measurement drifter – was first used in 2011 to characterize radiated noise around a prototype, scale-model wave energy converter deployed by C-Power in Puget Sound, WA. A similar system was used in 2014 to

[1] https://dosits.org/galleries/technology-gallery/locating-objects-by-listening-to-their-sounds/difar/

characterize radiated noise from a prototype river current turbine. At the start of the project in 2017, the DAISY still utilized a version of the wave spar buoy, equipped with a commercial hydrophone package (OceanSonics icListen HF) and augmented by multiple autonomous data loggers to capture metadata describing hydrophone depth, drifter location, ambient metocean conditions (e.g., wind speed), and orientation. This prototype was functional, but faced three challenges:

1. *Limited opportunities to reduce cost*: The majority of system cost was the commercial hydrophone package and could not be reduced by project team effort.
2. *Labor-intensive and error-prone instrument configuration*: In the field, individual sensors (i.e., hydrophone, GPS logger, pressure logger, and inertial measurement unit) had to be time-synchronized at the start of each day, offloaded after measurements, and recharged. This meant that DAISYs required several hours of preparation and demobilization each day by a team of trained personnel and it was not uncommon for one or more sensors to be incorrectly configured, resulting in data loss.
3. *Flow-noise and self-noise*: In currents, propagating sound was often masked by flow-noise at frequencies < 50 Hz and, in waves, flow-noise and self-noise made detecting propagating sound challenging at frequencies < 200 Hz.

To overcome these challenges, with support from the team at Pacific Northwest National Laboratory (PNNL), the project evolved the DAISY through three budget periods:

- *Budget Period 1*: Baseline Evaluation (Jan. 2017 – Aug. 2017);
- *Budget Period 2*: System Improvement (Sep. 2018 – Apr. 2020); and
- *Budget Period 3*: Testing in an Energetic Environment (May 2020 – Dec. 2024).

The first, brief budget period evaluated the baseline DAISY performance in currents at PNNL's Marine and Coastal Research Laboratory in Sequim, WA and performance in waves in the adjacent Strait of Juan de Fuca. During the second budget period, which constituted the majority of project activity, DAISYs were upgraded to integrate autonomous sensors and replace the commercial hydrophone package with a less expensive unit and custom-built analog-to-digital converter. Over successive rounds of testing, DAISY reliability improved and issues with flow-noise and self-noise were addressed through flow-shield and suspension system development. The third budget period was also intended to be relatively brief and focus on DAISY deployment around a wave energy converter at the U.S. Navy's Wave Energy Test Site (WETS). However, unforeseen difficulties delayed any wave energy converter deployment until mid-2024. In the intervening time, the project team made further updates to the DAISY architecture, developed an understanding of flow-noise mechanisms through further field testing in Admiralty Inlet, WA with support through TEAMER, and published a paper describing DAISY development and performance benchmarks. In July 2024, a group of three DAISYs was deployed around C-Power's SeaRAY at WETS – ironically, a larger version of the scale-model prototype characterized by the first DAISY prototype in 2011. DAISYs were effective at identifying range-dependent noise attributable to the wave energy converter's power take-off and localizing both wave energy converter noise and odontocete vocalizations. This field deployment was executed by two personnel and the data processing pipeline allowed initial review and characterization of wave energy converter noise by the end of the first day's deployment.

Since project initiation, DAISYs have also been used to characterize noise around multiple current turbines and adapted to a "shallow" version for low-clearance environments that resembles the original wave drifter. Manufacturing plans and processing scripts are freely available through pmec.us/research-projects/daisy. In addition, for those less inclined to build their own instruments,

a commercial variant is offered for sale by project partner MarineSitu, Inc. Overall, the project met nearly all its objectives, delivering a step change in our ability to cost-effectively contextualize underwater noise from marine energy converters.

1 Introduction and Overview

Because underwater noise is used by marine animals for communication, foraging, and navigation, introducing additional sounds into the marine environment – as a byproduct of harnessing the power in waves and currents – is a matter of regulatory concern. This project developed a purpose-built drifting hydrophone system – the Drifting Acoustic Instrumentation SYstem or DAISY – that could provide high-quality measurements of radiated noise in marine energy environments.

In energetic waves and currents, there are two mechanisms that degrade the fidelity of acoustic measurements: "self-noise" and "flow-noise". Self-noise is propagating sound produced by an element of the instrumentation system (e.g., metal-on-metal contact for shackles connecting the hydrophone package to the compliant suspension system). Suppressing this is primarily a matter of identifying potential self-noise sources and deploying engineering solutions that mitigate them (e.g., potting shackles in sound-dampening urethane). Flow-noise is non-propagating sound of hydrodynamic origin that is produced by acoustic pressure fluctuations around the hydrophone. This is analogous to the "wind in your ears" that one hears when riding a bicycle but is inaudible to a stationary observer nearby. For a drifting hydrophone, flow-noise arises from either relative motion between the hydrophone and surrounding water that causes turbulent eddies to be shed by the hydrophone element or turbulence advected over the hydrophone.

An initial DAISY variant – a hydrophone rigidly coupled to the hull of a spar buoy wave measurement drifter – was first used in 2011 to characterize radiated noise around a prototype, scale-model wave energy converter deployed by C-Power in Puget Sound, WA. A similar system was used in 2014 to characterize radiated noise from a prototype river current turbine. At the start of the project in 2017, the DAISY still utilized a version of the wave spar buoy, equipped with a commercial hydrophone package (OceanSonics icListen HF) and augmented by multiple autonomous data loggers to capture metadata describing hydrophone depth, drifter location, ambient metocean conditions (e.g., wind speed), and orientation. This prototype was functional, but faced three challenges:

1. *Limited opportunities to reduce cost*: The majority of system cost was the commercial hydrophone package and could not be reduced by project team effort.
2. *Labor-intensive and error-prone instrument configuration*: In the field, individual sensors (i.e., hydrophone, GPS logger, pressure logger, and inertial measurement unit) had to be time-synchronized at the start of each day, offloaded after measurements, and recharged. This meant that DAISYs required several hours of preparation and demobilization each day by a team of trained personnel and it was not uncommon for one or more sensors to be incorrectly configured, resulting in data loss.
3. *Flow-noise and self-noise*: In currents, propagating sound was often masked by flow-noise at frequencies < 50 Hz and, in waves, flow-noise and self-noise made detecting propagating sound challenging at frequencies < 200 Hz.

These were addressed through a multi-year engineering development and testing program that integrated individual sensors in a common architecture, replaced the commercial hydrophone with a custom-designed recording package and lower-cost element, and updated the DAISY's mechanical design to improve ease of use and repairability.

1.1 System Overview

Each DAISY consists of a surface expression connected to a hydrophone package at depth by a suspension system (Figure 1). For DAISYs in currents (C-DAISY, Figure 2), flow-noise is immediately reduced by a hydrophone that drifts with the dominant flow, but some residual relative velocity can remain and is mitigated by a flow-shield. For DAISYs in waves (W-DAISY, Figure 3), the main issue is that the surface expression is forced by the wave field and its motion transferred to the hydrophone package at depth, generating relative motion. This can be addressed by a suspension system functionally similar to the one used in sonobuoys[2] and consists of a mass, spring, and damper (rubber cord and "heave plate"). In addition to acoustic measurements, DAISYs collect co-temporal metadata, including hydrophone package depth, drifter position, orientation, wind speed/direction, and condition health (e.g., battery state of charge). While individual DAISYs can provide useful information about the characteristics of radiated noise around marine energy converters, groups of DAISYs can localize these sounds to attribute them to specific sources.

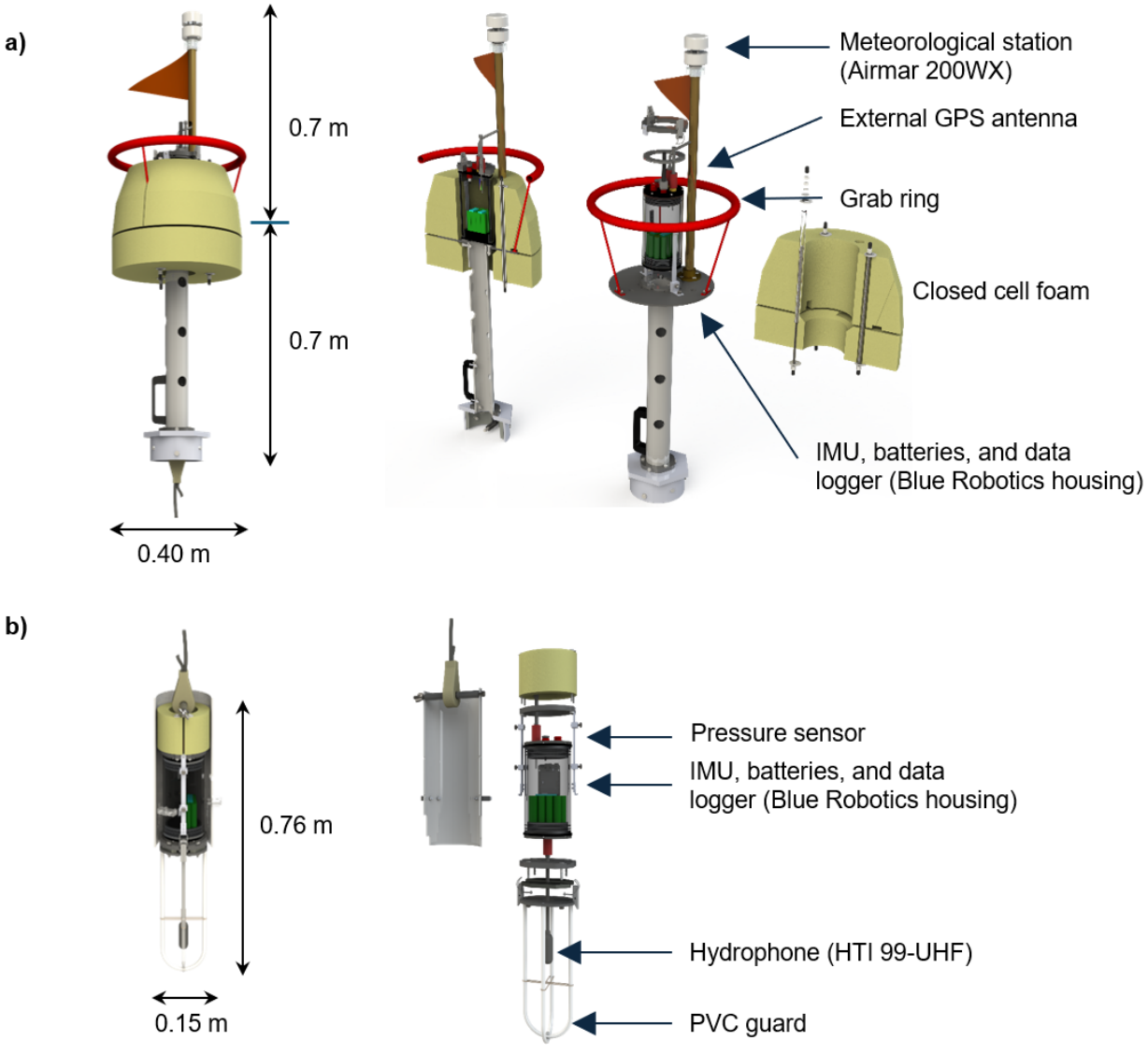

[2] https://dosits.org/galleries/technology-gallery/locating-objects-by-listening-to-their-sounds/difar/

Figure 1: Exploded views of (a) surface expression and (b) hydrophone package common to both DAISY variants with key dimensions.

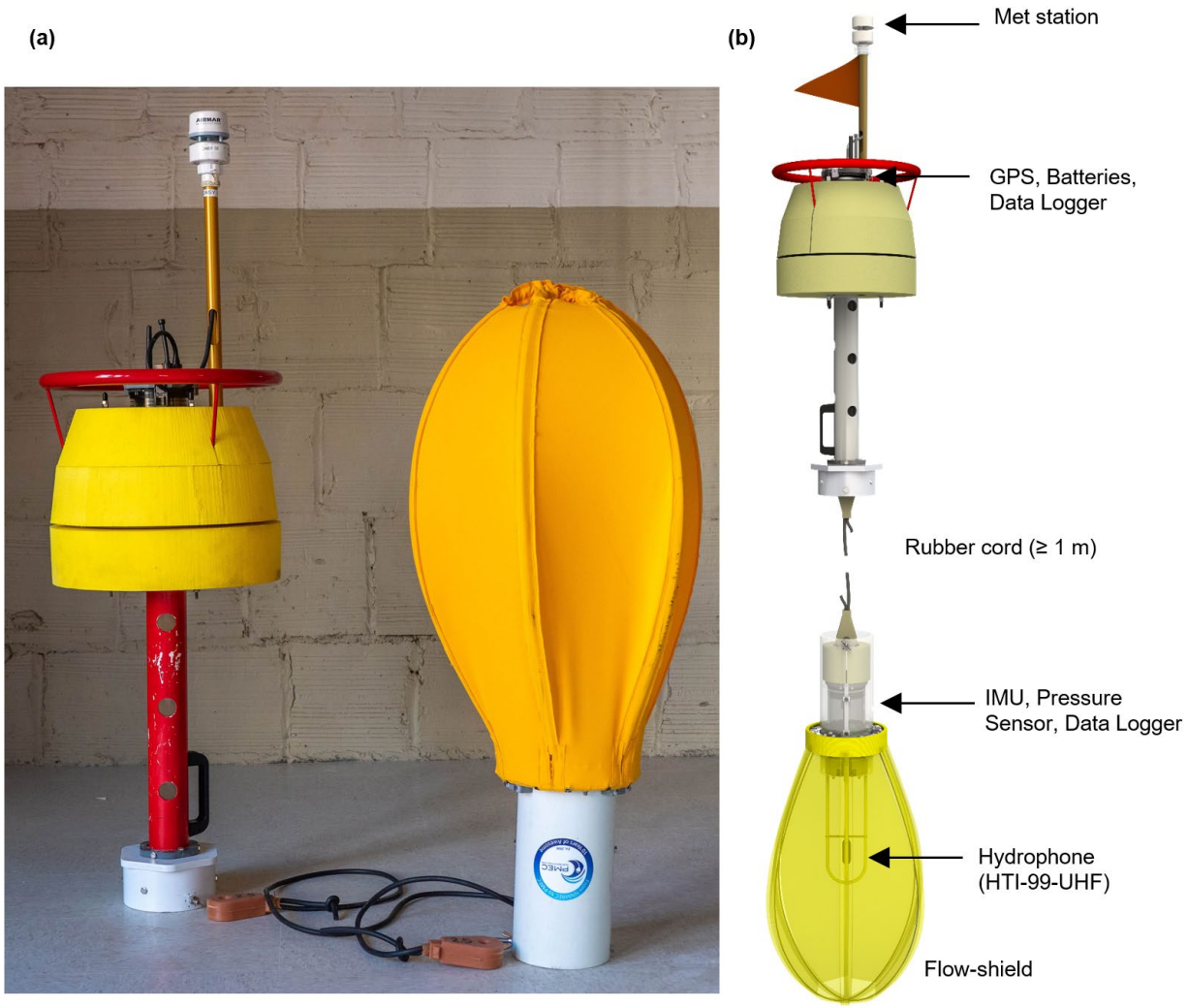

Figure 2: C-DAISY (a) as-built configuration (credit: Andy Freeberg) and (b) annotated rendering.

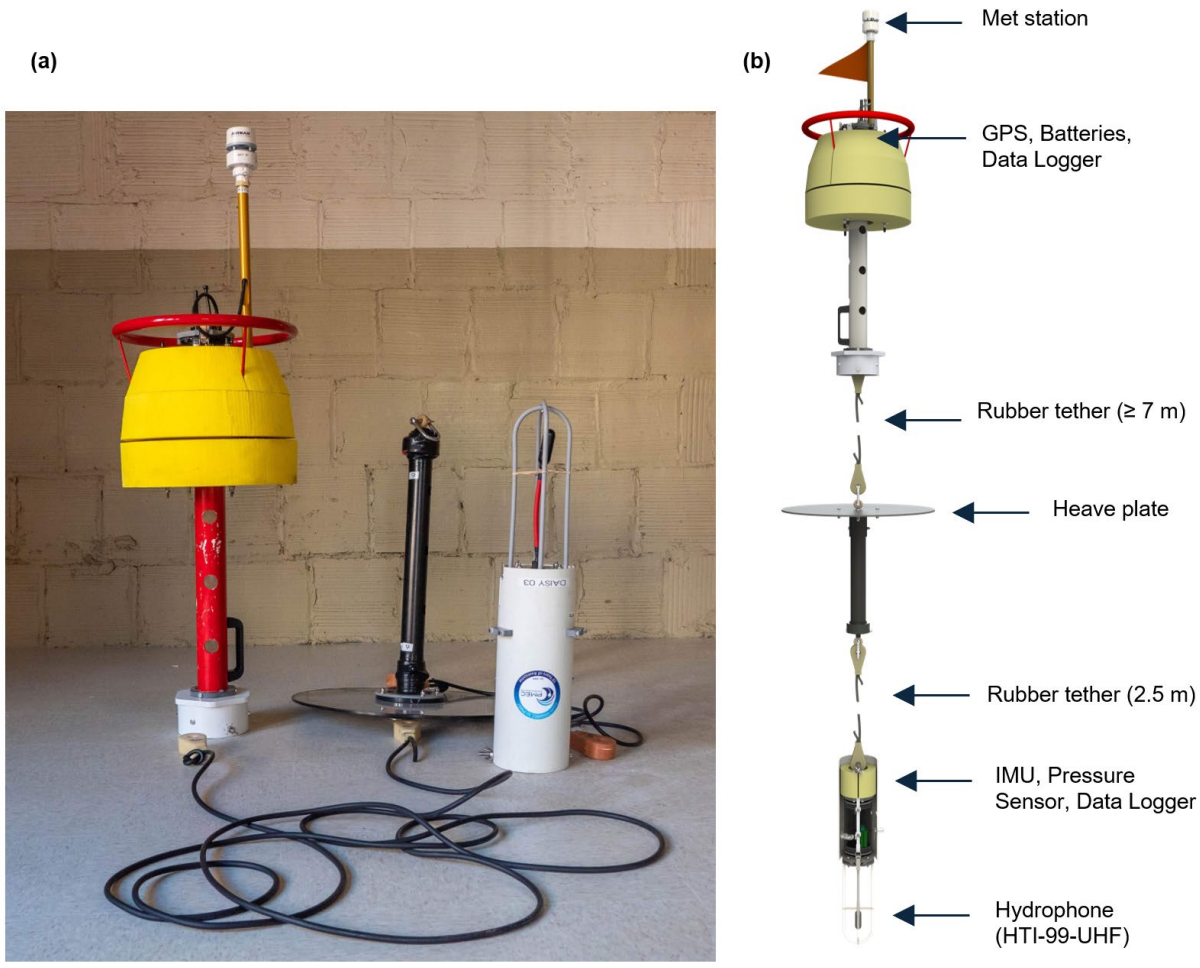

Figure 3: W-DAISY (a) as-built configuration (credit: Andy Freeberg) and (b) annotated rendering.

1.2 Project Outcomes and Lessons Learned

The project was able to realize multiple objectives:

- Demonstrating a suspension system that minimizes flow-noise and self-noise in energetic waves using a heave plate and lengths of solid rubber cord to isolate hydrophone motion from wave action;
- Demonstrating a flow-shield that minimizes flow-noise in energetic currents, but does not substantially attenuate or otherwise distort propagating sound;
- Demonstrating that DAISYs can be easily deployed and recovered by a team of two operating from a relatively small work boat;
- Implementing a high-fidelity recording package for underwater noise at substantially lower cost than available commercial products;
- Integrating multiple sensor streams (wind speed, position, orientation) using a commercial microcontroller (Beagle Bone “Pocket Beagle”);
- Demonstrating that this integration provides benefits, such as disabling hydrophone recording when DAISYs are on the surface to minimize irrelevant volumes of data;

- Developing a software suite to rapidly analyze and review data streams; and
- Demonstrating that information from groups of DAISYs can be used to attribute sound to marine energy converters through source localization.

These successes required multiple, iterative field tests to realize and it is difficult to understate the benefit of the opportunity to work with the team at Pacific Northwest National Laboratory throughout this process.

At the same time, there were a few project elements that did not come to fruition.

First, we had initially planned to replace the commercial tracker on the DAISYs (a Garmin dog collar) with a ruggedized tablet and radio-frequency (RF) transmitter integrated into the DAISY surface housing. In early testing, the RF transmission range was ineffectively short, which was eventually corrected through updates to the power supply architecture. Similarly, the ruggedized tablet software proceeded through several iterations intended to replace "pen and paper" recording and provide real-time access to DAISY component status in the field. These developments remain attractive but were ultimately set aside. While the tablet and RF transmitter can provide similar functionality to the commercial tracker, that system's independent power supply and durability, combined with a small handheld unit, confer reliability and use benefits that remain elusive for the tablet. Similarly, while a ruggedized tablet can theoretically replace "pen and paper" notetaking, typing information through a touch screen while on a moving boat (possibly being tossed by waves and splashed by water) is substantially more difficult than jotting down a quick note on a waterproof pad. It is possible that the continuing evolution of voice to text recognition could make this approach more feasible in the future.

Second, to avoid the need to open any of the electronics housings (which risks incorrect re-sealing and water ingress) we planned to offload all acoustic and metadata via WiFi. While this approach is effective for the limited data streams captured by the upper housing, the WiFi support through the Beagle Bone proved to be a substantial bottleneck for acoustic data transfer. This may be resolved by the new version of the Pocket Beagle, released in early 2025, which supports more rapid USB-C transfer.

Third, we had planned to use dynamic simulations of the DAISYs to inform hardware design decisions. While initial modeling in the first budget period reproduced some elements of DAISY motion in waves and currents, fidelity was insufficient for decision making. This highlights the significant effort required to build accurate digital twins for hydrodynamic responses in energetic waves and currents – a difficulty that wave energy converter developers routinely encounter.

Finally, there were several instances where initial conclusions were proved erroneous with the benefit of additional time and testing. Flow-shields, which were ultimately shown to reliably increase data fidelity in high-current environments, were considered a non-viable option by the end of the first budget period, a focus of development for much of the second, and confoundingly seen to provide no additional benefit at the start of the third. Only with additional testing in a more energetic environment and analysis of the available metadata streams from the DAISY (i.e., hydrophone depth and orientation) was the project team able to identify the factors that cause flow-noise in drifting measurement systems and how a flow-shield can mitigate those. Similarly, persistent low-frequency self-noise at 7-8 Hz was initially concluded to be tether strum from the suspension system. This hypothesis, which was based on good agreement with theory, was investigated in depth in the second budget period. It was not until we changed the hydrophone type on a subsequent project that we realized this was actually hydrophone vibration *excited* by tether

strum, which has a broader set of solutions than suppressing tether strum itself. Retrospectively, we realized that the "strum" peak was absent in all cases involving hydrophones with elements rigidly connected to the drifting package as opposed to a hydrophone on longer stem to reduce acoustic shadowing. Both of these examples highlight the benefits of a deliberate, multi-year technology development program with ample opportunities for iteration and course correction.

1.3 Practical Use Limitations

Practical use limitations for the DAISYs are summarized in Table 1, with more comprehensive information given in Table 2 in the following section. In addition, for source localization, the following considerations generally lead to higher quality results:

- DAISYs bracketing the source, as opposed to the source lying outside the DAISY array perimeter;
- Closer DAISY proximity to source, which increases the signal to noise ratio and reduces multi-path distortion;
- Acoustic events with well-defined start times (e.g., impulsive collisions) and/or appreciable frequency and amplitude structure (e.g., oscillatory power take-off tones for a wave energy converter) which improve cross-correlation accuracy between units; and
- Repetitive acoustic events of a similar type, allowing algorithmic outliers to be eliminated.

At least three DAISYs are required to localize a source in the horizontal plane and at least four with varying receiver depth are required to localize a source in three dimensions. Increasing the number of receivers can improve localization accuracy so long as all receivers detect the same acoustic event with limitation distortion and appreciable signal-to-noise ratios. If not, incorporating additional, poorly defined arrival times into the solution can actually decrease accuracy.

Table 1: Practical use limitations for DAISYs

Use Limit	Currents (C-DAISY)	Waves (W-DAISY)
Recommended suspension system	Tether ≥ 1 m with a flow-shield surrounding the hydrophone and its recording package	Surface-to-heave plate tether ≥ 7 m and heave plate to hydrophone tether ≥ 2.5 m
Flow-noise masking	Unlikely for f > 20 Hz Limited for f > 10 Hz	Unlikely for f > 20 Hz Limited for f > 10 Hz May be more prevalent as sea state worsens
Self-noise masking	Sporadic other than hydrophone vibration at 6-8 Hz	Sporadic other than hydrophone vibration at 6-8 Hz

1.4 Technical and Cost Performance Tables

This section summarizes elements of DAISY technical and cost performance through a set of tables:

- Table 2: Technical performance specifications;
- Table 3: Instrumentation cost (i.e., sensors, data acquisition systems, and power);
- Table 4: Platform cost (i.e., hardware surrounding the instrumentation);
- Table 5: Cost to collect data; and
- Table 6: Cost to analyze and interpret data.

As shown in Table 2, the DAISYs meet nearly all of the technical performance targets established at project initiation and, in several cases, exceed them. The only targets that were not met are the noise floor at 100 and 1000 Hz, but even this requires context. The target value corresponds to the original baseline, which was an icListen HF hydrophone (Ocean Sonics). These instruments are exceptionally sensitive and their noise floors are lower than ambient noise even in the quietest ocean conditions. Indeed, even in the quietest quiescent conditions encountered in this project (the interior of Sequim Bay, WA on a calm night), ambient noise levels at 100 Hz were ~60 dB re 1 µPa2/Hz, a full 15 dB above the instrument noise floor. The IEC 62600-40 Technical Specification establishes a higher noise floor requirement at 50 dB re 1 $\mu Pa^2/Hz$ because a marine energy converter generating sound of interest would exceed this threshold by a wide margin. Below this threshold, the radiated noise would be entirely irrelevant from a regulatory standpoint as it would be unlikely to ever exceed ambient levels. As result, the inability to meet these specific noise floor targets is of no practical consequence for monitoring a marine energy converter and the DAISYs are fully compliant with IEC 62600-40.

Further, by altering the system architecture and replacing the icListen HF with a custom data acquisition system and HTI 99-UHF hydrophone, the project was able to substantially exceed its cost targets – offsetting the higher cost of a more capable platform (Table 4) with larger cost reductions for instrumentation (Table 3). Similarly, the project was able to meet or exceed both operational and analysis cost targets (Table 5 and Table 6).

1.5 Report Structure

This report is written in a manner contemporaneous to each budget period and arranged by major tasks in the Statement of Project Objectives. For example, the narrative for Budget Period 1 does not generally reflect further knowledge on similar topics obtained in future budget periods except where specifically noted (e.g., the Budget Period 1 conclusion that a flow-shield would be ineffective is retained even though this decision was reversed with new data near the start of Budget Period 2).

Sections are organized as follows:

- Section 2: Budget Period 1 activities to establish baseline performance and early prototype configurations
- Section 3: Budget Period 2 activities to develop and test core hardware and electronics
- Section 4: Budget Period 3 activities to refine the system and demonstrate it in energetic environments
- Section 5: A brief summary of collaborations and system use outside of this project
- Section 6: A brief summary of scientific and technical information repositories associated with the project
- Appendices: Details of flow-shield testing, as well as bills of materials for hardware and electronics (live versions of the bills of materials are available with other open-source information at pmec.us/research-projects/daisy)

Much of the information provided in this report is described in a more concise manner in an archival publication on DAISY development and benchmarking (Polagye, et al., 2025). This also includes information about W-DAISY testing at the U.S. Navy's Wave Energy Test Site in Kaneohe, HI to evaluate system performance in energetic waves and use of localization to identify the source of chain noise at one of the site's berths.

Table 2: DAISY technical performance evolution from baseline to end-of-project status.

	Baseline	**Target**	**End-of-Project Status**	
	Value/Description	Value/Description	Value/Description	Comment
Low-frequency limit	75 Hz (flow-noise, self-noise)	10 Hz (instrument sensitivity limit)	10-20 Hz (flow-noise, self-noise)	Remaining self-noise (< 10 Hz) could be reduced by changing how hydrophone is secured
High-frequency limit	256,000 Hz (acquisition limit)	200,000 Hz	200,000 Hz	
Noise floor (100 Hz)	45 dB re 1 $\mu Pa^2/Hz$	45 dB re 1 $\mu Pa^2/Hz$	~60 dB re 1 $\mu Pa^2/Hz$	Lowest noise condition that could be evaluated in quiescent conditions in Sequim Bay, WA – actual noise floor at 100 Hz likely closer to ~50 dB
Noise floor (1 kHz)	30 dB re 1 $\mu Pa^2/Hz$	30 dB re 1 $\mu Pa^2/Hz$	~50 dB re 1 $\mu Pa^2/Hz$	Improved through further revision, but unable to match icListen HF performance
Location accuracy for monitoring device	3-10 m (based on comparison to met station GPS)	1-5 m	1-5 m	Higher-quality GPS antenna than baseline
Method and accuracy of MEC sound identification	*Ad hoc* comparison to distant reference Spatial variations in frequency bands associated with likely MEC sound	+ Frequency-dependent localization	+ Frequency-dependent localization	Demonstrated using vessel emissions, high-frequency tones, and WEC
Method and accuracy of flow-noise and self-noise removal	Automated *ad hoc* sound level comparison between frequency bands (incorrectly removes some MHK converter sound) or manual classification	*No change from baseline*	Automatic identification of strum with true positive rate > 80 % and false positive rate < 20 %. Flow-noise < 10 Hz.	Generally obviated by major reduction in flow-noise and self-noise achieved through hydrodynamic optimization
Classification metadata	Asynchronous GPS, IMU, and meteorological data	Synchronous GPS, IMU, and meteorological data	Synchronous GPS, IMU, and meteorological data	

Endurance	6 hours	6 hours	> 20 hours	~11 hours of storage 512 kHz, 24-bit recording time and records acoustic data only when submerged
Maximum sea state	$H_s \leq 3$m, $T_e \geq 5$ s	*No change from baseline*	System tests at WETS in $H_s > 2$ m	
Maximum current	No practical limit	*No change from baseline*	Stable in Admiralty Inlet at > 3 m/s	
Ability to detect source and remove ambient and flow-noise in variety of conditions	*Ad hoc* acoustic level comparison between frequency bands (also removes some MEC sound)	Automated removal based on machine learning from labeled data	Automatic identification of strum-induced self-noise and flow-noise masking using hand-engineered attributes	Machine learning approaches would require more training data to achieve similar outcome
Maximum water depth	No limit	*No change from baseline*	*No change from baseline*	
Minimum water depth	~ 2 m	*No change from baseline*	4.5 m for C-DAISY 13 m for W-DAISY	Set by minimum recommended tether lengths (Table 1) "Shallow" variant developed under separate project has a minimum water depth of ~1.5 m

Table 3: Instrumentation cost performance evolution from baseline to end-of-project status.

	Baseline		End-of-Project Status		Target		Comment
	Description	Cost ($)	Description	Cost ($k)	Description	Delta ($)	
Hydrophone	OceanSonics icListen HF	8925	HTI 99-UHF	1710	*No change*	-	Introduced significant time delays in the project, but central to exceeding cost targets
GPS	QStarz BT-Q1000eX	200	Board-level GPS	20	Board-level GPS	(200)	Included in integration line item
IMU	Lowell Instruments MAT-1	840	Board-level IMU	35	Board-level IMU	(840)	Included in integration line item
Pressure logger	None	0	Board-level pressure sensor	88	Board-level pressure sensor	(600)	Included in integration line item
Meteorological station	Airmar WX-200	1100	*No change*	1100	*No change*	-	Optional equipment
Instrument integration	Self-contained GPS, IMU. Battery, logger, and storage for met station	100	Microcontroller, batteries, and board-level sensors (upper and lower housings)	2358	Microcontroller, batteries, and board-level sensors (upper and lower housings)	1921	BP 2 Deployment includes electronics and housing for one upper and lower
RF tracker	Garmin dog collar	250	*No change*	250	Xbee Pro	(250)	Retained dog collars for ease of use and durability
Total		**11,415**		**5561 (-5854)**		**31**	Substantial reduction in total system cost by moving to custom data acquisition for hydrophone

Table 4: Platform cost performance evolution from baseline to end-of-project status.

	Baseline		End-of-Project Status		Target		Comment
	Description	Cost ($)	Description	Cost ($)	Description	Delta ($)	
Surface Expression	Schedule 80 PVC Metal spar Closed cell foam float collar Acrylic electronics housing	400	+ Waterproof housing + On/off switch + Waterproof charging + Wireless offload	1228 (+828)	+ Waterproof housing + On/off switch + Waterproof charging + Wireless offload	+526	Cost higher than targeted, but surface expression design balances cost against ease of operation and maintainability
Lower Housing	Schedule 80 PVC	100	+ Waterproof housing + On/off switch + Waterproof charging + Wireless offload	111 (+11)	+ Waterproof housing + On/off switch + Waterproof charging + Wireless offload	+157	Costs lower than targeted, partially offsetting cost of surface expression
Ballast	Lead disk	85	*No change*	0	*No change*	-85	Included in surface expression
Cabling	Airmar cable	50	Airmar cable	60 (+10)	*No change*	0	Airmar cable cost increased by manufacturer
C-DAISY suspension system	None	0	Rubber cord and flow-shield	263 (+263)	Rubber cord and Microstar drogue	+610	Microstar ineffective at suppressing flow-noise. Flow-shield production labor not included.
W-DAISY suspension system	None	0	Rubber cord and heave plate	148 (+148)	Rubber cord and heave plate	+279	Costs similar to target
Total		**635**		**1547-1662 (+912-1027)**		**+880-1210**	**W-DAISY – C-DAISY**

Table 5: Deployment, retrieval, operations & maintenance cost performance evolution from baseline to end-of-project status.

	Baseline		End-of-Project Status		Target		Comment
	Description	Value	Description	Value	Description	Value	
Field deployment	2 operators for duration for field survey	6 hours	*No change*		*No change*		
Turn-around time / DAISY	Manual offload of data, disassembly of spar, and individual instrument charging	4 hours	Manual data offload and common instrument recharge	< 1 hour	Automatic data offload and common instrument recharge	< 1 hour	Requires opening instrument housing to directly read SD card data
Maintenance	Annual full disassembly	16 hours	Design for disassembly	1 hour	Design for disassembly	6 hours	Substantial simplifications in hardware design

Table 6: Data management and analysis cost performance (single deployment) evolution from baseline to end-of-project status.

	Baseline		End-of-Project Status		Target		Comment
	Description	Value	Description	Value	Description	Value	
Collection automation	Manual sorting of files to directory structure	1 hour	Automatic sorting of files to directory structure	10 minutes	Automatic sorting of files to directory structure	< 5 minutes	
Analysis automation	Manual review and QA/QC	3 hours	Semi-automated review and QA/QC	3 hours	Automatic and accurate identification of flow-noise and self-noise	< 30 minutes	Automatic flow-noise and self-noise identification, but manual review still beneficial to identify acoustic events
Processing time	Manual review to obtain useful information	1-2 weeks	Improved code base with semi-automated review	< 1 day	Automatic post-processing	< 2 days	Process not fully automated, but similarly effective
Data generated	Hydrophone recording to resolve cetacean hearing limit (512 kHz)	~30 GB	*No change*		Hydrophone recording to resolve MEC high-frequency limit (56 kHz)	~3 GB	IEC 62600-40 requires collection to 200 kHz by default, so not possible to meet target and comply.

2 Budget Period 1 (Jan. 2017 – Aug. 2017)

2.1 Overview

The objective for the first budget period was to establish performance for the baseline, rigid hull DAISY and evaluate its performance against a pair of prototypes intended to reduce flow-noise in currents and waves. The baseline, rigid hull system (Figure 4a) consistsof a surface expression equipped with a GPS logger, meteorological station, and GPS tracker to facilitate recovery. A hydrophone (OceanSonics icListen) is coupled to the surface expression by a rigid spar, resulting in a submergence depth of 1.2 m. This system has demonstrated durability but is known to be susceptible to flow-noise and self-noise (e.g., noise from excitation of surface expression transmitted to hydrophone). The prototype C-DAISY (current-specific variant) and W-DAISY (wave-specific variant) compliantly couple the surface expression to the hydrophone. These “suspension systems” offer additional degrees of freedom to mitigate flow-noise and self-noise. For the C-DAISY (Figure 4b), this consists of a drogue (omnidirectional drag and inertial element) connected to the surface expression by a solid rubber cord. The drogue’s drag is hypothesized to maintain its velocity with the surrounding water, while its inertia (from added mass) isolates the hydrophone from the motion of the surface expression in waves and wind. For the W-DAISY (Figure 4c), the suspension system consists of a heave plate between two sections of rubber cord. This is hypothesized to act as a mass-spring-damper system with a resonant frequency lower than typical wave frequencies and thereby isolating the hydrophone from the motion of the surface expression. For both the C-DAISY and W-DAISY configurations, the hydrophone assembly includes a pressure sensor to monitor the hydrophone depth and an inertial motion unit (IMU) to monitor the hydrophone orientation and acceleration.

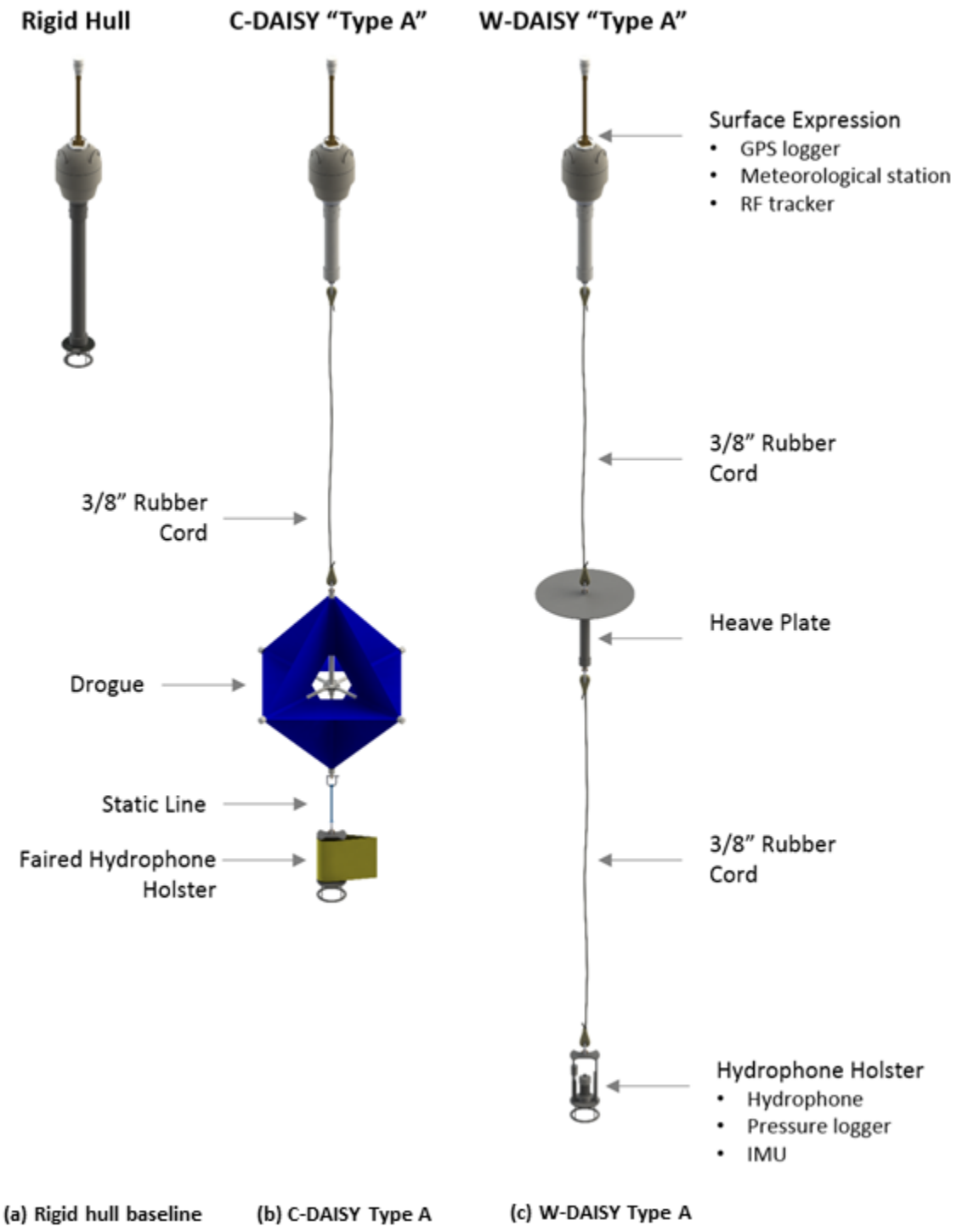

Figure 4: System configurations (to scale)

Budget Period 1 was structured into three tasks. Task 1 focused on dynamic simulation of DAISYs using a mid-fidelity software framework. While this was a conceptually attractive approach to low-cost design refinement, we found that the model accuracy was insufficient for decision making and did not continue this activity in future budget periods. Task 2 focused on testing the baseline system, prototypes (Figure 4), and variations of the prototypes. The formal scope for this was

centered on field testing proximate to PNNL's MCRL, but prototypes were also tested through separate projects in more energetic currents and waves. Task 3 focused on formalizing the electrical and mechanical design. While intended to be completed in the first budget period, we instead pursued continued design refinements throughout this and subsequent projects that substantially improved DAISY performance and reliability. Milestones associated with Budget Period 1 are summarized in Table 7.

Table 7: Budget Period 1 Milestones

	Description	Status
Task 1: Dynamic Simulation		
1.1	Simulate heave, surge, and sway acceleration amplitudes for a rigid hull DAISY and compare to observations.	Complete
1.2	Estimate relative water velocity at hydrophone for a rigid hull and C-DAISY deployed in currents.	Complete
1.3	Estimate relative water velocity at hydrophone for a rigid hull and W-DAISY deployed in waves.	Complete
1.4	Compare rigid hull, C-DAISY, and W-DAISY motion observed during baseline testing at MSL to simulations with similar environmental forcing.	Complete
Task 2: Baseline Testing		
2.1	Obtain necessary permits for field testing of baseline system.	Complete – no permits required
2.2	Establish test parameters with PNNL, including characteristics of acoustic source, range of currents, and range of waves.	Complete
2.3	Conduct measurements in quiescent conditions using rigid hull, C-DAISY, and W-DAISY.	Complete
2.4	Conduct measurements in currents using rigid hull and C-DAISY prototype.	Complete
2.5	Conduct measurements in waves using rigid hull and W-DAISY prototype.	Complete (limited testing at MCRL due to wave climate)
2.6	Report on effectiveness of flow-noise mitigation and sources of self-noise in waves and currents.	Complete
Task 3: Improvement Precursors		
3.1	Operate integrated sensor package on bench for six hours to verify feasibility and assess battery requirements for deployment.	Complete

3.2	Select configuration that minimizes flow-noise and self-noise, while maintaining ease of deployment	Complete

2.2 Dynamic Simulation (Task 1)

Because of the time and cost associated with open water testing, the project team developed a mid-fidelity model in ProteusDS to allow faster, more cost-effective design iteration. The model was used to simulate the baseline, rigid hull DAISY, a C-DAISY equipped with a drogue, and W-DAISY equipped with a heave plate. While the simulation was able to reproduce some general behavior (e.g., average speed over ground), it did not accurately predict important parameters, such as hydrophone motion and dynamic simulations were not continued into subsequent project phases.

2.2.1 Dynamic Model

2.2.1.1 ProteusDS Simulation Overview

Hydrodynamic models of the rigid hull system, C-DAISY, and W-DAISY prototypes were created in ProteusDS (DSA Ltd), a commercially available software used to model the motion of dynamic systems forced by wind, waves and currents.

Analysis with ProteusDS requires fewer computational resources than computational fluid dynamics (CFD) and, therefore, allows faster design iteration at the cost of reduced fidelity. For example, ProteusDS cannot model turbulent features and the forces they generate on rigid bodies. Rather, drag forces are calculated by bulk coefficients, which are prescribed by the user for each component in a system. Equations of motion governing rigid bodies and cable elements are solved using a 4^{th} order adaptive Runge-Kutta method. The “environment”, composed of layers of air, water, and sediment, is discretized into a gridded domain of uniform resolution. Waves, currents and wind are generated in this domain, which then impart forces onto model objects. The forces acting on dynamic objects are dependent on their geometry and their mechanical, mass, and hydrodynamic properties. Examples of the modelled rigid hull baseline system, the C-DAISY/W-DAISY surface expression are shown in Figure 5, and examples of the modelled drogue, heave plate, and holster are presented in Figure 6.

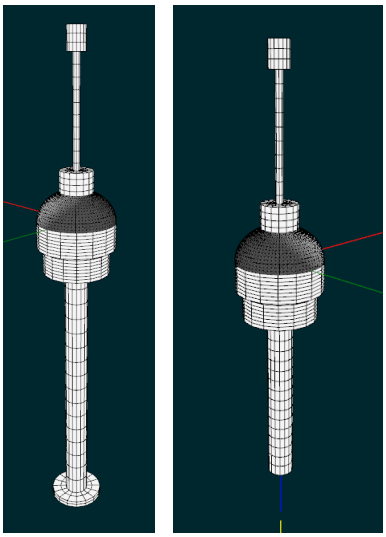

Figure 5: Rigid Hull DAISY (left) and C-DAISY / W-DAISY surface expression (right) as modelled in ProteusDS.

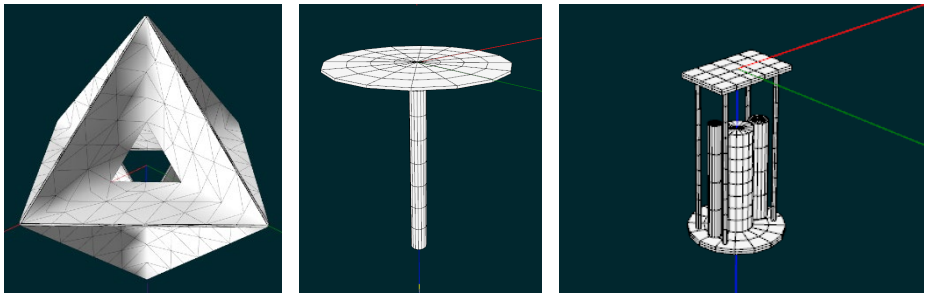

Figure 6: Drogue, heave plate, and hydrophone holster as modelled in ProteusDS.

2.2.1.2 Evaluation of Experimental Parameters

Coefficients of drag and added mass for circular plates oscillating in a quiescent fluid have been shown to depend on the non-dimensional Keulegan-Carpenter (*KC)* number (Keulegan & Carpenter, 1958). The *KC* number for a circular plate in sinusoidal oscillation is given by

$$KC = \frac{2\pi A}{D} \qquad \text{Eq. 1}$$

where *A* is the amplitude of oscillation and *D* is the diameter of the plate.

An experiment was conducted to determine the coefficients of drag and added mass of the W-DAISY heave plate. A linear oscillator was mounted to a dock at the Applied Physics Lab (APL) on Lake Union in Seattle, WA. The DAISY heave plate was fixed to the end of a 1" diameter rod extending into the water and oriented as it would be deployed in the field. Force was measured by a load cell at the connection between the rod and the oscillator carriage and position by a linear encoder. Sinusoidal motion was achieved using feedback position control. A sample rate of 200 Hz was used for both position and force measurements. The oscillator was operated at a range of amplitudes to quantify the coefficients of drag and added mass over a range of KC numbers. Although a similar experiment was conducted to evaluate the hydrodynamic parameters of the hydrophone housing, the signal to noise ratio was too low to be useful.

The phase-dependent results for each reveals a substantial dependence on the phase of oscillation, as well as an asymmetry in the coefficient of drag depending on the direction of motion

(Figure 7). Drag forces vary as turbulence develops in the wake of the heave plate, which is thought to contribute to the varying drag coefficient. Additionally, translation of the body through its wake with each oscillation may partially explain the sharp changes in added mass coefficients around the midpoint of each stroke. Notably, acceleration is at its minimum in these regions, which would result in minimal added mass even for large coefficients of added mass.

It is hypothesized that the proximity of the heave plate to the surface at the top of its stroke influenced the formation and shedding of turbulent structures, resulting in the asymmetry in drag coefficients during down-stroke and up-stroke. These results are also called into question by the deviation from a true sinusoidal shape seen in the depth data. Because of uncertainty in the experimentally-derived coefficients, simulations utilized approximate coefficients from literature describing circular plates oscillating in a quiescent fluid.

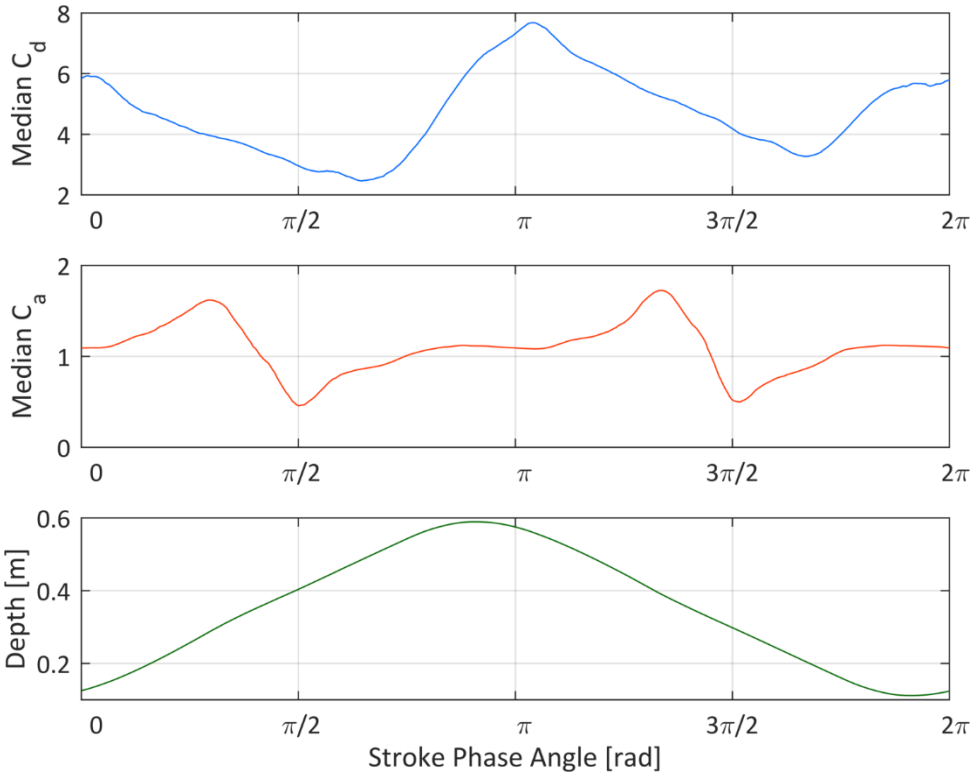

Figure 7: Median phase-dependent coefficients of drag (top), added mass (middle), and heave plate depth as a function of phase angle with an oscillation. A = 0.5 m, KC = 2.62.

2.2.2 Rigid Hull Baseline System

2.2.2.1 Model Accuracy in Currents

A rigid hull system deployed at MCRL in currents was compared to a model simulating similar forcing. Currents were measured by an Adaptable Monitoring Package (AMP), which was concurrently deployed at MCRL. Constant wind at a speed of 5 m/s and a heading of 180 degrees from north was modelled to match field data.

Figure 8 shows the path length and speed over ground of a rigid hull DAISY and its modelled counterpart. Because the rigid hull system was not instrumented with an IMU, it was not possible to evaluate the accuracy of simulated acceleration, but the results suggest that the model accurately predicts the DAISY's average speed over ground. The field data exhibits significantly more variation in speed over ground around its mean value, likely a result of the complex currents during a tidal

exchange in Sequim Bay and the presence of wind driven waves. Because co-temporal ADCP data provided only a "snapshot" of the current profile at one location, it was not possible to resolve these features in simulation.

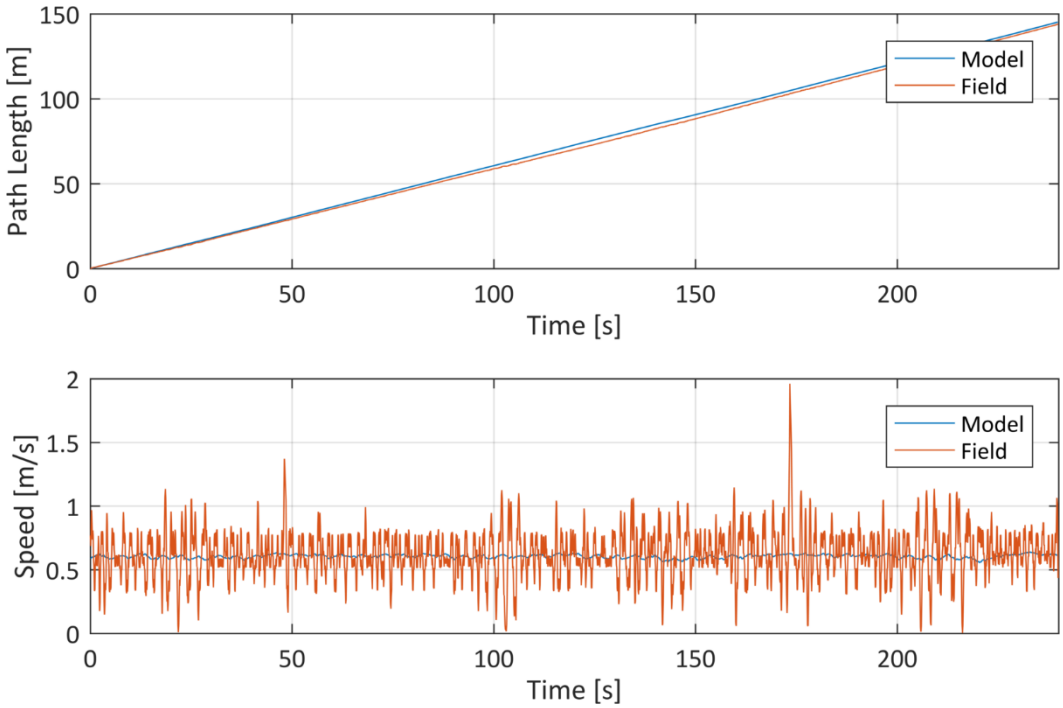

Figure 8: Rigid Hull DAISY surface expression path length and speed over ground.

2.2.2.2 Model Accuracy in Waves

A rigid hull system deployed at the U.S. Navy's Wave Energy Test Site (WETS) in Kaneohe Bay, Hawaii was compared to simulation under similar forcing. Water depth at this site was approximately 60 m and wave climate was modelled as a JONSWAP spectra with a significant wave height of 2.1 m and a peak energy period of 8.4 seconds (CDIP Buoy 198). Wind of 1 m/s at a heading of 200 degrees from North was modelled to match field data gathered by the DAISY met station.

Modelled hydrophone depth varied substantially (and unrealistically) from field measurements with the simulated hydrophone occasionally leaving the water entirely (Figure 9). Because the mass and geometric properties of the model are known to a reasonable certainty, the errors are attributed primarily to inaccurate estimations of the coefficients of drag and added mass. These coefficients were determined from empirical data for each primitive shape (primarily cylinders) comprising the rigid hull system. Although each component's coefficients may be accurate, the hydrodynamic forcing on the composite shape appear to differ considerably. As a consequence, the simulation predicts a high relative velocity between the hydrophone and surrounding water, with would lead to commensurately high-amplitude flow-noise.

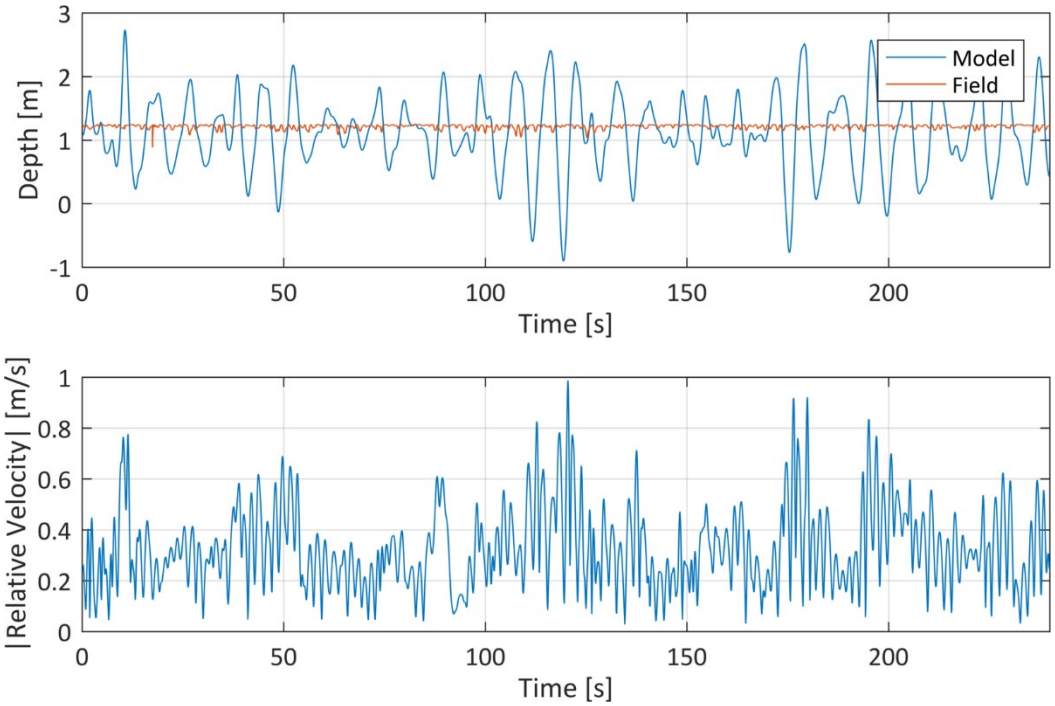

Figure 9: Rigid Hull DAISY hydrophone depth and relative water velocity.

2.2.3 C-DAISY

2.2.3.1 Comparison to Rigid Hull Baseline System

A simulation was run comparing a C-DAISY and a rigid hull system deployed in northbound currents with a surface velocity of 2 m/s and a current profile decaying according to a $1/7^{th}$ power law to a depth of 30 m. A constant wind speed of 5 m/s was modelled with a 180 degree heading (South-bound).

The path lengths, speeds over ground, hydrophone depths and relative water velocities of the simulated C-DAISY and rigid hull variants are shown in Figure 10 and Figure 11, respectively. Here, path length and average speed over ground were similarly predicted in both models, though the C-DAISY surface expression exhibits periodic variations. Model visualization showed that the drogue steadily pitched up and down in the current, generating oscillating forces on the surface expression. The surface expression, which generally lagged behind the drogue due to opposing winds, was periodically pulled upstream as the drogue dove. The average relative water velocity experienced by the C-DAISY's hydrophone was lower than that of the rigid hull's, but periodically exceeded it when the surface expression was pulled forward. This suggests that the C-DAISY should be less affected by flow-noise than the rigid hull.

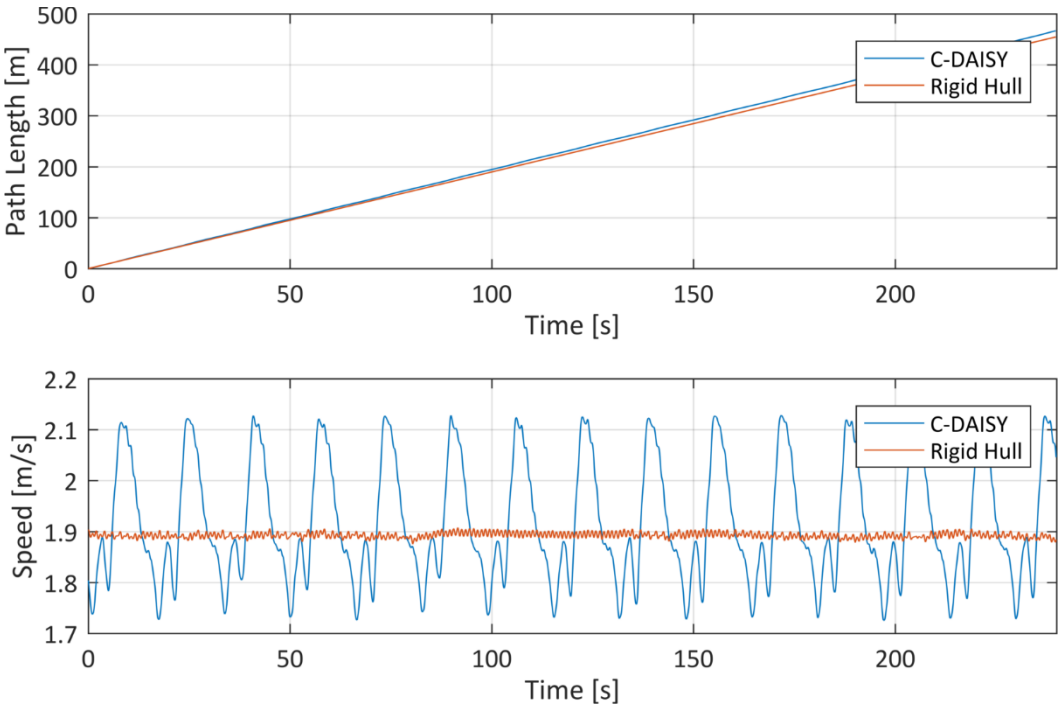

Figure 10: C-DAISY and rigid hull path lengths and speeds over ground.

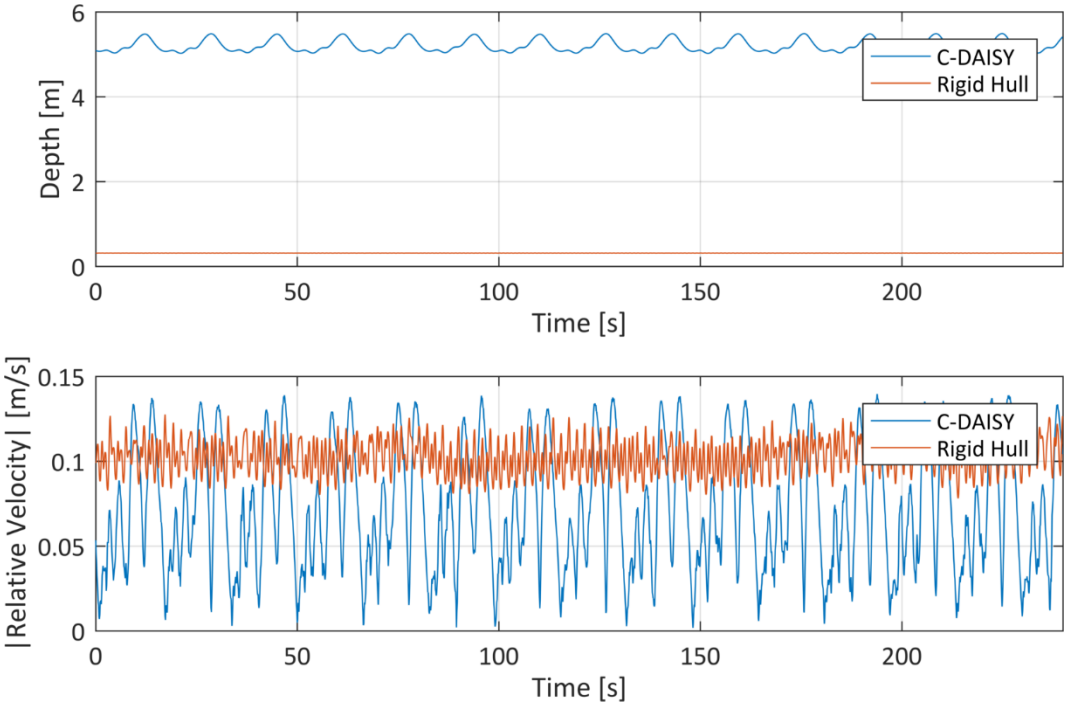

Figure 11: C-DAISY and rigid hull DAISY hydrophone depths and relative water velocity.

2.2.3.2 Model Accuracy

A C-DAISY deployed at the Marine Science Laboratory (MCRL) in currents was compared to the model with similar forcing. As for the simulation of the rigid hull system, prescribed currents were

those measured by the Adaptable Monitoring Package (AMP). Wind with an average speed 10 m/s and a heading of 120 degrees from North was measured by the C-DAISY and included in the model.

Hydrophone depth and co-spatial relative water velocity of a C-DAISY deployed at MCRL and its modelled counterpart are shown in Figure 12. The field measurements demonstrated more variability in depth than predicted by the model and the modeled depth variations differed appreciably from the simulation comparing the C-DAISY to the rigid hull configuration (Figure 11). This suggests a strong model sensitivity to specific forcing.

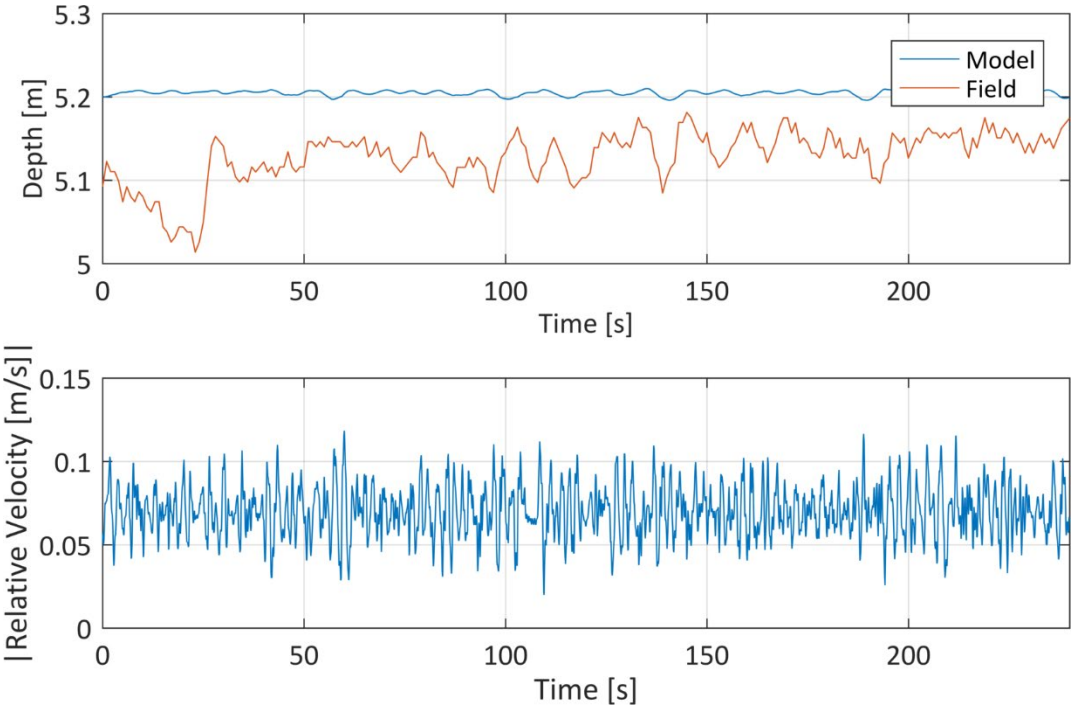

Figure 12: C-DAISY hydrophone depths and relative water velocity.

2.2.4 W-DAISY

2.2.4.1 Comparison to Rigid Hull Baseline System

A simulation was run comparing a W-DAISY and a rigid hull DAISY deployed in waves described by JONSWAP spectrum with a significant wave height of 2 m and a wave period of 7 seconds.

Hydrophone depths and co-spatial relative water velocities are presented in Figure 13, which shows that the average relative water velocity at the hydrophone was predicted to be approximately 50% lower for the W-DAISY hydrophone.

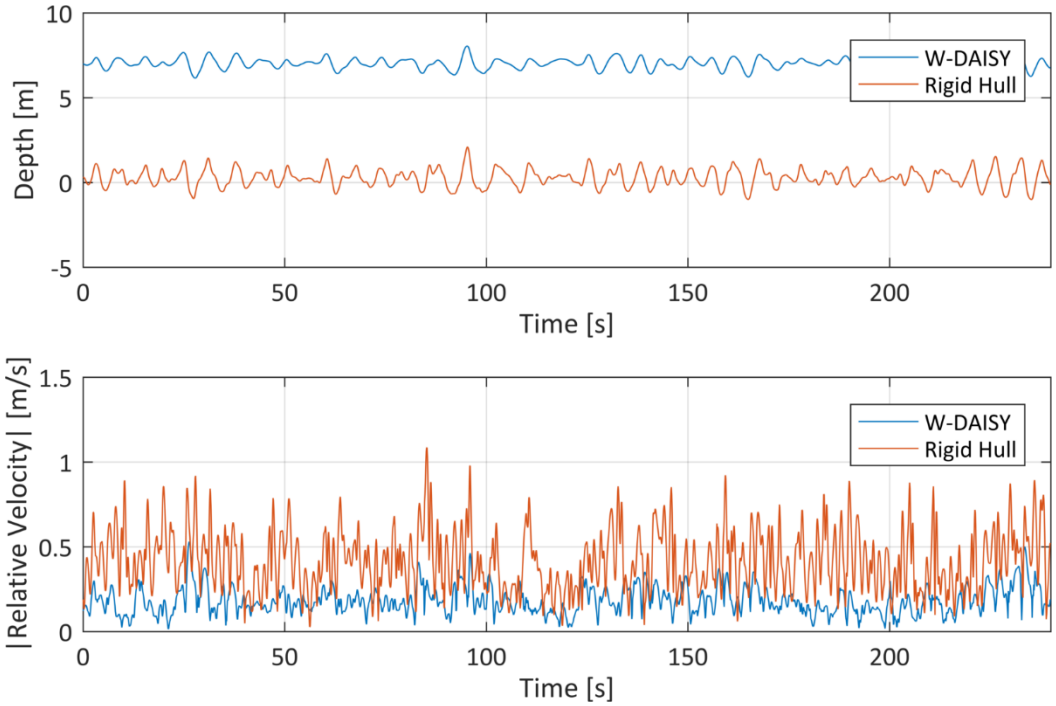

Figure 13: W-DAISY and rigid hull DAISY hydrophone depths and relative water velocity.

2.2.4.2 Model Accuracy

Data gathered by a W-DAISY deployed in the Strait of Juan da Fuca were compared to a modelled W-DAISY under similar forcing. Water depth on site was approximately 40 m. Wave spectra were measured co-temporally with a WaveRider deployed by PNNL. A mean wind speed of 7.5 m/s with a mean wind direction of 130 degrees from North was measured by the W-DAISY's met station and included in the model.

The hydrophone depths and co-spatial relative water velocities are shown in Figure 14 and the horizontal and vertical accelerations of the holsters are presented in Figure 15 for the W-DAISY deployed in the Strait of Juan de Fuca and a W-DAISY simulation with similar forcing. Depth variation of the simulated hydrophone exceeds what was measured in the field, suggesting inaccuracies in hydrodynamic parameters (as for the rigid hull simulation). The predicted relative velocity at the hydrophone is also substantially higher than would be inferred from field observations of flow-noise.

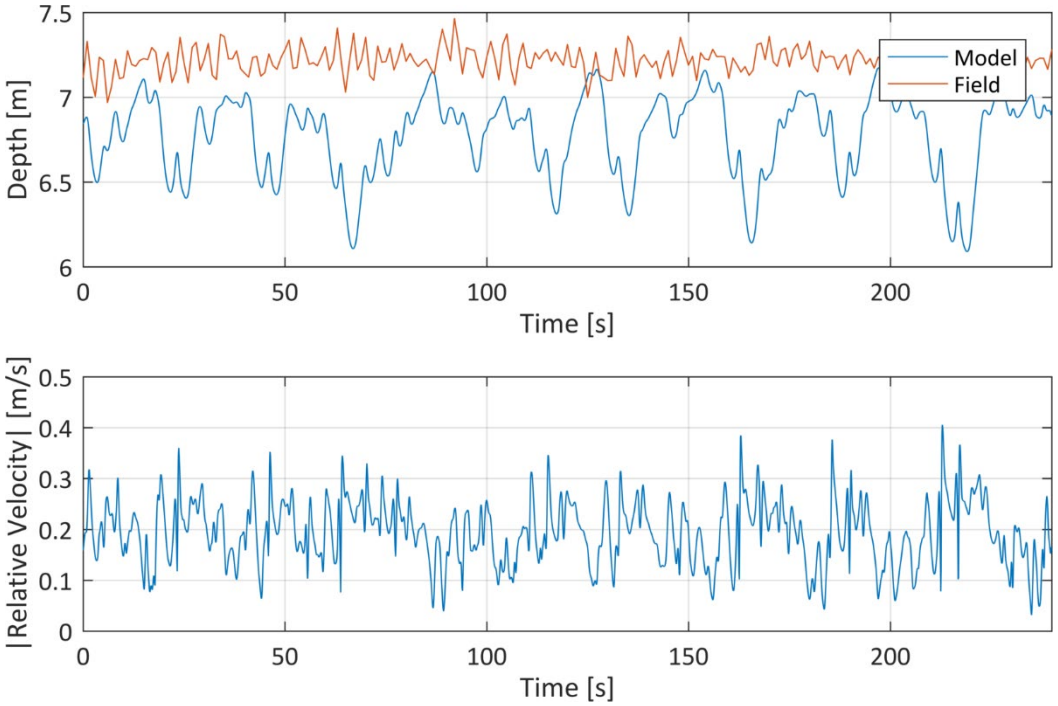

Figure 14: W-DAISY hydrophone depth and relative water velocity.

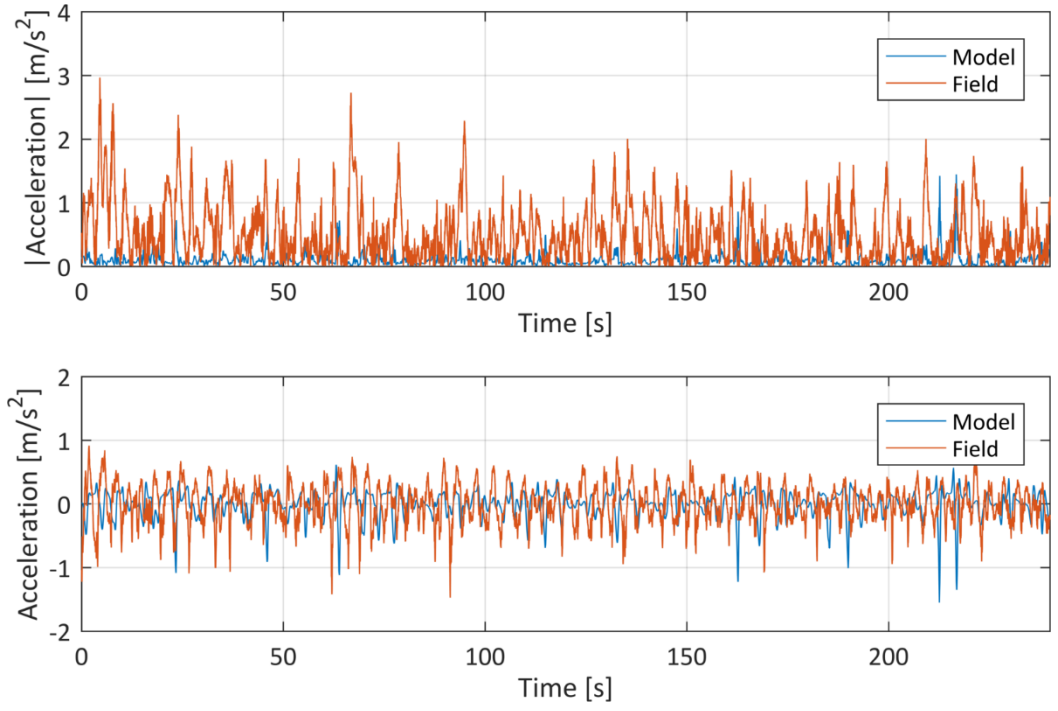

Figure 15: W-DAISY holster horizontal and vertical accelerations.

2.2.5 Discussion

The ProteusDS simulations produced results with variable utility. Comparisons between modelled rigid hull systems and W-DAISYs/C-DAISYs support the hypothesis that the suspension systems should be decrease flow-noise. However, simulations failed to accurately predict the behavior of

rigid hull DAISYs and W-DAISYs in wave environments when compared to field data. Because the geometries, mechanical, and mass properties of the DAISYs were known to a reasonable certainty, it is likely that inaccuracies in the coefficients of drag and added mass, compounded by the fidelity of the simulation in ProteusDS, contributed to the majority of these errors. Hydrodynamic coefficients were calculated for primitive shapes, which was likely a poor approximation for the relatively complex shapes of the surface expression and holster. The method used to measure the coefficients of drag and added mass of the W-DAISY heave plate was generally successful and could be repeated with other, large components (e.g., surface expression). Comparisons of field data and simulations suggest higher fidelity in current environments. This is most likely a result of the diminished effects of added mass in currents, where small accelerations (after the rigid bodies have reached steady state with the currents) reduce the influence of uncertainty in the coefficients of added mass.

The W-DAISY and C-DAISY simulations provide qualitative insight into their behavior, such as the periodic rise and fall of the drogue in currents, though some behaviors commonly observed in the field, such as the "leafing" of flat plates as they descend in the water column, were entirely unseen in simulations due to the limitations of model fidelity.

In summary, while hydrodynamic simulation of the rigid hull systems, C-DAISYs, and W-DAISYs in ProteusDS was able to provide directional guidance about the magnitude of flow-noise associated with variants, quantitative comparisons were marginal. The DAISY design has several similarities to point-absorbing wave energy converters (e.g., high-inertia heave plate against which a surface float reacts). Simulation of those systems is known to present multiple challenges and the assumption that simulation of the DAISYs would be simpler appears, in retrospect, naïve. Because of uncertainty around the effort required to refine the models and achieve more accurate results, the project team chose to focus subsequent efforts on design iteration through field testing.

2.3 Baseline Testing (Task 2)

2.3.1 Test Objectives

The objective of the baseline testing was to compare the acoustic performance and handling of the baseline, rigid hull DAISY with current-specific and wave-specific variants that compliantly coupled a hydrophone to a surface expression. For the purposes of this discussion, the rigid hull system is described as the "baseline" which was compared to prototype C-DAISYs and W-DAISYs.

2.3.2 Test Locations

Tests were carried out in three locations in and around Sequim Bay at the Pacific Northwest National Laboratory's Marine & Coastal Research Laboratory (March 2017), with supplemental information from more energetic locations in Admiralty Inlet (May 2017) and the US Navy Wave Energy Test Site (December 2016).

At MCRL, quiescent testing was conducted in the deeper waters of Sequim Bay. This was intended to establish a noise floor for the variants under test. Testing in moderate currents (less than 1 m/s) was conducted in the entrance channel to Sequim Bay, adjacent to Travis Spit. Limited testing in moderate waves (significant wave heights on the order of 1 m) was conducted in the Straits of Juan de Fuca.

2.3.3 System Configuration

Primary testing focused on the C-DAISY and W-DAISY "Type A" configurations shown in Figure 4. In several variants were evaluated, including:

- Replacement of the icListen HF hydrophone with an icListen hydrophone equipped with a Reson element with slimmer form factor (C-DAISY and W-DAISY)
- Incorporation of an open-cell foam flow-shield around the hydrophone (C-DAISY and W-DAISY)
- Incorporation of a data and power cable between the surface expression and hydrophone (C-DAISY)
- Incorporation of a fairing around the hydrophone assembly (C-DAISY)[3]
- Replacement of the compliant connection between drogue and hydrophone assembly with a rigid connection (C-DAISY)
- Incorporation of longer rubber cords between the surface expression and heave plate (W-DAISY)[4]

The intent of these modifications was to assess the sensitivity of flow-noise and self-noise to variations in system configuration. Because of differences in ambient noise in time and space, co-temporal/co-spatial comparisons proved to be the most reliable for benchmarking system performance.

2.3.4 Test Approach

2.3.4.1 Acoustic Source

An acoustic source was desired to produce a repeatable sound signature during testing. Because marine energy converters may produce sound from 10's of Hz to 10's of kHz, a source with a broad frequency response was desired. For these reasons, a US Navy J11 transducer was selected as a sound source. A source waveform was generated with a constant pressure-amplitude from 30 Hz – 1 kHz and a roll-off of 10 dB per decade from 1 kHz to 10 kHz and was calibrated to account for the transmit-voltage-response of the J11 and amplification system. The resulting source levels varied in amplitude from 30 Hz – 1 kHz, possibly due to a local interference pattern, but generally declined in amplitude from 1 kHz to 10 kHz as desired. The amplification level for the source was selected to yield a broadband (30 Hz – 10 kHz) sound pressure level less than the 120 dB re 1 µPa threshold for marine mammal harassment.

2.3.4.2 Quiescent Conditions

For quiescent testing, the baseline rigid hull, C-DAISY, and W-DAISY were deployed in a deep, calm part of Sequim Bay. At this location, the primary metocean forcing on the systems was wind, such that motion was substantially reduced relative to operation in currents or waves.

Systems were tested in an ambient environment and with the J11 suspended from *R/V Strait Science* as an acoustic source. While the vessel was operating dead ship, power for the J11

[3] The independent effect of the fairing was not tested at MCRL (i.e., no co-temporal comparisons were made between hydrophone assemblies where the only experimental variable was the fairing). However, a review of literature related to sonobuoy development makes a strong case for its inclusion in the C-DAISY. Specifically, while turbulent eddies are inefficient noise sources, if they occur in close proximity to a hydrophone, the resulting pressure fluctuations may be measurable. A hydrodynamic fairing on the hydrophone assembly reduces the intensity of shed vortices and, therefore, flow-noise produced by the structure.

[4] These configurations were not tested in waves at MCRL, but a variety of cord lengths were tested at WETS with good results, including a two-element vertical array with hydrophones at 12.3 and 26.3 m depth.

required a portable generator, which was suspended from the stern A-frame. This minimized, but did not eliminate, propagation of generator sound into the water. Further, substantial variations in received levels were observed over relatively small changes in source-receiver separation due to interference patterns, as shown in Figure 16. As a consequence of this, analysis from the quiescent testing focused on ambient noise conditions.

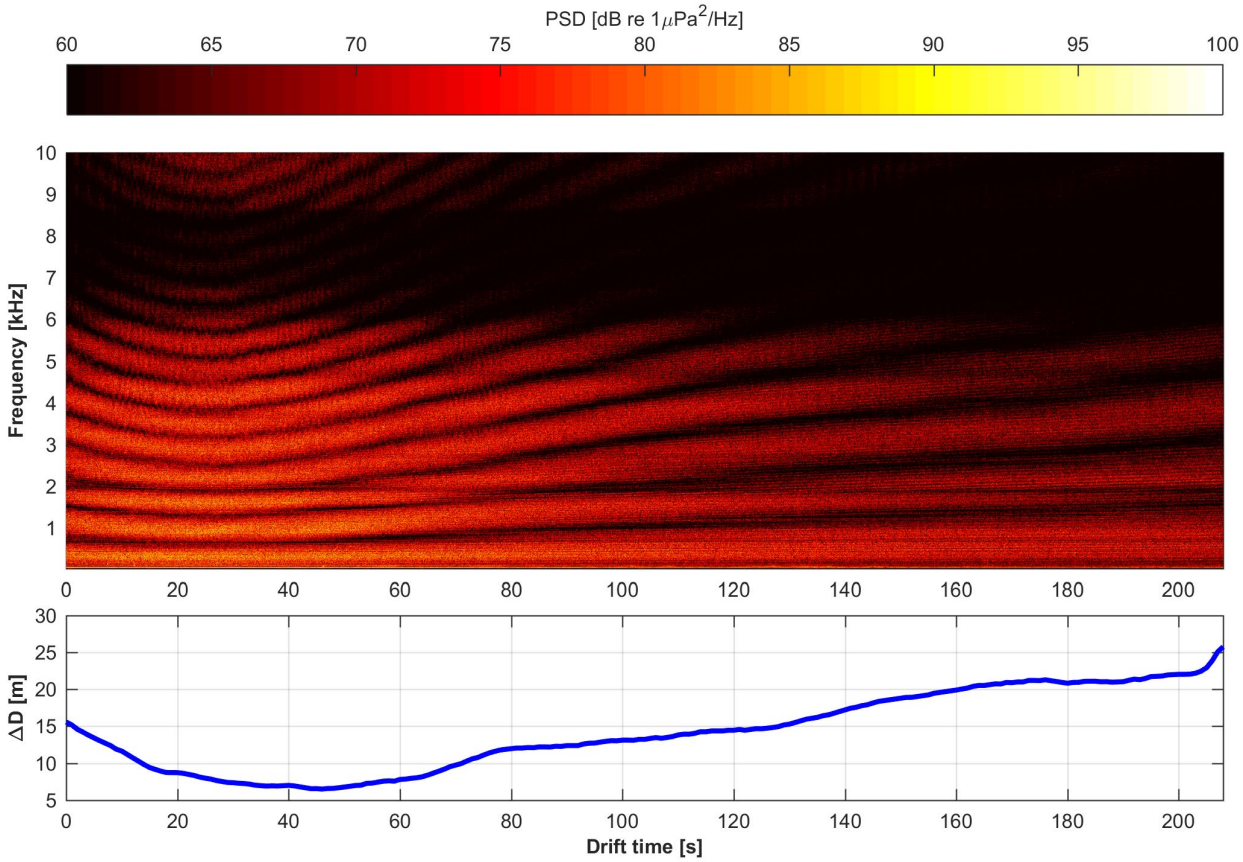

Figure 16: Received levels and proximity to J11 during quiescent testing (C-DAISY – Type A). (top) Received pressure spectra density as a function of drift time. (bottom) Horizontal separation between source (J11) and receiver (C-DAISY) as a function of drift time.

2.3.4.3 Testing in Currents

For testing in currents, DAISYs were released from the PNNL SAFE boat and carried through the narrow channel in the dominant current direction (ebb for all tests). For each test, a rigid hull system was deployed, along with a pair of C-DAISYs. The J11 transducer was deployed from a floating dock and enabled when the C-DAISYs were at relatively close range.

In addition, the C-DAISY Type A was used to characterize sound for a marine mammal playback study in Admiralty Inlet, which allowed testing in currents exceeding 3 m/s.

2.3.4.4 Testing in Waves

W-DAISY performance in waves was benchmarked in the Strait of Juan de Fuca. Due to the sea state and vessel working conditions, only a single comparison was possible between the rigid hull system and W-DAISYs with and without flow-shields.

Additional testing in larger significant wave heights was carried out at the U.S. Navy Wave Energy Test Site (WETS) in Kaneohe, HI.

2.3.5 Data Analysis

Data from each sensor was converted to MATLAB format and merged to a single file associated with each drift. Hydrophone recordings were reviewed with a MATLAB script to identify segments contaminated by anthropogenic sources (e.g., vessel traffic) and quarantined from analysis. Similarly, pressure sensor data was reviewed in time series format to identify the time that the hydrophones reached steady state depth in the water column.

Acoustic data were processed using Fast Fourier Transforms of windows with 2^{16} points tapered by a Hamming filter and overlapped by 50%. This yielded estimates of pressure spectral density (PSD) with a frequency resolution of 8 Hz and temporal resolution of 0.064 s. For periodograms (i.e., PSD as a function of frequency), the median PSD was calculated in pressure-squared space, as well as the 25th and 75th percentiles.

For C-DAISY drifts, periodograms were calculated for the 20 seconds centered on the closest point of approach (CPA) to the acoustic source. For W-DAISY drifts, periodograms were calculated for 50 seconds associated with quasi-stationary acoustic statistics. For quiescent testing, periodograms were calculated for the duration of the test during which ambient noise was statistically stationary (on the order of a few minutes).

2.3.6 Results

2.3.6.1 Quiescent Comparison

PSDs from all quiescent tests with rigid hull systems (March 21 and March 24, 2017) are shown in Figure 17. In all periodogram figures, the thick line represents the median PSD, while the transparent shading denotes the interquartile range. At frequencies above 1 kHz, the acoustic environment in Sequim Bay is relatively stationary. However, at lower frequencies, particularly below 100 Hz, variations of up to 20 dB were observed between tests. This exceeded quiescent variability observed between C-DAISY and W-DAISY variants. Consequently, a noise floor cannot be definitely assigned to each variant. Further, during these tests, drift rates from wind were on the order of several cm/s, which produced flow-noise below 30 Hz for all measurement systems.

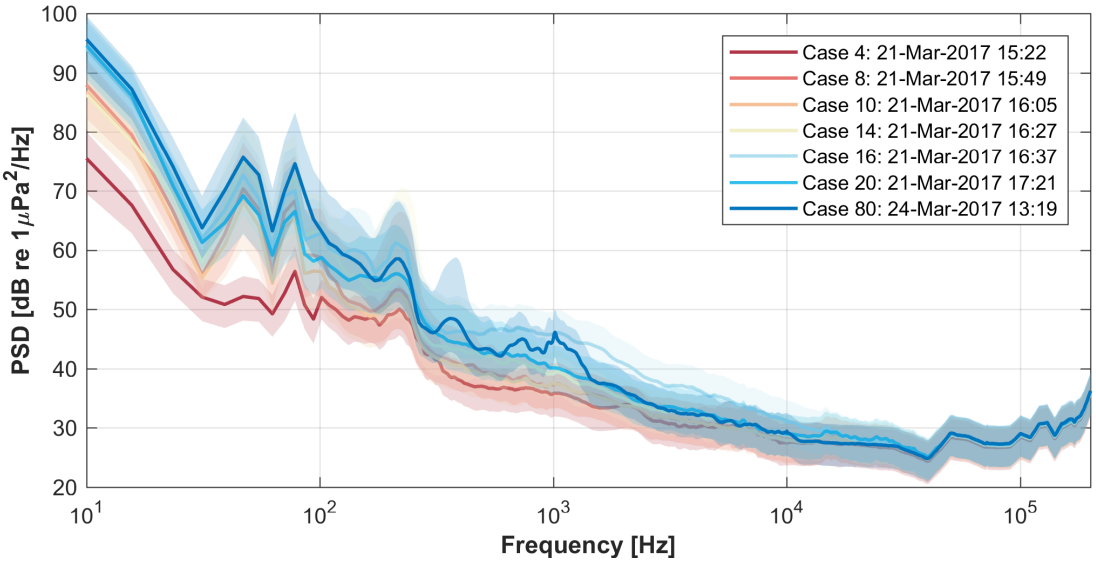

Figure 17: Periodograms from quiescent testing with rigid hull system.

2.3.6.2 Testing in Currents

C-DAISY variants were tested in currents generally less than 1 m/s. Testing was conducted in pairs to contrast design variants. Based on mapping of received levels during slack water in the channel, the sequences are dominated by sound produced by the J11 between 30 Hz and 10 kHz. Testing suggested the following:

- The incorporation of a open-cell foam flow shield flow-shield around the C-DAISY hydrophone reduced the flow-noise floor by 10 dB below 20 Hz, but at the cost of attenuating frequencies above 1 kHz by as much as 30 dB. This is likely a consequence of acoustic scattering by the air bubbles retained by the foam.
- Equipping icListen hydrophones with Reson elements may make them less susceptible to flow-noise than the standard GeoSpectrum elements, but confirming this requires a low-frequency calibration for the Reson unit.
- "Sistering" the data and power cable to the rubber cord that connects the surface expression to the drogue reduced the flow noise floor by 10 dB below 30 Hz. This suggests that the drag profile of the tether can beneficially reduce relative motion between the hydrophone and surrounding water.
- A rigid connection between the drogue and hydrophone assembly appears to have a similar flow-noise floor to the compliant connection but produces higher levels of self-noise between 30 Hz and 200 Hz. This may be because the rigid connection more efficiently propagates drogue self-noise to the hydrophone assembly.
- The "Type A" C-DAISY appears to have a flow-noise floor 5-10 dB higher than the rigid hull DAISY at frequencies less than 20 Hz, but produces a much "cleaner" signal with a significant reduction in self-noise. Quantitative comparisons are complicated by the differing depths of the hydrophones in each system.

Testing in Admiralty Inlet demonstrated favorable performance for the "Type A" C-DAISY in currents exceeding 3 m/s. As summarized in Figure 18 and Table 8, the flow-noise floor for the C-DAISY was largely unchanged in higher currents. In "quiescent" conditions with a drift rate of 7 cm/s, the flow-noise floor is over 20 dB lower, which suggests that relative hydrophone velocity is regularly exceeding this value.

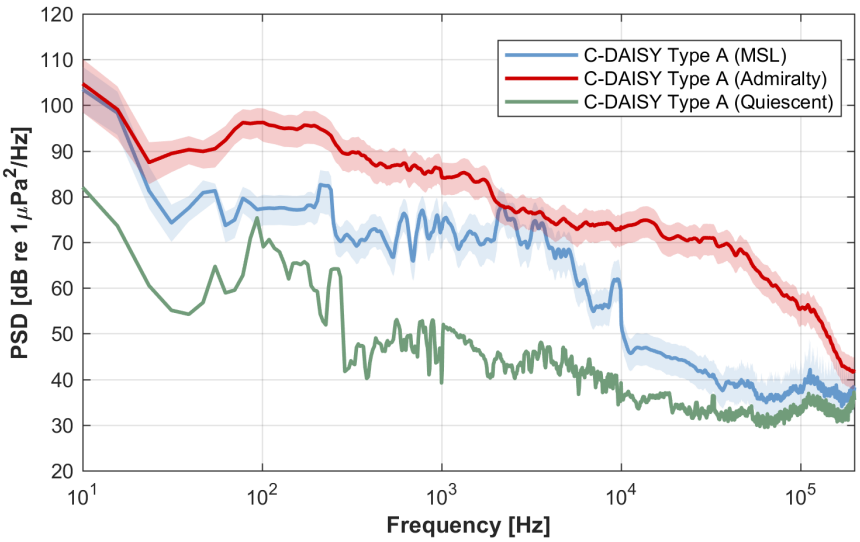

Figure 18: C-DAISY "Type A" – velocity comparison. "MSL" refers to PNNL's Marine Science Laboratory, the prior name for the MCRL facility.

Table 8: Metadata for C-DAISY Type A in moderate and high currents

Case ID	Speed over Ground [m/s]	Wind speed [m/s]	Hydrophone Depth [m]
C-DAISY A (MCRL)	0.69 ± 0.16	3.7 ± 0.58	5.2 ± 0.0061
C-DAISY A (Admiralty)	3.2 ± 0.09	4.3 ± 0.36	5.1 ± 0.011
C-DAISY A (Quiescent)	0.073 ± 0.016	2.5 ± 0.27	5.6 ± 0.0028

2.3.6.3 Testing in Waves

Due to unfavorable test conditions[5], only a single test of W-DAISYs was conducted in the Straits of Juan de Fuca. During these tests significant wave heights were on the order of 1 m in a wind-dominated sea with irregular direction and period. Testing compared the performance of "Type A" W-DAISY to a W-DAISY equipped with a flow-shield and a rigid hull system. As shown in Figure 19 and Figure 20, the open-cell foam flow-shield did reduce the flow-noise floor by approximately 7 dB below 30 Hz, but degraded measurements above 200 Hz for similar reasons to the C-DAISY. The flow-noise floor for the unshielded W-DAISY was approximately 20 dB lower than for the rigid hull system. This is consistent with results from testing in swell with higher significant wave heights at WETS. There, we have observed that as significant wave height increases, the rigid hull systems produce increasing self-noise, which can mask propagating sound at frequencies up to 1 kHz.

[5] Multiple members of the UW crew were actively seasick and recovery of DAISYs from R/V Strait Science was difficult do the high freeboard and short working deck. In over a decade of field work with DAISYs, these remain the most challenging conditions the PI has encountered.

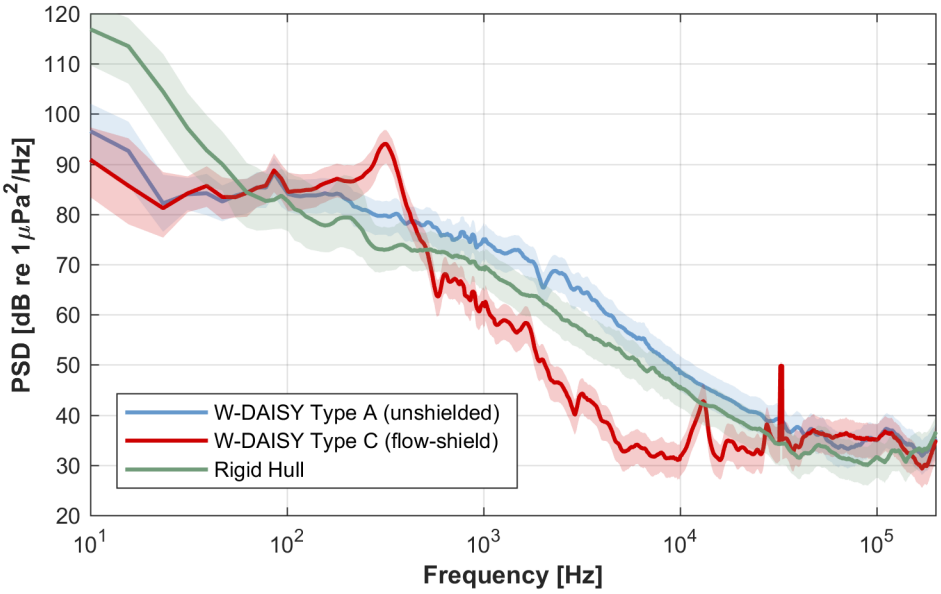

Figure 19: DAISY periodograms in waves in the Straits of Juan de Fuca.

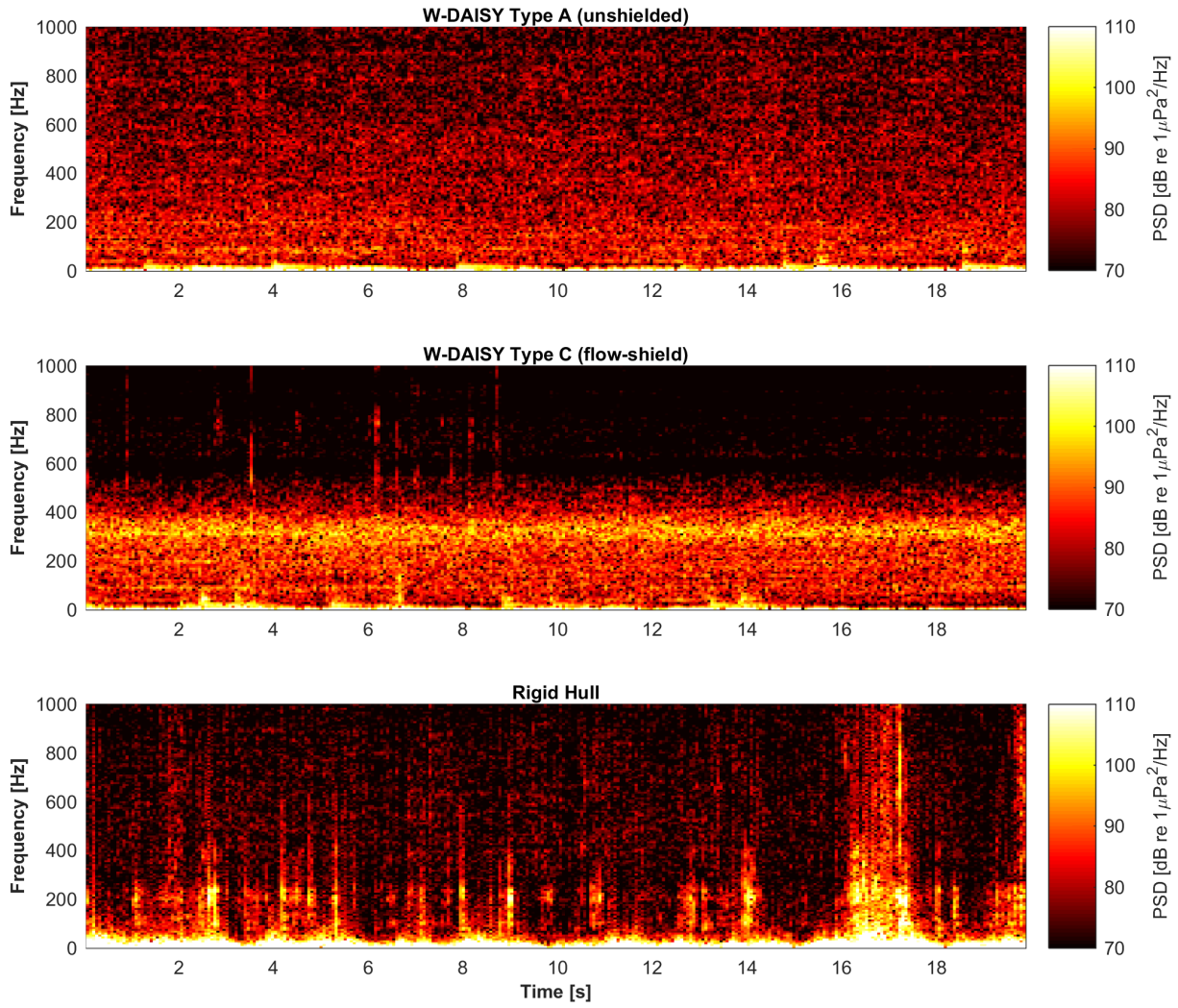

Figure 20: DAISY spectrograms in waves in the Straits of Juan de Fuca.

2.3.7 Discussion

Handling Considerations

The C-DAISY and W-DAISY variants produce substantially less self-noise than the rigid hull baseline systems and, in the case of the W-DAISY variant, substantially less flow-noise. However, the compliant systems were more difficult to handle aboard a vessel and hd an increased risk of entanglement with mooring lines or debris. This suggested that the compliantly coupled system designs would benefit from features that facilitated deployment and recovery, as well as survival in the case of temporary immersion.

Submersion Risk in Currents

In testing in Admiralty Inlet, a C-DAISY was pulled under by downwelling currents. This was caused by the omnidirectional drag profile of the drogue. However, this geometry has important benefits in currents with moderate winds and waves where it decouples the hydrophone from the motion of the surface expression. Consequently, an increase in reserve buoyancy represented a better path forward than moving to a two-dimensional drogue (e.g., a sail) with limited drag in the vertical direction.

Flow-noise Reduction

Flow-noise is the dominant feature in the C-DAISY acoustic spectra below 20-30 Hz, with the rigid hull systems performing slightly better. This indicates that the hydrophones on both the rigid hull system and C-DAISY variants are still experiencing some relative water velocity – with interactions between the surface expression and hydrophone on the C-DAISY exacerbating relative motion.

The relatively large drag from drogue in the C-DAISY system means that this element should remain in phase with the average currents acting over its cross-sectional area. However, the drogue is likely unresponsive to ambient turbulence with shorter length scales. While the compliant connection between the drogue and hydrophone holster allows the suspended assembly to respond to shorter length scales, that assembly still acts as a filter to turbulence smaller than its physical extent. This includes turbulence on the length scale of the hydrophone element. Considering that turbulence intensities are typically on the order of 10% at tidal energy sites, this means that for an average current speed of 1 m/s, turbulent eddies with velocities greater than 10 cm/s are common and velocities of 30 cm/s are probable.

Completely eliminating these contributions to the acoustic spectra requires either isolating the hydrophone from these fluctuations or digitally filtering them. The former is the purpose of a flow-shield, but the open-cell flow shields were found to distort accuracy at higher frequencies. The latter requires a second hydrophone in close proximity, which would substantially increase the cost of the C-DAISY[6]. Therefore, neither of these solutions appears practical for general-purpose monitoring.

Given this, it may still be possible to achieve incremental reductions in flow-noise. As noted previously, the icListen hydrophone equipped with a Reson element may have a superior form factor and increases the distance between the hydrophone element and bluff body housing (as source of turbulent eddies). Similarly, the flow-noise floor appears sensitive to the tether between the drogue and surface expression (i.e., a tether with a sistered power and data cable produced lower-amplitude flow-noise). Finally, adding a fairing the surface expression could reduce drag on this element, reducing non-drogue hydrodynamic forcing.

These issues are substantially less acute for the W-DAISY, particularly as hydrophone depth increases, due to lower ambient turbulence and reduction in wave orbital velocity. This is likely the reason that the W-DAISY flow-noise floor is generally lower than the C-DAISY flow-noise floor.

Testing in Waves

The Strait of Juan de Fuca adjacent to MCRL is problematic for testing under realistic wave conditions. Pacific Ocean swell, typical of wave energy sites, requires a specific wave direction to propagate down the Straits. The “confused” seas experienced during field testing of the W-DAISY systems make for difficult working conditions. For future testing, two measures were adopted. First, W-DAISY operations were conducted from a vessel with a continuously accessible, low freeboard (e.g., the SAFE boat or, in future tests, *R/V Desdemona*). During recovery operations from *R/V Strait Science*, it was difficult for the captain to maneuver the vessel alongside a W-DAISY without a high risk of running over the surface expression or entangling the rubber cord in a propeller. Second, W-DAISY operations were conducted closer to the mouth of the Straits where swell conditions occur more frequently and predictably.

Variant Comparison Procedure

[6] At approximately $10k, the hydrophone is, by far, the most expensive component in the system.

While several mechanisms were proposed for quantifying the absolute performance of DAISY variants, the most effective quantitative method proved to be a relative comparison between drifts that were effectively co-temporal and co-spatial. This eliminated the complications of temporally and spatially varying ambient noise.

Further quantification of system performance at specific frequencies could be facilitated by driving an acoustic source[7] over a narrower band of frequencies (e.g., 30 Hz – 300 Hz) where differences between variants were most pronounced. Using a narrower band of frequencies would allow a greater signal-to-noise ratio at these frequencies, while respecting the 120 dB broadband site threshold.

Finally, when benchmarking the C-DAISY and W-DAISY designs are all hydrophones should be deployed to the same depth. Testing demonstrated that variations in depth on the order of a few meters could significantly change received levels, particularly in the shallow entrance channel to Sequim Bay.

2.4 Electronics Design (Task 3.1)

Data integrity is of utmost import in any data acquisition system, and doubly so when working with acoustic data that requires a high degree of timing accuracy to minimize error in acoustic source localization. The baseline DAISY electronics package includes multiple autonomous sensors that log to individual storage. This setup poses several issues when working with the system:

- It is necessary to "sync" all sensor clocks using a PC prior to deployment, but these still drift independently by up to a few seconds over a normal survey period;
- Sensors must be configured manually and with a start time, and reconfigured if the start time changes (e.g., delayed deployment); and
- Deployment data must be manually retrieved from multiple instruments.

These problems all stem from the main drawback of the existing system: asynchronous data collection. In addition, most of the sensors do not have on/off switches and not all sensors have ways to verify functional status in the field (e.g., a wireless interface or blinking light). The prototype design for the new integrated electronics package overcomes these obstacles. The electronics are divided into two packages: an upper electronics housing for the surface expression and a lower (sub-surface) electronics housing that connects to the hydrophone. Instrumentation is summarized in Table 9 and a working prototype upper housing is shown in Figure 21.

[7] Ideally, PNNL would lease the J11 transducer from the Navy for use in multiple Triton projects. The icTalk LF currently on hand at Triton does not produce sound at sufficiently lower frequencies for this purpose.

Table 9: Instrumentation summary

Components	Details	Advantages Over Previous Design
Controller	BeagleBone Black (BBB) microcontroller	-Data synchronization between sensors -Single logging location and directory -Automatic log file rotation and timestamping
GPS	Board level GPS unit w/ timekeeping PPS output	-GPS synced system time -Synchronization of data across array of DAISYs and synchronization to external data repositories
IMU	9-Axis IMU (board level)	-True IMU (previous unit has no gyroscope) -Increased configuration options
Pressure Sensor (lower housing only)	30 bar pressure sensor with rated 2 mm resolution.	-Accurate pressure data and system timestamping for calculating reliable hydrophone depth
Meteorological station (Optional – upper housing only)	Airmar 200WX meteorological station	-Same device as previous design, but integration with BBB allows for device configuration through software interface
Power Monitoring	Battery voltage and current sensors	-Allows monitoring of system power consumption
RF tracker (upper housing only)	Networked 900 MHz RF Modules	-Send any desired system data to base station, not only GPS coordinates -Send commands to DAISYs from base station -Ability to swap out module for module operating at different frequency for use internationally (if required)
Wireless	2.4 GHz USB WiFi Module	-Device communication - Automatic backup of log files to Dropbox or other cloud storage

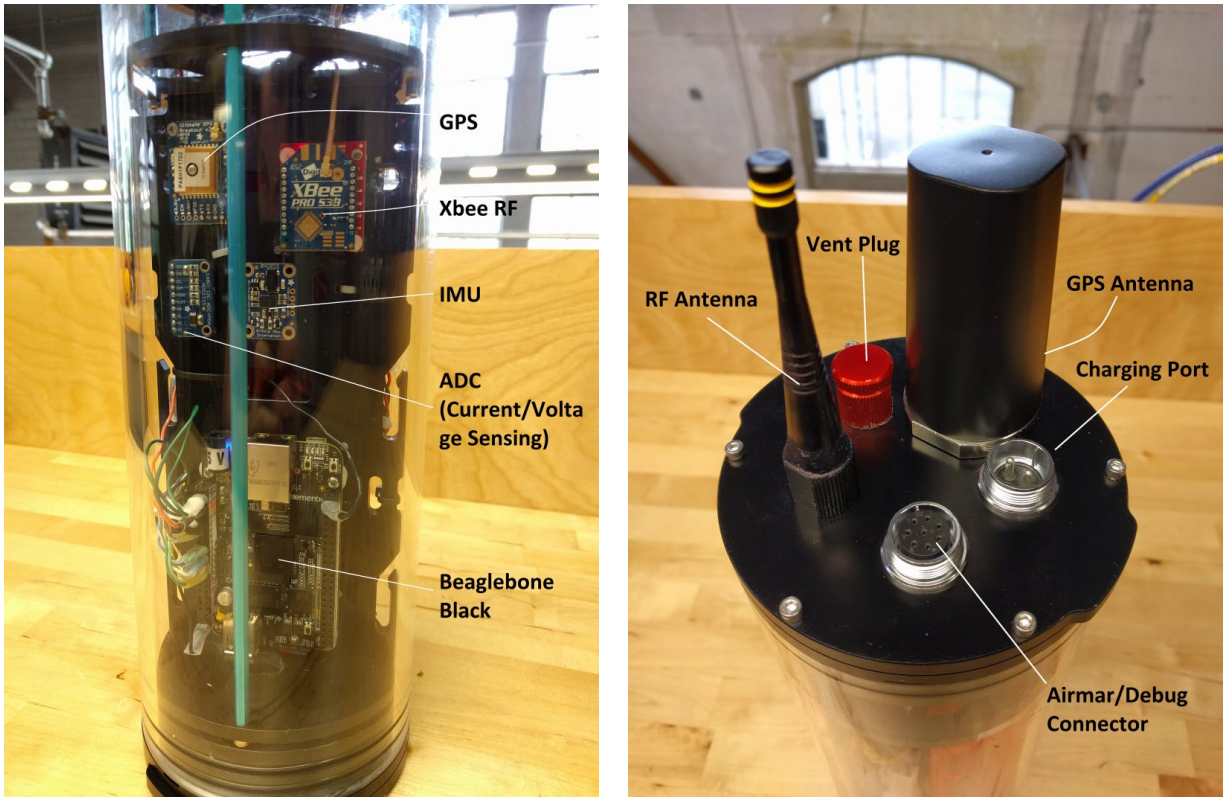

(a) Electronics assembly (batteries on reverse side)

(b) Antennas and connectors

Figure 21: Prototype upper electronics housing

2.4.1 Upper Housing

2.4.1.1 Controller

The prototype design of the upper housing features many improvements over the baseline design, of which the most crucial is the addition of a microcontroller acting as the controller and data acquisition system. The chosen microcontroller is an open source design called the Beaglebone Black (BBB), which is based on a 1 gigahertz Texas Instruments single-core CPU with 512 megabytes of RAM. This controller was chosen for its low power consumption, number of communication busses available, and technical support. It interfaces with the sensors and communication devices in the upper housing, and controls the logging and timestamping of data to ensure consistency between sensors. The sensors included in the upper housing design include: a GPS module with a timekeeping pulse-per-second (PPS) output, a 9-axis inertial measurement unit (IMU), and a battery power consumption monitor. The design also includes a bulkhead connector for attaching an optional Airmar meteorological station to the system, and a bulkhead connector on the bottom of the housing for the possibility of a communications tether between the upper and lower electronics packages. The package also contains a wireless module and an RF transmitter/receiver for communication and tracking. The BBB can handle many more devices, so expansion of the electronics package is possible as desired.

2.4.1.2 Sensors

The GPS is not only used to track the system location as in the baseline version of the electronics package, now it also provides GPS timestamp and PPS signals to a NTP (Network Time Protocol)

server that runs on the BBB microcontroller. The NTP server tracks the PPS ticks and GPS message timestamps to accurately set the system clock time and keep it from drifting away from UTC time. This process keeps the system clock within microseconds of UTC time while the GPS module has a 3D position fix. The parsed GPS data is logged by the system, eliminating the need to parse GPS data in post-processing. The GPS in the upper housing has an externally mounted antenna to improve position accuracy over the baseline system.

In the baseline system, the inertial measurement unit (IMU) used (Lowell Instruments MAT-1) is not a true IMU since it does not contain a gyroscope. Without a gyroscope, it is much more difficult to obtain accurate orientation from the raw data. The addition of a 9-axis IMU to the prototype design allows for more accurate device movement and orientation measurements. It is also possible to let the IMU do the orientation processing and calculate Euler and/or quaternion angles, which can be output along with the raw data, thereby reducing effort needed for post-processing of deployment data.

The existing system has sensors that all run on independent batteries. The upgraded system has a shared battery bank with current and voltage monitoring so that the battery charge can be calculated. It also allows for tuning system power usage by testing various sensor configuration parameters and optimizing them for specific deployment objectives.

The Airmar weather station is an optional attachment to the baseline system, so it was decided to make it an optional attachment in the prototype design. The Airmar systems do not save configuration setup at shutdown, so it is not possible to configure the device for deployment without reprogramming the instrument on a PC. Integrating the weather station into the BBB controller allows for custom setup configurations to be selected in the field.

2.4.1.3 Communication

The BBB controller has a USB wireless module that allows the device to stream data back to the user when within range of a properly configured wireless network. It also allows for the device to automatically upload log files to a Dropbox or another data server, reducing post-deployment effort since it is no longer necessary to manually retrieve log files from multiple sources[8].

As with the baseline system, it is necessary to have an RF module ping the device location back to the user in the common occurrence that it moves out of visual and wireless range during a deployment. The chosen RF module has a rated range of 9 miles at a 1.25 kB/sec throughput (4 miles at 25 kB/sec) and, when used in the native API mode, multiple modules can be networked together to increase the overall range of a single module by routing packets from one DAISY to another. Using these RF modules instead of the Garmin dog collars used by the baseline system allows for retrieving all system data (not just location), and for sending commands to the devices from the user while the systems are on the water.

An external connector for a debugging cable is also included in the unlikely event that both RF and wireless communications fail.

2.4.1.4 Power

The upper housing is powered by a 12 volt rechargeable lithium-ion battery pack. The design specification for the battery rates it at 14 amp-hours, giving a nominal rating of approximately 160 Watt-hours. An external port is included to allow for charging the system without the need to open the electronics housing.

[8] This also eliminates the need to open the electronics housing to offload data, which is time consuming.

To reduce the complexity and cost of the electronics housing, we are using a magnetically activated reed-switch to power on and turn off the system. Other options included an externally mounted, waterproof switch, or a shorting plug. However, those options are both more expensive to implement than an inexpensive reed-switch and relay.

2.4.2 Lower Housing

2.4.2.1 Controller

The prototype design of the lower housing uses the same BBB microcontroller. The sensors in the lower housing design include: a GPS module with a timekeeping pulse-per-second (PPS) output, a 9-axis inertial measurement unit (IMU), an external pressure sensor for monitoring hydrophone depth, and a battery power consumption monitor. The design also includes a bottom bulkhead connector for attaching the OceanSonics hydrophone package, and a bulkhead connector on the top of the housing for the possibility of a communications tether between the upper and lower electronics packages. The package also contains a wireless module for communication when in air.

2.4.2.2 Sensors

The GPS is mainly be used to provide GPS timestamp and PPS signals to a NTP (Network Time Protocol) server that runs on the BBB microcontroller. As with the upper housing, the NTP server tracks the PPS ticks and GPS message timestamps to accurately set the system clock time and keep it from drifting away from UTC time. This process keeps the system clock within microseconds of UTC time while the GPS module has a 3D position fix. As the lower housing is sent to depth for deployment it loses its GPS fix and the NTP server no longer receives GPS timestamps or PPS signals, so clock drift may occur. Options for mitigating or eliminating that clock drift are discussed in Section 2.4.3.

The same IMU used in the upper housing is used in the lower housing and operates in the same way as the IMU on the upper housing and with the same setting for consistency. The same power monitoring scheme is also used in the lower housing.

An externally mounted pressure sensor on the lower housing is be used to monitor the hydrophone depth. The chosen sensor has a rated resolution of 2 mm and max pressure rating of 30 bar.

By connecting the OceanSonics hydrophone to the BBB controller in the lower housing it should be possible to send commands to the hydrophone for configuration and for clock syncing. It should also be possible to send the GPS's PPS signal to the hydrophone for syncing the hydrophone clock to GPS time along with the system clock. Instantaneous acoustic data or other information could also be retrieved from the hydrophone.

2.4.2.3 Communication

The lower housing is deployed with the same type of USB wireless module as the upper housing and serves the same purpose, with the exception that it is disabled when the housing is at depth to conserve power and reduce the risk of electromagnetic interference. An external connector for a debugging cable is also available on the lower housing and is fitted with a submersible dummy plug during deployments.

2.4.2.4 Power

The lower housing is powered by the same type of 12 volt rechargeable lithium-ion battery pack as the upper housing. An external charging port with a submersible dummy plug is included to allow for charging the system without the need to open the electronics housing. As with the upper housing, a reed-switch is used to power on and off the device.

2.4.3 Localization Approach

2.4.3.1 Time Synchronization

Reliable time stamping and time synchronization between devices is essential for accurate acoustic localization, as is knowledge of hydrophone positions across DAISYs in an array. The baseline system does not have a way to ensure that device clocks stay synced between clock set commands or to ensure that the clocks do not drift. This problem is overcome in the upper housing with the use of a GPS module that has a PPS timekeeping output. The GPS message timestamps and the PPS signal are used by an NTP server running on the BBB to keep the system clock within, at most, 10 microseconds of UTC time.

This same method is employed in the lower housing. When the lower housing is at the surface the GPS achieves a 3D fix, and the NTP server updates the system clock. However, as the GPS module only outputs a PPS signal when it has a 3D GPS fix, the NTP server loses its time source when the lower housing is sent to depth. This leads to a possible source of clock drift in the lower housing during deployments. There are three practical solutions to this problem: 1) drift durations short enough that system clock drift is negligible, 2) add an external battery-backed real-time clock to system, or 3) provide a tethered connection between upper and lower housings to continually transmit PPS signals.

- **Solution 1:** This solution is simplest and acceptable if testing shows that clock drift over average deployment time is negligible. This was found to be the case in testing during Budget Period 2 and remains the approach taken for DAISYs.
- **Solution 2:** An external battery backed real-time clock (RTC) could be added to both the lower and upper housings. The DS3231 RTC device that would be used for this solution has a maximum clock drift of less than 4 milliseconds per hour and is an inexpensive solution, if required.
- **Solution 3:** Having a tether between the upper and lower housings would allow for sharing of the upper housing's GPS and PPS signals with the BBB in the lower housing. However, a tether is expensive, makes it more difficult to reconfigure hydrophone depth on the fly and makes the system more complicated to deploy and recover. Because of this, the solution was not pursued.

2.4.3.2 Elimination of RTK GPS in Favor of SPP GPS

We initially planned to incorporate a real-time kinematic (RTK) GPS in system to achieve cm-level localization of surface expression. For the rigid hull DAISYs, in combination with an IMU, this could be used to calculate the location of the hydrophone with cm-level accuracy. However, for the compliantly coupled systems, precise upper hull location does not translate to precision in hydrophone location. Further, the cost of an RTK GPS module and the required high-gain antenna (> $500), led to a decision to put aside the RTK GPS in favor of a standard single point precision (SPP) GPS module. The SPP GPS modules have approximately 1.5 meters of error with a clear view of the sky, and, as the DAISYs operate in open water, it is unlikely that substantial portions of the sky will ever be blocked long enough to seriously impact GPS signal quality.

2.4.4 Power Consumption

An initial bench test of the prototype upper housing verified power consumption for the system relatively to battery capacity. Power consumption was stable at 8.45 W with all sensors active and logging data at their maximum rates, as shown in Figure 22. This suggests an endurance > 12 hours

(significantly exceeding the 6 hour design target), as estimated by the battery specifications (161 Watt-hours) and the average power consumption.

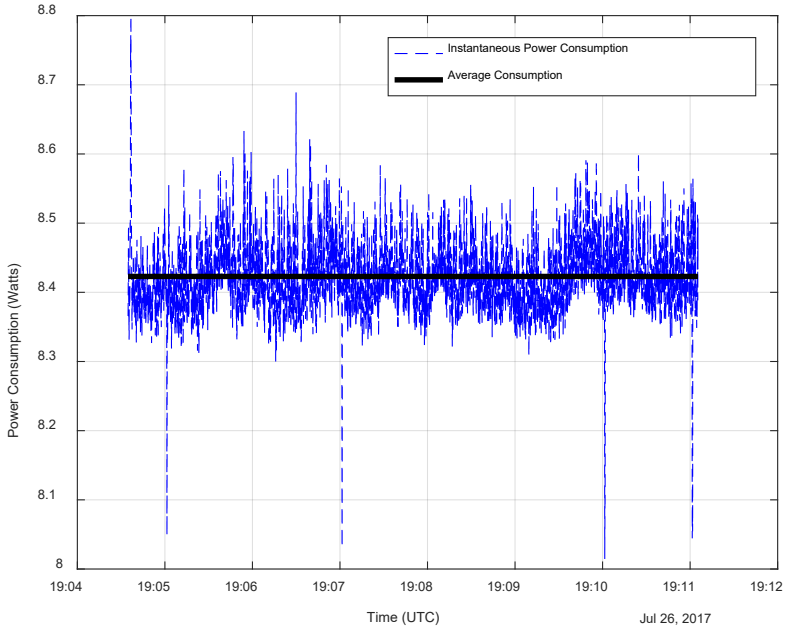

Figure 22: Snapshot of power consumption data from benchtop testing.

2.5 Mechanical Design (Task 3.2)

The mechanical design was undertaken with two primary goals: improve the quality of acoustic measurements and reduce the time required for operation and maintenance of the system. The baseline rigid hull system was taken as a starting point for the design, as it has the advantages of being easy to deploy from a vessel and proven durability in the field. However, the rigid hull system has several disadvantages, in addition to the elevated levels of self-noise and flow-noise:

- Requires several hours of mobilization and demobilization effort around each day of surveying, largely to extract asynchronous instruments for data offload and recharge.
- Some fasteners cannot be inspected for corrosion without breaking glue joints.
- The “anti-splash” domes on the top of the surface expressions reduce self-noise, but make it difficult to hook the retrieval U-bolts due to decreased clearance.

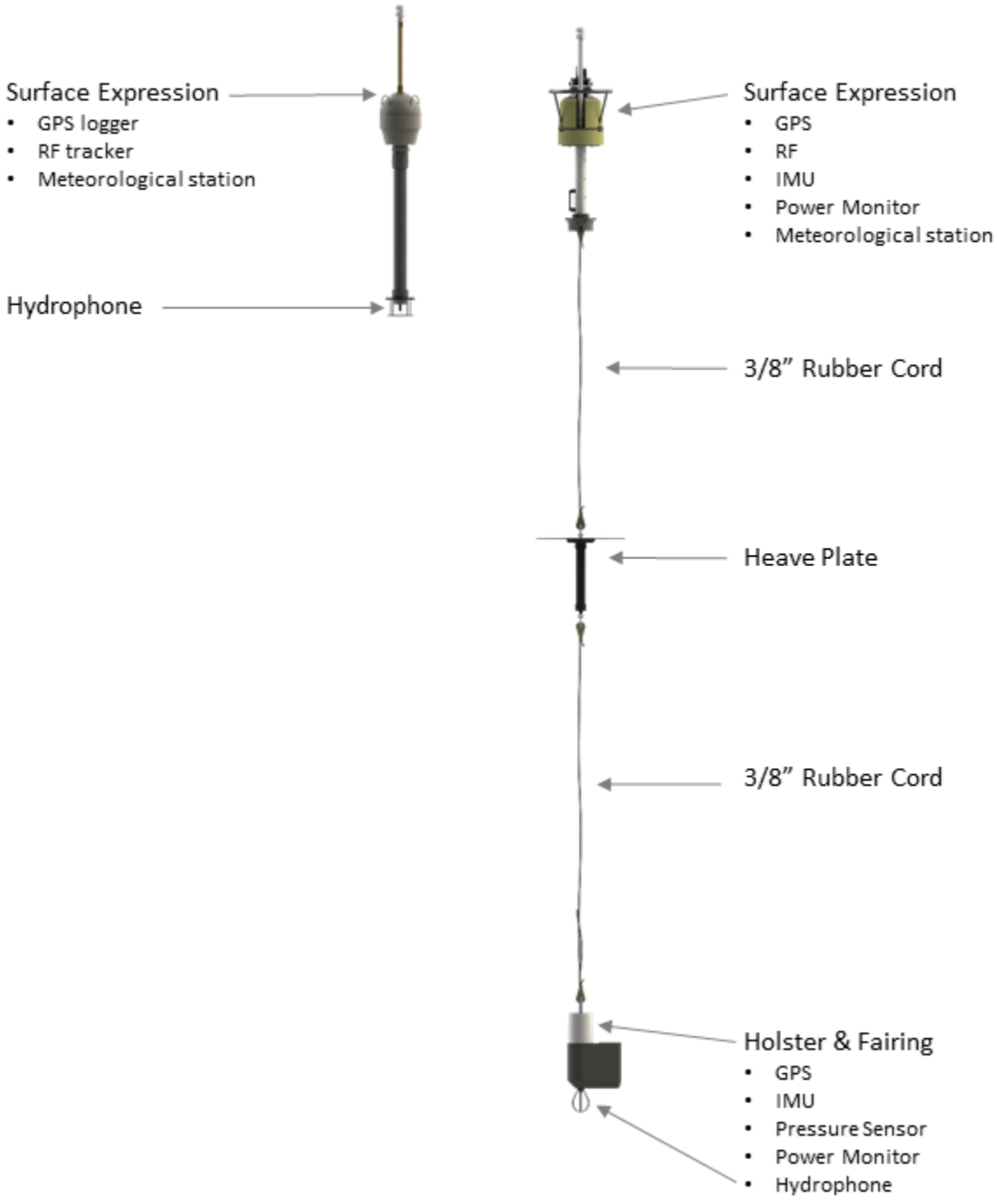

Figure 23: Rigid hull baseline and proposed DAISY

The proposed mechanical design shown in Figure 23 uses the suspension system demonstrated during Budget Period 1 to reduce the self-noise and flow-noise. The suspension system consists of compliant rubber cords with potted urethane connections and an inertial element (heave plate) for a W-DAISY. For the C-DAISY, this would be replaced with a drogue. As described in Section 2.4, the proposed DAISY electrical design should reduce mobilization and demobilization time by integrating all electronics and instruments into waterproof housings with bulkhead connectors for charging, a single external power switch to energize and initialize all systems, and wireless

communication to offload data and verify system health during field operations. The following sections describe mechanical design improvements to address remaining challenges with the rigid hull systems.

2.5.1 Surface Expression

The most important design change in the surface expression is the addition of a waterproof housing (Blue Robotics, Figure 24). The acrylic housing is sealed by two aluminum endcaps with bulkhead connectors for communications, recharging, and cabled instruments. The housing can remain sealed for deployments and only need to be removed from the surface expression for periodic maintenance. The housing is attached to the surface expression by the PVC collar placed on top of the housing and the twist latches. The housing can be easily removed without tools by twisting the latches and removing the PVC collar. The housing can then be lifted out of the surface expression without removing the closed cell foam that provides the primary buoyancy. Once removed, the housing can be unsealed by simply sliding the endcaps out of the acrylic tube. This improvement is expected to reduce mobilization and demobilization time by several hours per survey.

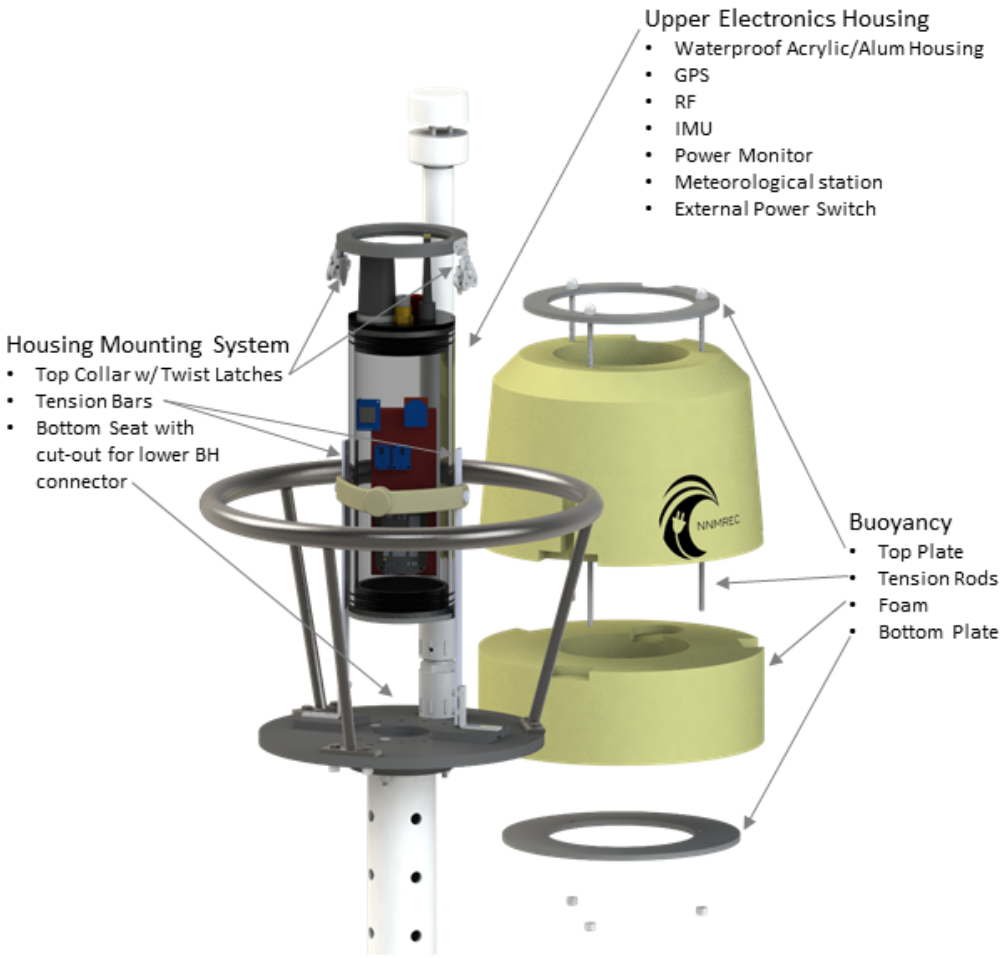

Figure 24: Exploded view of surface expression

The incorporation of the suspension systems to the C-DAISY and W-DAISY allows us to make further improvements to the surface expression. With the hydrophone decoupled from the surface

expression, the surface spar length can be reduced to maintain a righting moment without being awkward to deploy and recover.

During field tests in Admiralty Inlet (currents > 3 m/s) it was discovered that down-welling currents can generate enough force on the suspension system drogue to fully submerge a C-DAISY. This risk is mitigated by increasing the volume of closed cell foam on the surface expression.

Figure 25: Surface expression

To improve handling during deployment and recovery, the new DAISY design includes a 40 cm diameter circular grab bar and an oversized handle at the bottom of the spar (Figure 25). The grab bar is easier to snag by boat hook or hand than the relatively narrow U-bolts on the rigid hull. Switching to yellow buoyancy foam (previously dark grey) will also make it easier for recovery teams to spot the instrument. The hexagonal base at the bottom of the spar provides a flat edge on deck to prevent the surface expression from rolling during vessel operations, and the larger diameter spar

allows cables to be connected to the bottom of the electronics housing and hang down through the center of the spar[9].

All mounting systems that might need to be serviced in the field have been designed to operate with a minimum of tools. Changing the compliance cord only requires snipping the safety zip-tie and removing a wing nut, and the mast can be removed by snipping a safety zip-tie and unscrewing it from its base. For security in the field, threaded connections include (as appropriate) zip-ties, lock washers, and/or adhesives to prevent fasteners from backing out. Care has also been taken to ensure that all connection points are tightly fastened and reduced to the fewest degrees of freedom possible to reduce the potential for self-noise in the acoustic measurements.

To extend the lifespan of the DAISY and reduce the maintenance burden, drainage has been designed into all areas on the surface expression. Further, non-corroding PVC has been used wherever possible. Where metal is required for strength, stainless steel 304 or 316 has been chosen and the grade of the adjacent metal parts has been matched (i.e., all SS304 for the grab bar assembly, all SS316 for the tension rods and their fasteners) or galvanically isolated.

During major maintenance or breaking the system down for shipping, removing three nuts from the tension rods through the foam allows the rods and foam to be lifted away from the surface expression (Figure 24) making all fasteners and mounting hardware accessible. Once the buoyancy foam is removed, the spar can be separated from the base plate by removing three more bolts.

2.5.2 Suspension System

As discussed previously, the suspension system serves to isolate the hydrophone from motion of the surface expression and, in the case of the C-DAISY, more closely match the velocity of the surrounding water.

For compliant connection, EPDM rubber cord was chosen for its combination of strong resistance to environmental degradation by UV and saltwater and its modulus of elasticity that allows fast strain rates and up to 400-600% elongation before material failure (depending on cord diameter). Tension tests were performed to determine stress-strain curves for several different diameters of EPDM rubber cord. The suspension systems tested in the field had a maximum positive buoyance of approximately 220 N (50 pounds), and the rubber cord termination method was designed for a maximum elongation of 100% in the field. The results of the tension testing showed that these criteria were met by a 3/8” diameter EPDM rubber cord (220 N pounds generated 100% elongation). This diameter of rubber cord was used in all subsequent field tests and shown to perform well.

[9] The current design does not propose to have cables routed through the spar. However, there are at least two situations in which this would be desirable. The first would be a case where a real-time measurement of underwater noise is required. This could be communicated via the RF or wireless transmitters in the surface expression if a data cable connected the upper housing and lower housing. The second is for use of the DAISYs as a long-baseline positioning system for swarms of underwater floats. In this configuration, a power and data cable would connect to a transducer mounted at the base of the spar.

(a) As-built heave plate **(b) Deployed heave plate orientation**

Figure 26: Heave plate for W-DAISY

For wave-dominated conditions a flat, 0.6 m diameter circular heave plate was chosen as an inertial element. This shape was chosen because the simple geometry has high added mass and drag force from a small amount of material. Literature also describes the hydrodynamics of oscillating, circular heave plates, and manufacturing is simple and inexpensive. Initial simulations in ProteusDS (not shown) helped narrow the diameter range to between 0.5 m and 1.0 m for effective damping of holster relative velocity, the final diameter of 0.6 m was chosen for ease of handling in the field. As shown in field testing, this configuration successfully reduced flow-noise in wave environments. The circular heave plate did have a difficulty that was discovered early in field testing, specifically, a tendency to cut sideways or "leaf" as it falls through the water column. This was corrected by adding a ballasted spar to introduce a righting moment (Figure 26). The heave plate is relatively free from self-noise, as all fasteners are tightly fixed with no degrees of freedom to produce clanking or creaking sounds. The simple design and tough, corrosion-resistant materials of the heave plate and spar (PVC) make this component robust in the field and should ensure a long, low-maintenance lifespan. The simple connections between spar and heave plate (3 bolts) also allow easy disassembly for convenient shipping and storage.

For current-dominated conditions, an omnidirectional drogue (Pacific Gyre Microstar) was selected and appears suitable based on baseline tests. The drogue is designed to easily collapse for transport and storage.

The design for the DAISY suspension system includes a few features to help reduce self-noise. All mechanical connections that would be metal-to-metal (e.g., shackle to eyebolt) have one component of the connection potted in urethane material. Similarly, the thimble terminations for the rubber cord are potted in urethane (Figure 27). This prevents self-noise of the thimble against the shackle and also seals the rubber cord and thimble in a urethane block that ensures the rubber cord wrapped around the thimble will not stretch, rub or wear against the thimble surfaces, increasing the lifespan of the rubber cords.

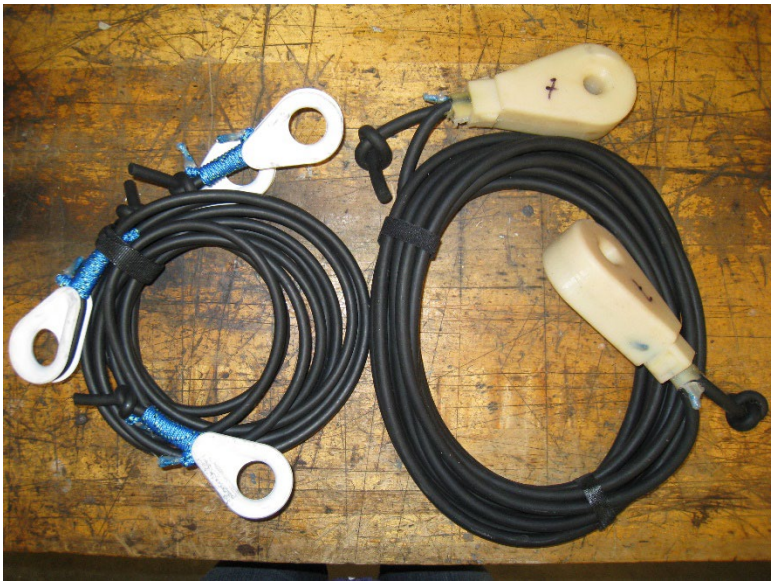

Figure 27: Rubber cords and termination – (left) prior to potting) (right) after potting terminations in urethane

2.5.3 Holster and Lower Housing

The primary purpose of the holster is to support the hydrophone and ancillary electronics. Prototype field testing of the W-DAISY and C-DAISY configurations used a simple PVC structure to mount the self-contained hydrophone, IMU, and pressure sensor (Figure 28a). The new DAISY holster design (Figure 28b) integrates the instruments into one package with single connection points for communications and charging. The housing, internal electronic systems, external power switch and twist-latch mounting system are duplicated from the surface expression. The batteries and a small amount of lead weight provide ballast at the bottom of the housing to provide slightly negative buoyancy and sufficient righting moment to keep the holster and hydrophone vertically aligned.

(a) Baseline C-DAISY and W-DAISY hydrophone holster (without fairing)

(b) Proposed C-DAISY hydrophone assembly with fairing and hydrophone guard

Figure 28: Hydrophone holster assemblies

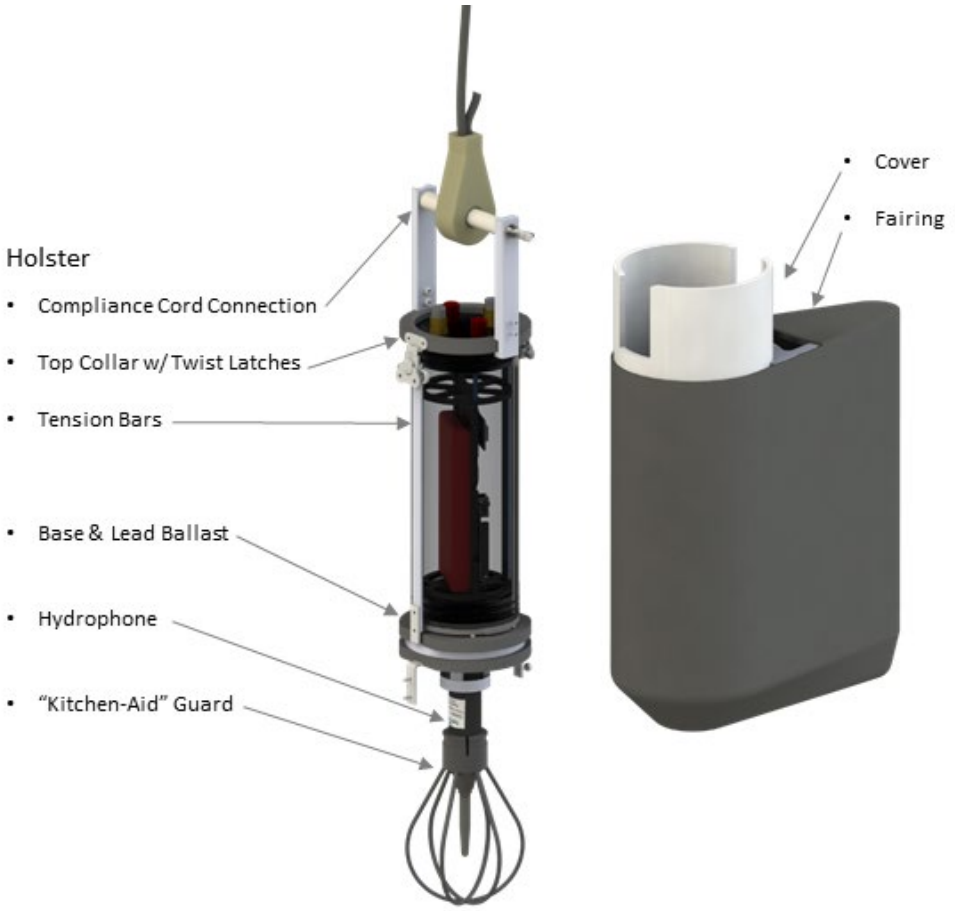

Figure 29: Exploded view of holster and lower housing

The connection point to the rubber cord (W-DAISY) or static line (C-DAISY) is designed to be simple and robust, while maintaining clearance for dummy plugs on the bulkhead connectors. The wingnut connection used on the surface expression is duplicated here to allow tool-free rubber cord swaps in the field. A robust cover created from 6 inch diameter PVC pipe is connected to the housing mounting system at four points to protect the acrylic housing and the bulkhead connection at the base of the hydrophone during deployments. The PVC cover also provides a mounting space for a neoprene fairing along the bottom edge of the cover. The neoprene fairing serves two purposes: reducing the drag coefficient of the holster and reducing the turbulent vortices that would be shed from the PVC cover's hard edges closest to the hydrophone.

Field testing at MCRL demonstrated an additional challenge related to the holster design. Self-noise was observed at MCRL for a C-DAISY configuration in which the holster was rigidly connected to the drogue. This highlighted a risk associated with rigid connections between the hydrophone and housing. A simple mitigation method to help reduce vibrations transmitted through the holster is to place soft rubber pads at connection points between components (e.g., rubber layer between housing endcaps and PVC mounting plates, rubber pads between metal L-bracket and PVC cover). It would be particularly important to ensure that a rubber layer is placed between the hydrophone body and the hard mounts that grip the body of the hydrophone. The hydrophone mounting system has been designed with an eye towards future-proofing – the mounts should be adaptable to either

the existing OceanSonics icListen HF or the smaller “Platform 4” design that would utilize the internal data storage and batteries in the DAISY electronics housing.

The final component in the holster design is a molded plastic guard to protect the hydrophones. This was designed using the rule of thumb that turbulent wakes produced by cylindrical objects typically dissipate at a distance of 10 diameters. The diameter of the rib is 0.5 cm, and the guard is separated from the hydrophone transducer by at least 5 cm. The guards can be cast from a high-durometer poly-urethane material that will provide necessary strength, while causing less acoustic scattering than metal and having no susceptibility to corrosion.

3 Budget Period 2 (Sep. 2017 – May 2020)

3.1 Overview

The primary objective of Budget Period (BP) 2 was to implement the design plans for BP 1, testing and iterating as required, to ready the DAISYs for an acoustic survey at the U.S. Navy's Wave Energy Test Site (WETS). Activity was structured around three tasks:

- Task 4: DAISY Improvement: Implementation of proposed hardware and software from BP 1.
- Task 5: Post-processing Software: Demonstrating localization of acoustic sources and an ability to automatically identify instances of flow-noise and self-noise in measurements.
- Task 6: Improved System Field Testing: Demonstrating hardware and software functionality through testing in waves and currents.

The tasks are presented out of sequence for interpretability since Task 5 (post processing software) relied on data from Task 6 (improved system field testing). Milestones and milestone status for each BP 2 task are summarized in Table 10.

A major change of direction, which occurred early in BP 2 and is discussed in Section 3.2.2, was the decision to replace the existing hydrophone recording package (icListen HF) with a lower cost hydrophone (HTI 99-UHF) and recording package developed by the project team. While initial implementation was relatively straightforward, multiple board revisions were required to achieve an acceptable noise floor and further revisions to the boards were required in BP 3 to eliminate remaining artifacts. Ultimately, this investment of time and resources benefited project outcomes by reducing the overall cost of the system and the potential degree of customization.

Table 10: Budget Period 2 Milestones

	Description	Status
Task 4: DAISY Improvement		
4.1	Complete fabrication of improved DAISY components.	Complete (hydrophone acquisition board requires revision to reduce electrical self-noise)
4.2	Characterize effect of hull configurations on hydrophone directivity and sensitivity at frequencies greater than 5 kHz.	Complete
4.3	Demonstrate deployment and offload software on bench.	Complete
Task 5: Post-processing Software		
5.1	Label data containing stereotypical WEC and CEC sound, flow-noise, and self-noise from prior DAISY deployments and baseline measurements.	Not completed (Not helpful for algorithm development due to significant differences in flow-noise and self-noise between baseline and improved DAISYs)
5.2	Label data containing acoustic source, flow-noise, and self-noise from field testing of DAISYs.	Complete (Labeling restricted to strum, which is only persistent form of self-noise)
5.3	Implement automatic self-noise and flow-noise identification and isolation.	Complete (Strum identification algorithm has true positive rate > 80%

		and false positive rate < 20%. Maximum flow-noise masking at f < 10 Hz.)
5.4	Implement localization algorithm and test using synthetic data.	Complete
5.5	Evaluate effectiveness of localization approach during improved system testing.	Complete (Effectiveness depends on array layout relative to source, multi-path interference, and signal-to-noise ratio)
Task 6: Improved System Field Testing		
6.1	Obtain necessary permits for field testing of improved system.	Complete
6.2	Conduct measurements in quiescent conditions with C-DAISYs and W-DAISYs.	Complete
6.3	Conduct measurements in currents using C-DAISYs	Complete
6.4	Conduct measurements in waves using W-DAISYs	Complete (Conditions in Clallam Bay not wave dominated.)
6.5	Demonstrate flow-noise reduction in acoustic spectra relative to baseline.	Complete (Flow-noise appears to be systematically eliminated to f < 10 Hz.)
6.6	Report on effectiveness of flow-noise mitigation and sources of self-noise in waves and currents.	Complete (Primary source of self-noise is line strum.)
6.7	Compare C-DAISY and W-DAISY performance to COTS system.	Complete (Comparison to OSU spar buoy, fixed shielded hydrophone, and fixed unshielded hydrophone.)

3.2 DAISY Improvement (Task 4)

DAISY improvements during BP 2 consisted of hardware modifications to the hull and suspension system, electronics modifications to integrate instrumentation and reduce hydrophone cost, and modifications to software to automate data offload.

The initial DAISY concepts (Figure 4) tested in Budget Period 1 provided evidence for improvements that could be made to the DAISY hardware. For example, the testing found that a longer compliant cord improved performance in wave conditions. However, testing also demonstrated that the drogue was difficult to handle on the deck of a ship and did not do enough to reduce flow-noise in high-current conditions. The time-consuming deployment preparation and offload process had many opportunities for improvement.

The improvements carried out during BP 2 resulted in the revised DAISY systems shown in Figure 30. The mass-spring-damper suspension systems were revised to improve their hydrodynamic performance, the surface expression was revised to support new electronics and the new suspension systems, and the lower housing was revised to protect the integrated electronics and hydrophone.

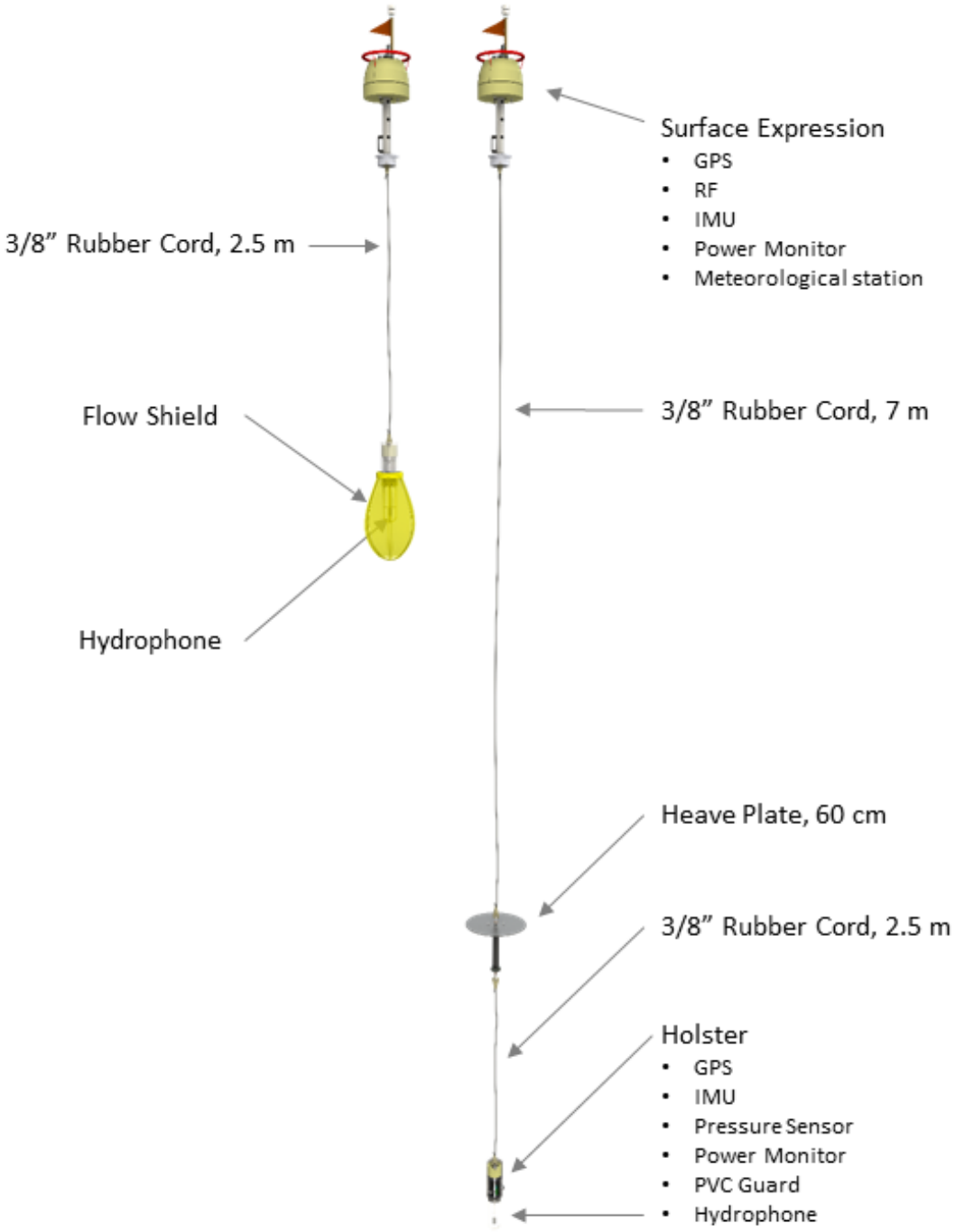

Figure 30: Revised system configurations tested in BP 2 (to scale)

3.2.1 Hardware Modifications

The redesigned Surface Expression (Figure 31) includes several improvements:

- Increased reserve buoyancy to minimize submergence risk identified during tests in Admiralty Inlet;
- Waterproof electronics housing with cabled weather-station and simple attachment hardware;
- Simplified connection hardware for suspension systems;
- Improved recovery hardware (i.e., grab bar, LED lights); and
- Easy disassembly and reassembly using minimal tools for shipping and inspection/maintenance.

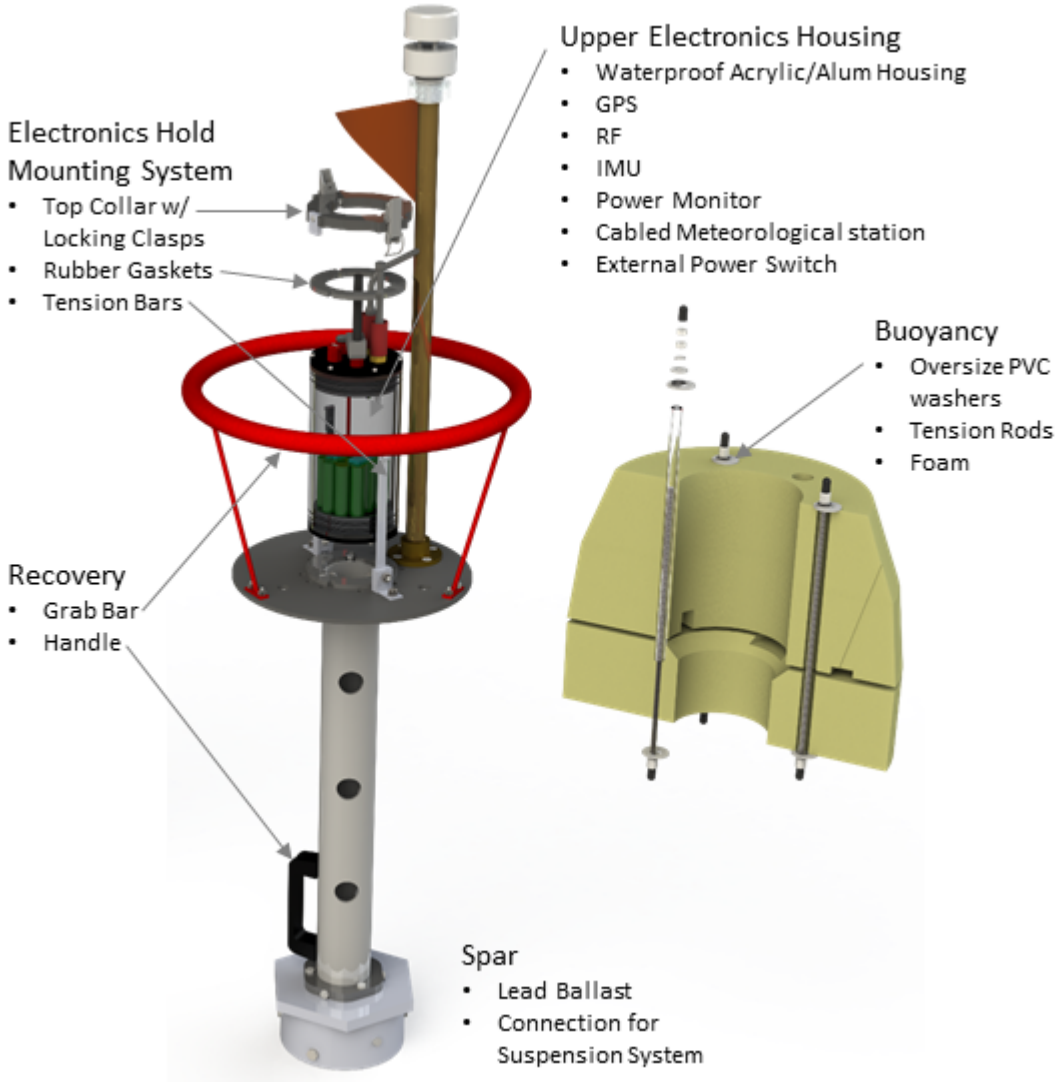

Figure 31: Surface expression components.

The surface expression's reserve buoyancy was increased from 80 N (18 lb) to 230 N (52 lb) by increasing the volume of buoyant foam. This brings the reserve buoyancy up to the operational limit

of the compliant cords in the suspension system and passively prevents overload of the cords that could sever the lower housing from the surface expression.

The improved electronics package with integrated instrumentation and a new waterproof housing was significantly larger and heavier than the rigid hull baseline system, moving the center of mass upwards in the surface expression. Additional lead ballast at the bottom of the spar was needed to achieve a desirable offset between the center of mass and buoyancy and, thereby, maintain a sufficient passive righting moment. The larger electronic housing also required a significant redesign of the attachment hardware, but the revised hardware allows the surface expression to be quickly assembled for deployment with minimal tools. During deployment, the electronics housing is quickly secured by a collar with locking clasps, the compliant cord is secured with a wingnut, and the only tool required is a pair of snippers to trim safety zip ties placed around the clasps and wingnut.

To further improve the ease of deployment and recovery, a large black plastic handle is included at the base of the spar and a 40 cm (16 in) red stainless-steel grab bar was fabricated and attached to the base plate of the surface expression. The red grab bar is much easier to snag with a boat hook than the small U-bolts used previously, reducing recovery time.

3.2.1.1 Lower Housing

The redesigned lower housing (Figure 32) includes:

- Protection for the new integrated electronics package and hydrophone;
- Improved passive stability by addition of buoyancy foam and lead ballast;
- Barely negative wet weight; and
- Simple hardware and easy assembly.

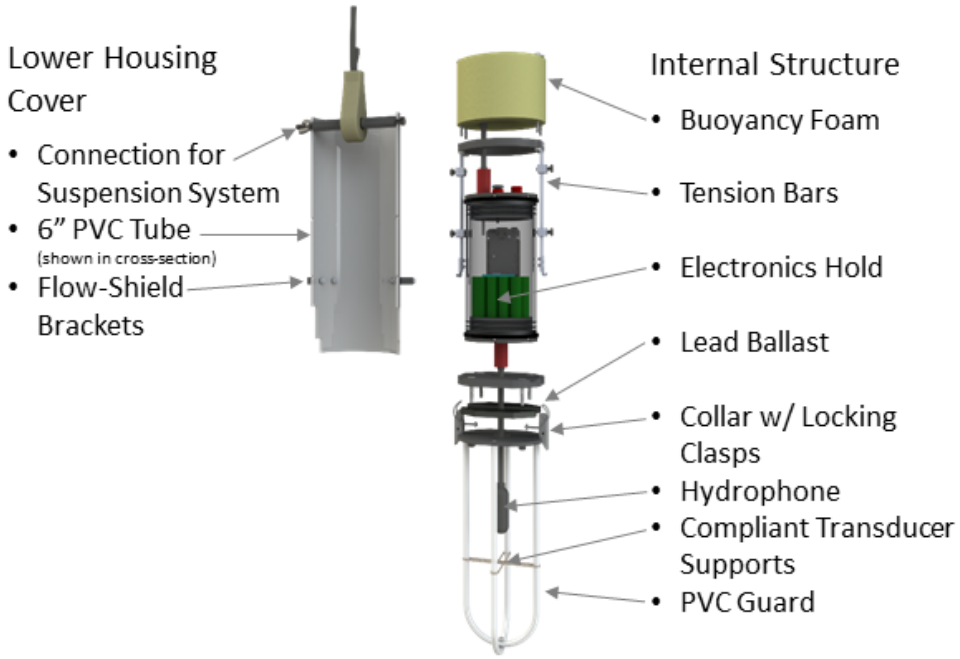

Figure 32: Lower housing components.

The lower housing required a completely new design, as the previous housing was designed to hold three independent data loggers (pressure, IMU, hydrophone) (Figure 28). The new lower housing uses the same integrated electronics and waterproof housing as the surface expression and the

waterproof housing is captured in the same method as the surface expression, with tension bars and a collar with locking clasps. The tension bar support frame is bolted inside a PVC tube to provide a simple protective cover for the electronics, and a PVC guard attaches to the collar to protect and support the transducer of the HTI-99-UHF hydrophone. The only tool required during deployment is zip tie clippers. The guard scatters directed sound at frequencies above 50 kHz, but is transparent to lower frequencies (Appendix 1).

The lower housing's passive stability and righting moment were improved with buoyancy foam (rated to 100 m) and lead ballast to maintain a vertical orientation and avoid inconsistent acoustic shadowing by the housing. The lower housing is ballasted to be barely negative, minimizing gravitational forcing on the lower housing which can lead to undesirable tilt as a consequence of the offset between the center of motion and tether attachment point.

3.2.1.2 Suspension System for W-DAISY

The W-DAISY suspension system for wave conditions (Figure 30b) was redesigned with one longer compliant cord (7 m from surface expression to heave plate) and reused the 2.5 m cord from heave plate to lower housing. This moved the lower housing to a depth of 12 m and the correspondingly reduced wave orbital motion around the hydrophone. Switching to the longer 7 m compliant cord also allowed large extensions of the rubber cord with minimal spring force as the surface expression followed the wave surface. This reduces forcing on and displacement of the heave plate. This decoupling of the lower housing from the surface expression movement reduces relative velocity between the lower housing and surrounding water, thereby reducing flow-noise. The system is analogous to the suspension system on sonobuoys used in anti-submarine warfare.

3.2.1.3 Suspension System for C-DAISY

The C-DAISY suspension system for current conditions was redesigned (Figure 30a) with a flow-shield instead of a drogue. The flow-shield provides similar drag properties to the drogue, but has additional flow-noise reduction benefits and couples the drag element directly with the hydrophone. For both drogue and flow-shield, the large cross-sectional area reduces flow-noise from relative velocity between the lower housing and the surrounding water by generating a large drag force acting on the combined flow-shield and lower housing, accelerating the housing until it is moving with approximately the same velocity as the surrounding water.

However, even with a high-drag element installed on the lower housing, the housing can develop a relative velocity due to forces transmitted by the tether. This can occur if the tether is sufficiently long, such that there is significant shear in the water currents in the vertical direction or if wind forcing on the surface expression is significant. If this occurs, the flow-shield surface area acts to average turbulent eddies over a large surface, causing flow-noise to roll off faster than it would for a bare hydrophone experiencing the same forcing. This is a significant benefit of the flow shield design over the drogue.

3.2.1.4 Flow-Shield Development

The flow-shield (Figure 33a) was an unexpectedly difficult mechanical element to develop. Flow shield testing in BP 1 used open cell foam to create a volume of quiescent water around the hydrophone, but this caused unacceptable distortion of the acoustic signal at higher frequencies.

The idea of a fabric flow shield came from conversations with Ben Wilson at the University of Highlands and Islands about "hooped" ocean drifters used to shield their Drifting Ears system. The ocean drifter is a fabric cylinder with hoop-shaped supports along the length. One challenge to this design was the formation of air bubbles on the fabric and hoops which caused acoustic scattering

and attenuation. This is the root cause of the problem with the open-cell foam flow shields that retained significant air, even after pre-treatment in a surfactant mixture.

The air bubble challenge was solved by using a specialty fabric, a polyester-spandex blend that is surface treated to make the outer layers hydrophilic. This fabric rapidly wicks fluid into the outer layers, dislodging even small air bubbles from the surface. The core layer of the fabric is hydrophobic, and prevents water from flowing through the fabric, forming a quiescent volume inside the flow shield. The small amount of spandex in the blend allows the material to flex and stretch under load, and it is a tough, durable ripstop material that prevents small tears and punctures from spreading. These qualities produce low attenuation of acoustic signals (Appendix 1) and durability during field use.

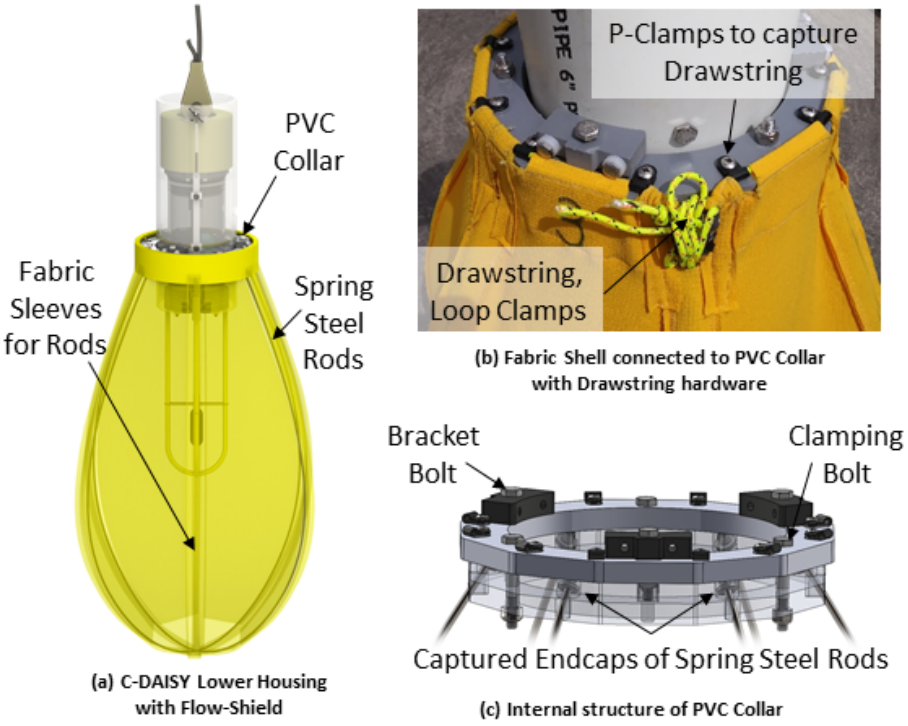

Figure 33: Flow-shield components.

Initial prototypes of the DAISY fabric flow shield used fiberglass rods to provide structure to the fabric shell and form an oblong shape that minimizes pockets of trapped air during deployment relative to a sphere. However, these fiberglass rods proved too delicate for field use and were prone to failure in fracture and/or delamination. Consequently, the fiberglass rod was replaced with a stainless steel 316 spring-tempered rod of diameter 0.162” (4.1 mm) and length 72” (1.8 m) that provided the necessary strength to survive the stress generated during deployment and recovery. The spring steel rods partially deform and provide slightly less spring force, but their performance has been satisfactory and they do not significantly distort propagating sound (Appendix 1).

Securing the fabric shell and spring rods to the lower housing was also unexpectedly challenging. In the final design, the fabric shell and spring steel rods are held in place at the top of the flow-shield in a collar made of three layers of PVC plate (Figure 33c). The spring steel rods have stops welded to both ends, and these are captured in a small cutout in the middle layer of PVC. The top and bottom

PVC layers sandwich the end-stops to prevent them from sliding out of the collar. Three bolts clamp the layers of PVC together.

The fabric shell is secured to the PVC collar with a drawstring that passes through the horizontal sleeve along the top of the fabric shell, then into a P-clamp on the top side of the collar (Figure 33b). The drawstring alternates threading through fabric sleeve and P-clamp around the entire top of the fabric shell. The drawstring is pulled tight so that the fabric shell is tight around the PVC collar, then the cord is secured with line clamps. Excess length of cord is bundled and tightly secured to one rod with zip ties to prevent self-noise.

To ensure the flow-shield is simple to work with in the field, the fabric shell and PVC collar can remain fully clamped and secure whether the flow-shield is installed on the lower housing or in storage. The flow-shield is quickly and easily connected to the lower housing by dropping three bolts through brackets on the lower housing into square nuts captured inside the PVC collar's middle layer.

3.2.2 Electronics Modifications

The electronics system underwent several modifications and revisions over BP 2. The initial prototype of the integrated electronics system, shown in Figure 34 and deployed in BP 1, used individual breakout boards and a complicated wiring harness. This system, while difficult to manage because of the wiring harness, showed that the concept of integrating the required sensors with a central microcomputer was possible, and would allow for a significant improvement in terms of usability and data collection when compared to the baseline system.

The initial goals of integrating all the sensor streams with a single microcomputer were:

- substantially reduce pre-deployment, deployment, and post-deployment complexity;
- reduce effect of clock drift between sensor streams by using a single system clock;
- increase timing accuracy using GPS with PPS based clock syncing; and
- reduce system cost.

The development of the integrated electronics system moved from the initial prototype to the second revision of the integrated printed circuit board system (both shown in Figure 34), each time improving upon the last design while adding features and functionality. The initial prototype only contained the minimum required sensors, required removing the battery to charge it, and still included a standalone hydrophone system (OceanSonics icListen HF) with an independent clock and battery. The prototype of the integrated printed circuit board system for the electronics added internal battery charging circuitry allowing charging via an external connection, removed the complicated wiring harness, and added an ethernet connection to the standalone hydrophone. This system had several design issues but showed that it would be feasible to reduce the size and complexity of the system by designing a custom printed circuit board solution. The prototype PCB system led to the first revision of the PCB system, shown in Figure 36.

One of the outcomes of the initial prototype PCB system was the decision to adjust the project scope to integrate a custom-built hydrophone data acquisition system into the electronics package. This decision was made in the interest of system cost (dominated by the icListen HF recording hydrophone), difficulty ensuring time-synced data, and greater ability to customize the overall system (e.g., begin data acquisition when the hydrophone reaches a specified depth). This change substantially extended the duration of BP 2 due to multiple revisions required to achieve acceptable performance for the new configuration.

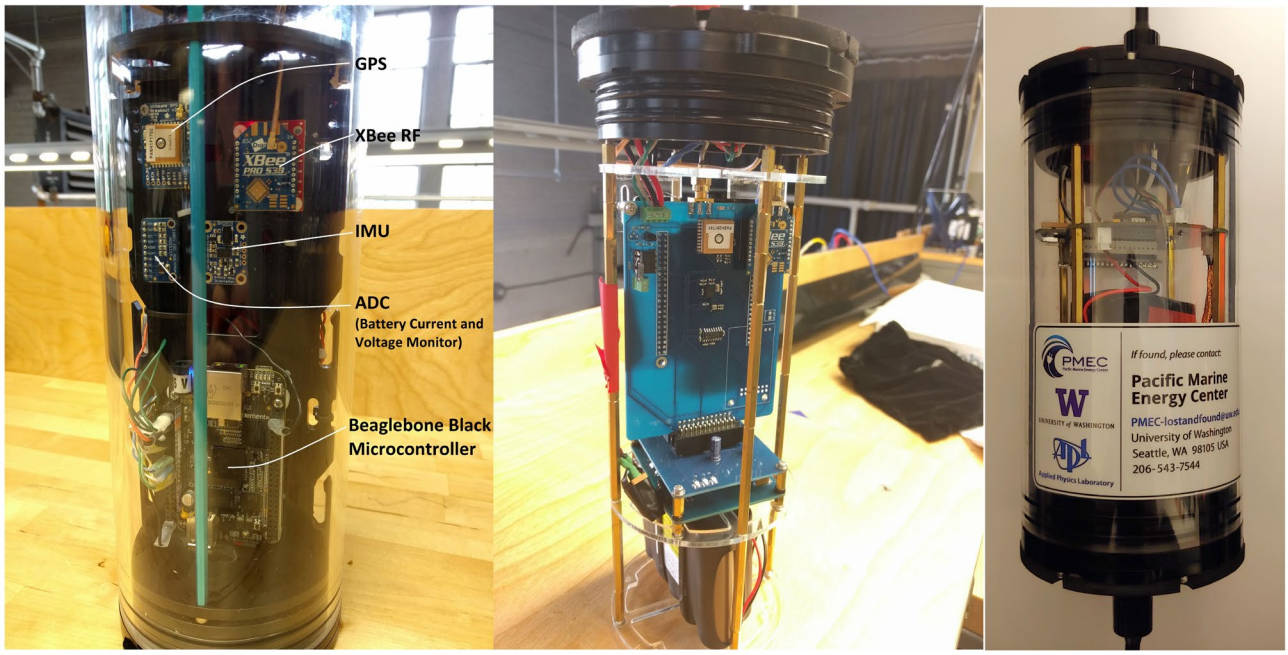

Figure 34: (left) Prototype electronics (2017), (center) prototype PCBs (2018), and (right) V2 electronics.

The first revision of the PCB system solved many of the problems with the prototype PCB design and substantially reduced the footprint and size of the electronics system. As can be seen in Figure 34, the length of the housing was reduced from approximated 12 inches to 9 inches. This size is still larger than necessary to house the required battery and electronics, but this preserves the option for additional batteries to extend system endurance and/or incorporate additional sensors in future use cases.

Most of the electronics development time between the prototype PCB and V2 electronics (Figure 37) was spent developing the integrated hydrophone data acquisition system. After development of the prototype PCBs for integrated control, we designed a small, test PCB as a prototype for an integrated, hydrophone data acquisition. This prototype was also used to assess the suitability of the Beaglebone Black microcomputer to handle the large amount of data generated by a 24-bit, 500k sample per second DAQ. Despite high-frequency electrical noise present on the prototype board, testing showed that the microcomputer could handle the data throughput from the hydrophone and the other sensors in the package. This success led to the decision to move forward with designing the integrated rev 1.0 PCBs (Figure 36).

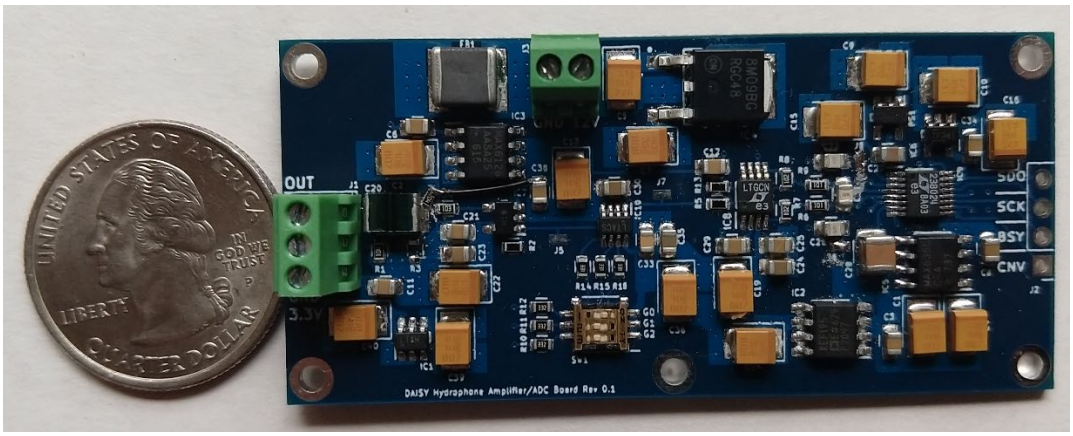

Figure 35: Prototype 24-bit, 500ksps hydrophone amplifier and ADC (quarter for scale).

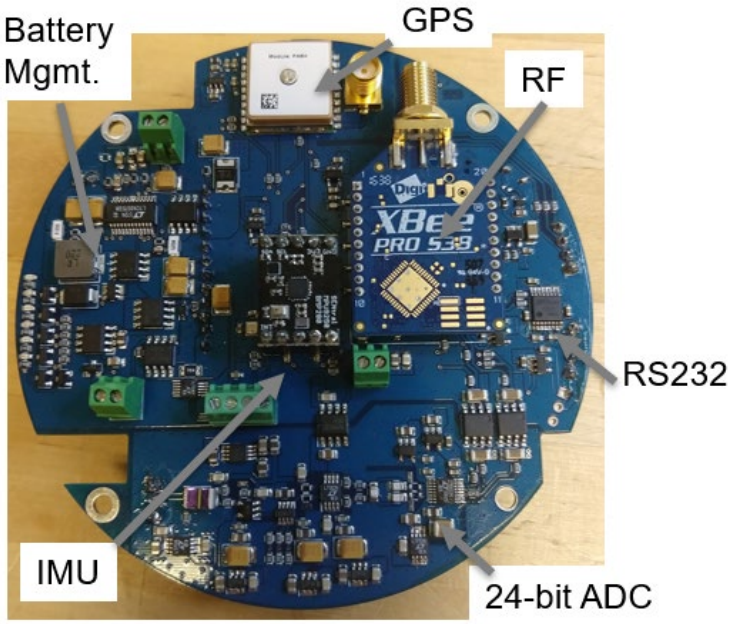

Figure 36: Rev. 1.0 of the DAISY electronics PCB, including first version of high-fidelity hydrophone DAQ (24-bit ADC).

The rev 1.0 PCB system was a large step forward in the DAISY electronics. The two main features of this design were the addition of the high-fidelity hydrophone data acquisition and a substantial reduction in the size of the PCB. The size reduction was the result of a newly released version of the Beaglebone Black microcomputer, called the “PocketBeagle”, that is less than half the size of the original Beaglebone Black while retaining nearly all the functionality of the standard version. This allowed us to reduce the size of the electronics housing by approximately 25%. While this PCB design saw significant improvements in terms of functionality and reduced noise in the hydrophone data acquisition system, the amplitude of high-frequency electronic noise present in the hydrophone data was unacceptable. In order to reduce the high-frequency noise, a second revision of the PCB was designed with some major changes to the hydrophone DAQ.

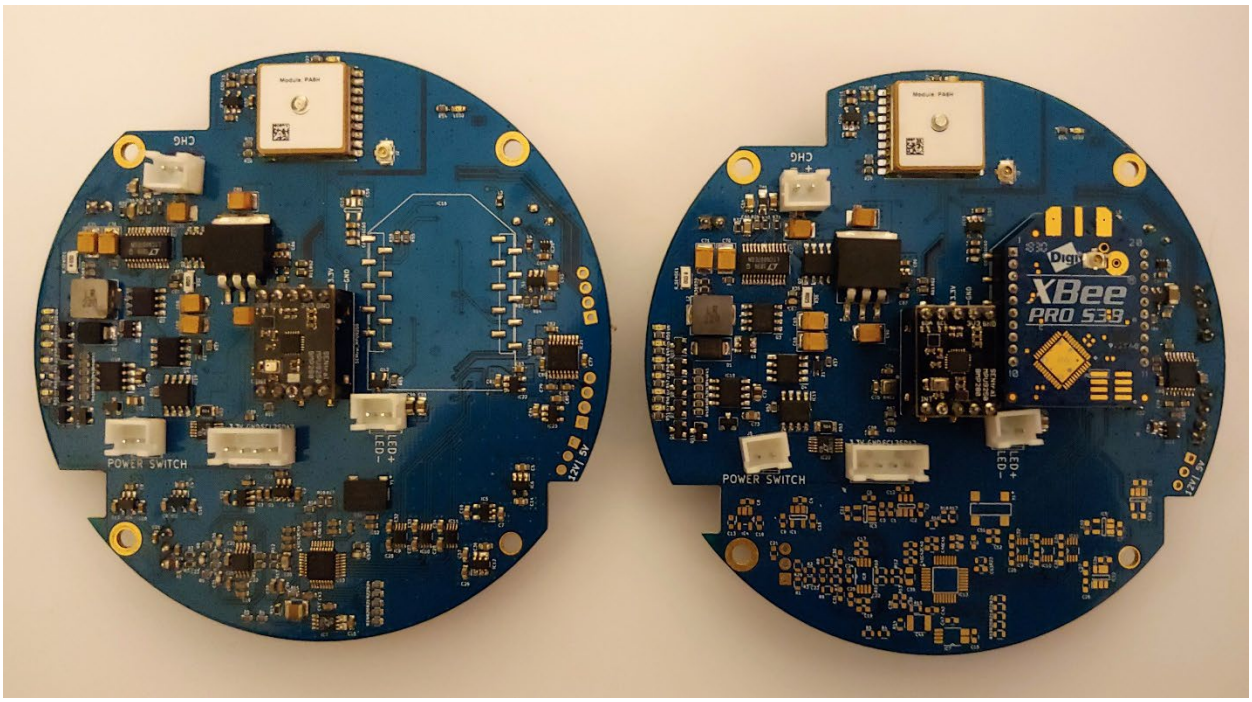

Figure 37: Rev 2.0 DAISY PCBs; lower PCB (left) upper PCB (right).

Rev 2.0 of the DAISY electronics PCB saw major updates to the hydrophone DAQ, including changing to a lower noise ADC and a different amplifier design. The new ADC includes additional features relative to the Rev. 1.0 ADC; such as a high over-sampling rate and integrated filtering, resulting in much lower noise compared to the Rev. 1.0 PCB design. The Rev. 2.0 design (Figure 37), like the Rev. 1.0 design, can be configured for either an upper electronics housing or a lower electronics housing.

While the Rev. 2.0 PCB design did substantially reduce the electrical noise present in the hydrophone data, it did not completely remove it. There are still high-frequency electrical artifacts present in the data that affect the fidelity of measurements, particularly at frequencies greater than approximately 10 kHz. Each iteration of the design thus far has resulted in substantially reduced electrical noise, so the team is confident the electrical noise and high-frequency spurs can be mitigated with another revision of the PCB design.

3.2.3 Software Modifications

For a DAISY deployment there are three separate software packages that are used: the onboard DAISY data acquisition and communication software, the Android tablet application software used for deployment management and tracking DAISYs in real-time (developed with support from PNNL), and the MATLAB based data offload/processing software used post-deployment.

The onboard DAISY data acquisition software contained a few bugs that impacted performance during testing at MCRL earlier in 2019, so time was spent to remove the code bugs and update the overall system software structure in order to improve the DAISYs' robustness and performance. The onboard system is run by a Debian Linux based microcomputer (PocketBeagle), and the default operating system kernel software contained some issues that affected the performance of the DAISYs, including:

- errors in the USB bus driver that would cause dropped data packets and high CPU load;

- errors in the inter-processor communication library that would cause missed interrupts (especially during times of high CPU load); and
- errors in the default Wi-Fi driver that pushed the USB bus to its limit making the first two issues worse.

The performance impact of these issues was not noticeable on the bench because the DAISYs were able to maintain a continuous Wi-Fi connection. It was only during testing in 2019, when the DAISYs would lose Wi-Fi connection, that the issues with the driver would begin to impact system performance. As soon as it was discovered that the Wi-Fi was the cause of the issues, work began to solve that problem, which led to the USB bus and inter-processor communications error being found and solved as well. Now, bench tests with the DAISYs, where the Wi-Fi gateway is intermittently turned off and on again, show good performance and no signs of the kernel or driver issues that were present previously.

Currently, the data offload and software allows a user to easily connect to and offload data from multiple DAISYs simultaneously without manually sorting through the data files on each DAISY. The improvements to the data acquisition software/drivers has also increased the Wi-Fi transfer rates of the DAISYs, so retrieval of the data takes less time than it did previously. Now, the DAISYs are capable of offloading data at an average rate of 5.5 MB/sec, whereas previously the offload rate averaged less than 2 MB/sec. This increase in Wi-Fi transmit speed makes offloading data over Wi-Fi acceptable (though still relatively slow), moving the DAISYs closer to the point of only needing to open the electronics housings for maintenance. The data offload GUI also contains features to request a status check from each DAISY connected to the network and to delete the log files currently stored on the DAISYs connected to the network.

The Android tablet deployment software is still in a pre-alpha state. There are issues with the device access permissions between the software and Android tablet operating system that would need to be overcome to ensure a robust and fully working application. On one hand, this interface could provide substantial benefit by allowing real-time updates in the field and replacing pen-and-paper logs with a time-stamped electronic record. On the other, on a boat pitching in rough seas, writing on a pad is difficult, but still easier than typing on a screen interface.

3.3 Improved System Field Testing (Task 6)

3.3.1 Test Overview

In BP 2, DAISYs were tested in three locations on the Olympic Peninsula in Washington:

- the interior of Sequim Bay – a representative “quiescent” environment with limited wave or current forcing (C-DAISY and W-DAISY).
- the entrance channel to Sequim Bay – a representative “energetic” current environment with peak velocities approaching 1.5 m/s and limited wave forcing (C-DAISY only); and
- the Straits of Juan de Fuca adjacent to Clallam Bay – a representative “energetic” wave environment (W-DAISY only).

The purpose of testing in a quiescent location was to benchmark the performance of the DAISYs in relatively still water to identify sources of self-noise and inter-unit variability. Energetic locations were intended to represent environments around current turbines and wave energy converters. In all three locations, tests consisted of consistency checks across the three prototype DAISYs and localization trials for acoustic sources (icTalk LF, icTalk HF, and vessel) using DAISY arrays.

Acoustic data were primarily processed per the guidance in IEC 62600-40 (IEC 2019) by separating the measured acoustic time series into sequences 1 s in duration overlapped by 50 % and tapered by a Hann window. Each of these sequences was detrended, then processed by a Discrete Fourier Transform with a variance-preserving correction, yielding an estimate for mean-square voltage spectral density level with a 1 Hz bandwidth. A frequency-dependent calibration consisting of hydrophone manufacturer specification for $f > 750$ Hz and an Ocean Networks Canada calibration for lower frequencies (down to 0.1 Hz) was applied to yield a mean-square sound pressure spectral density level (PSD) in dB re $1\mu Pa^2/Hz$.

To evaluate the time-evolution of higher frequencies acoustic data were also processed using a 0.1 s sequence window, yielding a frequency resolution of 10 Hz at a comparably reduced time interval. This is helpful to visualize the evolution of higher-frequency sounds over relatively short time scales. Similarly, to evaluate the evolution of low-frequency ($f < 30$ Hz) sound over longer time scales, 10 s sequence windows, yielding a frequency resolution of 0.1 Hz were employed in a limited manner. When evaluating statistics of low-frequency sound (e.g., flow-noise, mechanical self-noise), 10x 1-second PSDs were averaged in pressure-squared space to increase the statistical confidence in the realization.

To evaluate the quality of data, two types of QA/QC check were employed. First, metadata from ancillary sensors were reviewed to ensure that GPS positions were accurate (e.g., comparing GPS estimates from the primary receiver to a receiver on the met station) that the hydrophone had reached a steady-state depth, and that no unexpectedly high vibrations were occurring on the lower housing. Second, acoustic data were reviewed using a tool that allowed us to listen to a playback of recordings while visualizing the acoustic spectra. This was helpful to identify sources of self-noise, verify the signal-to-noise ratio of sources in localization studies, and identify conditions during which ambient noise from other anthropogenic sources (e.g., vessel traffic) were significant. During testing, we did not encounter any operational limitations due to battery capacity or on-board storage.

Overall DAISY performance was acceptable, particularly for prototype systems. We encountered no mechanical or electrical failures over four days of testing. Notably, while earlier versions of the flow shield had been able to substantially reduce flow-noise, durability had been poor and these tests demonstrated that the current build overcomes this limitation. Testing did reveal several new software bugs (e.g., time stamping of some log files, processor “lock-up” due to Wi-Fi reconnect frequency), all of which have been subsequently resolved. A key improvement was the straightforward deployment and recovery, requiring less than a minute for a crew of two to get each system over the side and back aboard.

3.3.2 Quiescent Testing

We conducted quiescent inter-comparisons of three W-DAISY (compliant cord, heave plate) and C-DAISY (compliant cord, flow-shield) configurations. During these trials, the DAISYs were approximately co-located. Figure 38 shows the W-DAISY inter-comparison periodograms and Table 11 shows the associated metadata. Close agreement is seen between all three units for frequencies > 10 Hz, with a common peak associated with propagating sound around 215 Hz and high frequency tonal noise above 10 kHz[10]. This is indicative of low inter-unit variability.

[10] The significance of these peaks is exaggerated by the logarithmic scale and progressive frequency averaging. In a linear periodograms without any smoothing, these are isolated, narrowband artifacts. They are electrical self-noise.

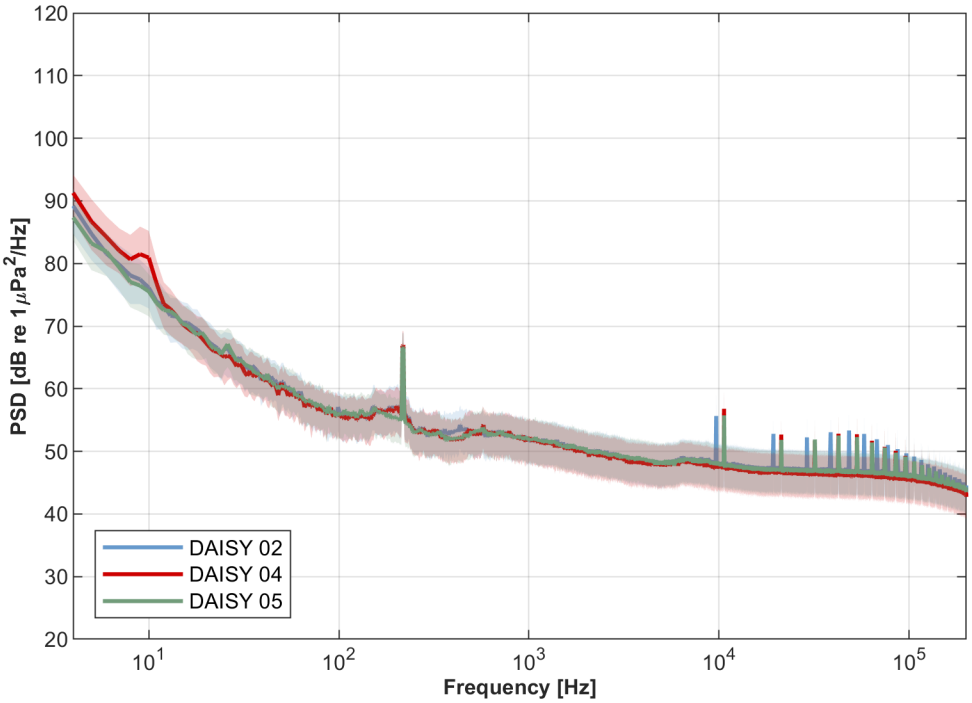

Figure 38: W-DAISY inter-comparison in quiescent conditions.

Table 11: Metadata for quiescent testing of W-DAISY configuration.

Drift	DAISY	Location	SOG [m/s]	Wind Speed [m/s]	Depth [m]
147	02	Sequim Bay	0.13 ± 0.2	4.8 ± 1.1	11.4 ± 0.01
148	04	Sequim Bay	0.15 ± 0.3	3.9 ± 1.1	11.5 ± 0.01
149	05	Sequim Bay	0.2 ± 0.2	4.9 ± 1.4	11.5 ± 0.01

Figure 39 shows a similar quiescent comparison for the C-DAISY configuration, with associated metadata in Table 12. As for the W-DAISY builds, inter-unit variability is low for frequencies > 10 Hz. At lower frequencies, elevated received levels for two of the DAISYs are a consequence of line strum (Section 3.3.6.2). Received levels are generally higher than during the W-DAISY test due to the approach of a vessel.

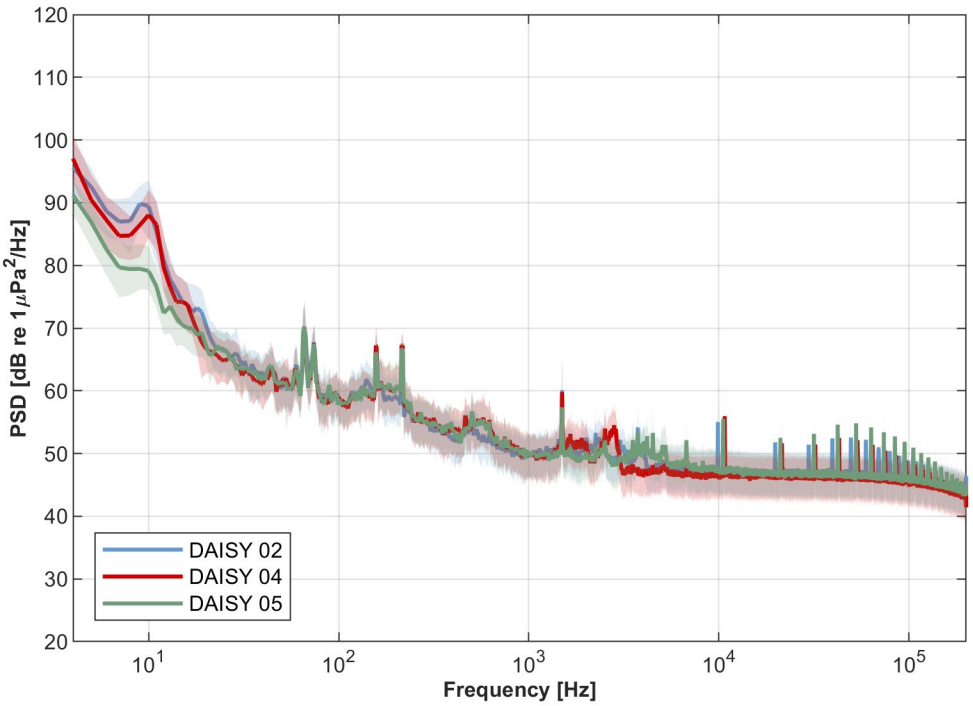

Figure 39: C-DAISY inter-comparison in quiescent conditions.

Table 12: Metadata for quiescent testing of C-DAISY configuration.

Drift	DAISY	Location	SOG [m/s]	Wind Speed [m/s]	Depth [m]
186	02	Sequim Bay	0.08 ± 0.02	-	3.3 ± 0.01
187	04	Sequim Bay	0.09 ± 0.02	3.5 ± 0.76	3.32 ± 0.01
188	05	Sequim Bay	0.07 ± 0.02	3.7 ± 1	3.43 ± 0.01

3.3.3 Testing in Currents

Figure 40 shows the inter-comparison of C-DAISYs drifting in close formation in the Sequim Bay channel with associated metadata given in Table 13. At frequencies > 10 Hz, as for the quiescent inter-comparison, agreement between DAISYs was excellent, generally within 1-2 dB between units. At lower frequencies, there is a deviation between units centered on a peak with a frequency of ~10 Hz attributable to line strum (Section 3.3.6.2).

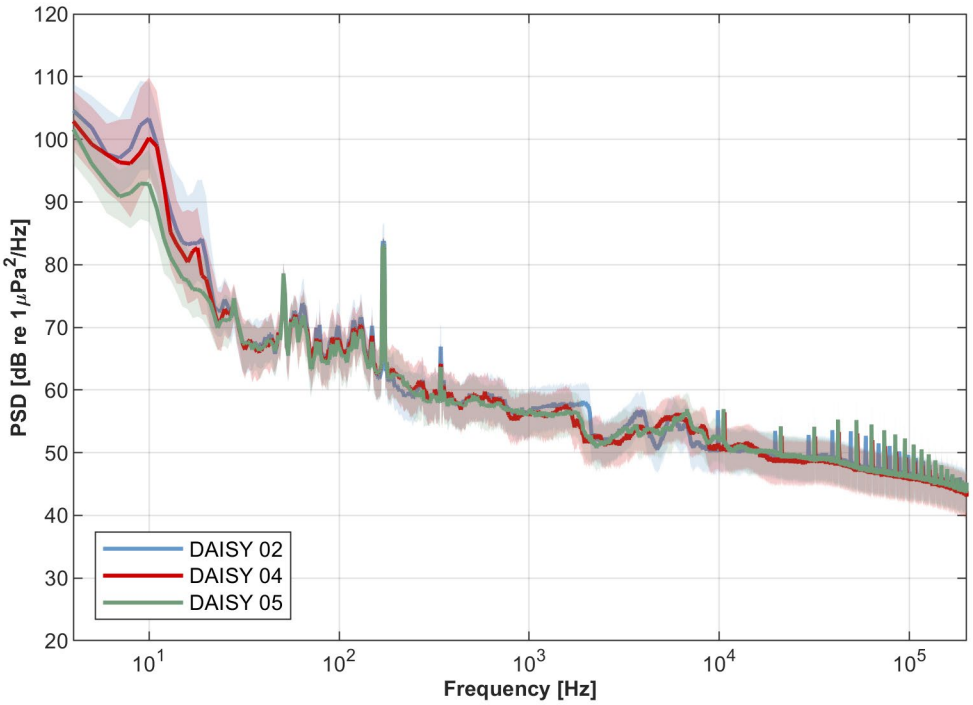

Figure 40: C-DAISY inter-comparison in Sequim Bay channel.

Table 13: Metadata for C-DAISY inter-comparison test.

Drift	DAISY	Location	SOG [m/s]	Wind Speed [m/s]	Depth [m]
171	02	Channel	0.89 ± 0.1	4.1 ± 0.6	3.29 ± 0.04
172	04	Channel	0.86 ± 0.2	3 ± 0.5	3.26 ± 0.07
173	05	Channel	0.86 ± 0.1	3.2 ± 0.6	3.36 ± 0.04

Our intention had been to ground truth performance in currents by a simple comparison between measurements in the channel and in the quiescent region at the interior of Sequim Bay. However, this proved ineffective because of temporal and spatial variations in propagating sound and fluctuations in low-frequency self-noise and flow-noise. Specifically, in some cases, low-frequency measurements were lower amplitude in the channel with a relatively high speed over ground than they were in the quiescent bay. Based on the analysis presented in Section 3.3.6.2, we now understand this difference to be a consequence of variable wind forcing on the surface expression.

3.3.4 Testing in Waves

Figure 41 shows the comparison between W-DAISYs in Clallam Bay with associated metadata in Table 14. The purpose of testing in Clallam Bay was to access a more energetic wave field than adjacent to Sequim Bay. While moderate waves were forecast for the area during testing, they did not materialize and, in retrospect, Clallam Bay appears to be on the eastern end of the forecast zone for Neah Bay, such that the forecast was likely accurate closer to the western ends of the Strait of Juan de Fuca. Because wind speeds were relatively high and currents were significant, this is better considered a "hybrid" forcing case than testing in waves. Measurements using prototype

DAISYs at WETS (separate funding) have demonstrated the system's ability to acquire reliable data in significant wave heights > 2 m.

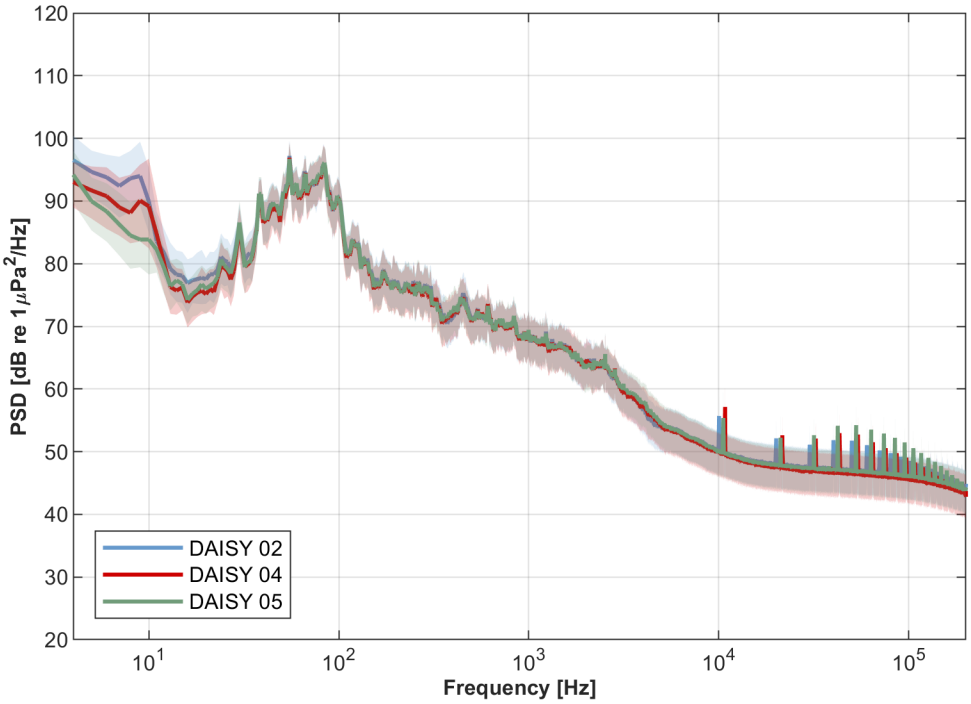

Figure 41: W-DAISY inter-comparison in Clallam Bay.

Table 14: Metadata for W-DAISY inter-comparison test.

Drift	DAISY	Location	SOG [m/s]	Wind Speed [m/s]	Depth [m]
1	02	Clallam Bay	0.43 ± 0.2	7 ± 1.0	11.6 ± 0.05
2	04	Clallam Bay	0.43 ± 0.2	6.4 ± 0.9	11.4 ± 0.05
3	05	Clallam Bay	0.43 ± 0.2	6.1 ± 1.4	11.7 ± 0.06

3.3.5 DAISY Performance Benchmarks

DAISY performance was benchmarked against three other measurement platforms:

1. A spar buoy developed by Oregon State University (OSU) that is optimized for measurements in waves. A comparison was made in quiescent conditions in Sequim Bay and "hybrid" conditions in Clallam Bay.
2. An unshielded hydrophone on the Adaptable Monitoring Package (AMP) deployed in the Sequim Bay entrance channel.
3. A shielded hydrophone on the Integral Consulting NoiseSpotter platform deployed in the Sequim Bay entrance channel.

3.3.5.1 Comparisons with OSU Spay Buoy

During testing in Clallam Bay, a cargo vessel passed abeam of the hydrophones at a range of 1-2 km. For these comparisons, the W-DAISY configuration was used and the hydrophone suspension system at the base of the OSU spar buoy was adjusted to drift at approximately equal depth to the

DAISYs. Considering the comparisons between the spectra in Figure 42, there are three distinct regions:

- From 20 Hz to 5 kHz, there is near-perfect agreement in received levels between the three DAISYs and the OSU spar buoy. This is an excellent result, as these are the frequencies of greatest interest for marine energy monitoring.
- Below 20 Hz, the DAISY received levels exceed the OSU spar buoy by ~20 dB, with some variation between DAISYs. There are likely at least two factors in play. First, the differential forcing between the wind and tidal currents likely produced more flow-noise on the DAISYs than the OSU spar buoy. This is because the spar buoy's larger cross-section in the water column produces more drag from the currents, reducing the contribution from wind on buoy motion. Second, OSU has not had their hydrophone calibrated at the lowest frequencies and is relying on the manufacturer specification for sensitivity. The DAISY hydrophones have been calibrated at low frequencies by Ocean Networks Canada and a substantial roll-off in sensitivity at the lowest frequencies is present and accounted for in the DAISY results. We emphasize that accurate measurements at these frequencies is difficult and of less importance than the higher frequencies where good agreement is observed.
- Above 5 kHz, the DAISY received levels are also elevated relative to the OSU spar buoy. Here, a combination of two factors is likely in play. First, the DAISY analog-to-digital conversion noise is significant at these frequencies (notably at the tonal peaks), such that the deviation could be entirely explained as ambient noise dropping below the DAISY noise floor. Second, neither the DAISY nor the OSU hydrophones have been calibrated at these frequencies and we are both relying on manufacturer specifications. Above 5 kHz, OSU substantially increases its pre-amplifier gains, which may be exacerbating underlying deviations between actual and manufacturer-specified sensitivity at these frequencies.

In contrast, as shown in Figure 43, for the comparison in Sequim Bay there are disagreements of at least a few dB at all frequencies, with the worst disagreement at the highest and lowest frequencies observed. DAISY electrical self-noise likely explains the deviations at higher frequencies (Section 3.3.6.1), the disagreement in mid-range frequencies could be a matter of depth (the OSU spar buoy hydrophone was at a depth of 6 m vs 12 m for the DAISYs), and the low frequency disagreement is likely an artifact of line strum (Section 3.3.6.2) and of the manufacturer sensitivity used by OSU, as the disagreement widens with decreasing frequency. As discussed in Section 3.3.8, the lowest frequencies are below the propagation cut-off frequency in Sequim Bay, such that differences in measurement depth may also play a role.

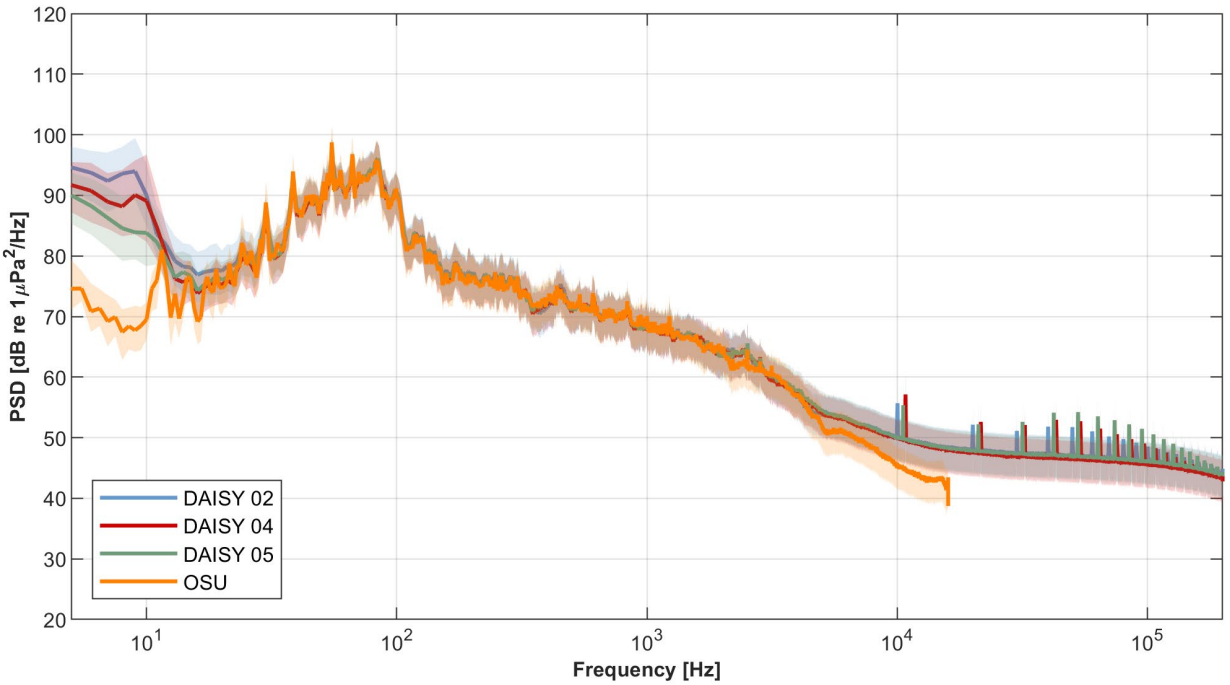

Figure 42: Comparison to OSU spar buoy in Clallam Bay, WA.

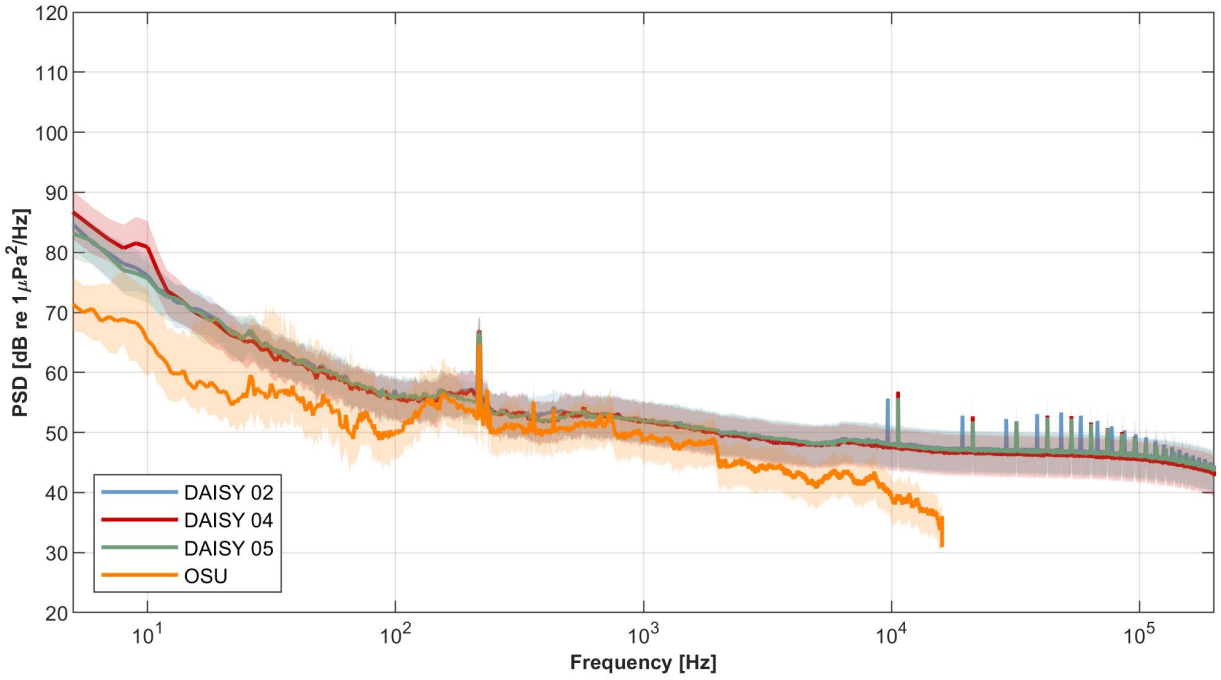

Figure 43: Comparison to OSU spar buoy in Sequim Bay, WA.

3.3.5.2 Comparison with Fixed Hydrophones in Sequim Bay Entrance Channel

Figure 44 shows an approximately co-temporal/co-spatial (20 m time offset) comparison between a DAISY and a fixed, unshielded hydrophone on the AMP (icListen HF). Flow-noise masking is apparent in the frequency range shown (4 – 500 Hz) and exceeds ambient noise by up to 50 dB. Further, we note that, while the gap between these measurements seems to narrow at lower

frequencies, this is an artifact of the lack of a low-frequency calibration for the AMP icListen. The true AMP hydrophone spectrum is likely a constantly increasing linear slope.

Figure 45 shows a similar comparison with a DAISY and a fixed, shielded hydrophone on the Integral Consulting Noise Spotter platform (icListen HF). The flow-shield on the fixed hydrophone reduces, but does not eliminate flow-noise, with deviations of up to 40 dB due to flow-noise and shield self-noise. The frequencies affected by flow-noise are, however, substantially reduced – from a maximum of 500 Hz for the unshielded hydrophone to 300 Hz for the shielded hydrophone.

While the low-frequency DAISY measurements do contain some flow-noise and self-noise, the drifting flow-shield does substantially mitigate the flow-noise that would mask propagating sound for shielded or unshielded hydrophones.

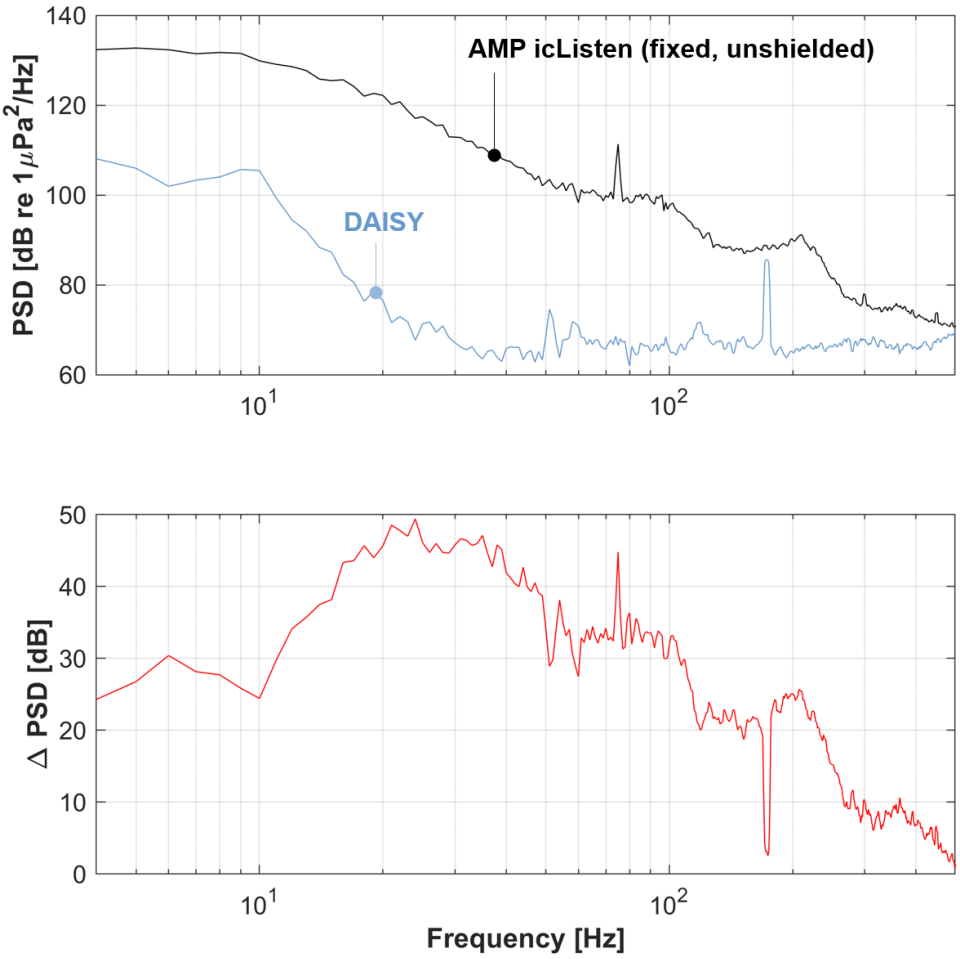

Figure 44: Comparison between DAISY and fixed, unshielded hydrophone (icListen on AMP). (upper panel) Mean-square sound pressure spectral density level (PSD) for each receiver. (bottom panel) Difference in PSD between receivers.

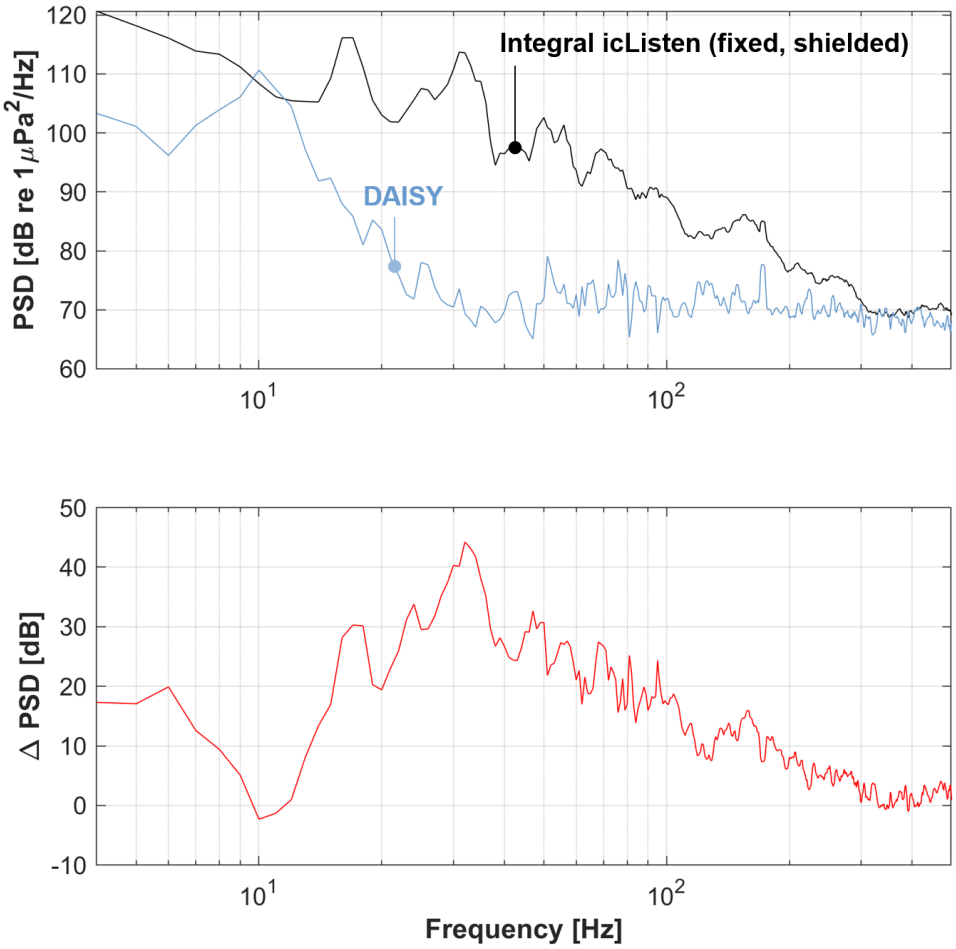

Figure 45: Comparison between DAISY and fixed, shielded hydrophone (icListen on Integral Consulting Noise Spotter). (upper panel) Mean-square sound pressure spectral density level (PSD) for each receiver. (bottom panel) Difference in PSD between receivers.

3.3.6 Sources of Self-Noise

Based on DAISY testing at MCRL, there are two persistent sources of self-noise common across all DAISY variants and test conditions, with other intermittently occurring self-noise specific to the C-DAISY variant. The persistent sources are shown in Figure 46. At $f < 1000$ Hz (top panel), for this drift, the dominant source of low-frequency self-noise is strum at $f < 30$ Hz, with flow-noise affecting $f < 10$ Hz. These low-frequency, high-amplitude sounds drive the time-variation in the broadband sound pressure level (bottom panel). Because these low-frequency sounds are of limited biological significance and low-frequency measurements are difficult obtain with high fidelity, broadband sound pressure levels are often reported with a low-frequency limit of at least several Hz. At higher frequencies (middle panel), ambient noise is relative homogenous, but we see persistent, tonal self-noise from electrical sources starting around 10 kHz and recurring at 10 kHz intervals.

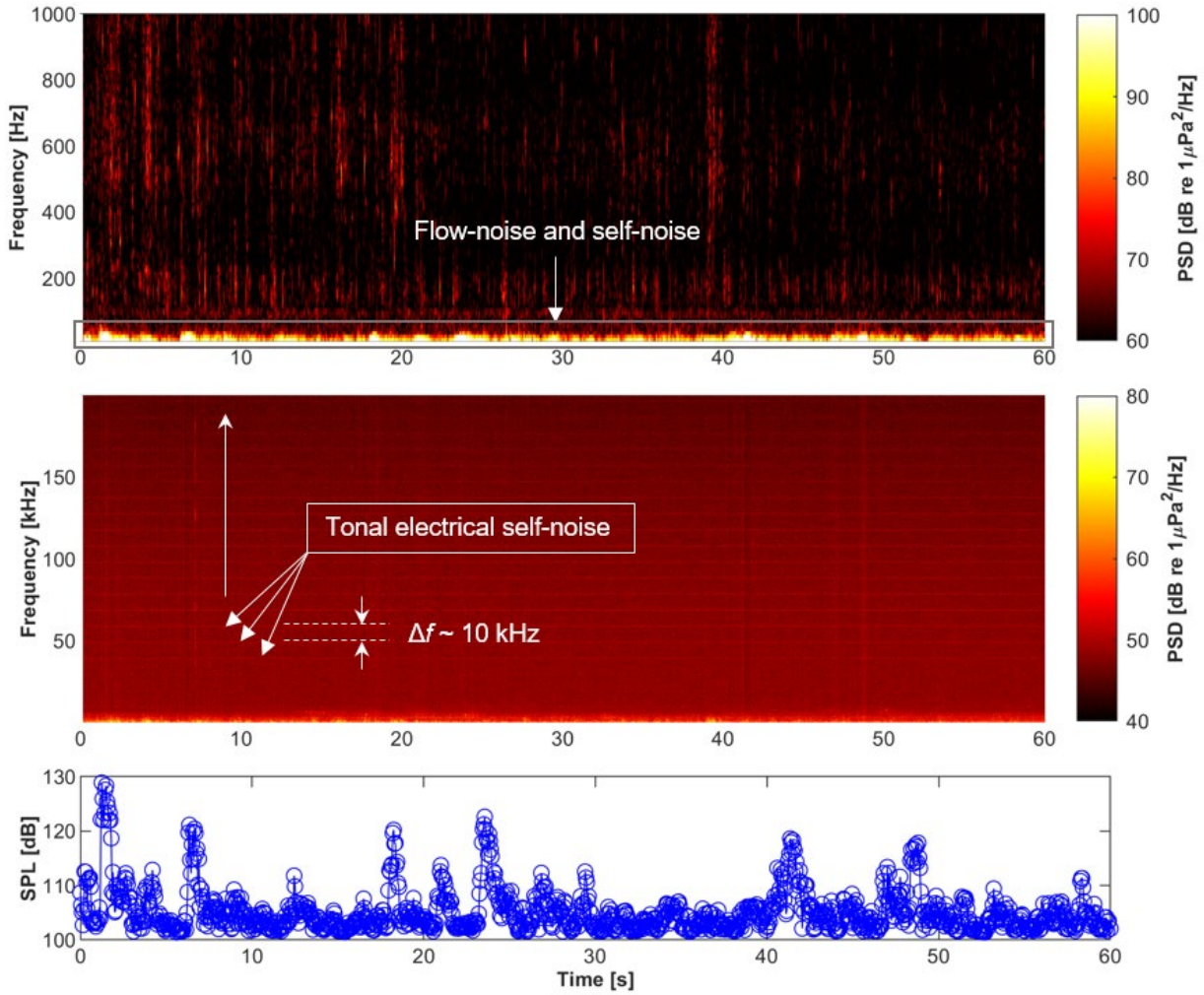

Figure 46: Representative time series from a C-DAISY drift in the Sequim Bay entrance channel annotated to emphasize persistent self-noise. (top) *f* < 1 kHz (1000 Hz) to emphasize low-frequency sound. (middle) *f* < 200 kHz to emphasize high-frequency sound. (bottom) broadband (1-200 kHz) sound pressure level.

To evaluate the significance of self-noise and the most appropriate approach to mitigating it, we consider three questions:

1. *Does self-noise substantially bias the results of measurements?* This depends on the amplitude of self-noise relative to propagating sound and the persistence of self-noise. Persistence is critical because IEC 62600-40 emphasizes median statistics, which are unaffected by outliers. This choice was made to intentionally focus on sounds that are commonly produced by marine energy converters, rather than infrequent acoustic emissions.
2. *Can the source of self-noise be addressed through a mechanical or electrical modification to the DAISY?* This is the most attractive approach to mitigating self-noise as it removes the contamination at its source.
3. *Can this source of self-noise be addressed through post-processing software?* This is a low-cost mitigation measure, as it is implemented in software, but if self-noise is persistent,

identification in post-processing simply establishes the frequencies masked by its presence. This mitigation measure does not allow propagating sound at such frequencies to be determined.

3.3.6.1 Electrical Noise

To evaluate the root cause for the tonal peaks in Figure 46, we tested the three data acquisition on the DAISYs built for this project and two others built for University of Hawai'i in three ways:

- in air, with the hydrophones muffled by foam;
- in a tank filled with water; and
- in a tank filled with water with the hydrophones disconnected.

Representative results for one DAISY are given in Figure 47. Two features are notable. First, with the hydrophone disconnected from the bulkhead on the housing, the electronic noise is substantially lower. This suggests that the electronic noise is not fundamental to the data acquisition chain, but rather originating from the HTI hydrophone. Based on diagnostics to date, we believe that the most likely source of this noise are the linear voltage regulators in the DAISY electronics used to power the hydrophone signal amplifiers. This could be adjusted through further revisions to the electronics boards. Second, evaluating the self-noise floor in water is preferred to evaluation in air, as the in-water data is similar to the in-water data, but with more noise at lower frequencies.

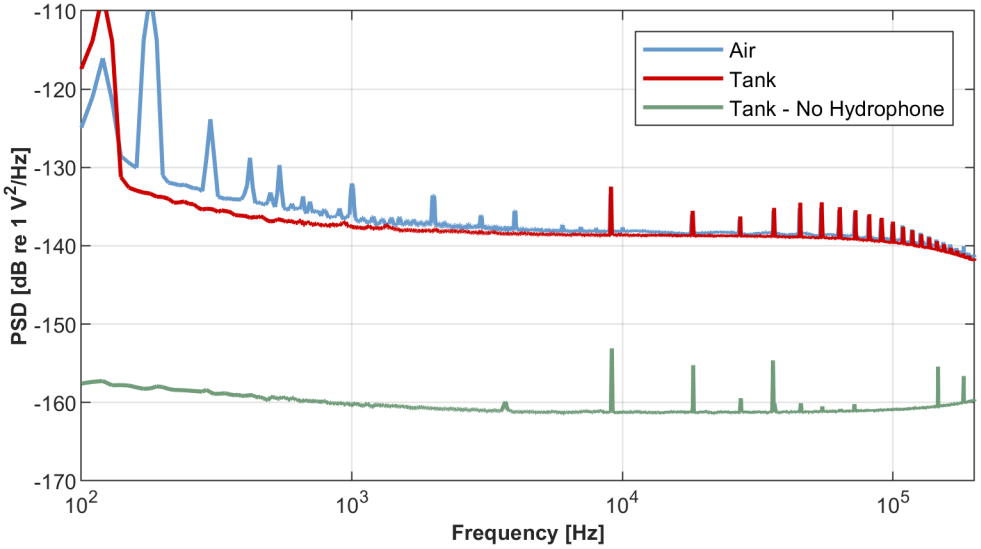

Figure 47: Uncalibrated voltage pressure spectral density for a representative DAISY under different conditions.

Figure 48 shows the results from tank testing with the hydrophone disconnected for all five DAISYs. First, at frequencies below a few kHz, data acquisition self-noise is similar, consistent with the results of low-frequency system calibrations previously conducted. Second, all of the data acquisition systems have the same electrical artifact around 10 kHz, though the frequency varies slightly between builds. Third, DAISY 03 and DAISY 05 have additional electronic noise not present in the other builds, likely due to sensitivity to internal cable routing.

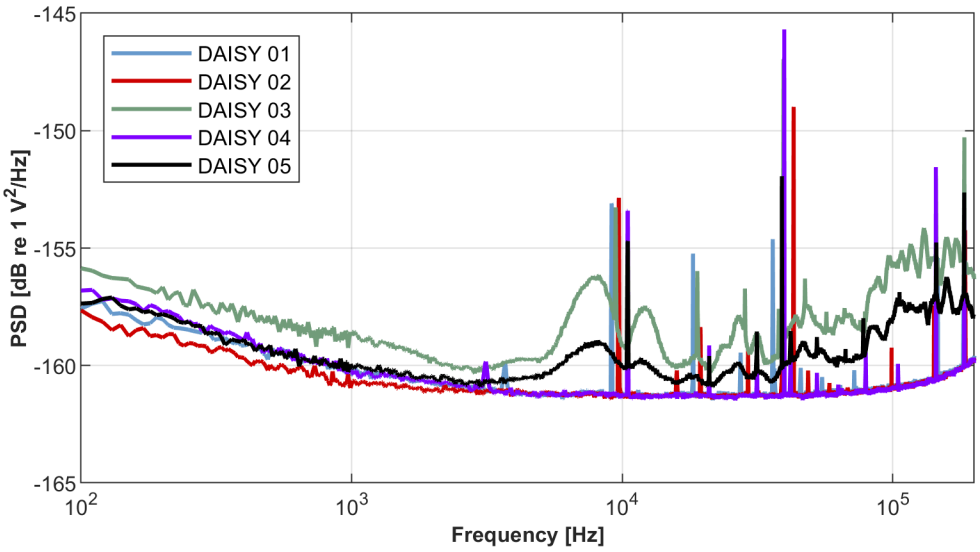

Figure 48: Uncalibrated voltage pressure spectral density for all DAISYs.

Finally, when pressure calibrations are applied to tank test data, as shown in Figure 49, we observe that the high-frequency noise floor is consistent with field measurements in the quiescent portion of Sequim Bay (i.e., noise floor of ~48 dB re 1 μPa^2/Hz, Figure 43). This confirms the hypothesis that the deviation between the OSU spar buoy and DAISYs in quiescent testing was a consequence of the DAISY noise floor. At frequencies below 100 Hz, the tank testing does not provide a reliable estimate of the DAISY noise floor, likely a consequence of ambient noise and vibration in the building (e.g., received levels are lower in the field).

Based on this analysis, we believe that the electrical self-noise is likely a consequence of electrical noise on the negative-rail input to the analog-to-digitals converter's differential amplifier, which operates at a similar switching frequency. Removing this component from future revisions of the DAISY electronics printed circuit board and connecting the negative-rail of the differential amplifier directly to analog ground would eliminate all components that contain switching from the analog portion of the hydrophone data acquisition. This will minimally impact the system's dynamic range as the differential amplifier's output will saturate at approximately 15 millivolts less than the existing system. However, this, along with upgrading the power supplied to the hydrophone pre-amplifier with additional filtering, should remove the artifacts currently present in the data and reduce the noise floor to levels more in line with COTS recording hydrophones. We note, however, that so long as the high-frequency tonal artifacts can be eliminated, the DAISYs will be compliant with IEC 62600-40 requirements for self-noise.

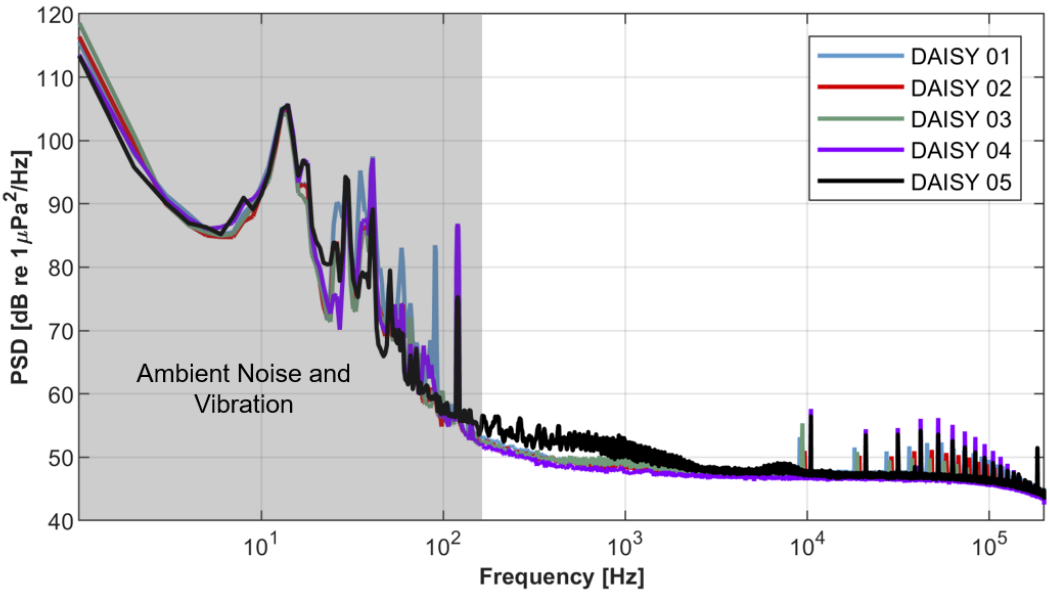

Figure 49: Self-noise evaluation. Grey shading denotes region of spectrum likely affected by ambient noise and vibration.

3.3.6.2 Line Strum Hypothesis

During testing at MCRL, the C-DAISY prototypes often, but not always, exhibited a spectral peak around 10 Hz. This occurred during quiescent testing in Sequim Bay and during testing in currents in the entrance channel. A similar peak was present in W-DAISY data from Clallam Bay (wave, wind, and current forcing), but not in most of the W-DAISY data from quiescent testing, nor in all W-DAISY data from measurements in more energetic waves at WETS.

To investigate the potential origin of this peak, we made use of the concurrent sensors on the DAISYs (e.g., pressure sensor, accelerometers on surface expression and lower housing). In Figure 50, we show the spectrogram from a quiescent drift during which the DAISY speed over ground was a relatively low 0.08 m/s. The 10 Hz peak is relatively obvious and intensifies over the five-minute drift. While there is a probable harmonic of this peak at ~20 Hz (barely apparent in a median periodogram representation, not shown), there is no peak at 5 Hz. Consequently, we can rule out the 10 Hz peak as being a harmonic of a lower frequency.

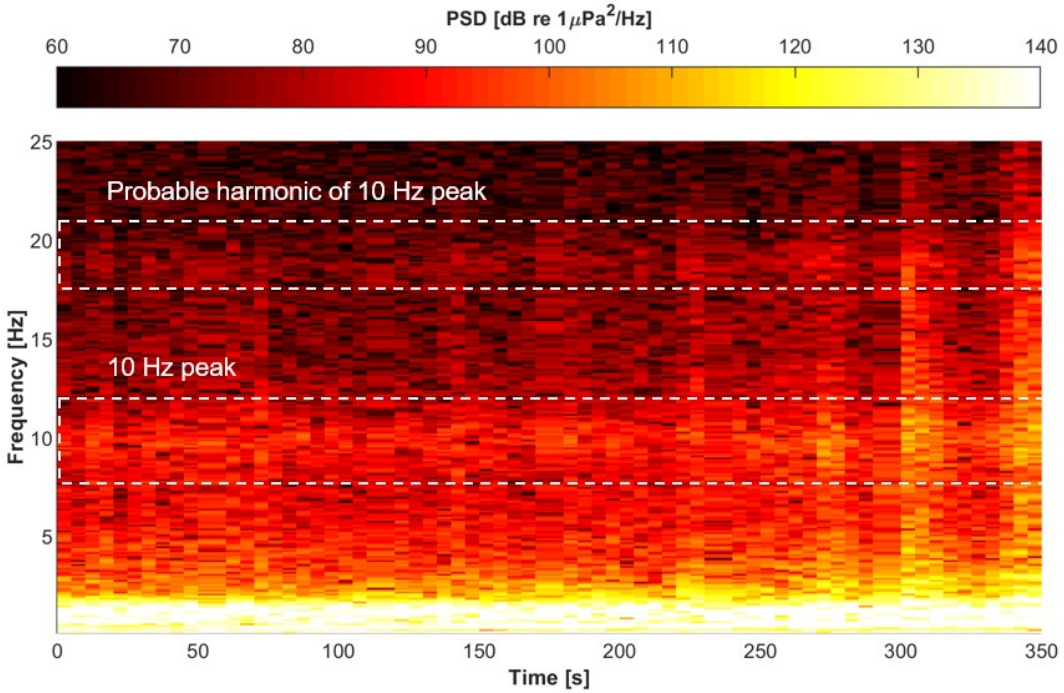

Figure 50: Spectrogram for quiescent drift of a C-DAISY with ~10 Hz self-noise peak and probable harmonic at ~20 Hz noted. Acoustic data have been reprocessed to yield a frequency resolution of 0.1 Hz and time resolution of 10 s.

Figure 51 shows semi-quantitative metadata for the same drift. Spectrograms are given for the pressure sensor on the lower housing, three-component acceleration for the surface expression and lower housing (IMU), and speed over ground measured by the GPS on the surface expression. Several features are notable:

- The surface expression experiences more motion than the lower housing, as evidenced by the more energetic acceleration for all three components than for the lower housing. This motion intensifies over time, as does the variation in the DAISY's speed over ground.
- The suspension system (rubber cord, flow-shield inertia) does not allow the majority of surface expression motion to translate to the lower housing, except for a tonal component in the vertical direction at ~0.7 Hz (apparent in both the pressure and z-axis acceleration).
- There is no motion apparent at 10 Hz.

Because there is no motion local to the hydrophone at 10 Hz, this suggests that the 10 Hz peak could be self-noise from the rubber cord (i.e., strum)[11]. The increasing motion of the surface expression over the course of the drift also suggests that this is a consequence of wind forcing slowly accelerating the DAISY. Further, during quiescent testing, DAISYs drifted in somewhat different directions and at somewhat different speeds, suggesting that, much like the sail on a boat, the wind-induced forcing depends on the orientation of a DAISY's surface expression.

[11] While this could also be a consequence of flow-shield self-noise, the appearance of a similar spectral feature in W-DAISY testing contradicts such a hypothesis.

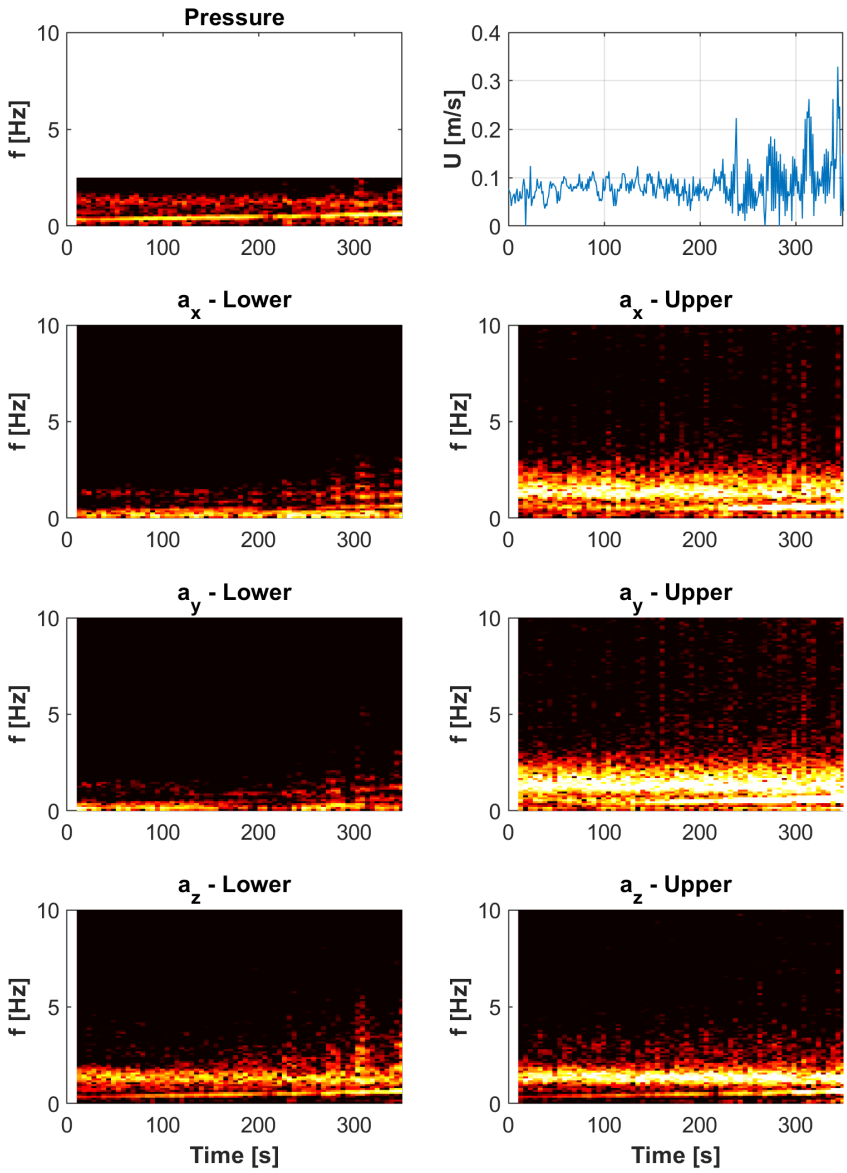

Figure 51: DAISY metadata from same drift as Figure 50. Pressure and accelerations shown as spectrograms and saturated to emphasize energy-containing frequencies. The pressure sensor acquires data at 5 Hz, resulting in a maximum frequency of 2.5 Hz for spectral analysis.

In fact, the average wind speed over a drift appears to be a strong predictor of this self-noise for the C-DAISY, as shown in Figure 52. The relatively limited number of data points suggests that this self-noise (PSD at 10 Hz) increases with wind speed up to 4 m/s and is relatively constant thereafter. The scatter observed in the data may be a consequence of wind direction or differential wind forcing on each DAISY. The leveling off at higher wind speeds may a consequence of an equilibrium being achieved between wind forcing and current drag as DAISY relative velocity increases.

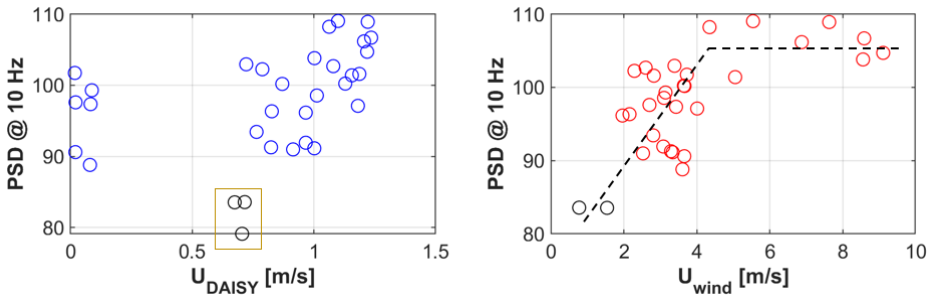

Figure 52: Drift-average (PSD) [dB re 1µPa²/Hz] in the 10 Hz band compared to the average speed of the C-DAISY over ground (U_{DAISY}) and wind speed (U_{wind}). Black circles denote channel drifts on Day 1 with limited strum.

Because this self-noise occurs at frequencies relevant to marine animal hearing, its potential to mask propagating marine energy converter sound could be problematic and warrants consideration of hardware mitigation approaches (its persistence obviates software mitigation). If This could be achieved by either increasing the drag on the submerged components or decreasing the drag on the air-side components. However, both options have significant downsides. Increasing the drag on the submerged components would generally require an increase in component size, which would complicate deployment and recovery. This design philosophy, which is expressed in the OSU spar buoy design, can be effective for individual drifting systems, but would be a significant challenge for localizing arrays, particularly if rapid deployment/recovery is required in close proximity to a marine energy converter (i.e., increased risk of mooring entanglement or collision with the energy converter). Decreasing the drag on the air-side components would require removing functionality (e.g., removing the mast with the meteorological station and visibility lights) or decreasing the margin for operational safety (e.g., removing foam to reduce reserve buoyancy and risking full submersion in moderate vertical velocity). Ironically, a benefit of the flow-shield, specifically, a low relative velocity that generally minimizes flow-noise, means that there is little forcing from currents and the low-frequency system performance can be affected by wind speed. This means that this effect will likely be independent of current velocity for the C-DAISY, as evidenced by the similar ranges of strum in quiescent and high-current environments at the same wind speed.

Alternatively, the natural frequency, f_n, of a tensioned, compliant line is given by Vandiver and Mazel (1976) as

$$f_n = \frac{n}{2L}\sqrt{\frac{T}{\mu}}$$

where n is the mode number, L is the line length in m, T is the line tension in N, and μ is the linear density in kg/m. For the 10 mm diameter rubber cord (volumetric density of 1522 kg/m^3), this suggests a tension of ~8 N would be sufficient to excite a first mode at 10 Hz. This is similar to the wet weight of the lower housing and flow shield and suggests that reducing this frequency to 5 Hz could be achieved by doubling the length or diameter of the rubber cord. As for modifications to

alter the wind/current drag balance, either of these approaches would make the system somewhat more difficult to deploy and recover[12].

3.3.6.3 Flow-shield (C-DAISY)

While line strum is common to all DAISY variants, the C-DAISY flow shield also produces three types of intermittent self-noise.

The first is "spar popping" and is highlighted in Figure 53. This is a short-duration event with relatively high amplitude to sounds like a staccato "pop". The highest amplitude sound is around 150 Hz and, depending on the severity of the event, can extend up to 1000 Hz. This self-noise occurred most frequently on the first of the three flow-shields that was fabricated. We believe that the root cause of this was that a smaller washer was welded to the end of the spring steel in this configuration (Figure 33c), which allowed the end to have some range of motion in the PVC collar. This was subsequently corrected and has not been observed since.

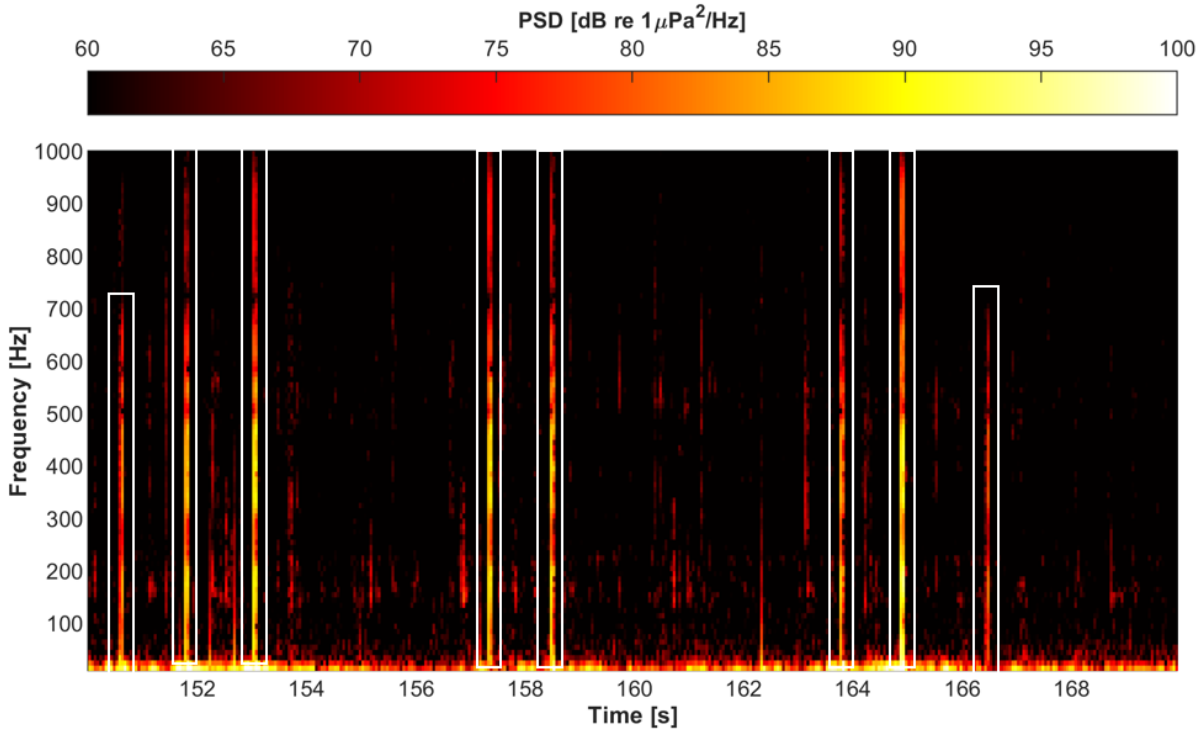

Figure 53: Representative example of "spar popping" self-noise for C-DAISY. Events are outlined by white boxes.

The second is "pumping" and is highlighted in Figure 54. This is a short-duration event with relatively low amplitude centered around 200 Hz that sounds like a low-frequency flutter. We believe that this is inherent to the flow-shield and is likely exacerbated by relative motion between

[12] Subsequent tests showed that increasing line length did not, in fact, substantially alter the frequency of this self-noise. However, during tests with a new version of the DAISY in July 2024, we observed that this peak had shifted to a lower frequency. The mechanical difference between the systems was change in the hydrophone cable diameter. In subsequent re-analysis, we determined that this peak was never present in data collected with the icListen hydrophones. The working hypothesis is that the peak is caused by hydrophone vibration which can be excited by strum from the tether. This suggests that effective mitigation measures could include suppressing strum on the tether or altering the hydrophone stem stiffness.

the flow-shield and surrounding water, as occurs during surveys with higher wind velocity. However, this acoustic signature was only apparent during quiescent testing and is, therefore, not likely a significant concern for operational use.

The third is “sloshing” and is highlighted in Figure 55. This is a relatively low-amplitude sound with a duration of < 1 s. This sound is also likely endemic to the flow-shield, but of sufficiently low amplitude and infrequent occurrence as to make a negligible contribution to median statistics.

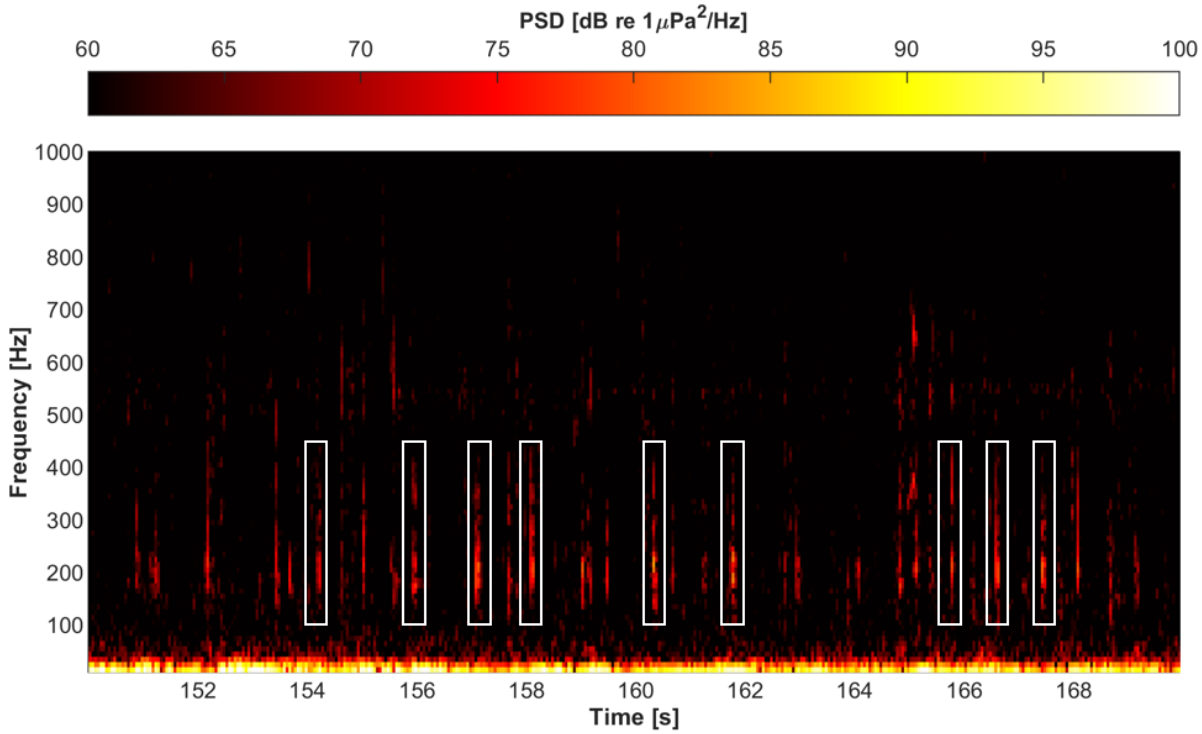

Figure 54: Representative example of “pumping” self-noise for C-DAISY. Events are outlined by white boxes.

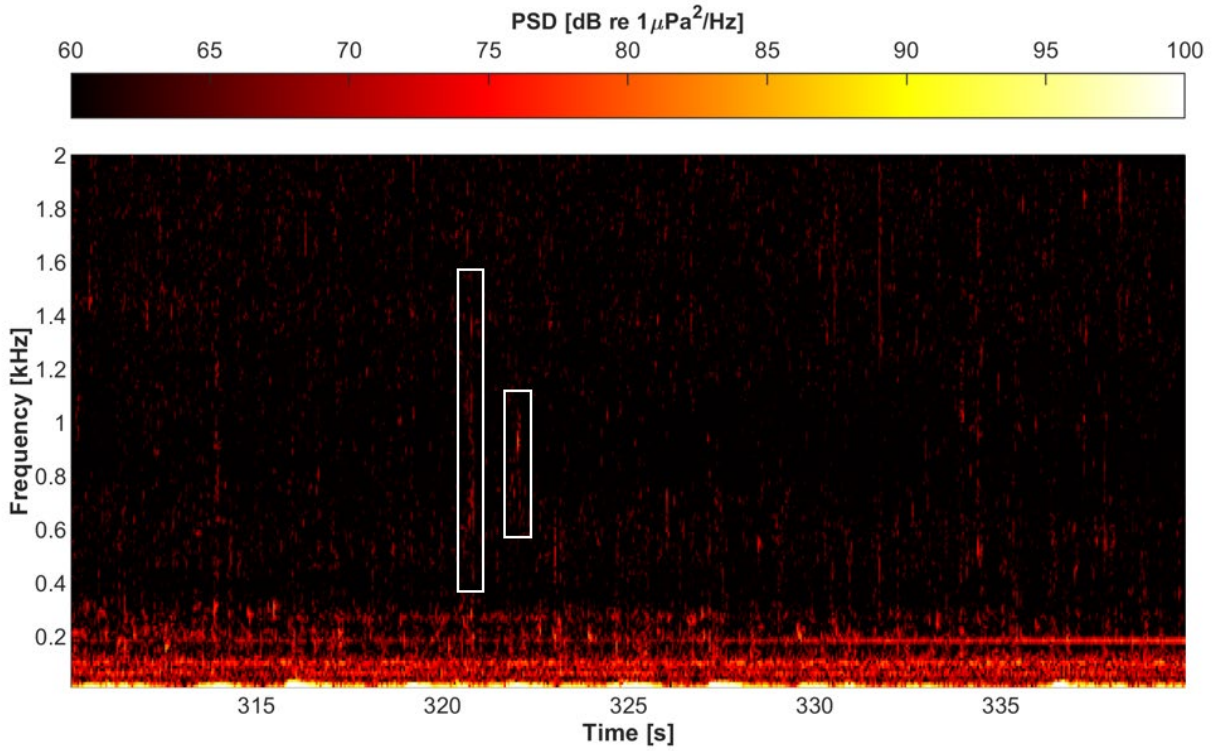

Figure 55: Representative example of "sloshing" self-noise for C-DAISY. Events are outlined by white boxes.

3.3.7 Sources of Flow-Noise

Flow-noise is a non-propagating sound arising from either relative motion between the hydrophone and water (causing turbulent eddies to be shed by the pressure-sensitive element) or ambient turbulence advected across the hydrophone (Strasberg, 1979). Flow-noise is generally identifiable in periodograms (sound pressure spectral density (PSD) as a function of frequency, *f*) as a monotonic decrease in amplitude with increasing frequency at a constant spectral slope. Mathematically, this can be described as

$$PSD_{\text{flow-noise}} = 10\log_{10}\left(Cf^{-n}\right)$$

where $PSD_{\text{flow-noise}}$ is the estimated PSD of flow-noise in dB re 1uPa^2/Hz and *C* and *n* are empirical constants obtained by fitting this equation to measurements over a specified frequency band with a constant spectral slot (e.g., 1-6 Hz). When turbulent length scales that produce flow-noise are sufficient to "engulf" a hydrophone, *n* = 5/3 (i.e., the slope of the inertial subrange in turbulent flow) and when turbulent length scales are smaller than the hydrophone, fluctuations partially cancel and the slope is proportional to f^{-n} where *n* > 5/3 (Bassett, Thomson, Dahl, & Polagye, 2014). The amplitude of flow-noise scales with the magnitude of the relative motion between the hydrophone and surrounding water. For relative velocities on the order of a few centimeters per second, flow-noise may only be identifiable at frequencies on the order of a few Hz. However, as relative velocity increases, flow-noise can mask propagating sound at frequencies up to 1 kHz (Bassett, Thomson, Dahl, & Polagye, 2014).

While the flow-shield around the C-DAISY hydrophone generally suppresses fluid motion in proximity to the hydrophone element and allows the C-DAISY to closely track the dominant flow

velocity, turbulence interacting with the shield can still produce pressure fluctuations. To evaluate the significance of environmental factors on flow-shield performance, PSD at 1 Hz (the frequency band with the highest amplitude flow-noise) is regressed against average C-DAISY speed over ground and wind speed during drifts. The PSD in this band relatively insensitive to speed over ground, but follows a similar trend with wind speed as strum, suggesting the same underlying mechanism: acceleration of the C-DAISY by the ambient wind field. Unlike strum, there are not simple mechanical modifications like increasing the line length to mitigate this effect. However, , flow-noise does not appear to mask propagating sound about 10 Hz and is, consequently of less importance for acoustic characterization.

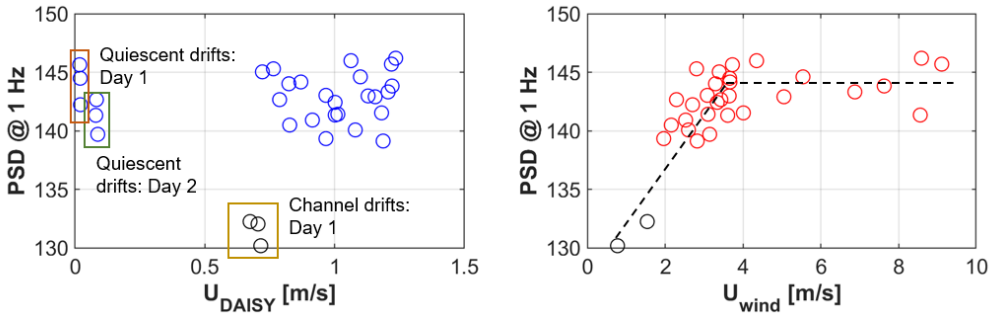

Figure 56: Drift-average (PSD) [dB re 1µPa^2/Hz] in the 1 Hz band compared to the average speed of the C-DAISY over ground (U_{DAISY}) and wind speed (U_{wind}). Black circles denote channel drifts on Day 1 with limited strum.

Further confirmation that sound at this frequency is flow-noise is given in Figure 57. The spectral slope, *n*, is relatively consistent and greater than 5/3 (consistent with the relatively large surface area of the flow shield), while the spectral amplitude, *C*, varies over orders of magnitude and is at a minimum when 1 Hz sound is at a minimum.

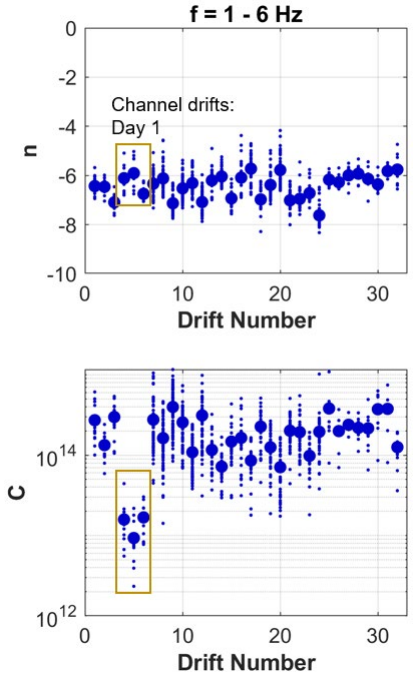

Figure 57: Spectral fits for C-DAISY drifts. Blue dots show mean values of fit coefficients over a drift and dots show instantaneous values each 10-second sequence.

3.3.8 Low-frequency Sound Summary

Figure 58 shows a representative periodograms for low-frequency (f < 100 Hz) measured sound during initial testing. The example is from a C-DAISY, but the spectral characteristics are similar for the W-DAISY. The acoustic spectrum can be broken into four regions with some overlap:

1. 1-6 Hz: Linear slope (in dB space), decreasing amplitude
2. 6-12 Hz: Spectral peak associated with self-noise
3. 12-30 Hz: Linear slope, decreasing amplitude
4. 30+ Hz: Relatively "flat" spectrum

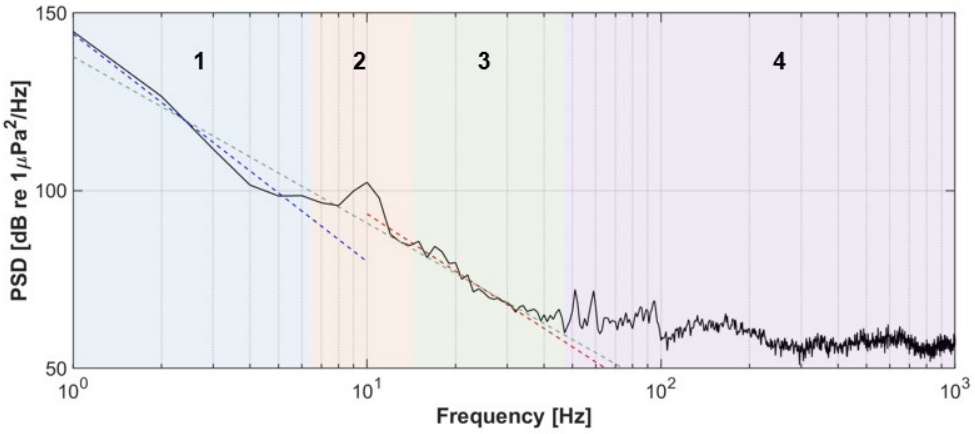

Figure 58: Low-frequency sound characteristics with annotated regions (C-DAISY). Dashed lines show spectral best fits for 1-6 Hz (blue), 12-30 Hz (red), and composite (green).

While Region 1 is likely flow-noise, Region 2 self-noise, and Region 4 ambient noise, it is possible that Region 3 is either ambient noise or self-noise. Because the slope in Region 3 is shallower than in Region 1, we can say, with some certainty, that this is *not* flow-noise.

To address this question, we consider a comparison between three co-temporal/co-spatial, quiescent C-DAISY drifts with differential levels of self-noise excited by strum. As shown in Table 15, the drifts occurred during wind speeds of ~4 m/s and the DAISYs were drifting at similar, though not identical, speeds over ground. Spectra are shown in Figure 59.

Table 15: Metadata for quiescent testing of C-DAISY configuration

DAISY	SOG [m/s]	Wind Speed [m/s]
02	0.08 ± 0.02	3.4 ± 0.3
04	0.08 ± 0.02	3.1 ± 0.7
05	0.07 ± 0.02	3.4 ± 0.9

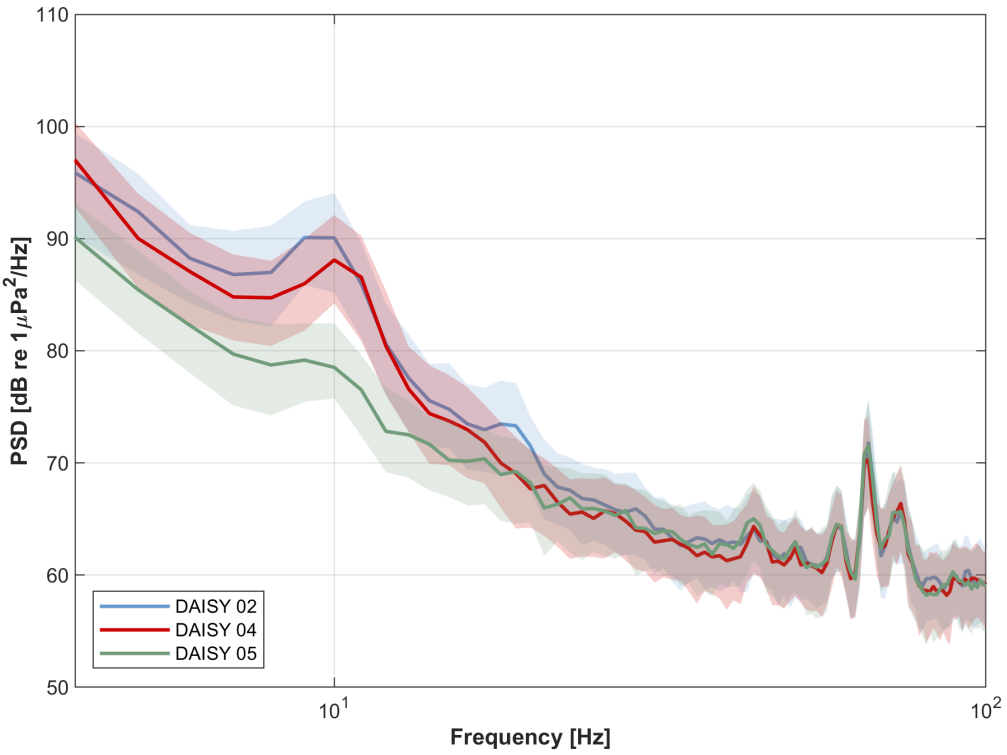

Figure 59: Comparison of quiescent C-DAISY drifts with differential strum at a wind speed of 4 m/s.

For this drift, the spectra for DAISY 02 and DAISY 04 show a significant strum-excited peak at ~10 Hz, with a harmonic at 20 Hz also apparent for DAISY 02. Neither peak is prominent in the spectra for DAISY 05, though a slight peak at 10 Hz suggests that some strum is present, albeit at much reduced amplitude. This is consistent in the relatively broad (~15 dB) range in the PSD at 10 Hz for the same wind speed shown in Figure 52. Beyond 25 Hz, the median spectra for all three drifts converge to within a few dB and the interquartile ranges overlap at ~15 Hz.

While this does not definitively resolve the ambiguity between ambient noise and consistent self-noise, two pieces of evidence suggest this represents propagating sound. First, during drifts in Clallam Bay when the W-DAISYs produced strum due to significant wind and current forcing, W-DAISY acoustic spectra were in close agreement with the OSU spar buoy at frequencies down to 30 Hz. Second, the low-frequency propagation limit in the portion of Sequim Bay where quiescent testing occurred is ~15 Hz. The lowest frequency that will propagate, f_{low}, (the "mode 1 cut-off") is given by

$$f_{\text{low}} = \frac{c}{4D\left(1 - c^2/c_s^2\right)^{1/2}}$$

where c is the sound speed of water, c_s is the sound speed of the sediment, and D is water depth (Jensen, Kuperman, Porter, Schmidt, & Tolstoy, 2011). As the sound speed profile of the sediments in Sequim Bay are not well-characterized, for the purposes of discussion, we assume a sound speed in water of 1500 m/s and a sound speed in sediment of 2500 m/s. In a depth of 30 m, f_{low} is ~15 Hz. Given this, it is plausible that wind shear at the water surface could produce propagating sound.

In summary, the low-frequency operational limit for the C-DAISY (i.e., the limit at which ambient noise is masked by self-noise or flow-noise) depends on wind speed. For wind speeds above 4 m/s, the evidence available suggests that the low-frequency operational limit is ~25 Hz (above this speed, flow-noise and self-noise are constant and independent of wind speed). Below wind speeds of 4 m/s, the low-frequency operational limit improves and is likely < 10 Hz in low wind conditions. In such conditions, in the water depths that current turbines are deployed (e.g., < 60 m), the C-DAISY would likely be able to accurately characterize all propagating sound emitted from a turbine.

3.4 Post-processing Software (Task 5)

At the beginning of this project, flow-noise and self-noise were persistent in measurements using rigid-hull DAISYs. These events were often broadband, masking propagating sound at frequencies up to several kHz. Consequently, at the outset, we assumed that identification and removal of these frequent events would be required to produce reliable data from DAISYs. However, over the course of testing, we were able to substantially mitigate these non-propagating sounds through hardware refinements (e.g., W-DAISY suspension system, C-DAISY flow-shield) without significantly compromising ease of deployment. Consequently, post-processing software developments focused primarily on identification of the persistent source of remaining mechanical self-noise (excited by line strum), flow-noise, and localization to attribute acoustic emissions to their source. For flow-noise and self-noise, the affected frequencies are low in absolute terms (f < 30 Hz) and, therefore, verging on infrasound that is only potentially relevant to fish and low-frequency cetaceans.

3.4.1 Self-noise Identification

Because self-noise was prevalent in energetic and quiescent testing of both DAISY variants at MCRL and has been observed intermittently at WETS, additional characterization and automatic identification are desirable. To facilitate this, a review tool was developed to annotate 10-s periodograms for the presence and frequency extent of strum. This was primarily identifiable as prominent, tonal peak (f ~ 10 Hz). Manual review was completed for 1083 examples from data acquired at MSL (74 % of total data) and 323 examples from Clallam Bay (39 % of total data). In the annotated data, self-noise attributable to strum can be identified in:

- 97% of quiescent C-DAISY data;
- 97% of energetic C-DAISY data;
- 58% of quiescent W-DAISY data; and
- 96% of energetic W-DAISY data.

For each 10-s sequence containing strum, the lowest and highest strum-contaminated frequencies (f_{min} and f_{max}) were identified and the following features were calculated:

- The peak frequency by prominence, with prominence defined as the y-axis separation between the measured periodogram and a linear trend between f_{min} and f_{max};
- The prominence of the peak, in dB;
- The strum bandwidth (i.e., f_{max} - f_{min}); and
- The “strum significance”, as quantified by the integral of the region between measured data and the linear trend between f_{min} and f_{max}.

Because the amplitude of the acoustic spectrum decreases as frequency increases, the prominence of strum relative to the linear trend proved to be a more effective estimator of the dominant strum frequency than the absolute PSD.

Strum statistics are summarized in Figure 60. For the C-DAISY, the strum peak frequency is centered around 11 Hz with a bandwidth of 5-10 Hz. The strum peak frequency rarely occurs below 6 Hz or above 20 Hz and the prominence of this strum peak can be up to 15 dB. For the W-DAISY testing in Clallam Bay, strum is centered around a lower frequency (9 Hz) and has a wider frequency distribution, but similar bandwidth, peak prominence, and significance as the C-DAISY. In conditions where W-DAISYs are less forced by currents, the prominence, bandwidth, and significance of strum are all likely to be reduced, as evidenced by quiescent tests where strum occurs less frequently and, when it does occur, is less significant.

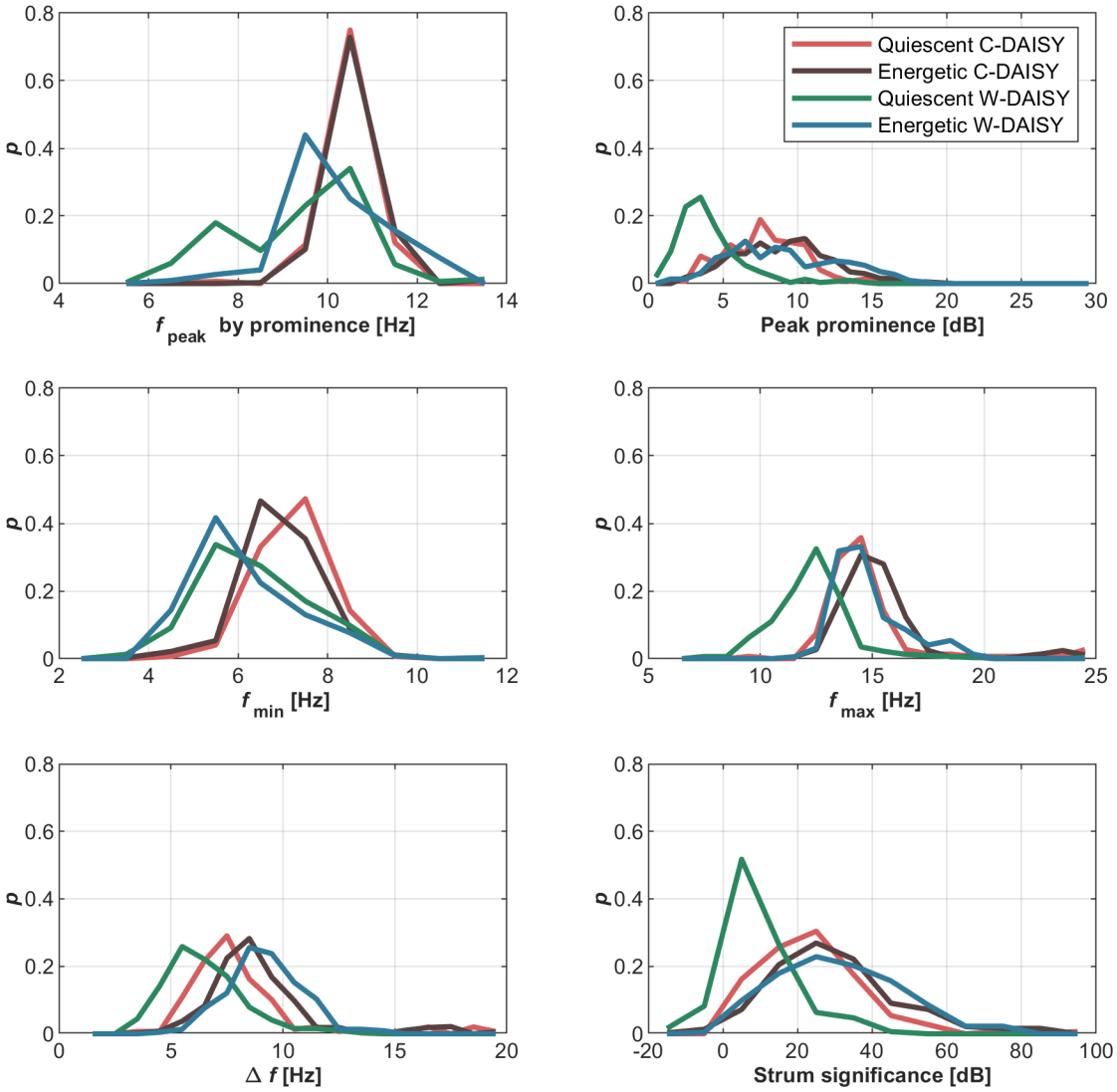

Figure 60: Strum statistics from testing at MSL and in Clallam Bay.

To identify when strum occurs and estimate the probable extent of masking, we make use of a number of properties of the measured spectrum highlighted in Figure 61:

- The spectral fit consistent with flow-noise (Cf^{-n}) is a good descriptor of the spectrum at low frequencies. Deviation from this either indicates a transition to a region where strum self-noise dominates or to a region dominated by propagating sound. This is quantified by the

deviation between the measurement and spectral fit. The start of a potential flow-noise region is identified by the tuning parameter $PSD_{threshold}$. The first time that the deviation (Δ in Figure 61) exceeds this threshold denotes the beginning of a potential strum region.

- From the properties of strum in the reviewed examples, we know that strum rarely occurs below some frequencies and rarely occurs above others. This is quantified by the tuning parameters f_{min} and f_{max}. If no potential strum events are identified within this frequency range, then strum is unlikely to have occurred.
- The tonal nature of most strum events means that they are typified by a local maximum in the deviation between the measurement and spectral fit. In addition to restricting the range of frequencies over which strum is known to occur, we also specify a minimum "peak prominence"[13] to avoid classifying spurious peaks as a strum event.

In summary, a strum event is identified by a peak of sufficient prominence between f_{min} and f_{max}. The start of the event is identified as the first frequency at which the deviation exceeds $PSD_{threshold}$. The bandwidth of the strum event is estimated as twice the frequency range between the identified peak and identified start (i.e., the strum peak is centered in the frequency domain).

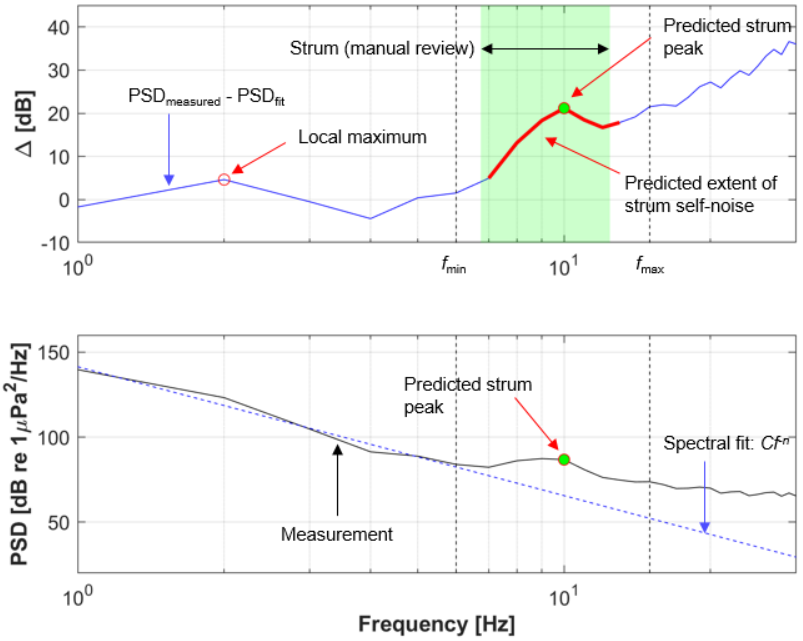

Figure 61: Strum identification example. Bottom panel shows the measured and fit spectra. Top panel shows the deviation between the two and key features, along with the frequency range manually identified as contaminated by strum self-noise.

Because there are several tuning parameters involved, it is instructive to consider their effect on algorithm performance. We quantify this with four parameters:

- *True positive rate*: the fraction of sequences containing strum that are correctly identified;
- *True negative rate*: the fraction of sequences without strum that are correctly identified;

[13] The "prominence" of a peak is defined by the y-axis distance between a local maximum and the highest adjacent local minimum.

- *False positive rate*: the ratio of the number sequences identified as containing strum (but did not) relative to number that did not actually contain strum; and
- *False negative rate*: the ratio of the number of sequences identified as not containing strum (but did) relative to the number that actually contain strum.

Figure 62 shows the parameter sensitivity. The algorithm is relatively insensitive to the choice of f_{min}, f_{max}, and $PSD_{threshold}$, but quite sensitive to the peak prominence. This makes sense, since, in the absence of strum, the measured spectra will deviate from the spectral fit and it is primarily the prominence of the peak that differentiates strum from ambient noise. We note that a peak prominence of 1.5 dB appears to produce an adequate performance trade-off: true positive and true negative rates > 80%, while false negative and false positive rates are < 20 %.

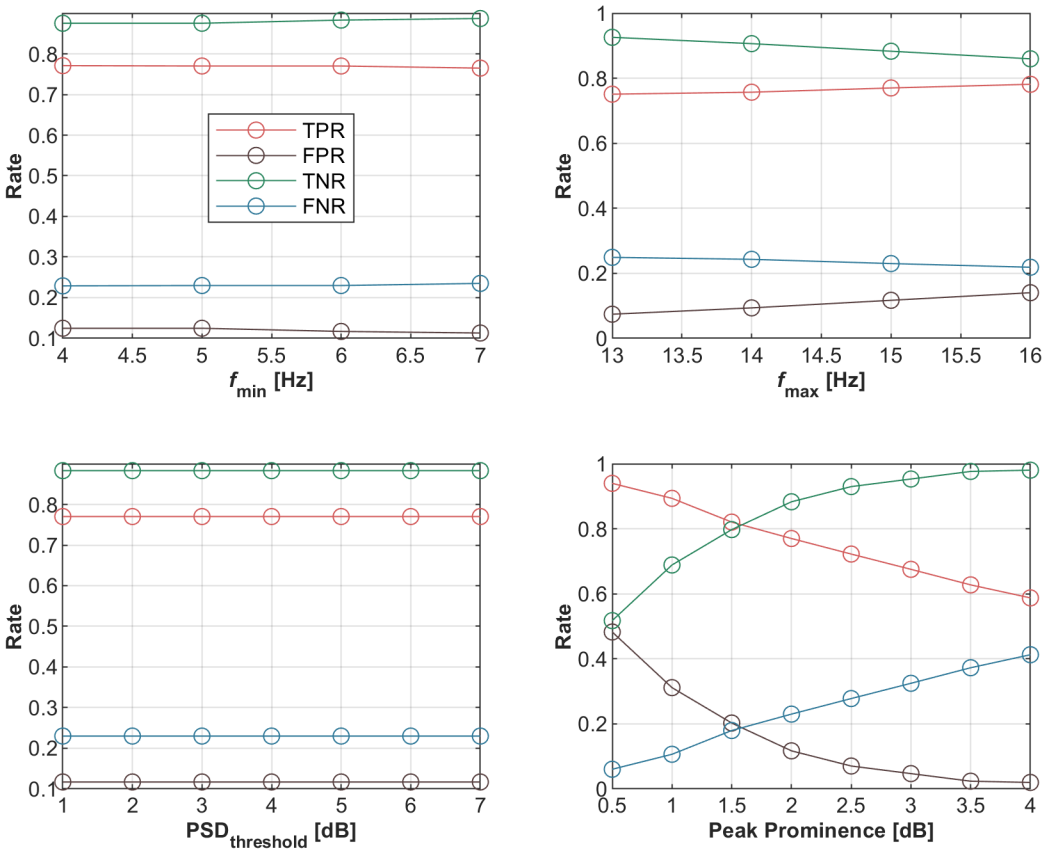

Figure 62: Strum detection sensitivity to algorithm parameters, given as the median of results for all sequences with the specified combination of parameters. In each plot, horizontal axis shows the varied parameter with other parameters at their median values (f_{min} = 6 Hz, f_{max} = 15 Hz, $PSD_{threshold}$ = 4 dB, peak prominence = 2 db).

Figure 63 shows a similar sensitivity in the frequency characteristics of strum. Specifically, each panel shows:

$$\Delta f = \text{median}\left(f_{x,\text{strum}}^{\text{manual}} - f_{x,\text{strum}}^{\text{automatic}} \right)$$

where the "manual" and "automatic" superscripts denote frequency identification by manual review versus automatic processing and x denotes a property, such as the minimum, maximum, or peak frequency affected by strum. On average, the algorithm predicts the strum peak frequency to

within a few Hz. However, this is a long-tailed distribution, with errors up to 15 Hz observed for some sequences and model parameters (not shown by the mean statistics). The algorithm also predicts the onset of strum at lower frequencies than observed, unless $PSD_{threshold}$ is increased to relatively high values and generally under-predicts the cessation of strum because the peak frequency is not exactly centered between onset and cessation. Because strum detection is insensitive to $PSD_{threshold}$, a relatively high value for this parameter appears appropriate. Classification accuracy degrades as peak prominence increases, which promotes a tendency to overshoot the actual strum peak, thereby increasing the bandwidth of strum and over-predicting cessation.

Overall, we note that, regardless of the selected model parameters, the deviations between predicted strum frequencies and observed strum frequencies are on the order of a few Hz, on average.

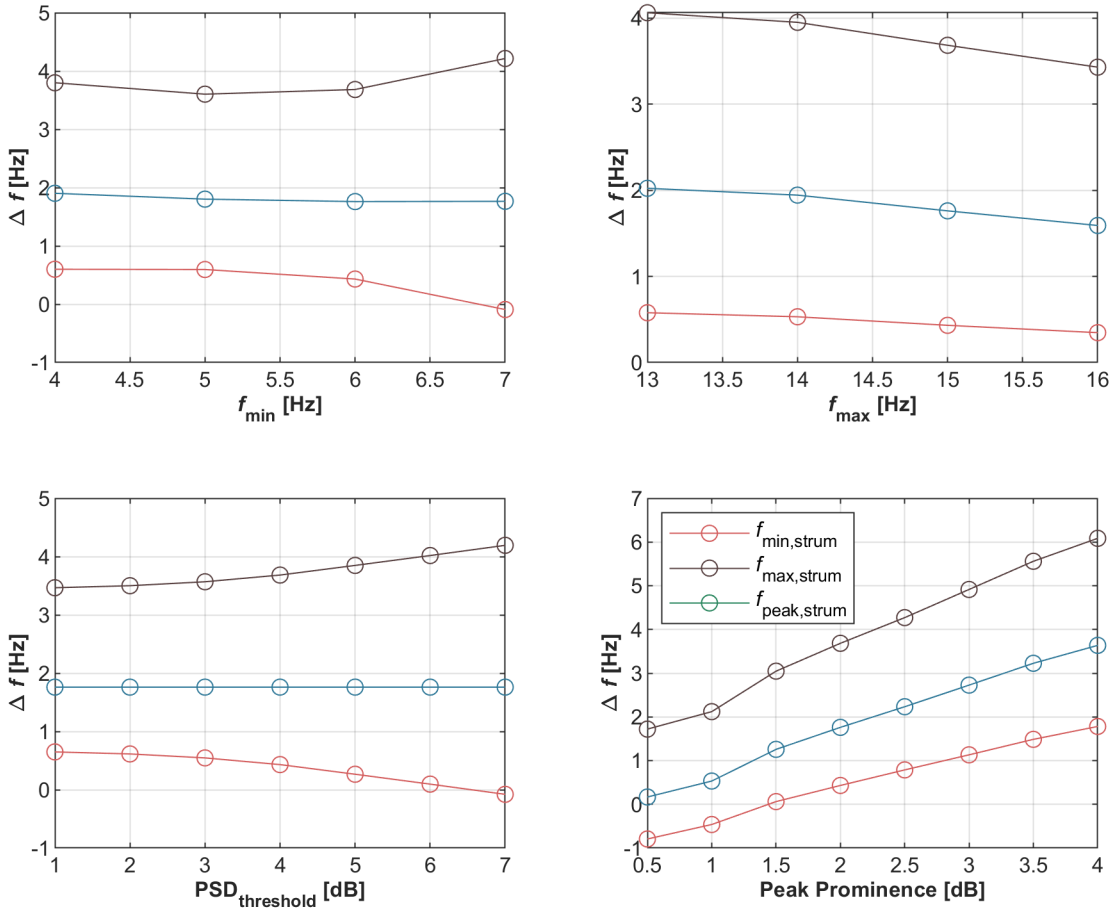

Figure 63: Strum classification sensitivity to algorithm parameters, given as the mean of results for all sequences with manually identified strum and combination of specified parameters. In each plot, horizontal axis shows the varied parameter with other parameters at their median values (f_{min} = 6 Hz, f_{max} = 15 Hz, $PSD_{threshold}$ = 4 dB, peak prominence = 2 dB).

Having addressed strum, we briefly consider the other three types of mechanical self-noise identified during testing:

1. "Spar popping": Attributable to a manufacturing weakness in the C-DAISY flow-shield on two of the units, this was addressed by a minor revision to the spring steel termination.

2. “Pumping”: Attributable to slow vertical oscillations of the flow-shield, this sound is only apparent in quiescent testing and not a concern for operational use. This could also be readily identified by a convolution algorithm given its consistent archetype.
3. “Sloshing”: Attributable to water motion inside the flow-shield, this sound appears in both quiescent and energetic testing. However, its spectral signature is ill-defined and low-amplitude. While these properties would make it difficult to automatically identify, it occurs infrequently (i.e., only a few seconds over a drift of several minutes).

We emphasize that these instances of self-noise are relatively low-amplitude compared to flow-noise on a fixed platform and, with the exception of self-noise induced by strum, are intermittent. Because IEC 62600-40 emphasizes median spectral representations, intermittent sound sources are naturally excluded and do not introduce substantial bias.

3.4.2 Flow-noise Identification

Flow-noise detection follows a similar approach to strum identification. However, the region affected by flow-noise is indicated by a *lack* of deviation between the measured PSD and a fit of the form Cf^{n}, which is indicative of flow-noise. As demonstrated in Figure 64, the highest frequency likely affected by flow-noise is characterized by a deviation greater than the tuning parameter $PSD_{\text{threshold}}$. To ensure that this deviation is sustained, it must also not be a local maximum. This is addressed by a peak prominence tuning parameter for peak identification.

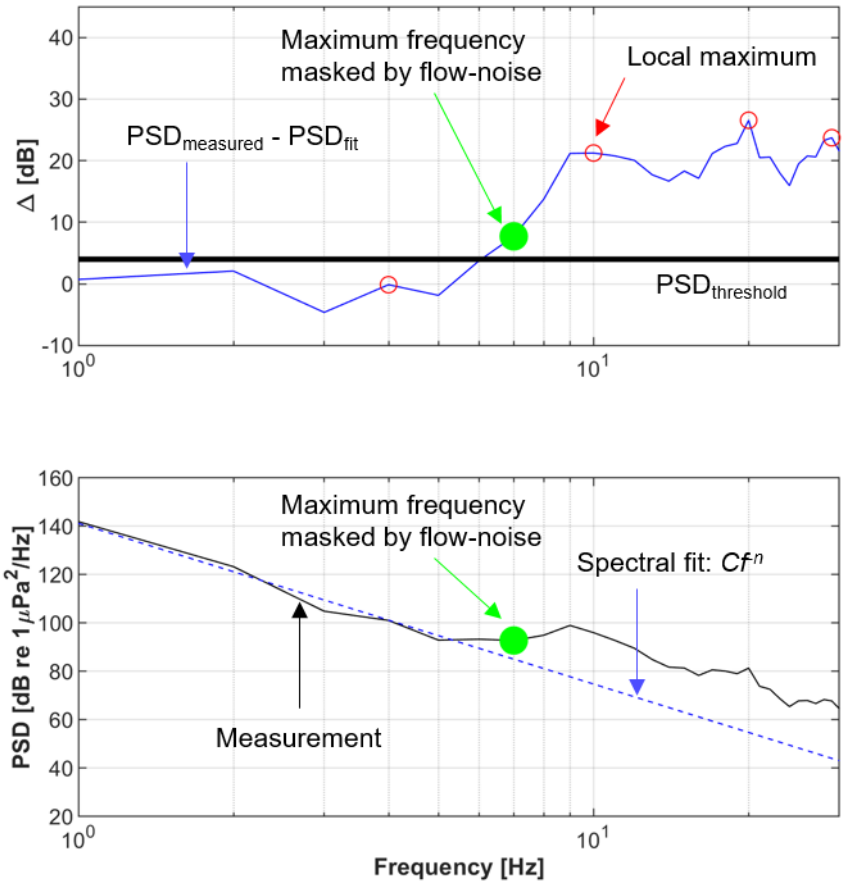

Figure 64: Flow-noise identification example. Bottom panel shows the measured and fit spectra. Top panel shows the deviation between the two and key features, along with the $PSD_{threshold}$ and identified peaks.

Results by DAISY variant and test condition are shown in Figure 65 for one set of tuning parameters. As expected, flow-noise masking persists to slightly higher frequencies in energetic than quiescent conditions. Also consistent with expectations, in energetic W-DAISY testing without strum, flow-noise is detected at higher frequencies (i.e., no strum to mask flow-noise). While the quiescent C-DAISY cases are anomalous in this regard, with flow-noise detected at *higher* frequencies for cases with strum, flow-noise and strum are both caused by wind-induced relative velocity and, in some sequences it is logical to expect that flow-noise amplitude would exceed strum amplitude.

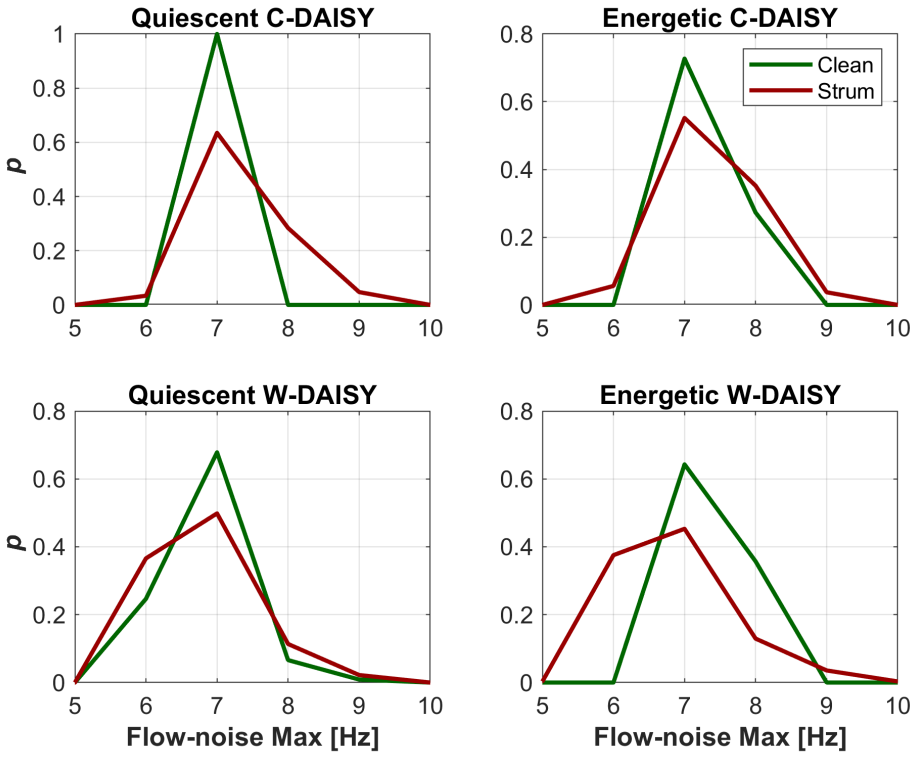

Figure 65: Histogram of maximum frequencies affected by flow-noise for each DAISY variant and test condition for $PSD_{threshold}$ = 4 and peak prominence = 1.5 dB. Results are partitioned by the presence of manually-identified strum.

Because there are some differences between sequences containing strum and not, only sequences without manually identified strum are presented in Figure 66. The general trend is that the maximum frequency masked by flow-noise increases with the $PSD_{threshold}$ tuning parameter and decreases with peak prominence parameter. Both results are to be expected. As $PSD_{threshold}$ increases, a greater deviation from a flow-noise spectrum is required and, as peak prominence increases, fewer local minima (which are contra-indicators of sustained deviations) are detected.

For any meaningful choice of tuning parameter, the maximum frequency masked by flow-noise contamination is < 10 Hz. This demonstrates the effectiveness of DAISY designs to suppress flow-noise contamination at low frequencies.

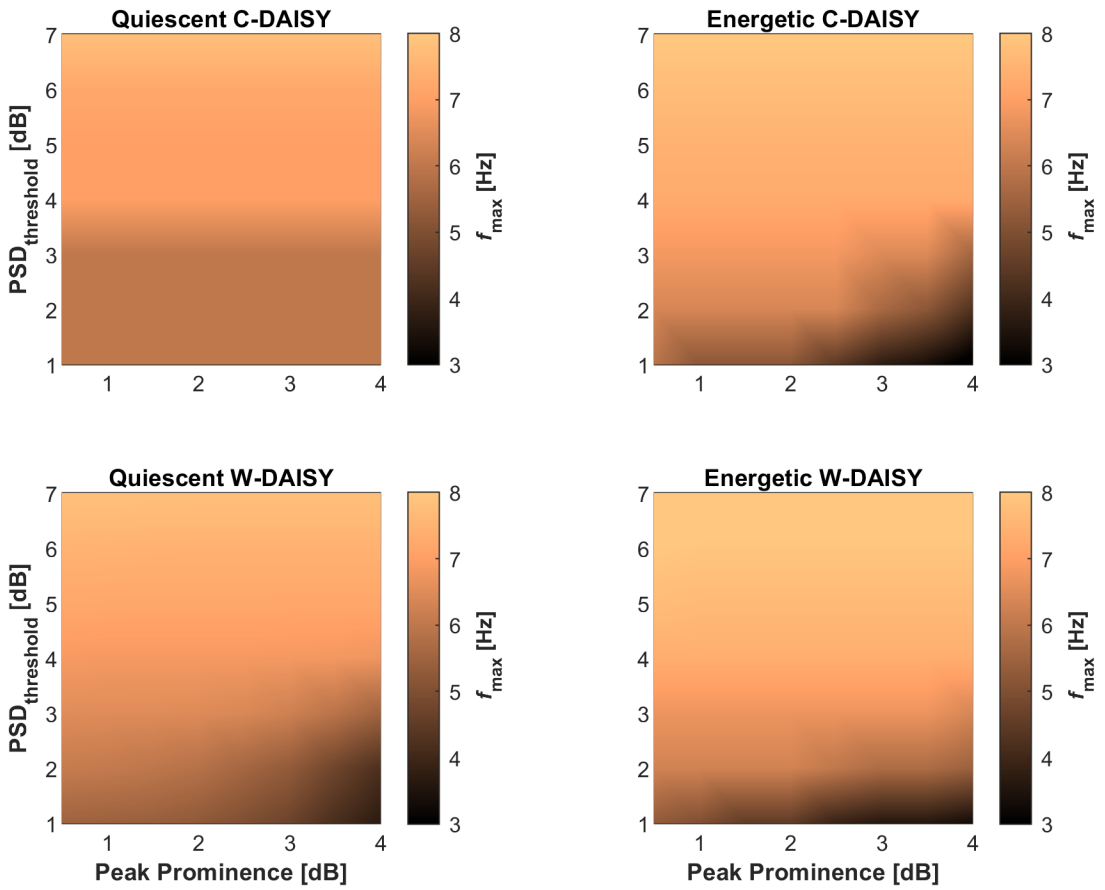

Figure 66: Maximum frequency affected by flow-noise for sequences without strum contamination as a function of model parameter for each DAISY variant and test condition.

3.4.3 Acoustic Localization

3.4.3.1 Hyperbolic Localization Theory

An acoustic source localization methodology was implemented based on (Wahlberg, Mohl, & Telberg Madsen, 2001). This method relies on the measurement of the differences in arrival times of a signal, known as the "time-differences of arrival" (TDOAs), between pairs of receivers. With knowledge of the receiver positions and the speed of sound in water, a set of points can be calculated that satisfy a "constant-difference distance" relationship for a pair of receivers, which is equal to the speed of sound, c, multiplied by the pair's time-difference of arrival, t. The set of points satisfying the constant-difference distance relationship produce a two-sheeted hyperboloid with foci at the receiver positions, as shown in Figure 67.

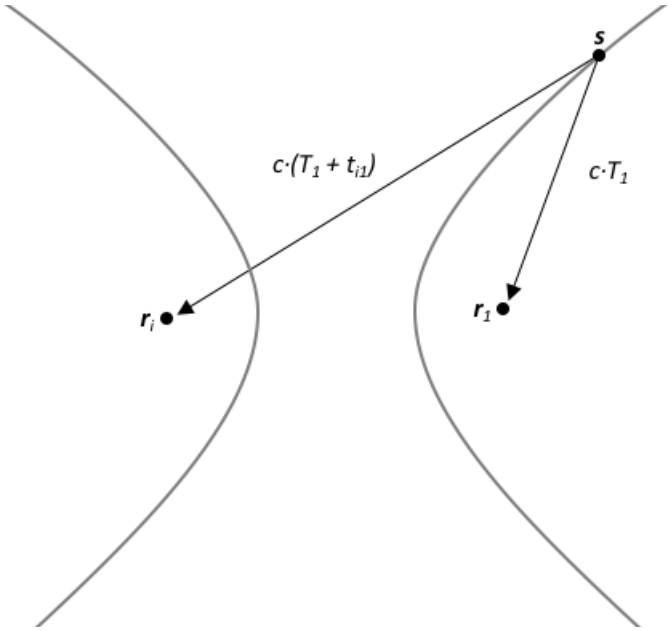

Figure 67: An example of a constant-difference distance hyperbola for an acoustic source and pair of receivers. Hyperbolae are composed of a set of possible source positions dependent upon the travel time from the source to receiver 1, T_1, and the time-difference of arrival, t_{i1}.

Taking the origin at $\boldsymbol{r_1} = [0,0]^T$, the lateral distance between a receiver with position vector $\boldsymbol{r_i} = \left[r_{xi}, r_{yi}\right]^T$ and a source with position vector $\boldsymbol{s} = \left[s_x, s_y\right]^T$ is related to the acoustic travel time from source to receiver 1, T_1, and the time-difference of arrival between receiver i and receiver 1 by

$$(r_{xi} - s_x)^2 + \left(r_{yi} - s_y\right)^2 = c^2(T_1 + t_{i1})^2, \qquad i = 2,3,4 \ldots, n. \tag{1}$$

Expanding the terms in equation 1, a system of linear equations can be written in the form

$$2r_{xi}s_x + 2r_{yi}s_y + 2c^2 t_{i1}T_1 = -c^2 t_{i1}^2 + \left|\left|\boldsymbol{r_i}\right|\right|, \qquad i = 2,3,4 \ldots, n. \tag{2}$$

Equation 2 has three unknowns: s_x, s_y, and T_1, and one such equation can be written for each receiver pair and accompanying TDOA measurement. Therefore, a minimum of four receivers are necessary to produce an unambiguous solution to the 2-D localization problem.

The method described by Wahlberg et al. can be used to solve the 2-D localization problem with only two receiver pairs (three receivers) by using the quadratic formula.

For a receiver matrix $\boldsymbol{R}$, given by

$$\boldsymbol{R} = \begin{bmatrix} r_{x2}, & r_{x3}, & r_{x4} \\ r_{y2}, & r_{y3}, & r_{y4} \\ r_{z2}, & r_{z3}, & r_{z4} \end{bmatrix},$$

a vector of TDOAs, $\boldsymbol{t}$, given by

$$\boldsymbol{t} = [t_{21}, t_{31}, t_{41}]^T$$

and a matrix, $\boldsymbol{b}$, given by

$$\boldsymbol{b} = -c^2 t_{i1}^2 + \left|\left|\boldsymbol{r_i}\right|\right|,$$

(2) can be rewritten as

$$2\boldsymbol{R}^T\boldsymbol{s} + 2c\boldsymbol{t}T_1 = \boldsymbol{b}.$$

Rearranging for $\boldsymbol{s}$ produces

$$\boldsymbol{s} = -c^2T_1\boldsymbol{R}^{-T}\boldsymbol{t} + \frac{1}{2}\boldsymbol{R}^{-T}\boldsymbol{b}. \tag{3}$$

The quadratic formula is used to solve for T_1 by using the relationship $c^2T_1^2 = \boldsymbol{s}^T\boldsymbol{s}$, where

$$T_1 = \frac{-p \pm \sqrt{p^2 - aq}}{a}, \tag{4}$$

and a, p, and q are given by

$$a = c^4\boldsymbol{t}^T\boldsymbol{R}^{-1}\boldsymbol{R}^{-T}\boldsymbol{t} - c^2,$$
$$p = -\frac{c^2\boldsymbol{t}^T\boldsymbol{R}^{-1}\boldsymbol{R}^{-T}\boldsymbol{b}}{2},$$

and

$$q = \frac{\boldsymbol{b}^T\boldsymbol{R}^{-1}\boldsymbol{R}^{-T}\boldsymbol{b}}{4}.$$

The solution(s) to (4) are substituted into (3) to produce an estimate of source position. If (4) results in two positive real solutions, additional information is necessary to determine the more accurate solution. Complex solutions and negative solutions to (4) are discarded.

Errors in estimates of source range are known to be high for acoustic sources with distances from the array centroid much greater than the distances between array receivers. However, the error is primarily in the magnitude of the source position vector, rather than the direction, such that azimuth and elevation angles calculated using the estimated source position may be accurate even if the estimated source position is not.

Another measure of solution robustness is the matrix condition number. This is the ratio of the largest to the smallest singular value of a system of equations and describes the sensitivity of a system's output to changes in its input. In the context of the localization solution in this form, it describes the sensitivity of position estimates to errors in DAISY GPS position, speed of sound, and TDOA measurements, and it can be used to determine array properties such as directional sensitivity and to bound solution error. Although calculations of directivity and error bounds have not been conducted here, the condition number has been shown to roughly represent the solution's sensitivity over a drift, which is strongly affected by the receiver geometry. To quantify the system's sensitivity to the GPS positions of the DAISYS and the source only, the terms of the form ct_{i1} in (2) were substituted for d_{i1}, the difference in direct path travel times between the source and each receiver, calculated using GPS positions. The condition number of the resulting matrix, A, given by

$$A = \begin{bmatrix} 2r_{x21} & 2r_{y21} & 2c \cdot d_{21} \\ 2r_{x31} & 2r_{y31} & 2c \cdot d_{31} \end{bmatrix},$$

was calculated at each time step.

3.4.3.2 Experimental Methodology

During the field trials in February 2019, experiments were conducted with cooperative sources to evaluate a core DAISY capability: localization of sound to attribute emissions to a source. Baseline performance testing took place in the inner waters of Sequim Bay, herein referred to as the "quiescent" tests. Tests of performance in currents took place in the Sequim Bay channel during a tidal exchange and tests in "waves" took place in Clallam Bay. The Clallam Bay case is best considered a hybrid, given that the significant wave height was < 1 m, winds were strong, and currents estimated to be approximately 1 m/s given the DAISYs' speed over ground.

For each test, three DAISYs were deployed such that their positions approximated the vertices of an equilateral triangle. Two acoustic projectors (Ocean Sonics icListen LF and icListen HF) were lowered from a vessel on a weighted line. A pressure logger (Onset HOBO) and an inertial measurement unit (IMU, Lowell Instruments MAT-1) were deployed with the sound sources to record their depth and orientation, and the position of the vessel was continuously logged using a handheld GPS unit (Qstarz).

The pair of acoustic projectors generated a range of tones, clicks, and frequency sweeps to evaluate the localization effectiveness for these sound archetypes. The icListen HF produced a repeating series of tones (3 second duration) and clicks (< 0.1 s duration) with frequencies increasing from 10 to 200 kHz in 10 kHz steps. The icListen LF simultaneously produced a series of tones (5 second duration) at 0.1, 0.2, 0.5, 1.0, 1.5, 2.0 2.5, and 3.0 kHz followed by three frequency sweeps (5 second duration) from 0.1 to 3.0 kHz.

Tests in quiescent and wave conditions were repeated with increasing distance from the centroid of the triangle to each DAISY. A minimum of three minutes of data were collected (approximately three repetitions of the sound sequences) at each range. Tests in currents were limited by the channel width, so repeated measurements had similar spacing between DAISYs.

3.4.3.3 Narrowband Localization Results

Localization results for all tones from 10 – 200 kHz from the 25 m quiescent test case are presented in Figure 68. Co-temporal position and bearing error estimates, matrix condition numbers, and hydrophones depths for this drift are presented in Figure 69. In this case, position error was typically less than the target upper bound, or 30% of the mean distance from the DAISYS to the source, when the sound source was "inside" of the triangle formed by the DAISYs. The error in this region may be within the uncertainty inherent to GPS measurements. GPS uncertainty is approximately ±2.5 m, but because the vessel's position and the DAISY positions were measured independently, the aggregate uncertainty in absolute position error, defined here as the difference in estimated target position relative to the vessel's measured position, could be as much as ±5.0 m. When sound sources were at the edges of the triangle or outside of it, the method frequently failed to find a solution (i.e., no gray pairing between purple estimated positions and blue known positions). This case demonstrates an anticipated limitation of the localization method: the accuracy of position estimation suffers significantly when the sound source is outside of the array. Bearing errors were generally lower than the 20° target bound even when position accuracy was poor.

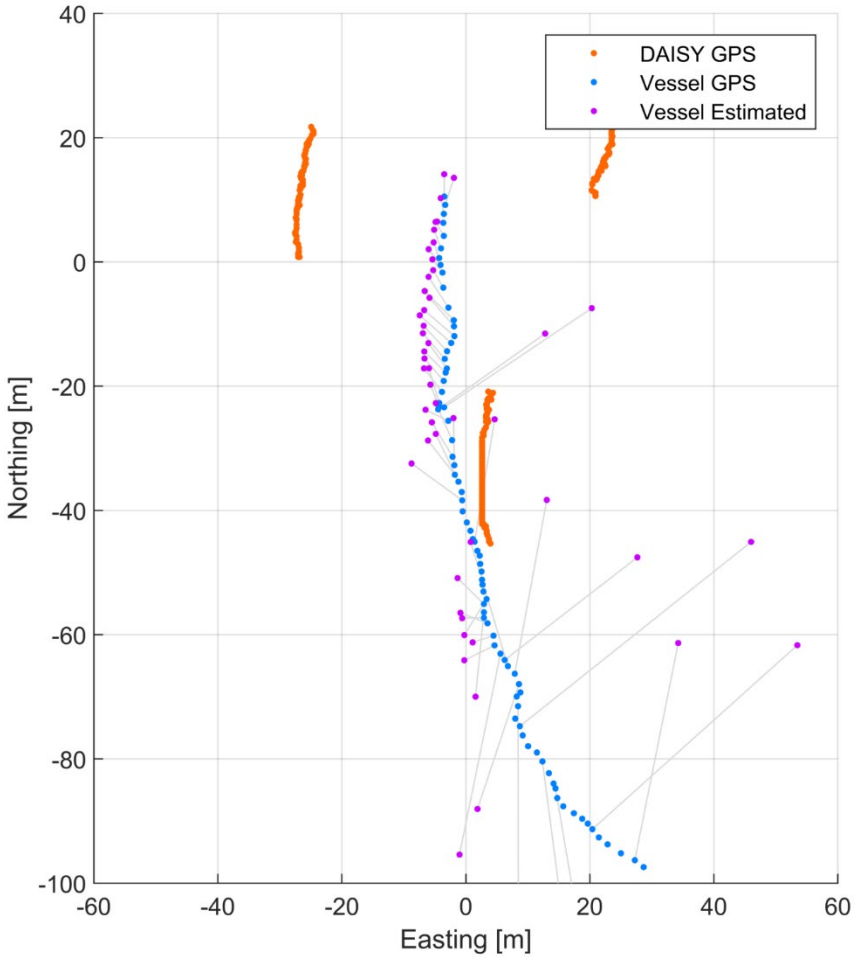

Figure 68: Results from quiescent testing (Sequim Bay) at 25 m range. Gray lines connect the estimated target position to its measured GPS position. Tones: 10 – 200 kHz.

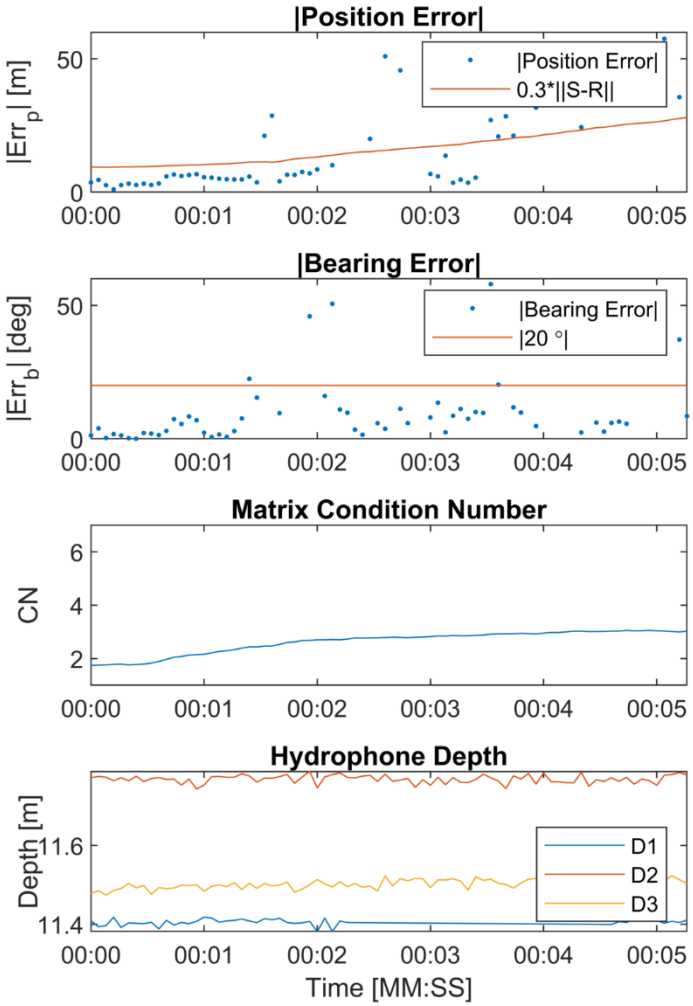

Figure 69: Co-temporal position and bearing error estimates, matrix condition numbers, and hydrophone depths from 25 m quiescent test in Sequim Bay.

Localization results for all tones from 10 – 200 kHz from a trial in currents are presented in Figure 70, and co-temporal position and bearing error, matrix condition numbers, and hydrophones depths are presented in Figure 71. As with the quiescent case, solutions were found when the sound source was located “inside” the array. However, both position and bearing errors exceeded the target performance. This error could have been caused by up to three sources. First, a software error (subsequently corrected) in the DAISY software running on the lower housings may have introduced slight errors in the hydrophone time stamps. Second, as the channel is relatively close to a cliff face, the available GPS satellites with direct line of sight to the DAISYs may have been limited, resulting in sub-optimal position data. Third, the sound sources were deployed on a static line which did not hang vertically in the water column, which would result in additional position uncertainty on the order of a few meters.

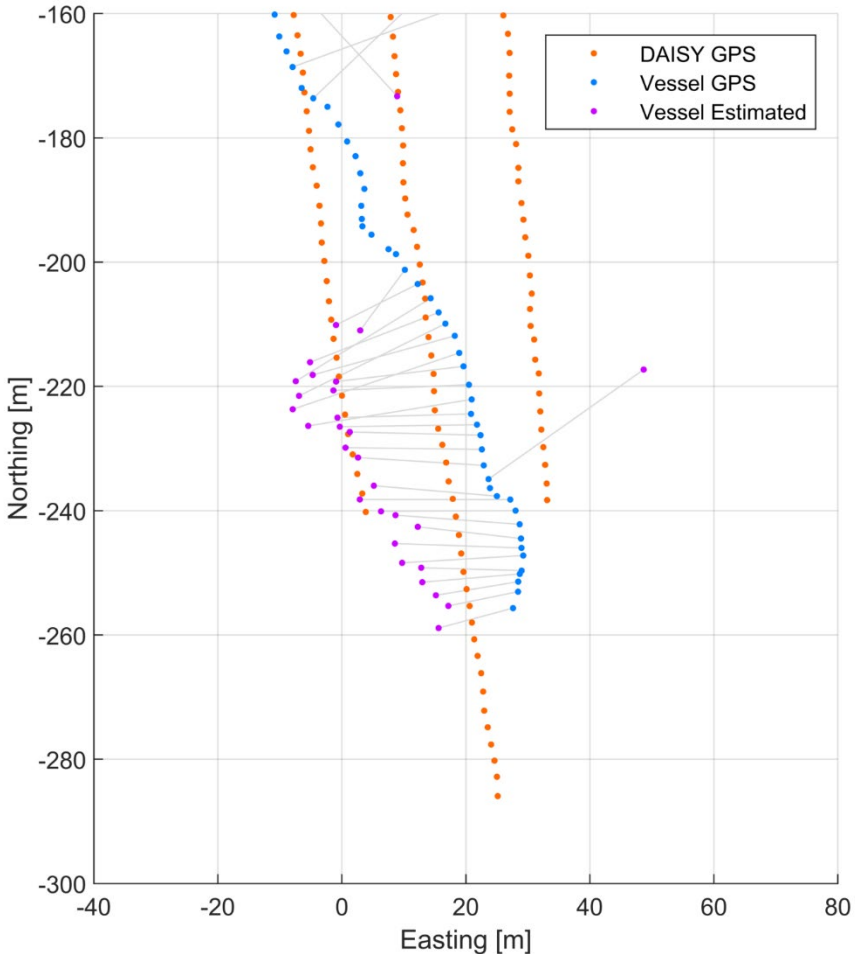

Figure 70: Results from current testing (Sequim Bay channel. Gray lines connect the estimated target position to its "actual" position (vessel GPS). Tones: 10 – 200 kHz.

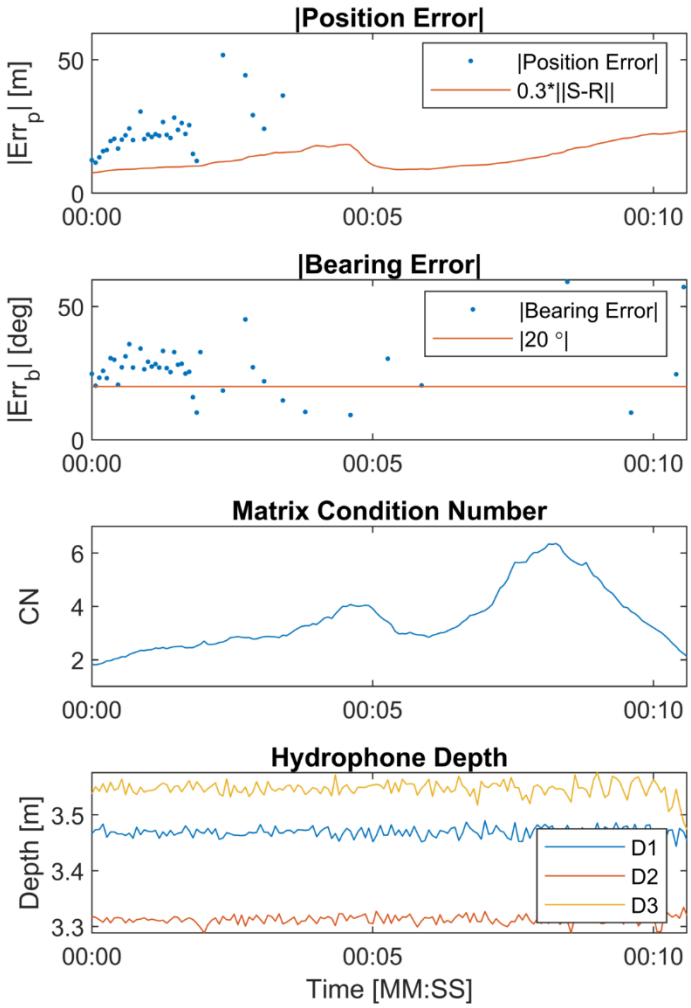

Figure 71: Co-temporal position and bearing error estimates, matrix condition numbers, and hydrophone depths from current testing in Sequim Bay Channel.

Localization of clicks and tones was difficult, principally, because it was difficult to determine their time-differences of arrival (TDOA), a fundamental input to the localization algorithm. TDOAs are commonly calculated as the lag at the point of peak cross-correlation between signals measured by two receivers. This method is less accurate when the signal to noise ratio (SNR) of a signal is low. SNR at all frequencies was a function of frequency dependent background noise levels and of the amount of multi-path interference (e.g., interaction of direct path sound with surface and bottom reflections). The SNR of mid- (10 kHz) through high- (200 kHz) frequency sources was acceptable in a number of trials, as the frequency-dependent absorption was offset by lower levels of ambient noise. SNR at lower frequencies (e.g., 100 – 500 Hz) was lower, which may have been a consequence of greater bathymetric interactions, lower source levels, and/or higher ambient noise.

Due to the poor performance of the cross-correlation method, an alternative approach was used to calculate TDOAs for clicks and tones. The times-of-arrival (TOAs) of each signal were measured manually by analyzing the filtered amplitude envelope of the pressure time series. For each DAISY, the time at which the signal amplitude had unambiguously risen above the noise was taken as the TOA. TOAs were then subtracted from one another to produce TDOAs. Fundamentally, this method

requires sufficient time between the direct arrival of sound and the first reflected arrival, as well as a sufficient signal-to-noise ratio (SNR) to unambiguously identify the initial rise.

3.4.3.4 Broadband Localization Results

The generated tones, clicks, and sweeps approximated some of the sounds measured around wave and current sites to date (e.g., narrowband tones with harmonics produced by generators), but were not representative of any broadband transient sounds (e.g. clicks, chain rattle, wave breaking). Therefore, the localization analysis was extended to vessel engine noise, a proxy for other broadband sounds. Unlike localization of icTalk clicks and tones, localization of engine sound from the deployment vessel did not require manual review to measure times-differences of arrival (TDOA) due to the vessel sound's relatively high SNR. Instead, cross-correlations of windowed co-temporal acoustic data were calculated and the time lag at the peak cross-correlation was taken as the TDOA for each DAISY pair.

Vessel and DAISY GPS positions and localization estimates for an array with DAISYs approximately 25 m from the array centroid are presented in Figure 72. Co-temporal DAISY acoustic spectra, inter-unit cross-correlations, position and bearing error estimates, matrix condition numbers, and hydrophone depths are presented in Figure 73.

Localization absolute position error, calculated as the range between the vessel's estimated position and its GPS position, was typically less than 10 m from approximately 01:00 to 04:00 (relative to start of survey) and from 11:30 to 12:00. In contrast, absolute position error grew steadily from ~10 m to ~100 m from 04:00 to 11:00. An explanation for this trend can be drawn from the DAISY acoustic spectra and from co-temporal array performance metrics such as cross-correlation and the matrix condition number. As seen in the acoustic spectra, the engines were off over this period and the icTalks were deployed (icTalk LF sweeps are visible in the spectra). Over this period, icTalk signals had the greatest SNR, resulting in local maxima in the cross-correlation signals. However, their SNR was still low, relative to the vessel's SNR, resulting in greater TDOA errors and, consequently, position estimation errors. The matrix condition number also increased over this period because the vessel drifted from "within" the array to a position almost 100 m south of the array centroid. Later, after the vessel's engines restarted, the position estimates did not immediately improve because SNR related errors were high, as a result of the range from the DAISYS, and the system of equations was still "poorly conditioned". It is thought that SNR related errors decreased as the vessel returned to the edge of the array at 11:30. Bearing estimation errors followed similar trends.

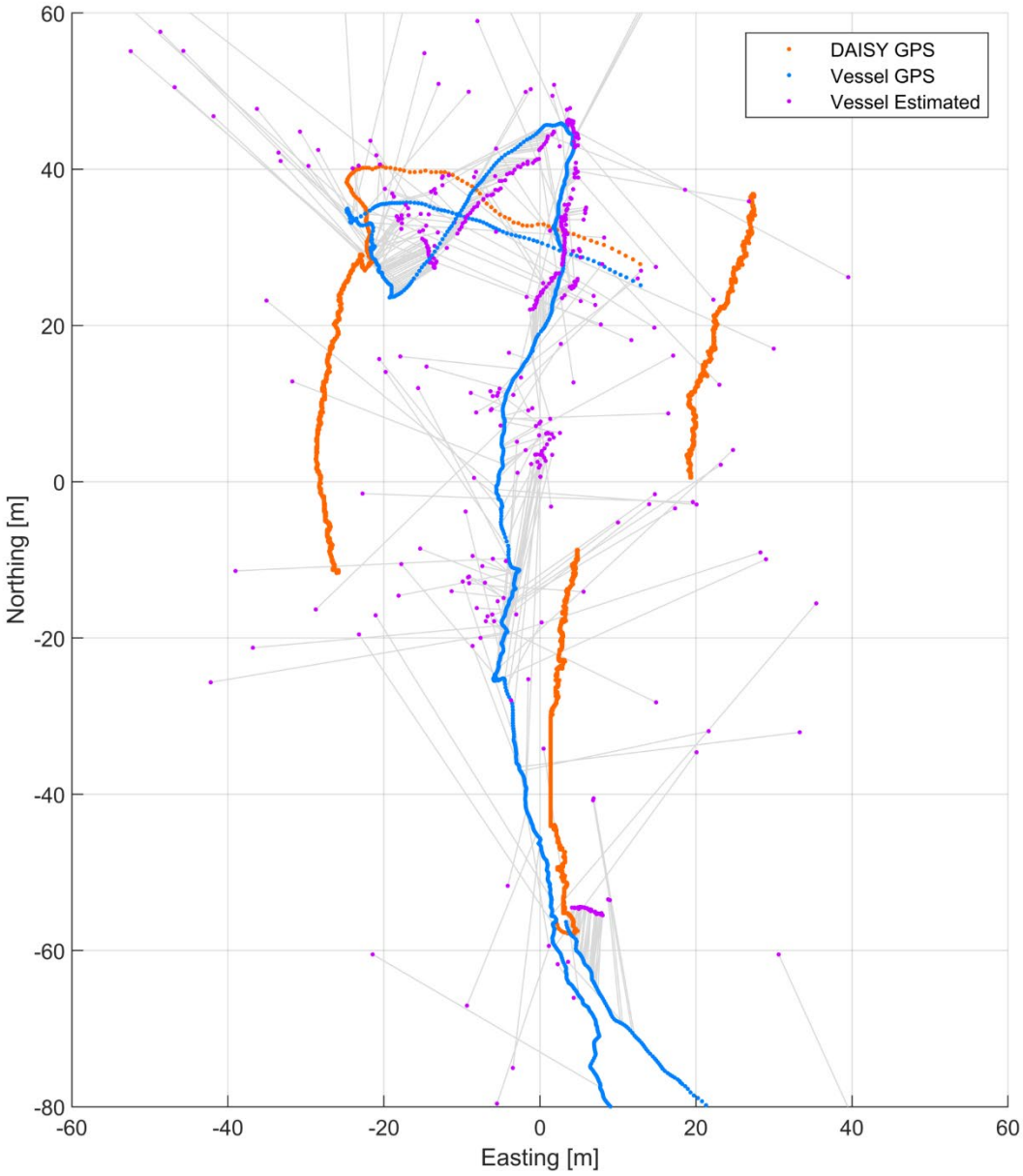

Figure 72: Vessel and DAISY GPS positions and localization estimates for an array with DAISY-centroid spacing of ~25 m. Gray lines indicate the range between an estimated vessel position and the co-temporal position recorded by GPS on the vessel.

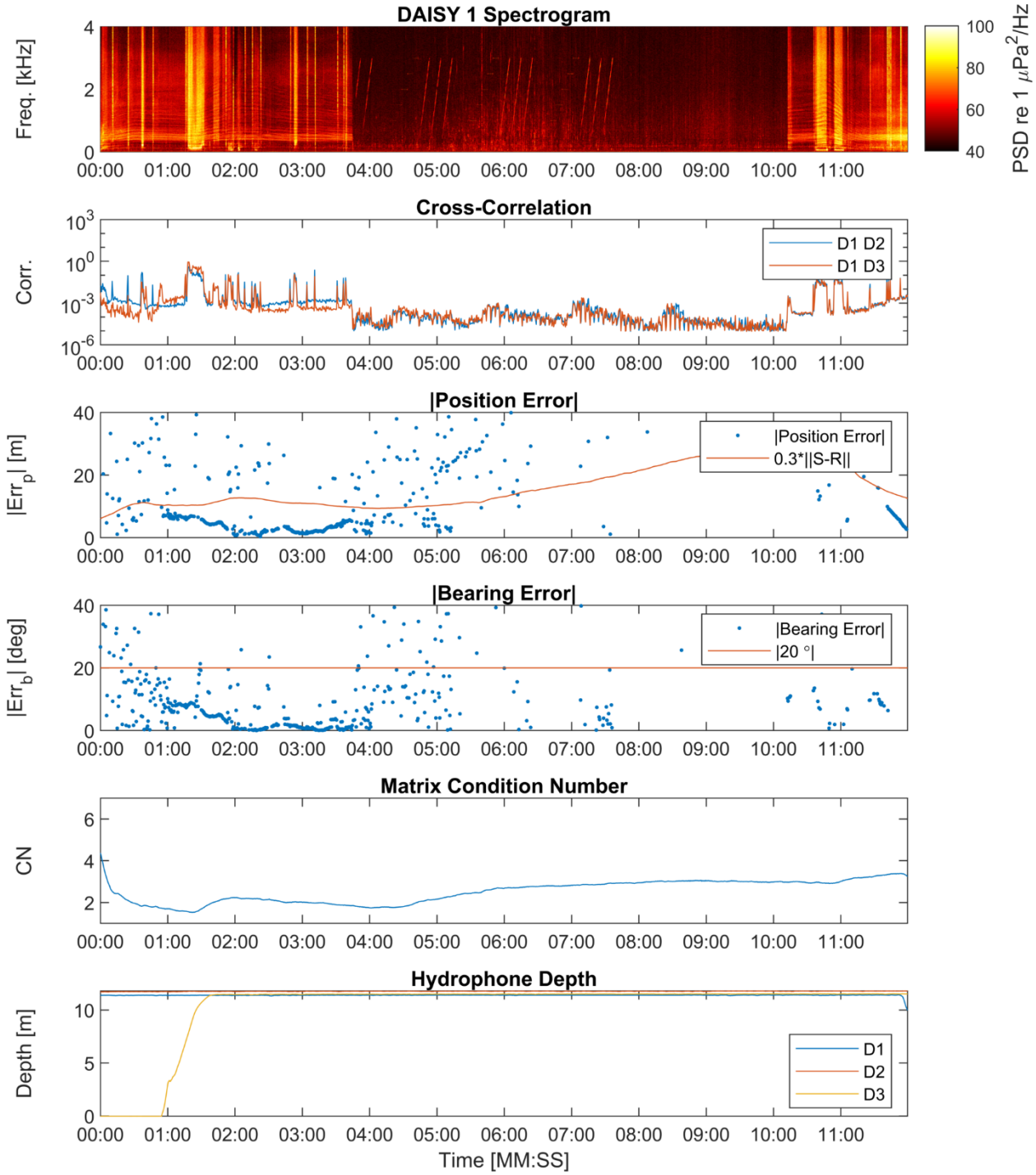

Figure 73: Co-temporal DAISY acoustic spectra, inter-unit cross-correlations, position and bearing error estimates, matrix condition numbers, and hydrophone depths from 25 m quiescent test in Sequim Bay.

3.4.3.5 Conclusions

The underwater soundscape around a marine energy device often contains multiple sources and attribution of each sound to its correct source can be a challenging task. Although pre- and post-installation acoustic surveys using stationary platforms can be used to observe changes in the soundscape, these observations do not always provide all necessary information. Furthermore,

they are not always possible due to economic and time constraints. Source localization with a drifting hydrophone array can help to rapidly identify the origins of sounds, thereby assisting in the accurate attribution of each sound to the correct source.

Wave energy converters, current turbines, and their supporting infrastructure, have been shown to generate sounds with a variety of bandwidths. The successful localization of both broadband and narrowband sounds is an encouraging accomplishment and suggests that a DAISY array will be capable of localizing sounds from marine energy devices, provided that specific criteria are met. Primarily, sources of interest must have sufficient SNR in order to accurately measure their time-differences of arrival, a critical parameter to the localization calculations. Because SNR degrades with increasing distance from source to each receiver, the maximum range that DAISYS can be deployed from a source of interest is set by the signals amplitude relative to other sources of noise (e.g., ambient noise, flow noise, etc.). The arrangement of DAISYs relative to one another and to the source is of secondary importance to source detectability, but can have a significant effect on solution accuracy. Solution error is minimized for equally spaced DAISYs and for a source positioned in the "center" of the array (equidistant from all DAISYs). Finally, confidence bounds on position and bearing estimates must account for measurement uncertainties, of which GPS uncertainty is a significant and unavoidable contributor.

Operationally, it was possible to repeatedly deploy DAISYs in acceptable arrangements in both currents and waves with ease. The experience of the PNNL vessel operators was particularly helpful in this task. Although the initial arrangement distorted over time due to heterogeneous currents, it was easy to reset position when necessary.

Several changes could be made to improve localization results. First, deploying hydrophones in deeper water and at greater depths would help to increase SNR by reducing the effect of surface reflections. However, in currents, there is a risk of the hydrophone becoming offset, beyond GPS positioning error, from the surface expression. Second, deploying a fourth DAISY would permit more accurate solutions to the 2D localization problem. Alternatively, deploying a fourth DAISY with a hydrophone at a different depth than the other three would permit 3D localization using the current method, and would thereby reduce the uncertainty introduced to the solution by depth variation between the DAISY hydrophones and the sound source. Deployment of additional DAISYs (e.g., four DAISYs for 2D localization, five DAISYs for 3D localization) would help considerably with error minimization, particularly in the event that one DAISY is experiencing high GPS uncertainty, timing error, or other failure(s), but could make operations more challenging

3.5 Lessons Learned

3.5.1 Low-frequency Sound Mitigation

Going into BP 2, the project team had concluded that flow-shields provided insufficient flow-noise reduction to justify attenuation at higher frequencies. Early success with a modified flow-shield in BP 2 reversed this thinking and led to significant effort to develop a durable, effective flow-shield. As demonstrated by the relatively low frequency ($f < 10$ Hz) at which flow-noise affects measurements, even in energetic currents, this effort appeared worthwhile[14].

[14] Additional tests conducted with TEAMER support in BP 3 demonstrated that flow shields are effective at reducing flow-noise, but that unshielded drifting hydrophones can also have relatively low levels of flow-noise depending on specific conditions during a drift.

We also note that isolating flow-noise and self-noise from ambient noise can be challenging at the lowest frequencies due to the relatively steep roll-off in hydrophone sensitivity. This factor complicated earlier attempts by the project team to reconcile measurements with analytical models for flow-noise. Calibration to low frequency (i.e., $f < 1$ Hz) can be extremely helpful in this regard.

The primary remaining source of low-frequency self-noise is attributable to line strum, which can mask propagating sound at frequencies up to ~25 Hz. This can be automatically identified in measurements using the algorithm developed under this project. As discussed, this self-noise is strongly correlated with wind speed, which produces relative motion between the DAISY and surrounding water.

3.5.2 Hydrophone Integration

The project team was able to achieve a significant cost reduction by switching to an OEM hydrophone and custom data acquisition system. This did, however, require significant effort from the project team and resulted in substantial project delays due to the general development cycle and long lead time for appropriate hydrophones. Further revisions in BP 3 were able to reduce electrical self-noise at high frequencies ($f > 10$ kHz).

3.5.3 Emphasis on Hardware versus Software

At the start of the project, there was an expectation that the broadband self-noise and flow-noise experienced by the baseline DAISY was unavoidable and that this would need to be addressed through machine learning algorithms to identify and "quarantine" measurement sequences with such contamination. Our experience during BP 2 has been that hardware modification can be effective at eliminating most sources of self-noise and flow-noise, to the point that remaining masking is persistent in time and restricted to low frequencies ($f < 25$ Hz), rather than being intermittent in time and affecting a wider range of frequencies ($f < 1$ kHz). Such masking can be detected by relatively simple and robust algorithms that rely on expected characteristics of the low-frequency acoustic spectra.

3.5.4 Benchmarking Challenges

At the start of BP 2, the intention was to benchmark the DAISY against one or more drifting COTS systems. This proved difficult as neither a "COTS" European system (Drifting Ears) nor a "COTS" U.S. system (M-AUE) could be mobilized. Ultimately, the project team was able to benchmark DAISY performance against a research-grade instrument developed by OSU and fixed, commercial hydrophones in energetic tidal environments. In addition to a limited number of COTS benchmarks, comparisons in a field setting are complicated by variations in received levels with position, hydrophone depth, and time. This means that deviations between systems must be greater than ~5 dB before they can be decisively concluded to be meaningful. This is not to say that benchmarking is unhelpful. Quite to the contrary, it would have been difficult to establish the significance of the electrical self-noise issues on the DAISYs without the comparison to the OSU spar buoy, nor would the benefits of drifting over fixed instrumentation at low frequencies been as apparent. However, the limitations of benchmarking across all frequencies, particularly in shallow, reverberant environments, such as the Sequim Bay entrance channel, must be acknowledged.

3.5.5 Importance of Local Wind Measurements

With the benefit of hindsight, the sensitivity of low-frequency ($f < 25$ Hz) measurements to wind speed could have been anticipated by the hydrodynamic design of the DAISY, which naturally keeps its speed relatively well-aligned to dominant water currents, but renders it sensitive to wind forcing.

However, without the local wind measurement provided by the DAISY met station, it is unlikely that we would have identified this trend. Specifically, had we relied on wind data for the general site, we would not have known that the "outlier" drifts with low self-noise in the channel were consistent with the calmest winds encountered during testing. Early in BP 2, the project team discussed removing the met station from the DAISY build to reduce cost since the wind measurements are not required under IEC 62600-40 and the met station has a relatively high cost ($1000) and more limited durability than other components[15]. In retrospect, this would have been "pennywise, pound foolish" and it is fortunate that we did not make this decision.

[15] Newer versions of the Airmar WX200 are submersible, but the original units were only splash proof.

4 Budget Period 3 (Jun. 2020 – Dec. 2024)

4.1 Overview

The primary objective for BP 3 was to deploy a group of DAISYs around a wave energy converter at the U.S. Navy's Wave Energy Test Site (WETS) in Kaneohe, HI. This would demonstrate DAISY core capabilities, including ease of use, rapid data offload, compliance with IEC 62600-40 survey methodology, and localization of sounds produced by a wave energy converter (WEC). Secondary objectives were to revise the electronics boards to reduce high-frequency (> 10 kHz) self-noise and demonstrate these through an additional round of testing at MCRL. BP 3 milestones are summarized in Table 16. In addition, to collect sufficient data to publish a journal article on DAISY development and performance, the project team collected additional field data in Admiralty Inlet with support from PNNL provided through TEAMER.

Activities during this budget period faced two major challenges: (1) disruption from the COVID-19 pandemic and (2) a historically long gap between WEC deployments at WETS relative to the 2015-2018 time period when multiple WECs were simultaneously operating at two of the berths. Despite these challenges, the end-of-project outcomes were positive with the DAISYs performing as designed and now being offered as a commercial product by commercialization partner MarineSitu.

Table 16: Budget Period 3 Milestones

	Description	Status
Task 7: Energetic Field Deployment		
7.1	Demonstrate that revised electronics boards are able to meet electrical self-noise targets for hydrophone recording system.	Complete (further reductions, potentially reaching hydrophone noise floor, achieved under DE- EE0009959)
7.2	Deploy DAISYs with revised electronics boards at PNNL MCRL to characterize quiescent performance and C-DAISY performance in a tidal channel.	Complete
7.3	Complete test plan for deployment at WETS.	Complete
7.4	Collect acoustic data from WETS.	Complete
7.5	Complete analysis of collected data as specified by test plan.	Complete (publication under review following minor revisions)
Task 8: Commercial Readiness		
8.1	Develop marketing material describing system capabilities and limitations.	Complete
8.2	Post open-source mechanical design and electrical design, as well as software, to pmec.us website.	Complete

4.2 System Refinement and Testing (Task 7.1)

4.2.1 Electronics Upgrades

4.2.1.1 Board Modifications

Going into BP 3, the custom data acquisition board for the HTI hydrophones had been revised to provide performance compliant with IEC 62600-40, except for tonal, high-frequency noise at frequencies greater than 10 kHz. We note that, to date, there are limited indications that marine energy converter produce substantial noise above 10 kHz, but the DAISYs are intended to be compliant with the IEC Technical Specification.

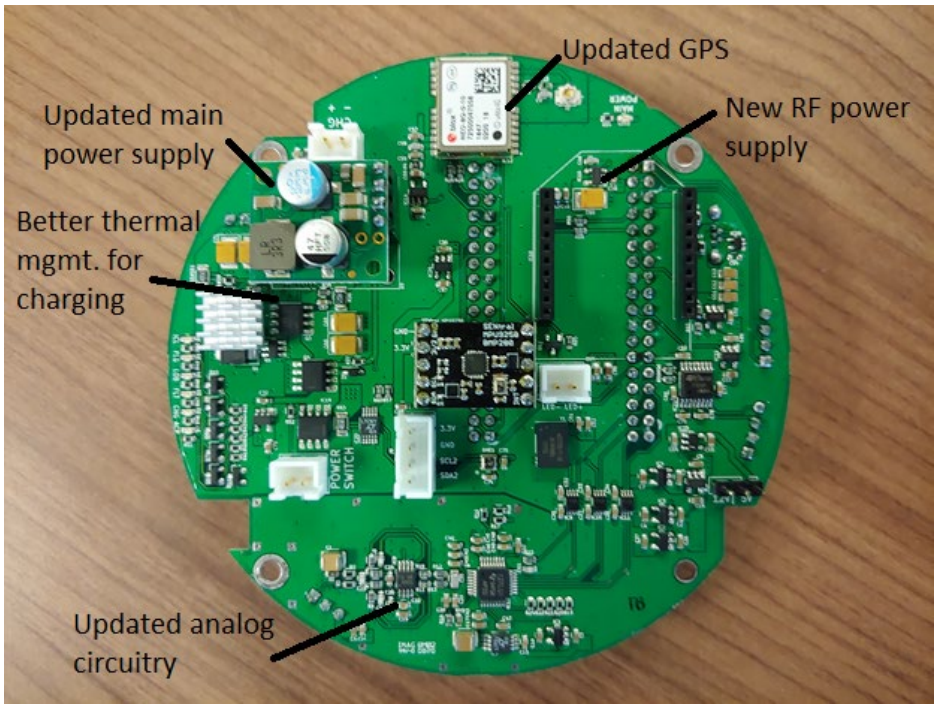

Figure 74: Upgraded electronics boards with major changes marked.

The updated electronics boards, shown in Figure 74 improved overall reliability and performance. A few of the notable improvements include an updated GPS receiver module, a socketed main power supply, improved thermal management, and upgraded power supplies for the RF and USB systems.

The updated GPS receiver has drastically reduced the time-to-fix and improved the DOP (dilution of precision) reported, while using the same GPS antenna as the previous electronics. The previous GPS receiver would generally take more than 30 seconds before receiving a GPS fix with a clear sky view and would report DOP values in the range of 3-5, which are considered “good”. The new GPS receiver generally receives a GPS fix in less than 20 seconds and will report DOP values in the range of 1-2, which are considered “excellent”. Better DOP values should mean improved position tracking and time-syncing – both of which are critical for source localization.

The updated main power supply replaced a linear regulator onboard the previous electronics boards. With the linear regulator in place, the overall electrical efficiency of the system was less than 50%, as most of the power used was being converted to heat by the main supply linear regulator. Moving from the onboard linear regulator to a socketed switching supply greatly improved the electrical efficiency and drastically reduced the internal temperature of the electronics housing.

Better thermal management of the battery charger circuit has reduced the charge time of battery by eliminating the thermal shutoffs that occurred with the previous electronics boards. During peak charge currents, the previous electronics boards would stop charging every 3-5 minutes for 30-60 seconds due to poor placement of the circuit thermistor and ground connectors. The new boards have fixed those issues and now are able to charge the battery without thermal shutdown.

A major problem with the previous board design was poor RF transmission distance, limiting our ability to replace the external GPS dog tracking collars with the DAISYs integrated RF module. The problem stemmed from insufficient power being supplied to the RF module due to poor documentation from the RF module manufacturer. With the power supply issue fixed on the current electronics boards, RF transmission distance no longer appears to be an issue. While maximum transmission distance has yet to be tested to its full extent, it does appear that RF range should be sufficient for most DAISY deployment use cases.

As shown in Figure 75, the updated analog circuitry eliminated the tonal, high-frequency electronic noise and EMI/RFI. Discussions with Texas Instruments component engineers have revealed additional minor changes that could be made in future board revisions. The revisions, which are being reserved for a future board revision, would result in minor improvements to the signal to noise ratio (~1 dB at frequencies > 100 kHz) and phase margin of the analog-to-digital converter driver circuitry.

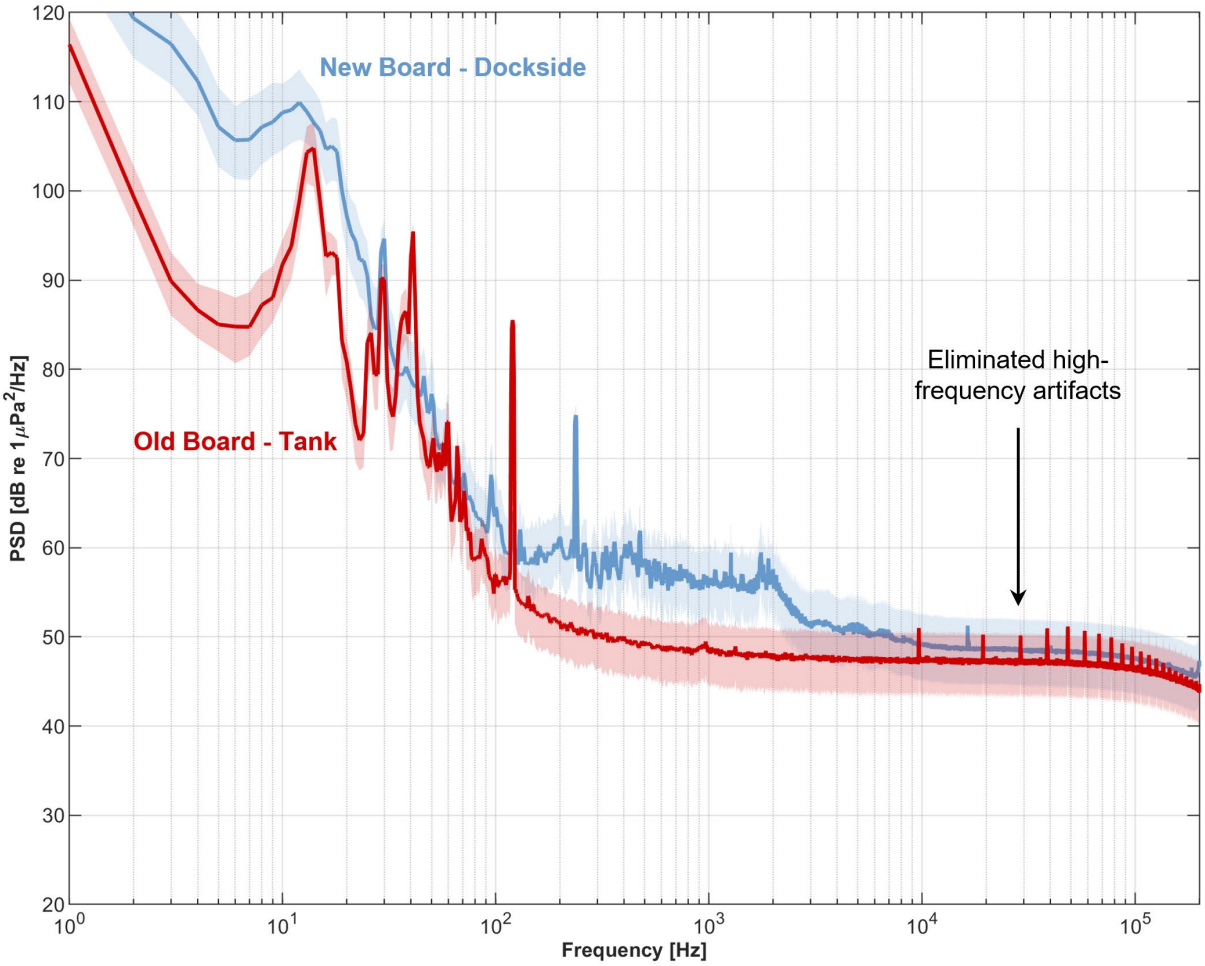

Figure 75: Comparison of new and old printed circuit boards for data acquisition. Note that the old board is tested in a tank with lower ambient noise while the new board is tested dockside in an urban environment.

4.2.1.2 System Calibration

Hydrophone recording packages with the revised electronics were calibrated by PNNL and Ocean Networks Canada (ONC). At PNNL, DAISYs were calibrated by PNNL from 50-200 kHz with azimuthal sensitivity evaluated at 50 kHz. At ONC, a benchtop calibrator was used for frequencies from 1-750 Hz and an in-water calibration against a reference hydrophone used from 2-100 kHz. In addition, both PNNL and UW conducted pistonphone field calibrations around 250 Hz with two types of calibrators.

Results from the calibrations are shown in Figure 76 for the full range of frequencies and in Figure 77 for high frequencies where the ONC and PNNL calibrations overlap. Results are consistent with expected DAISY sensitivities and the UW pistonphone calibration (G.R.A.S. 42AA) overlaps with the ONC low-frequency calibration (black dots in Figure 76). The PNNL pistonphone calibration (Bruel & Kjar at 251 Hz) departs from these, the reason for which could not be identified by PNNL. At high frequencies (Figure 77), the PNNL and ONC calibrations both show significant scatter (which is expected), but do not agree, with ONC predicting higher sensitivity than PNNL at most frequencies. As the two calibrations generally agree around 70 kHz, we have chosen to take as representative a calibration that uses ONC data for frequencies < 70 kHz and PNNL data for frequencies > 70 kHz.

PNNL and ONC evaluated potential reasons for the disagreement between the two calibrations, but were unable to identify a root cause. Different methods are used (tank at PNNL vs. free field at ONC) and the PNNL calibration is accredited, while the ONC calibration is not, but the azimuthal sweeps performed by PNNL at 50 kHz do not always overlap with their baseline measurement (Figure 77).

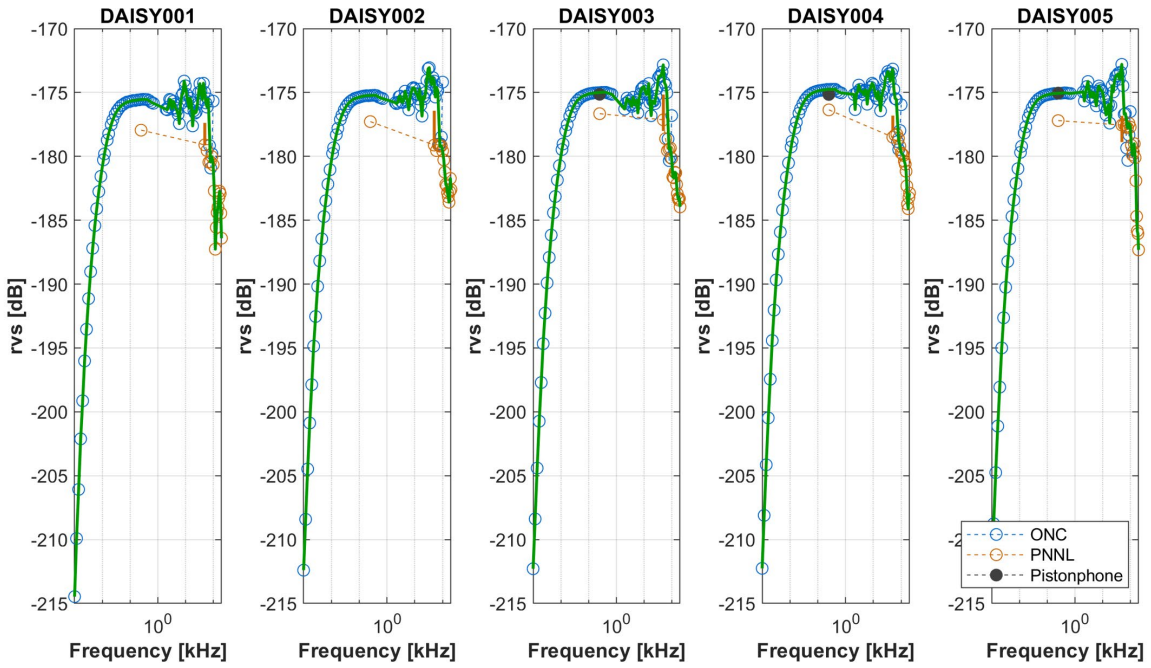

Figure 76: Receive voltage sensitivity from DAISY calibrations (full frequency range). "Pistonphone" refers to UW's G.R.A.S. 42AA field calibrator and was only applied to DAISYs 003-005 (001-002 staged at WETS).

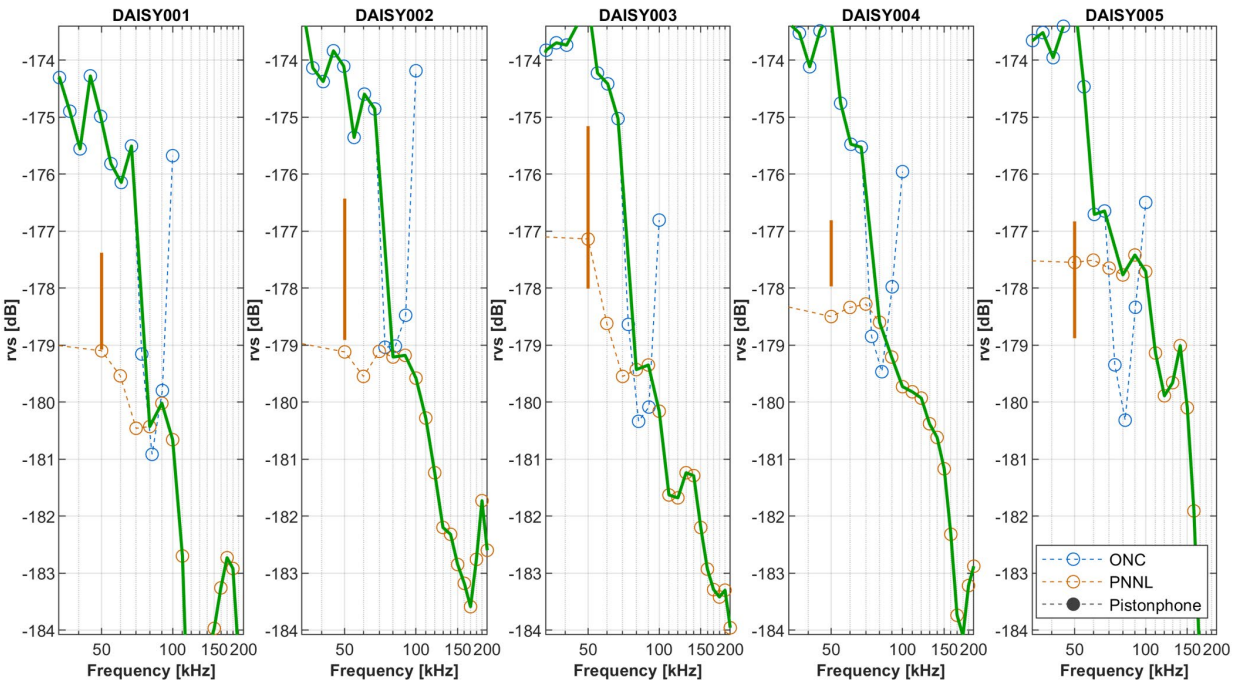

Figure 77: Receive voltage sensitivity from DAISY calibrations (high frequencies only). The orange bar denotes the range of azimuthal sensitivities reported at 50 kHz. The green line is the composite best fit calibration which uses the ONC calibration below 70 kHz and the PNNL calibration above. PNNL azimuthal sweeps do not intersect the frequency sweep for all DAISYs.

4.2.1.3 System Integration Updates

The DAISY firmware was updated to switch off hydrophone data logging while the system is in air, using the data stream from the pressure sensor. This is a small, but important, update to the system that had been planned since BP 1. By restricting hydrophone data logging to submerged periods, the overall data volume is significantly reduced, with commensurate reductions in offload time. The software controls for this had been used for several years to successfully switch off WiFi when submerged, so had been thoroughly vetted before this implementation.

The DAISY post-processing code base includes a suite of software tools built in MATLAB that:

- Parse raw data files, apply frequency-dependent calibrations to the hydrophone data, and merge all data products (e.g., georeferenced sound pressure spectral density levels) into a single file associated with a drift;
- Allow users to compare acoustic data between drifts; and
- Allow users to simultaneously review spectrograms, listen to the underlying audio data, and tag acoustic events of interest.

In the code base developed through BP 1 and BP 2, these post-processing steps significantly increase the files sizes for output files, such that a 5-minute drift might produce a data file > 1 GB. This complicates data sharing and slows down subsequent comparison, review, and annotation activities. However, the file size is significantly inflated by high frequency spectral information (e.g., pressure spectral densities at frequencies up to 200 kHz in 0.001 Hz bands). These high frequency data contain little useful information, since even a relatively tonal sound will have a frequency bandwidth proportional to its center frequency (e.g., a strongly tonal sound at 100 kHz would have a bandwidth of 10 kHz). Because of this, alternatives to constant bandwidth signal processing are

attractive. One such approach in use in the long-term acoustic monitoring community is "millidecade" processing (Martin, et al., 2021), which progressively coarsens the frequency bandwidth in the acoustic spectra at high frequencies, while preserving complete information at lower frequencies (e.g., < 1 kHz). This implementation in the DAISY code base and reduced output file size by approximately one order of magnitude.

4.2.2 Field Verification

4.2.2.1 Test Overview

C-DAISYs with upgraded electronics boards were field-tested at PNNL's Marine and Coastal Research Laboratory (MCRL) on September 28, 2020 (Figure 78). The tests had five objectives:

- Verify that the new electronics boards reduced noise artifacts present in previous builds;
- Verify that modifications to flow shields reduced incidence of self-noise;
- Evaluate the potential for different lengths of rubber cord to reduce the peak frequency for observed line strum;
- Benchmark the DAISYs in quiescent and energetic currents to assess inter-unit variability and performance relative to an unshielded reference hydrophone; and
- Collect additional data to demonstrate localization effectiveness.

Operations were conducted with three DAISYs (S/N 003-005). For most of the deployments, these were configured as C-DAISYs with 2.5 m of rubber cord connecting the surface expression to hydrophone package and oblong fabric flow shields installed around the hydrophones. The reference hydrophone was an icListen Reson previously calibrated by ONC for low frequencies and by Ocean Sonics for high frequencies[16]. This was deployed from an "F-DAISY", a localization float for an underwater drifter, which has a slightly smaller surface expression than a C-DAISY. The icListen Reson was mounted in a DAISY holster and instrumented with an autonomous pressure sensor and IMU, as for the prototype DAISYs tested in BP 1 (Figure 4).

Figure 78: DAISYs drifting as a group for inter-unit comparison study.

4.2.2.2 Results

Between February 2019 and September 2020, a number of final manufacturing tasks were completed for the flow shields to reduce self-noise described in Section 3.3.6.3. These included a "popping" noise attributed to the flow shield spars shifting in their collars. Manufacturing updates included increasing the size of the retaining washer on the end of the spring steel spar and potting the retaining washers in mold putty to restrict their motion. This appears to have been successful in reducing this self-noise. Spar popping only occurred on one DAISY, was intermittent (occurring

[16] Unlike the DAISYs, this was not calibrated at high frequency by PNNL, but prior calibrations of icListen hydrophones by PNNL have shown good agreement with the manufacturer calibrations.

every 10-20 seconds, as opposed to every few seconds), and did not occur on all tests (most prevalent during initial quiescent test).

The DAISY electronics packages recorded data throughout with two exceptions: (1) the met station data collection was intermittent due to an unhandled exception that occurs when the met station is placed horizontally and goes into a "sleep" mode – as occurs when DAISYs are set down on deck – and (2) a restart of one DAISY lower electronics package that was collecting data, but not connecting to the WiFi network. This was substantially better performance than during prior prototype tests where upper and low electronics packages required resets several times during the tests.

Figure 79 shows a comparison between the icListen Reson and two versions of the DAISY – one tested in February 2019 and one with revised electronics boards tested in September 2020. These tests occurred in a quiescent portion of Sequim Bay, with minimal currents, light winds, and limited anthropogenic sound. Several results are notable:

- As expected from dockside testing at UW, the electronics board revision was successful in removing the high-frequency artifacts (spikes) observed in February 2019 DAISY testing.
- The electronics board revision did *not* substantially reduce the high-frequency noise floor for the DAISY.
- The noise floor for the icListen Reson drops below the DAISY at ~100 Hz and is 15 dB lower than the DAISY at 30 kHz (DAISY noise floor ~50 dB vs. ~35 dB for the icListen Reson).

Note that the disagreement between the two DAISYs at lower frequencies is expected, given that these measurements were not co-temporal, with differences in ambient noise associated with wind and anthropogenic activity. During data review, we found that the data acquisition software deployment had a bit shifting error that resulted in jumps in the recorded waveform, which is likely responsible for the "ringing" observed between 100 and 1000 Hz with the DAISY with the revised electronics board. This was easily corrected with a subsequent software fix after a conversation with Texas Instruments application engineers. However, because this ringing would likely degrade the cross-correlation required for time-delay-of-arrival localization, no attempts were made to localize sound sources during these trials.

As the board revisions implemented between February 2019 and September 2020 had been intended to reduce the noise floor, not just remove the high frequency artifacts, this result is somewhat disappointing. While it does not significantly compromise DAISY performance when characterizing current turbines, as demonstrated in the next set of results, and complies with IEC 62600-40 requirements a lower noise floor should be achievable and would be desirable[17].

[17] A series of further upgrades were conducted through DE-EE0009959 and appear to have reduced the noise floor to the fundamental limit for the HTI 99-UHF hydrophone. Further reduction would require a more sensitive hydrophone element, such as the Reson element used in the icListen HF reference hydrophone.

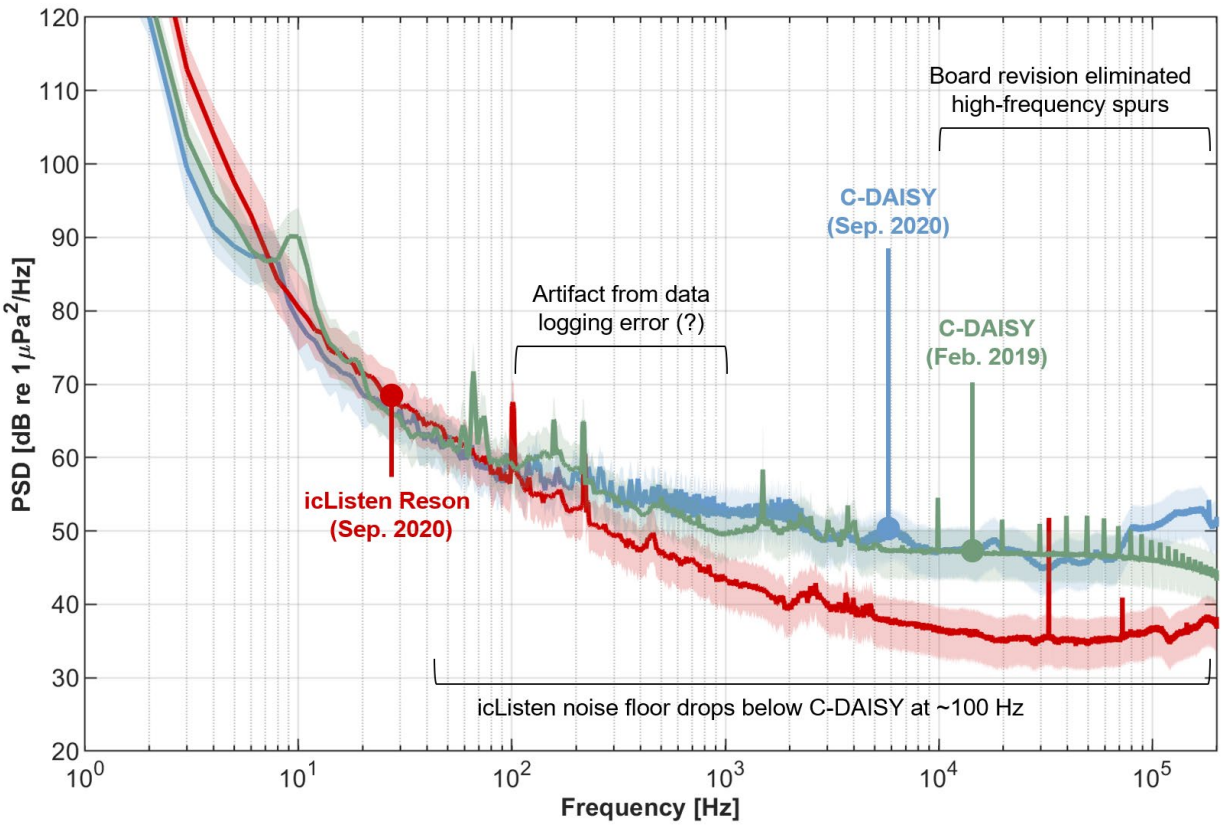

Figure 79: Quiescent comparison between icListen Reson and DAISY versions tested in February 2019 and September 2020. The icListen Reson test is concurrent with the September 2020 DAISY test.

Results from drifts in currents are presented in Figure 80 and produced similarly mixed outcomes. During these tests, DAISYs were released at the mouth of Sequim Bay and carried into the narrow channel by the currents (~1.7 m/s during the time period corresponding to the periodogram in Figure 80). DAISY 001 and 002 were equipped with flow shields, as for the quiescent test, while the flow-shield was removed from DAISY 003 and no changes were made to the icListen Reson from its quiescent configuration.

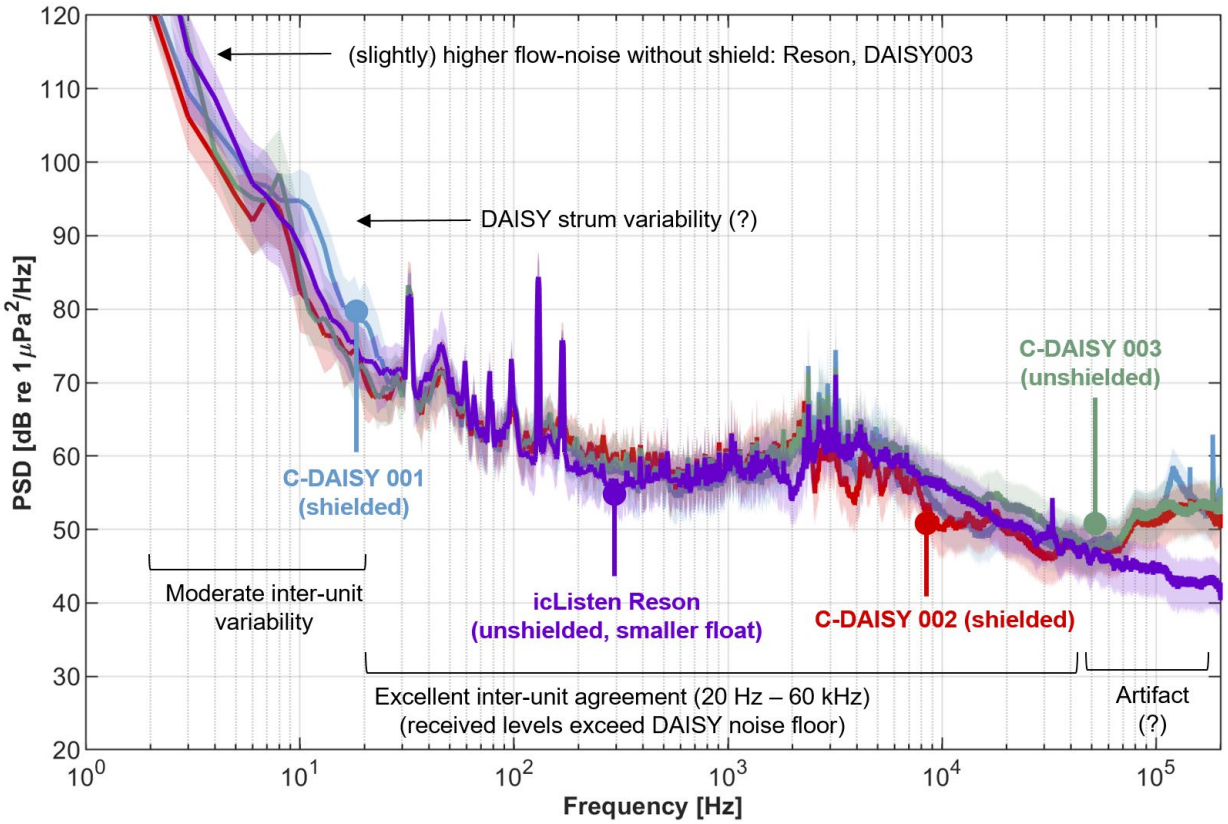

Figure 80: Energetic (1.7 m/s current) comparison between DAISYs and icListen Reson. DAISY 001 and DAISY 002 are equipped with flow shields, while DAISY 003 and the icListen Reson are not.

Because received levels are elevated in the channel at higher frequencies[18], the agreement in this portion of the acoustic spectra between the icListen Reson and DAISYs is much improved relative to the quiescent drift, with excellent inter-unit agreement between 20 Hz and 60 kHz. Above this, as for the quiescent drift, the noise floor for the DAISYs appears to pull away from the icListen Reson. This suggests that the DAISYs can accurately characterize propagating sound in tidal channels over a relatively wide range of frequencies, particularly those relevant to radiated noise from current turbines. At frequencies less than 5 Hz the shielded DAISYs outperform the unshielded DAISY or unshielded icListen Reson by 10 dB, but between 5 and 20 Hz, strum-excited self-noise produces considerable variability across the DAISYs. The unshielded Reson, while having slightly worse performance at the lowest frequencies does not produce strum and generally performs about as well as the shielded DAISYs. This was unexpected, given that tests in BP 2 at the site showed a much larger deviation between shielded and unshielded hydrophones, particularly in DAISY-to-DAISY comparisons. This is possibly explained by the test conditions. While these tests were conducted on a flood tide, most prior tests had been conducted on ebb tides, which may be more turbulent than flood or have greater vertical shear. Similarly, wind speed was quite low during these drifts (< 1 m/s), which minimized differential forcing on the surface expression.

Drifts with different lengths of rubber cords were also inconclusive. These had been intended to test the hypothesis that the peak frequency for line strum would be affected by the length of the tether to the surface expression, as predicted by theory. As shown in Figure 81, varying the length of

[18] A consequence of sediment generated noise, which is audible in all recordings.

rubber cord in the system had no significant effect on the peak strum frequency. As discussed under BP 2, this result is actually consistent with our current understanding that this strum peak is caused by hydrophone vibration that is excited by tether strum, but not directly observing tether strum.

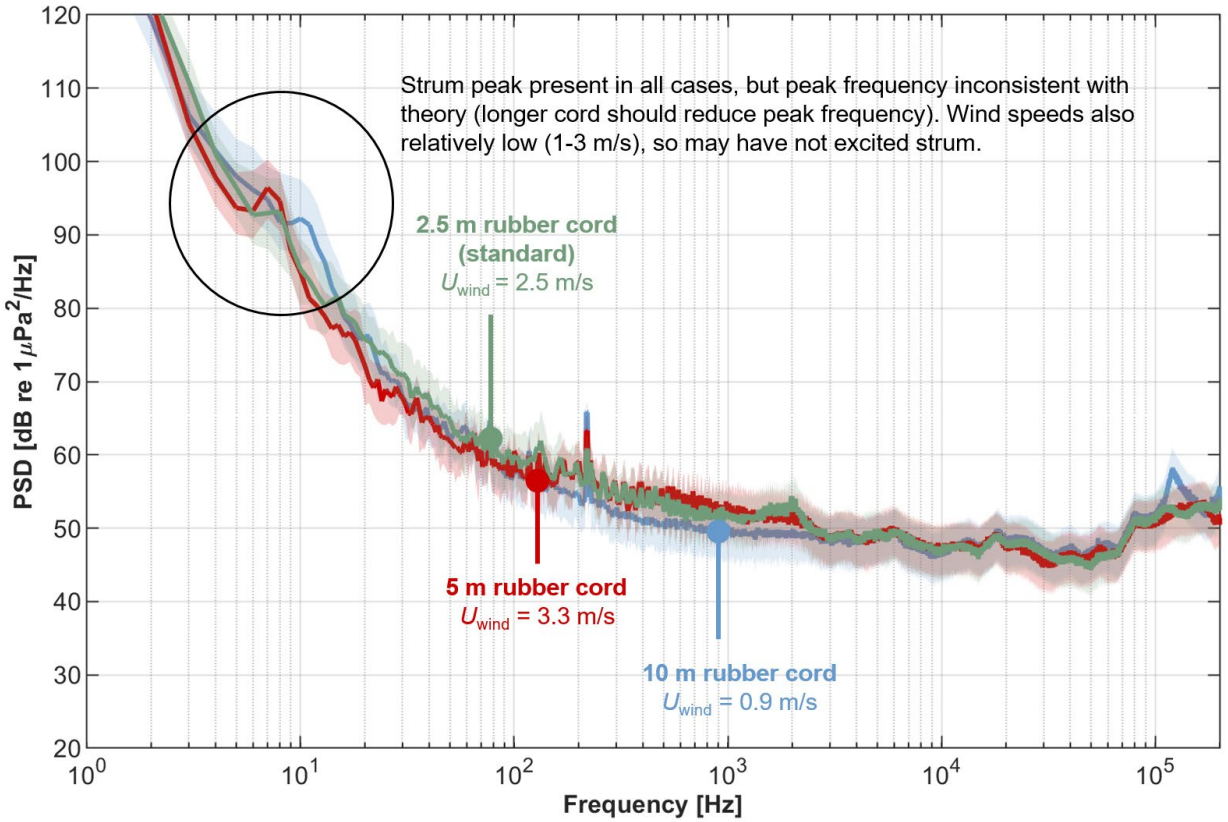

Figure 81: Quiescent comparison between DAISYs with different lengths of rubber cords.

4.3 Energetic Deployment in Currents

4.3.1 Test Overview

An overall project objective was to produce a publication describing the DAISY development and performance benchmarks. While the experiments in September 2020 had been intended to provide the final information for such a publication, the software bit-shifting issue and lack of flow-noise reduction observed for shielded DAISYs motivated an additional round of testing in Admiralty Inlet, WA. At this site, the greater water depth would allow longer tethers to be employed (more characteristic of conditions for a survey around a utility-scale current turbine) and stronger currents would pose a stringent test for flow-noise reduction. Because PNNL funding to support DAISY tests under Triton had been exhausted, their activities were supported through a successful TEAMER application. These tests were successful and were incorporated into the DAISY development publication (Polagye, et al., 2025).

4.3.2 Measurements

DAISYs were deployed in Admiralty Inlet, WA on July 14, 2022 in the high-current region adjacent to Admiralty Head. During these drifts, four DAISY variants were employed:

- *Configuration 1*: Standard DAISY equipped with a flow shield to suppress flow noise;
- *Configuration 2*: Standard DAISY with flow shield removed;
- *Configuration 3*: Standard DAISY without a flow shield and with the hydrophone replaced by an acoustic Doppler velocimeter; and
- *Configuration 4*: An early prototype DAISY with a smaller surface expression, more compact recording hydrophone system, and no flow shield.

4.3.3 Results

During deployment, DAISY speed over ground exceeded 3 m/s, nearly twice the maximum current speed during previous tests in the entrance channel to Sequim Bay. As shown in Figure 82, for unshielded DAISYs, flow noise contamination could be as high as 30 dB at frequencies up to 30 Hz. However, contrary to expectations, no clear trends were observed with tether length (either in terms of flow-noise amplitude or self-noise). As shown by simultaneous acoustic Doppler velocimetry (Figure 83), this is likely a consequence of limited variations in relative velocity and turbulence with depth.

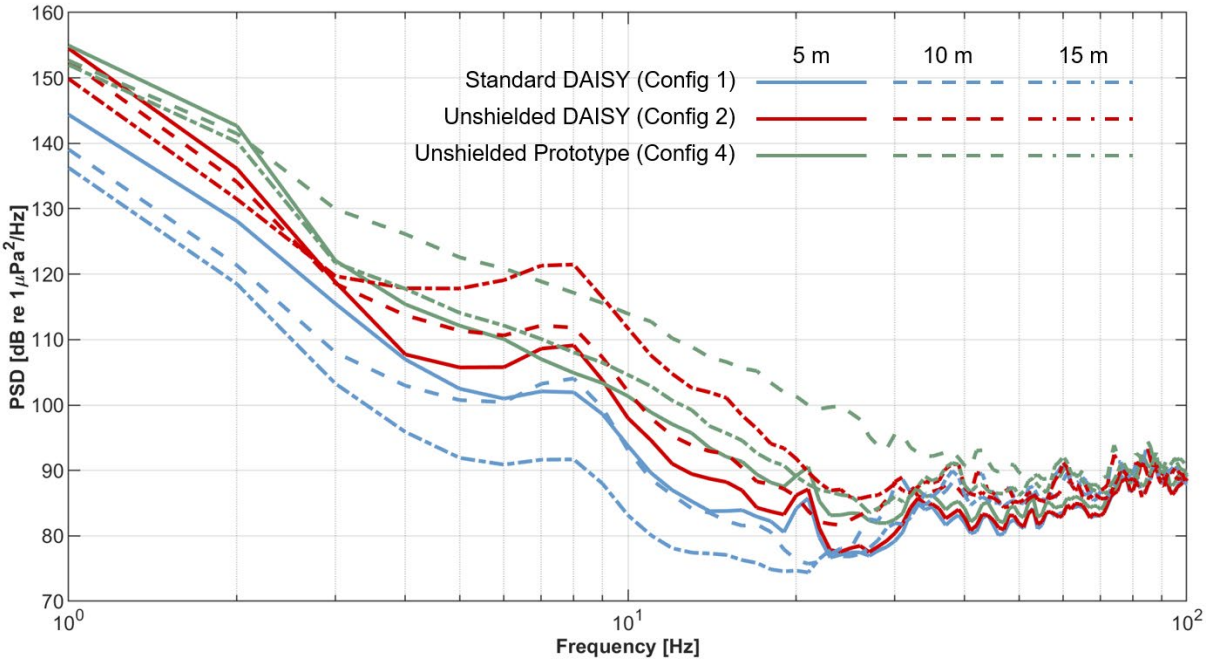

Figure 82: Median acoustic pressure spectral density levels across all DAISY variants and tether lengths, emphasizing the region impacted by flow noise and line strum (1-100 Hz).

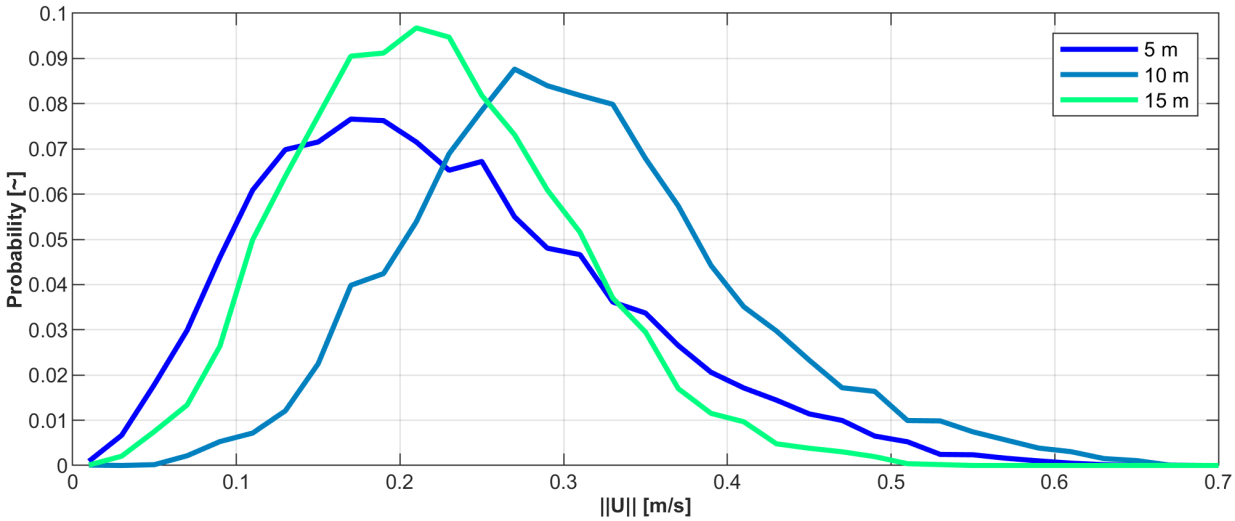

Figure 83: Probability distribution of relative velocity magnitude as a function of tether length as measured by drifting ADV.

Given that the relatively velocity measurements are not explanatory of the differences observed across the DAISY variants, we considered the implications of time series metadata from the pressure sensor and accelerometer deployed with each hydrophone. As shown in Figure 84, with a 5 m tether, hydrophone depth is relatively stable, tilt angles of the hydrophone relative to vertical are generally < 10° and there is limited flow noise for any of the configurations

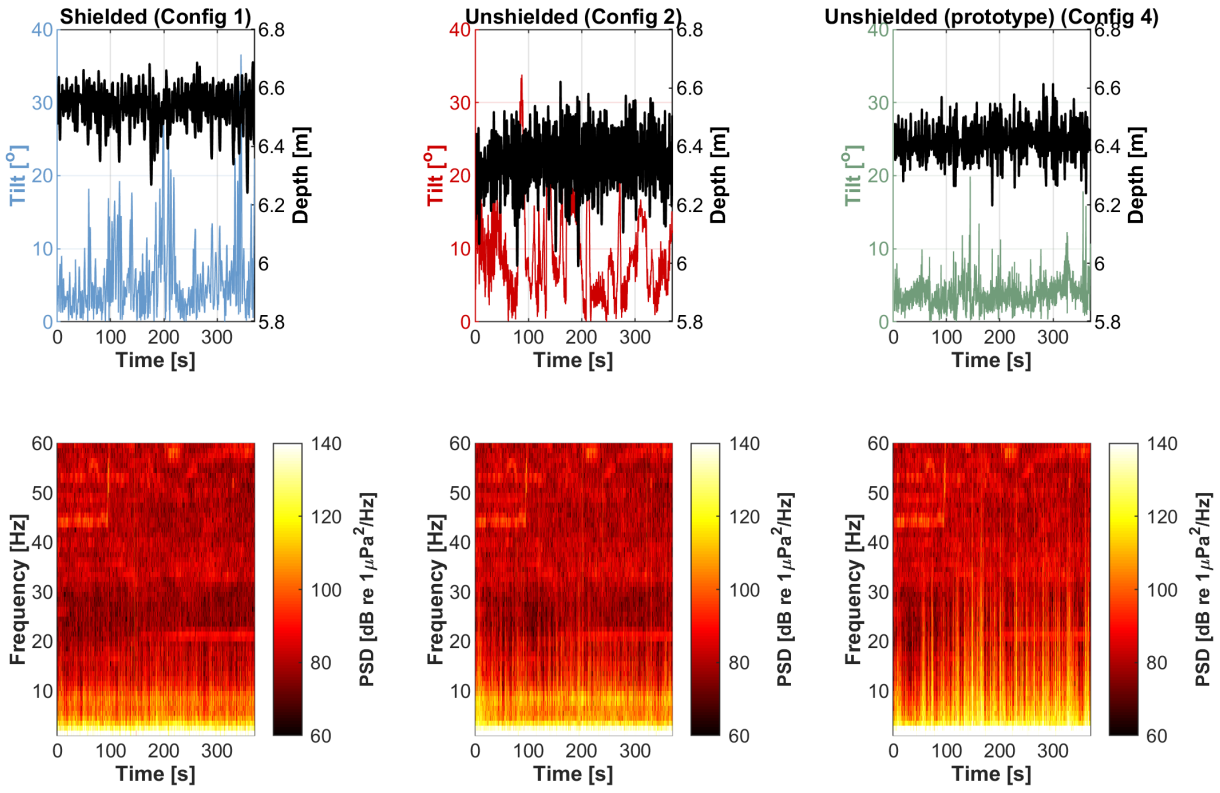

Figure 84: Comparison between DAISY orientation and low-frequency noise for 5 m tether length. (top row) Hydrophone tilt relative to vertical axis (colored by DAISY configuration) and hydrophone depth (black lines). (bottom row) Low-frequency spectrogram, emphasizing frequencies impacted by flow noise. Persistent hydrophone strum at ~7 Hz is apparent in the spectrograms for Configs 1 and 2.

With a 10 m tether (Figure 85), each hydrophone experiences significant depth excursions during different parts of the drift, likely because of interactions with coherent turbulent structures. However, these differences may have more to do with spatial and temporal evolution in the currents than a fundamental variation with depth as each set of drifts originated from a slightly different location and the structure of the tidal currents evolved over the survey. When interacting with coherent turbulent structures, hydrophone depth decreases and the tilt angle increases (e.g., around 250 s for Config 2). Given that these excursions are also the times during which flow-noise is elevated on the unshielded hydrophones, it is reasonable to interpret these as periods with higher than average relative velocity. While the shielded hydrophone also experiences a similar excursion in depth and tilt, this does not increase flow-noise due to the benefits of the flow-shield.

These trends extend to the 15 m tether (Figure 86). Here, the unshielded DAISY (Config 2) experiences a large depth and tilt excursion, with a correspondingly large increase in flow noise. The prototype unshielded DAISY (Config 4) has steady depth but experiences a tilt excursion near the end of the drift that is correlated with increased flow-noise. We interpret this as relative velocity producing drag on the hydrophone assembly, such that it slightly changes depth due to line angle and experiences a moderate relative tilt. A similar event is visible for the 10 m tether on Config 2 from ~10-100 s (Figure 85, note differences in y-axis depth scales). We hypothesize that such events become more probable as tether length increases due to vertical shear in the water column.

In summary, for an unshielded hydrophone, there are two mechanisms that likely increase relative velocity. The first is entrainment in a coherent structure, which manifests as a depth and orientation change for the hydrophone. The second is vertical shear between the surface expression and hydrophone, which manifests primarily as a sustained tilt excursion. This can occur when the surface expression is the dominant source of drag in the system.

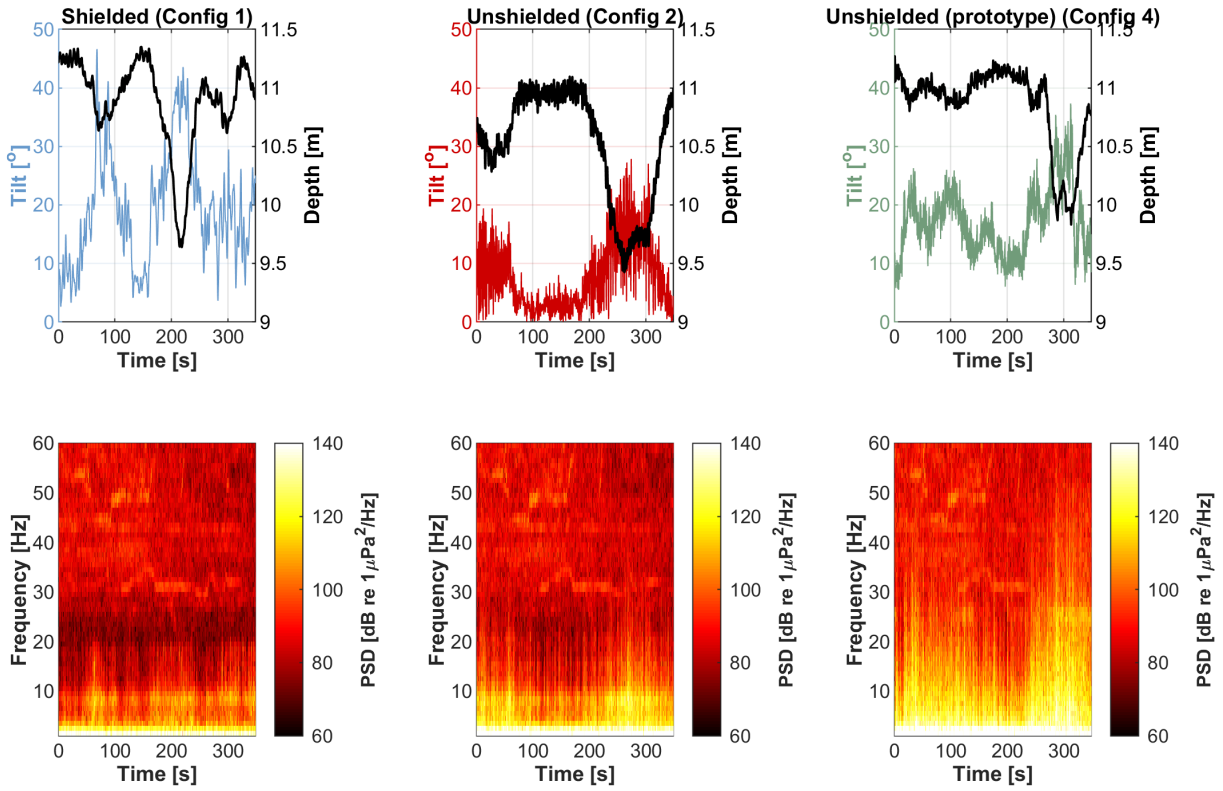

Figure 85: Comparison between DAISY orientation and low-frequency noise for 10 m tether length. (top row) Hydrophone tilt relative to vertical axis and hydrophone depth. (bottom row) Low-frequency spectrogram.

Neither of the mechanisms occurred continuously for all DAISY variants tested, such that unshielded hydrophones *could* achieve comparable performance to shielded hydrophones during favorable conditions. On the other hand, even when shielded hydrophones encountered turbulence and shear, flow-noise levels remained relatively low. These results indicate that flow shields for drifting systems can substantially increase certainty in high-quality data yield at low frequencies (< 100 Hz). Because flow-noise is relatively high intensity, it can rapidly mask ambient noise at these frequencies. As such, controlling flow-noise to the extent possible is essential to reporting accurate "broadband" acoustic quantities, such as sound pressure level, or pressure spectral densities at relatively low frequencies. If sound pressure levels are substantially inflated by flow noise, this can lead to substantial over-estimates for the acoustic footprints of marine energy converters.

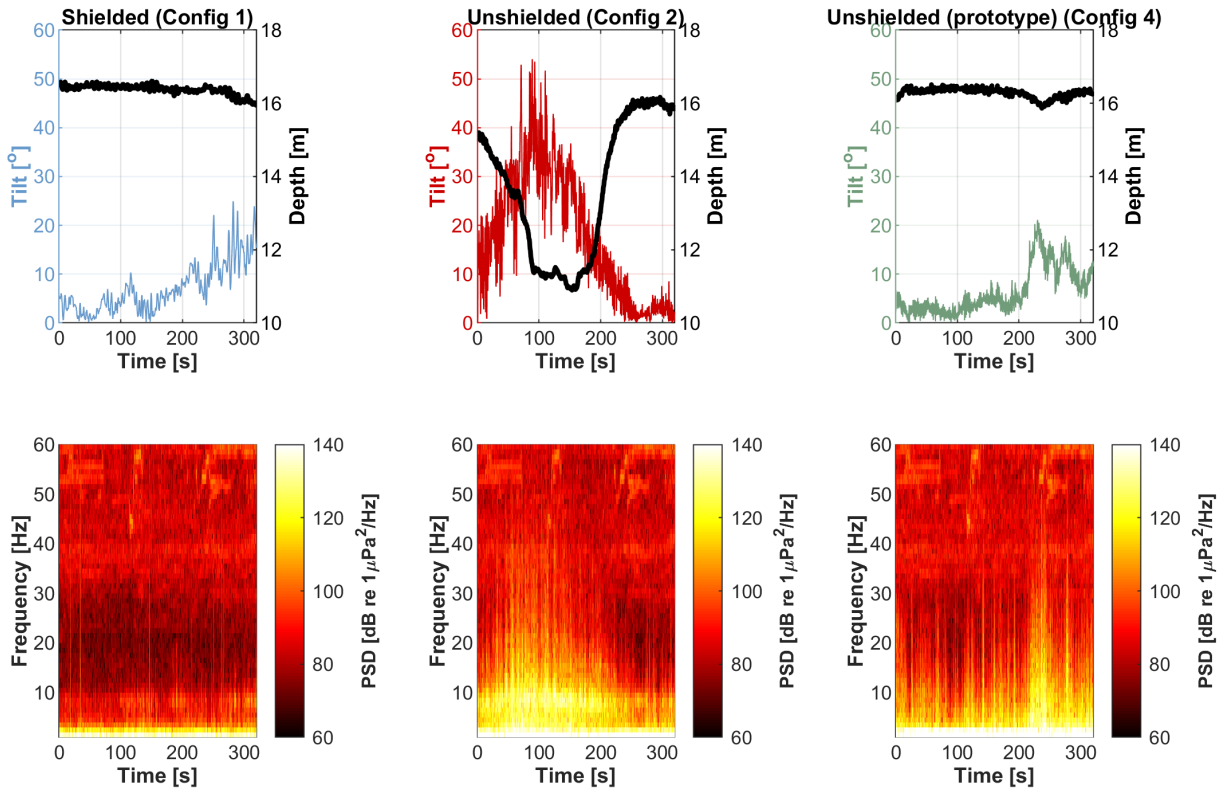

Figure 86: Comparison between DAISY orientation and low-frequency noise for 15 m tether length. (top row) Hydrophone tilt relative to vertical axis and hydrophone depth. (bottom row) Low-frequency spectrogram.

A secondary objective was to investigate approaches to reducing line strum relative to the standard rubber cord on the DAISY by testing the performance of DAISYs with a bare line and a faired line. Performance across tether types and lengths are summarized in Figure 87. In general, the bare line produced the most strum and the faired line the least. The rubber cord induced limited strum for one drift (10 m tether length), consistent with the variability in relative velocity observed in the DAISY variant tests. During these tests, hydrophone packages on all tether types experienced significant depth excursions and tilt variations, but the flow shield was universally effective in suppressing flow noise to a similar range as observed for the shielded hydrophone in the DAISY variant tests (Figure 82). In these conditions, unshielded hydrophones would likely have experienced high intensity flow noise.

We note that in prior tests at MCRL, strum was only observed in quiescent drifts when wind speeds substantially exceeded 2 m/s. Here, we observed significant strum at wind speeds < 1 m/s. Given the relatively shallow depth of prior trials in the Sequim Bay entrance channel, it is likely that the depth was insufficient for relative velocity from turbulence and/or shear to generate line strum from currents.

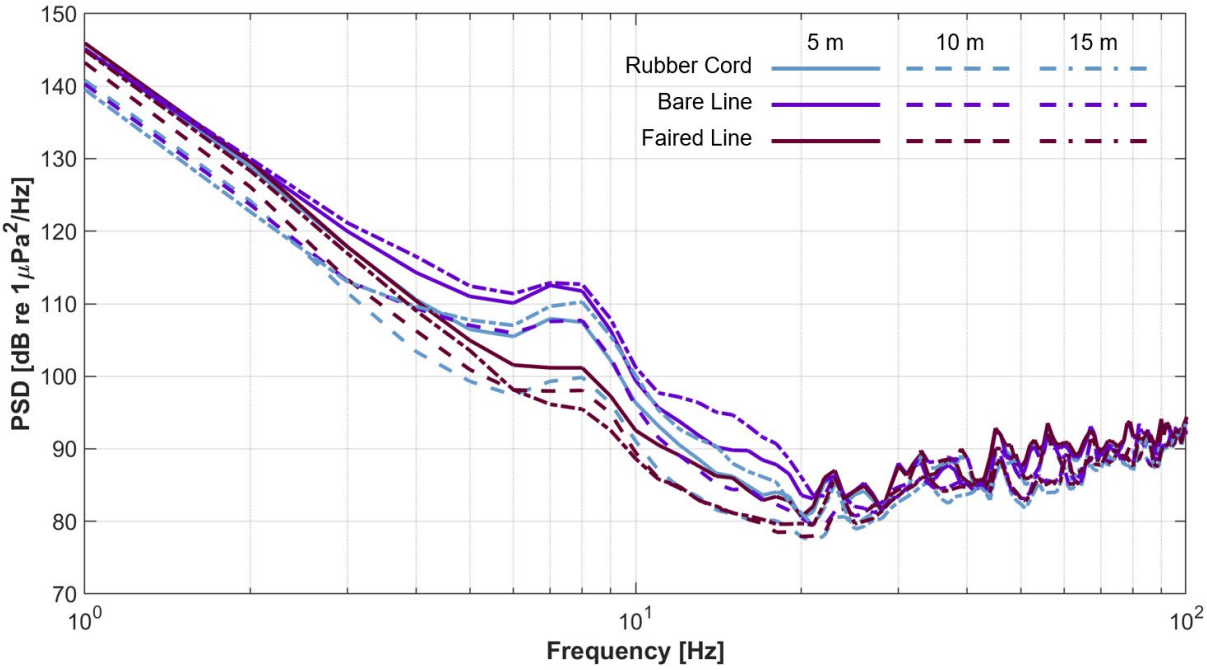

Figure 87: Median acoustic pressure spectral density levels across all tether types and lengths, emphasizing the region impacted by flow noise and line strum (1-100 Hz).

The faired line proved generally effective at reducing strum. However, the fairing approach taken for this study (flags of vinyl tape) is unlikely to be durable over multiple deployments. Faired lines of an appropriate diameter are produced by some line manufacturers but are not generally stocked by retailers. Similarly, commercial, modular fairings are available, but to equip a 15 m line with one type of modular fairing would cost $1000, which is ~50% of the cost of a DAISY. As with all low-frequency flow noise and self-noise mitigation measures, it is necessary to balance costs and benefits. In wave energy environments, the benefit from a faired line might be more limited, as the stretch in the rubber cord provides important benefits to the overall mass-spring-damper characteristics of the system that suppress flow noise from wave-induced motion of the surface float. It might be possible to reproduce these characteristics using a shorter section of tether with more compliance than a rubber cord and a faired static line over most of the depth.

Overall, this field test demonstrated the benefits of flow-shields, as well as identifying likely sources of flow-noise through analysis of available metadata.

4.4 Energetic Deployment in Waves (Task 7.2)

Three WECs were scheduled for near-term deployment at WETS in 2019:

- Ocean Energy's OE35 oscillating water column;
- Oscilla Power's Triton-C point absorber; and
- CPower's SeaRAY point absorber.

The initial deployment plans were scoped around the OE35 deployment, but the WEC suffered severe damage during its tow from Oregon to Hawai'i and several years elapsed as insurance claims were settled and dry dock time was scheduled for repair. This WEC was ultimately deployed at WETS in August 2024, but never connected to the grid to complete commissioning due to the lack of available weather windows. The Triton-C similarly arrived in Hawai'i in 2020, but is still

awaiting a suitable weather window for deployment. CPower's SeaRAY was successfully deployed in early July 2024 and served as the focus for the DAISY survey.

4.4.1 Test Plan Development

The primary objective of the test plan was to execute a "Level B" characterization under IEC 62600-40 specifications. This requires measurements to be obtained within one of four zones (squares, 25 m on edge) positioned at 90 degree offsets at a range of 100 m from a WEC (Figure 90). Because the SeaRAY was a relatively small WEC, a modified set of survey zones were established at closer range which would have higher signal-to-noise ratios. The original test plan included localization with five DAISYs, but because of the rapid response nature of the deployment and other project commitments, only three were available. While three DAISYs had been shown to be effective at localizing sound from vessels and prescribed sources (Section 3.4.3), experiments at WETS had found that localizing other noise (e.g., mooring chain) required five DAISYs. In retrospect, this was determined to be a methodological error but resulted in no emphasis placed on DAISY orientation relative to the WEC during this survey (i.e., arranging DAISYs to bracket the WEC).

4.4.2 Measurements

Each of the three W-DAISYs was configured with a surface expression, 7 m tether, heave plate, 2.5 m tether, and hydrophone recording package. Surveys were conducted on July 15 and July 16, 2024 (Figure 88).

Figure 88: DAISYs deployed around C-Power's SeaRAY wave energy converter at WETS on July 16 (credit: Aidan Hunt, UW)

On July 15, the following operations were conducted:

- An intercomparison of the three DAISYs at a reference location ~1 km from SeaRAY and similar depth (this confirmed that all three instruments had similar performance in the same soundscape);
- A survey at moderate range (~100 m) from SeaRAY with a pair of DAISYs, while the third DAISY remained at the reference location; and
- A survey at close range (< 50 m) from SeaRAY with a pair of DAISYs, while the third again remained at the reference location.

The reference location serves as a pseudo baseline in that sounds from distant sources will have similar intensity as around SeaRAY and, by choosing a similar water depth, the high-frequency (> 10 kHz) contribution from snapping shrimp should be similar between the two locations. This baseline can be a helpful method for identifying sounds attributable to a specific source by visualizing the differences between measurements at close range to the source and at the reference location.

The relatively limited set of measurements on July 15 was driven by two factors. First, working conditions were challenging with the significant wave height exceeding the forecast by ~0.7 m, a relatively short peak period (~5 s), and strong winds (20 mph). This resulted in steep, breaking waves throughout the survey. Second, because SeaRAY is on a single point mooring, it has a watch circle of roughly 100 m. While C-Power's real-time GPS was rendered inoperable during deployment, the back-up GPS, which reports position daily, had indicated a stable position roughly 50 m west of the as-deployed coordinates. On site, we assessed WEC position using a handheld GPS at close range, and found that this position was off by ~75 m and that the WEC position was appearing to change appreciably (~ 30 m) between the two surveys (this was later determined to be an optical illusion). Because the IEC survey methodology involves a zone-based survey at known distance and bearing to the WEC, this could not be executed without a better estimate of WEC position.

At the suggestion of the vessel captain, we procured a golfing range finder on the afternoon of July 15 to establish range to SeaRAY. On July 16, we again deployed and conducted four drifts with three DAISYs. Three of these involved measurements at ~100 m in an arc around the WEC and one of these involved measurements beginning at ~25 m range. Operational conditions were substantially less challenging with the significant wave height falling below the forecast by ~0.7 m and less gusty winds. The range finder proved effective at obtaining distances out to 100 m, but at greater ranges (e.g., 150 m), accuracy was likely on the order of ±10 m because of the difficulty of differentiating between laser returns from the WEC and intervening waves.

4.4.3 WEC Position Determination

As shown in Figure 89, trilateration of SeaRAY position during three recovery and redeployment cycles (six ranges from known vessel position in a relative short time window) produced three, closely-spaced estimates for SeaRAY position. These were consistent with handheld GPS waypoints obtained on July 15 at a range of roughly 10 m (visual estimate). Based on this information, we believe that SeaRAY location did not appreciably change over the two days of survey activity and used the average of the three positions as the best estimate for SeaRAY position.

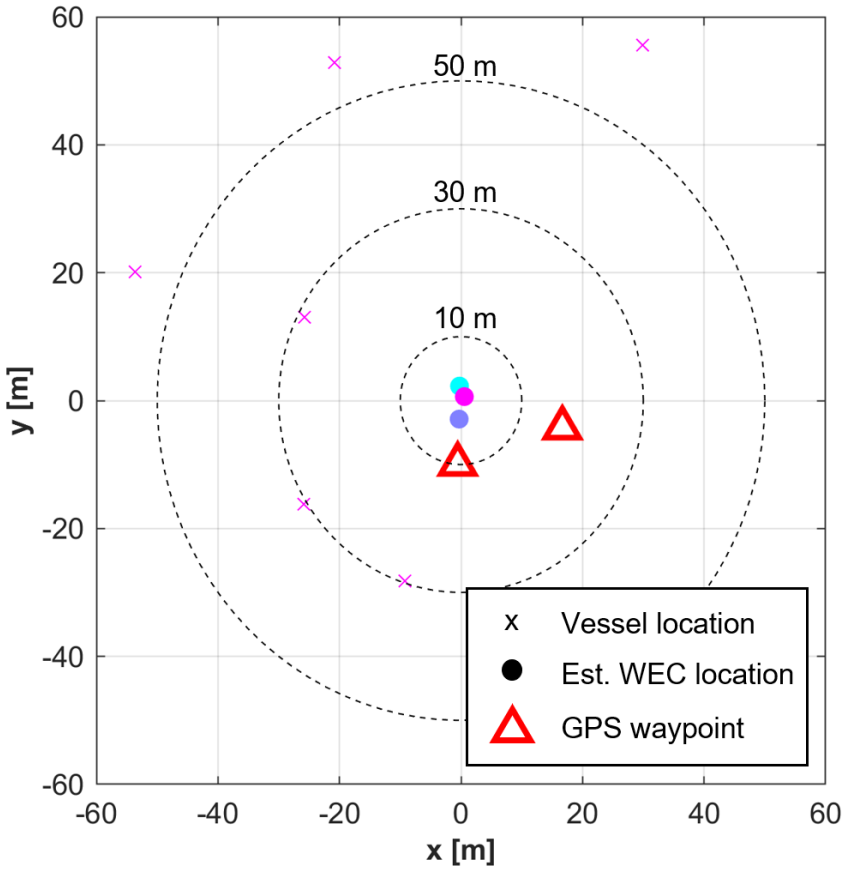

Figure 89: Estimated SeaRAY position based on trilateration and GPS waypoints

4.4.4 DAISY Data

DAISY tracks around the SeaRAY are shown in Figure 90, along with IEC survey zones. As seen in Figure 90, a limited number of tracks overlap the IEC survey zones and, as subsequently discussed, insufficient information was obtained from any zone to be fully compliant with IEC Level B methodology. This was a consequence of the necessity of defining the zones post-survey since accurate information about the WEC location was not available during the survey. While this could have been compensated for by deploying DAISYs in a "blind" manner to saturate the area around the WEC, this would have increased the required survey time by at least an order of magnitude.

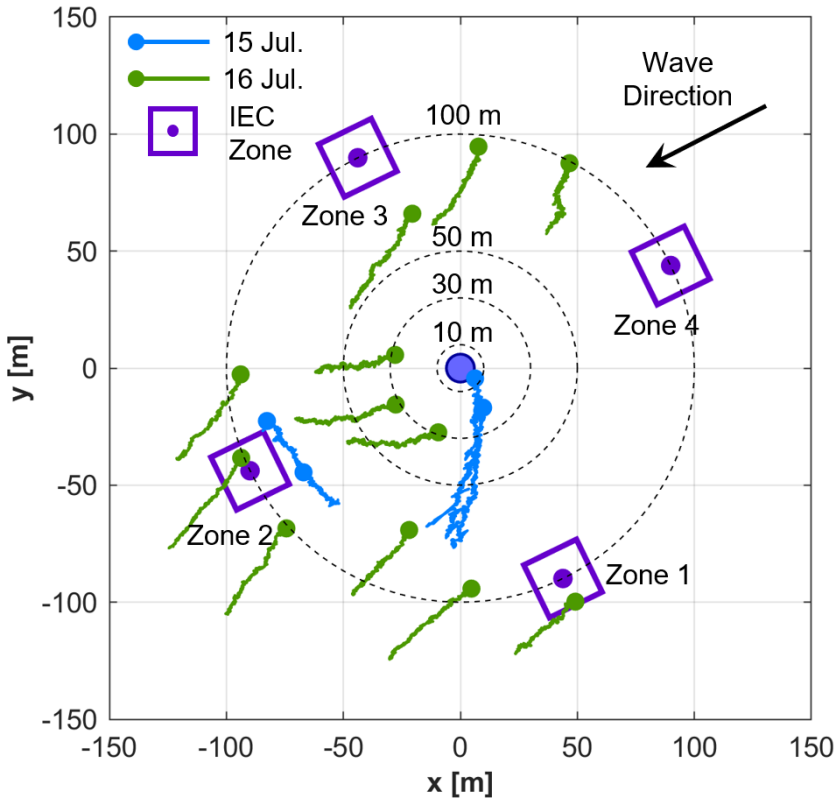

Figure 90: DAISY tracks around SeaRAY (coordinate origin). Concentric circles denote ranges relative to origin. Large dotes denote the starting position for each DAISY track.

DAISY metadata is summarized in Table 17. Sea state information is from CDIP buoy 225, which is positioned at WETS and maintained by the University of Hawai'i. The significant wave height and energy period were relatively consistent over both days of survey effort and winds were moderate throughout. DAISY hydrophone depths were consistent with expectations and reflect minor variations in tether lengths from the manufacturing process.

Table 17: DAISY metadata from SeaRAY deployment

DAISY S/N	Location	Speed over Ground [m/s]	Wind Speed [m/s]	Hydrophone Depth [m]	H_s [m]	T_e [s]	Dir. [deg]
			July 15, 2024				
001	Ref.	0.59 ± 0.34	6.4 ± 0.9	12.0 ± 0.1	1.7	5.9	68
002	Ref.	0.61 ± 0.36	6.5 ± 1.0	12.2 ± 0.1	1.7	5.9	68
003	Ref.	0.63 ± 0.36	6.5 ± 1.3	11.7 ± 0.1	1.7	5.9	68
001	SeaRAY	0.6 ± 0.35	6.1 ± 0.9	12.2 ± 0.1	1.8	6.1	64
002	Ref.	0.67 ± 0.36	6.3 ± 1.2	12.4 ± 0.1	1.8	6.1	64
003	SeaRAY	0.61 ± 0.35	6.4 ± 1.5	11.8 ± 0.1	1.8	6.1	64
001	SeaRAY	0.63 ± 0.38	6.3 ± 1.0	12.3 ± 0.1	1.9	6.2	61
002	Ref.	0.64 ± 0.38	6.4 ± 1.1	12.5 ± 0.1	1.9	6.2	61
003	SeaRAY	0.7 ± 0.5	7.0 ± 1.4	11.8 ± 0.1	1.9	6.2	61
			July 16, 2024				
001	SeaRAY	0.56 ± 0.3	5.4 ± 0.9	12.0 ± 0.1	1.6	6.3	64
002	SeaRAY	0.55 ± 0.28	5.8 ± 1.0	12.3 ± 0.1	1.6	6.3	64
003	SeaRAY	0.52 ± 0.29	5.7 ± 1.0	12.1 ± 0.1	1.6	6.3	64
001	SeaRAY	0.56 ± 0.3	5.1 ± 0.8	12.0 ± 0.1	1.6	6.2	62
002	SeaRAY	0.55 ± 0.31	5.5 ± 0.9	12.4 ± 0.1	1.6	6.2	62
003	SeaRAY	0.54 ± 0.32	5.4 ± 1.1	12.1 ± 0.9	1.6	6.2	62
001	SeaRAY	0.56 ± 0.3	4.6 ± 0.8	12.0 ± 0.1	1.6	6.1	63
002	SeaRAY	0.57 ± 0.32	4.9 ± 0.9	12.5 ± 0.1	1.6	6.1	63
003	SeaRAY	0.53 ± 0.31	4.8 ± 1.0	12.2 ± 0.1	1.6	6.1	63
001	SeaRAY	0.53 ± 0.3	4.4 ± 0.7	12.1 ± 0.1	1.6	6.1	66
002	SeaRAY	0.53 ± 0.3	4.8 ± 0.7	12.5 ± 0.1	1.6	6.1	66
003	SeaRAY	0.52 ± 0.3	4.4 ± 1.1	12.2 ± 0.1	1.6	6.1	66

4.4.5 IEC Analysis

IEC 62600-40 requires a minimum number of "sequences" for Level B acoustic characterization of a WEC. Specifically, 20 sequences, each 30 s in duration, are required from within a zone 25 m on edge located on-axis with the dominant wave direction at a range of 100 m from the WEC or perpendicular to the wave direction at a similar range. These zones, which were determined post-survey, are shown in Figure 90. Within the 30 s window, at least 80% of the underlying samples (1 s duration, 50% overlap) must be considered "valid" (i.e., not substantially contaminated by non-WEC noise sources). Here, we extend validity to include 30 s windows where at least 80% of the underlying samples were within the defined zone, excluding those from outside the zone. This subtly occurs when DAISYs are at the margin of a zone and move in and out of it within a 30 s window, but remain mostly inside the zone.

Because the zones were not known at the time of the survey, they could not be directly targeted and, consequently, only two of the zones were surveyed and each contained only 3 valid sequences, rather than the 20 specified in IEC 62600-40.

IEC 62600-40 defines WEC-band noise as

$$L_{P,WEC} = 10\log_{10} \int_{f_1}^{f_2} \frac{\overline{p_f^2}}{p_o^2}\, df$$

where f_1 and f_2 are the low- and high-frequency limits for WEC noise, p_o^2 is the reference value of 1 µPa²/Hz, and $\overline{p_f^2}$ is the mean-square sound pressure spectral density. Here, based on comparisons between measurements around SeaRAY and the pseudo-baseline reference location, we define f_2 as 10 kHz. However, we note that this encompasses persistent mooring noise around 1 kHz that is definitively *not* attributable to SeaRAY based on prior surveys that identified the source as a damaged mooring at the 60 m WETS berth (Polagye, et al., 2025). The low-frequency modal cut-off is approximately

$$\mathrm{f_{low}} = \frac{\mathrm{c}}{4\mathrm{D}\left(1 - \frac{\mathrm{c}^2}{\mathrm{c_s^2}}\right)^{0.5}}$$

where c is the speed of sound in water, c_s is the speed of sound in the seabed, and D is the water depth. Based on CTD measurements of the upper water column, c is ~1536 m/s, D is ~81 m, and c_s is estimated at 4000 m/s, which is consistent with the limestone substrate closer to shore. This results in a cut-off of ~6 Hz, so the default IEC 62600-40 cut-off of 10 Hz is employed. However, based on the slope of the low frequency spectra, it is likely that flow noise is appreciable for frequencies < 20 Hz, such that WEC band levels are biased slightly high.

WEC band levels in Zone 1 and Zone 2 were 103 dB and 102 dB, respectively. The difference between the two zones is likely within the bounds of temporal variability. This is likely the reason for the relatively limited differences in mean-square pressure spectral density for both zones (Figure 91). Frequency-specific variations would also likely be reduced with a decidecade representation of received levels.

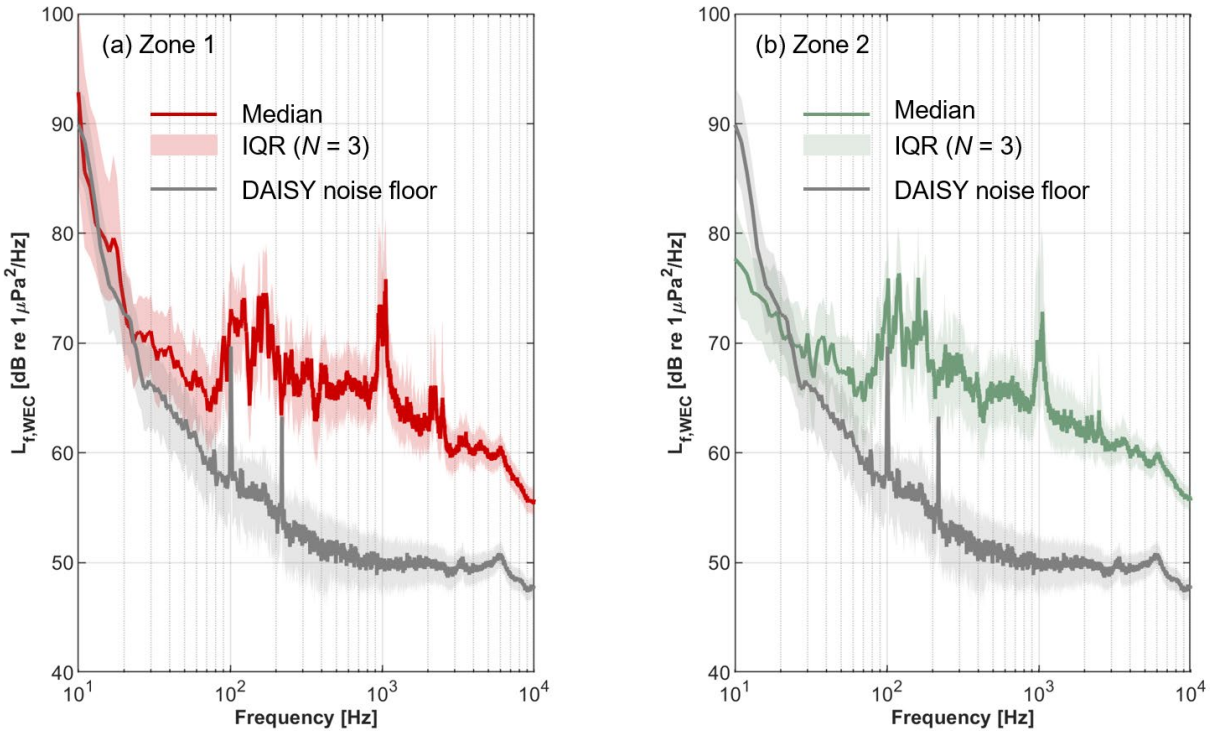

Figure 91: Mean-square sound pressure spectral density for survey zones. At all frequencies of interest, received levels exceed the DAISY noise floor established during quiescent drifts in Sequim Bay, WA. Solid lines denote the median and shaded regions denote the inter-quartile range (IQR).

4.4.6 Source Attribution

While IEC 62600-40 provides a standardized approach for quantifying sound in the vicinity of a WEC, it does not allow us to differentiate between noise radiated by the WEC and other ambient sources. A representative spectrogram from a distance of ~10 m is shown in Figure 92. The soundscape is a composite of period tonal sound at frequencies < 800 Hz (likely attributable to the power take-off), with intermittent sound around 1 kHz. The latter is chain noise from the damaged mooring at the 60 m berth (~1 km away). In addition, there are intermittent "booms" (likely attributable to waves breaking on the hull) and "squeaks". In manual review of the data, we also identified two intermittent non-WEC sources: marine mammal vocalizations by an odontocete (~13 kHz) and fish tag transmitters (69 kHz).

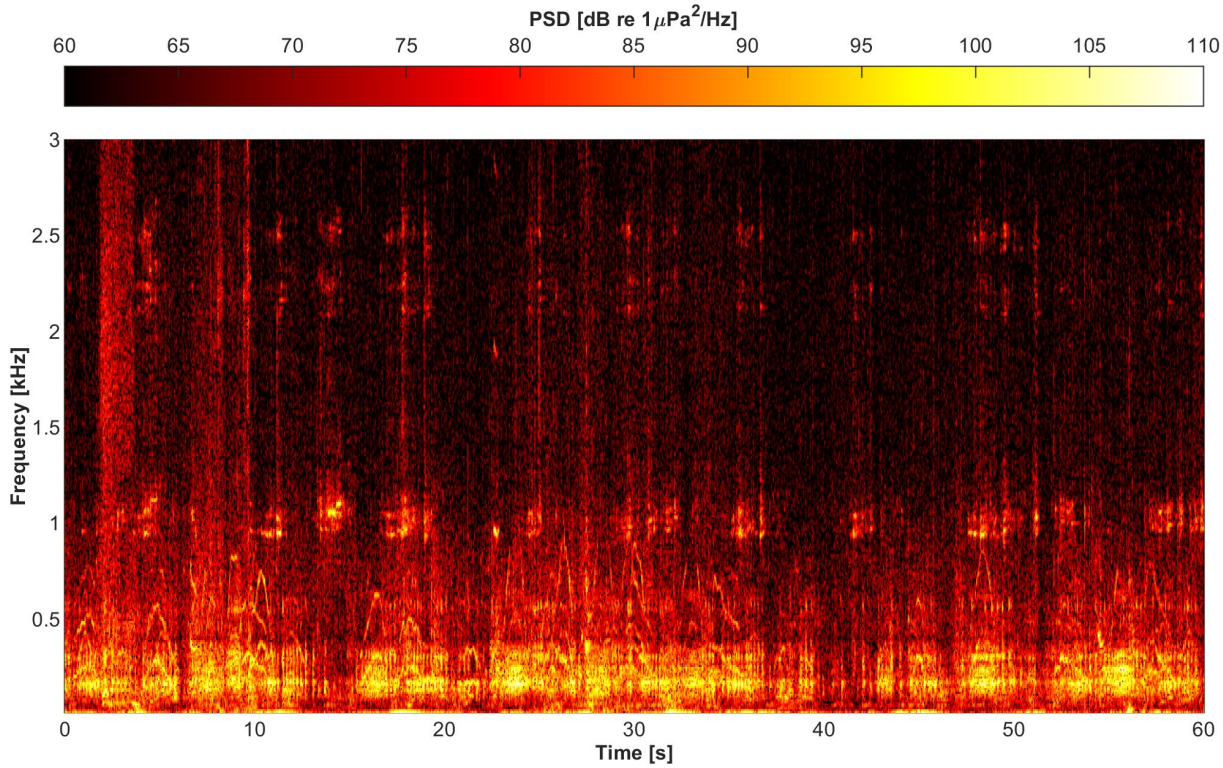

Figure 92: Spectrogram at range of ~10 m from SeaRAY.

Formal attribution of sounds to SeaRAY was performed through a combination of range dependence and localization. For frequently occurring sounds, we first compared range dependence in periodograms (time-averaged spectrograms) of radiated noise at relatively close range (~10 m), intermediate range (~80 m), and a pseudo-baseline measurement at much greater range (~1200 m). As previously discussed, the range for the latter is such that any radiated noise originating from SeaRAY is likely to fall below ambient levels at this location. For the two closer measurements, frequencies that show a clear range dependency are likely attributable to SeaRAY, while those that do not are likely attributable to other sources. An example of this analysis is shown for measurements on July 15 in Figure 93. Because the measurements are not co-temporal, we cannot directly compare the time-resolved spectrograms, but if we assume that the radiated noise from SeaRAY is statistically stationary, the periodigrams are informative. Specifically, these suggest that SeaRAY produces sound from 50 – 900 Hz, with sound from 90 – 400 Hz remaining slight elevated above ambient noise out to 80 m. For subsequently analysis, we take this to the "WEC

band". In contrast, the chain noise from the 60 m berth mooring is nearly constant for the two measurements around SeaRAY and still appreciable in the reference measurement.

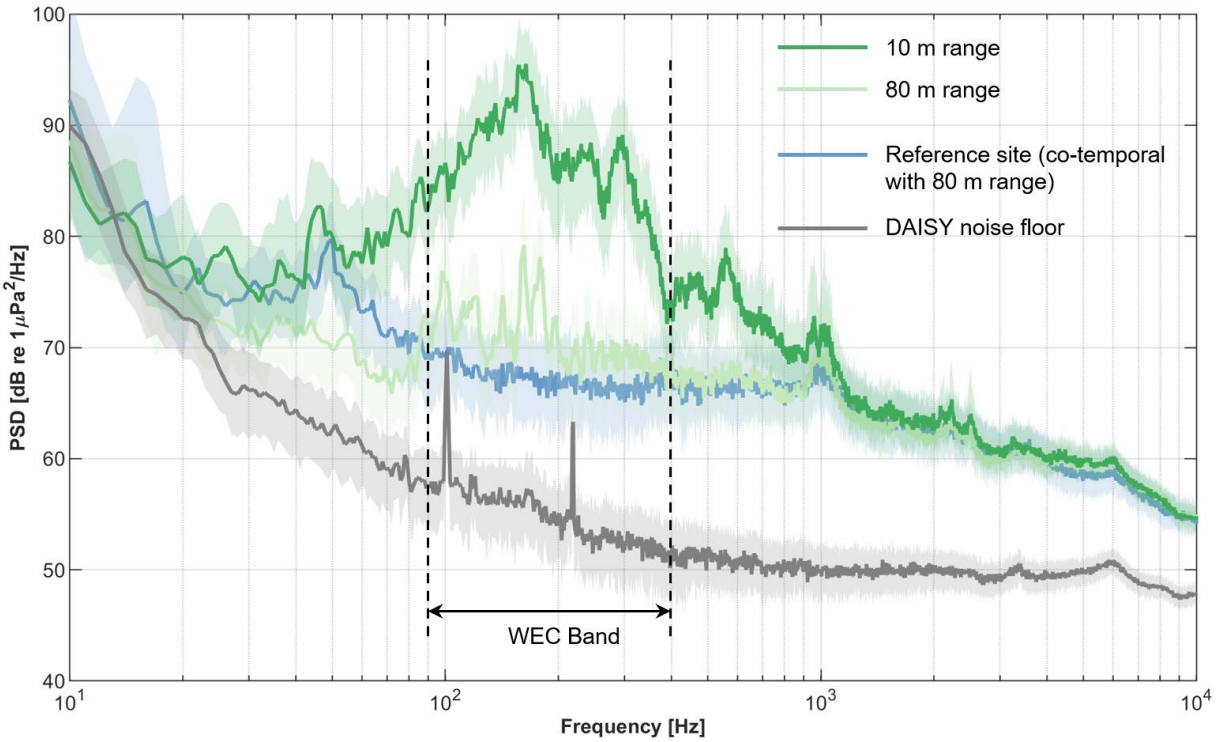

Figure 93: Periodograms from received levels at three ranges to SeaRAY. The "WEC Band" is defined as the range of frequencies that remain elevated about the pseudo-baseline at a range of 80 m. Solid lines denote median values and shaded regions denote the inter-quartile range.

Based on this, we can visualize the range and azimuthal dependence of "WEC band" noise around SeaRAY. As for IEC 62600-60, this is done by taking the median pressure spectral density for adjacent, 30-second sequences, and integrating over a relevant frequency range. While these frequencies do also contain non-WEC noises, such as breaking waves, these are limited in occurrence and, consequently, the median values as unaffected. As shown in Figure 94a, we observe a clear range dependence and limited azimuthal dependence. The dominance of range dependence over azimuthal variations is clear in Figure 94b where received levels roughly follow a practical spreading law of 15log$R$ where R is the distance between SeaRAY and receiver. Through discussions with CPower, we determined that the differences in radiated noise between the two days are primarily a consequence of differences in power take-off speed. In fact, the elevated cluster of points between 100 and 150 m range on July 16 corresponds to a power take-off control setting that allowed somewhat higher rotation rates.

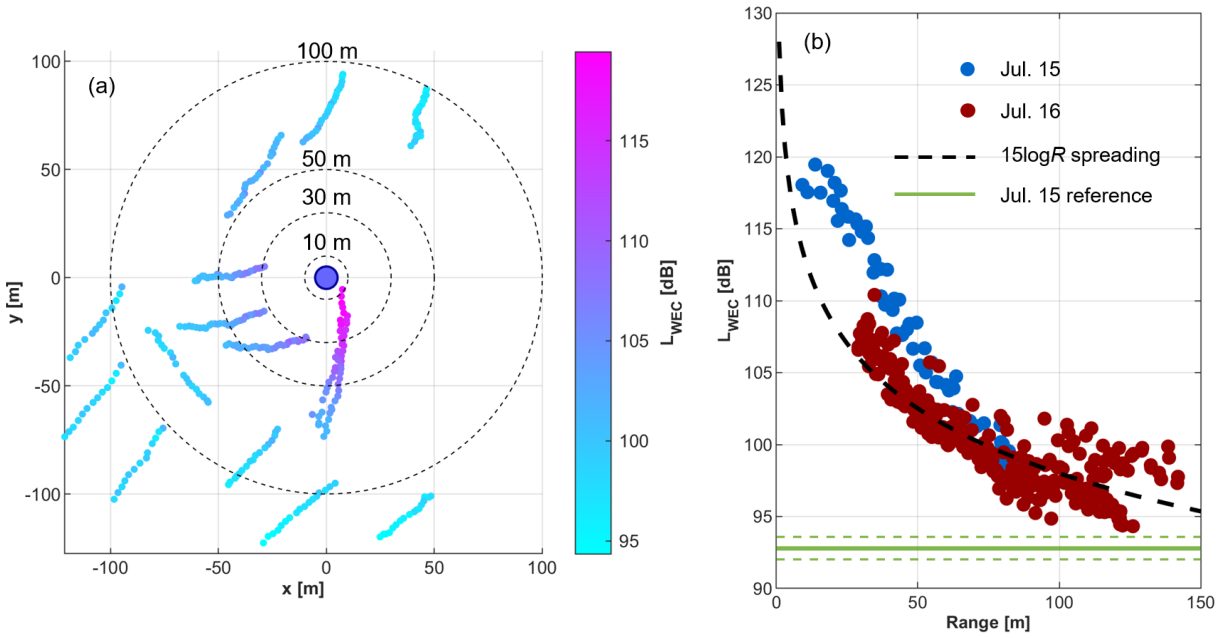

Figure 94: (a) Spatial variations in WEC-band noise around SeaRAY (b) range dependence. Each circle denotes band levels calculated from the median sound pressure squared in a 30-second window.

4.4.7 Localization

While assessing range dependence provides insight into sounds on an aggregate basis, localization can identify the source of individual events. Here, we use a time-delay-of-arrival method (Wahlberg, Mohl, & Telberg Madsen, 2001), as described in Section 3.4.3. We note that this scenario is somewhat simpler than in marine biology or defense applications as we know the location of our source of interest, such that our objective is to discriminate between sound originating from the WEC and those originating from other sources. To establish time-of-arrival across the three receivers, we cross-correlate filtered and Hilbert-transformed voltage waveforms for manually identified events in one DAISY data stream.

Table 18 provides a summary of initial localization results, grouped by sound type and receiver distance from SeaRAY. Events that could not be localized are excluded but are a relatively small fraction of localizations attempted (i.e., 2 out of 17 measurements at close range). Two "error" metrics are presented. This first is the average distance between the estimated location for a source and the nominal location of SeaRAY. The second is the difference in the estimated bearing from the centroid of the receiver array to the source relative to the actual bearing to SeaRAY's estimated location. While results are presented for a limited number of cases, they are informative of localization benefits. Specifically, at close range, all sources that are mechanical in nature (i.e., PTO, "boom", and squeaks/snaps localize to a similar position (within 20 m) and bearing (within 15°) as SeaRAY. The high-frequency biological source (odontocete vocalization) localizes to a similar range, but significantly different bearing, such that it is unlikely noise originating from SeaRAY. At greater range, absolute localization accuracy is relatively worse, but estimated bearings are less affected.

Table 18: Localization summary. *N* denotes the number of events of a particular type localized and distance/bearing metrics are averages from those populations.

	Close Range (30-50 m)			Distant (> 100 m)		
	N	Source Distance to SeaRAY [m]	Source Bearing to SeaRAY [deg]	*N*	Source Distance to SeaRAY [m]	Source Bearing to SeaRAY [deg]
PTO	6	17	-11	4	65	16
"Boom"	2	14	-14	-	-	-
Mechanical (squeak, snap)	4	20	-10	1	77	-25
High-frequency Biological	3	35	-40	-	-	-

Figure 95 provides a visual representation of the same information for the close range localizations. The sounds likely to have originated from SeaRAY are all clustered, while the high-frequency sound with biological structure is more distributed and may indicate a marine mammal moving through the area.

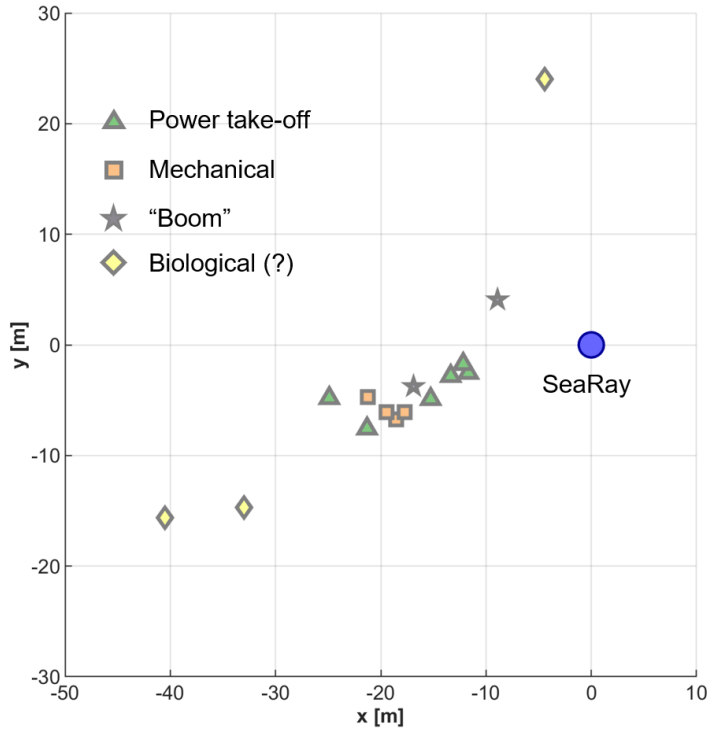

Figure 95: Spatial representation of close range localizations summarized in Table 18.

While all sounds likely originating from SeaRAY are localized to a position 10-20 m away from the best estimate based on range trilateration, this represents a limitation of localization accuracy and does not provide a better estimate of SeaRAY position. This conclusion can be better understood by visualizing the uncertainty in the estimated source location, as in Figure 96 for one instance of

power take-off sound. The black circle denotes the estimated source location by the exact solution to the hyperbolic equation set given by Wahlberg et al. If, instead, we consider all possible source locations on a relatively well-constrained grid (here, ±150 m in both directions), we can compute an error metric as the deviation in estimated time-of-arrival for this set of locations relative to the actual time of arrival across all three receivers. As visualized by the contours, the source location that results in the least error has a relatively wide uncertainty zone extending towards the actual location of SeaRAY. This is a consequence of the receiver orientation. If we had deployed receivers to bracket SeaRAY, uncertainty would likely be significantly reduced. However, because we did not expect to be able to localize sound from SeaRAY at all with an array of only three DAISYs, we instead, prioritized spatially distributed measurements. Localization accuracy could also be improved by deploying more than the minimum required number of receivers around a source.

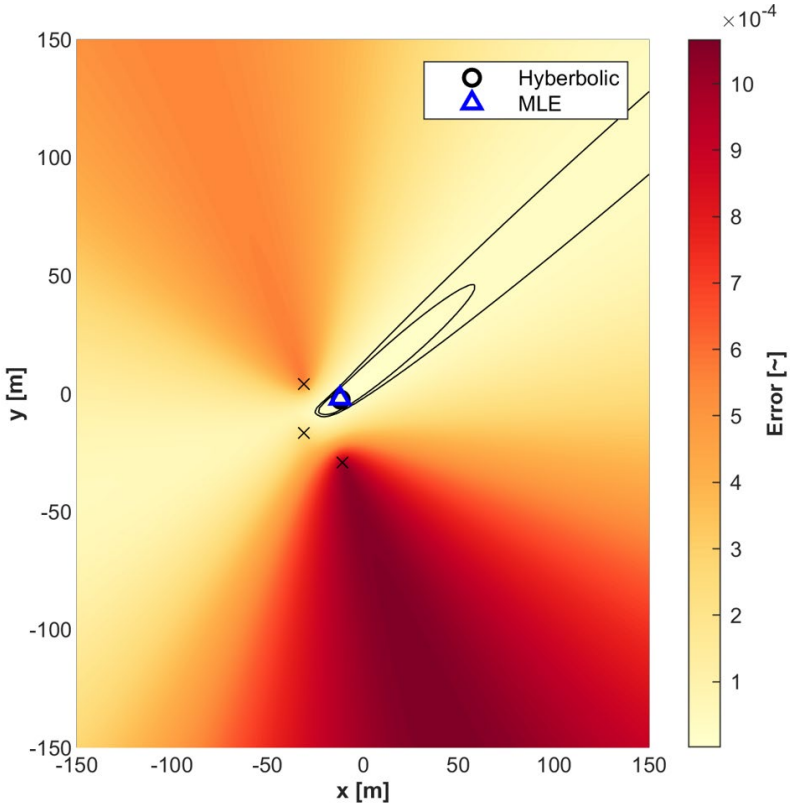

Figure 96: Visualization of source position uncertainty for one instance of power take-off noise. 'x' markers denote DAISY positions. Contours are all computed values with 1% and 5% of the lowest absolute uncertainty. Estimated SeaRAY position is at the coordinate origin.

4.4.8 Conclusions

While the data collected was unable to meet the requirements of a "Level B" IEC 62600-40 survey due to the unknown WEC location, it demonstrated several core DAISY capabilities:

- Collection of high-fidelity acoustic measurements without flow-noise or self-noise contamination above 20 Hz, while drifting in energetic waves;
- Safe and effective deployment and recovery by a team of two; and
- Attribution of sound to a marine energy converter through a combination of range-dependent analysis and localization.

These results are described in an archival journal publication that is currently under peer review.

4.5 Commercial Readiness

An overall project objective is to transition the DAISY from a research tool used by UW to a product available to and used by a broader community. This technology transition has taken two forms: an open-source option and commercial offering through a project partner.

First, the DAISY hardware and software are available open source through pmec.us/research-projects/daisy. This includes the bill of materials for all DAISY variants (including variants developed with separate funding, such as a "shallow" version that resembles the baseline rigid hull system), electrical and mechanical drawings, and manufacturing plans. The latter were used by PNNL to construct flow-shields for their drifting hydrophone system built around an OceanSonics buoy and hydrophone package.

Second, recognizing that many potential users would prefer not to build their own instruments, project partner MarineSitu, Inc. has made a commercial version available (https://www.marinesitu.com/daisy). Because the design is open source, this did not require MarineSitu to negotiate a licensing agreement with UW and other instrumentation companies would be able to develop similar products, if desired. Since launching the commercial version in late 2024, MarineSitu has received expressions of interest to procure DAISYs from U.S. and international customers.

5 Collaborations and Other Use

In addition to activities directly funded through this project, DAISYs have been used successfully in multiple additional contexts:

- By Integral Consulting to characterize noise from rocket launches off Vandenburg, CA
- By Integral Consulting to characterize radiated noise from a CalWave WEC deployed off San Diego, CA
- By PNNL and UW to characterize noise from a small tidal turbine in Portsmouth, NH
- By UW to characterize noise from a small tidal turbine in Agate Pass, WA and Sequim Bay, WA
- By UW to characterize noise from ORPC turbines in Millinocket, ME and Igiugig, AK
- By UW to characterize noise from the permanent moorings at WETS

6 Publicly Available Scientific and Technical Information (STI)

There are four repositories of STI associated with the project:

1. The DAISY information page on the PMEC website (pmec.us/research-projects/daisy)
2. An MHK-DR archive containing data from the variant and tether tests in Admiralty Inlet (https://mhkdr.openei.org/submissions/455)
3. An MHK-DR archive containing all data presented in the archival journal paper on the system development and benchmarking (Polagye, et al., 2025) (https://mhkdr.openei.org/submissions/570)
4. An MHK-DR archive containing all data associated with measurements around C-Power's SeaRAY (https://mhkdr.openei.org/submissions/593)

As additional measurements are acquired and analyzed, further MHK-DR submissions and publications are anticipated to continue building the knowledge base for radiated noise from marine energy converters.

7 References

Bassett, C., Thomson, J., Dahl, P. H., & Polagye, B. (2014). Flow-noise and turbulence in two tidal channels. *The Journal of the Acoustical Society of America, 135*(4), 1764-1774.

Jensen, F. B., Kuperman, W. A., Porter, M. B., Schmidt, H., & Tolstoy, A. (2011). *Computational ocean acoustics*. New York, NY: Springer New York.

Keulegan, G. H., & Carpenter, L. H. (1958). Forces on cylinders and plates in an oscillating fluid. *Journal of research of the National Bureau of Standards, 60*(5), 423-440.

Martin, S. B., Gaudet, B. J., Klinck, H., Degan, P. J., Miksis-Olds, J. L., Mellinger, D. K., . . . Moors-Murphy, H. (2021). Hybrid millidecade spectra: A practical format for exchange of long-term ambient sound data. *JASA Express Letters, 1*(1).

Polagye, B., Crisp, C., Jones, L., Murphy, P., Noe, J., Calandra, G., & Bassett, C. (2025). Performance of a Drifting Acoustic Instrumentation SYstem (DAISY) for characterizing radiated noise from marine energy converters. *ournal of Ocean Engineering and Marine Energy, 11*(1), 11-33.

Strasberg, M. (1979). Nonacoustic noise interference in measurements of infrasonic ambient noise. *The Journal of the Acoustical Society of America, 66*(5), 1487-1493.

Vandiver, J. K., & Mazel, C. H. (1976). A field study of vortex-excited vibrations of marine cables. *Offshore Technology Conference* (pp. OTC-2491). Offshore Technology Conference.

Wahlberg, M., Mohl, B., & Telberg Madsen, P. (2001). Estimating source position accuracy of a large-aperture hydrophone array for bioacoustics. *The Journal of the Acoustical Society of America, 109*(1), 397-406.

Appendix 1: Flow-shield and Hydrophone Guard Acoustic Characterization

The flow-shield and hydrophone guard were designed to mitigate flow-noise in currents and protect the hydrophone element from impact in waves, respectively. However, components of both structures shadow the hydrophone element from sounds, resulting in transmission loss. The magnitude of the loss depends on the frequency of sound and the size, shape, and material properties of the shield and guard components. Because the shield and guard are not axisymmetric, the signal losses are also dependent on the incident angle of the sound.

An experiment was conducted to measure the transmission loss resulting from the shield and guard as a function of frequency and signal direction. A DAISY, configured with an OceanSonics icListen HF hydrophone, was tested at the Acoustic Test Facility (ATF) on R/V Henderson. The DAISY was fixed to the end of the ram, a vertical member that projects through the vessel's moon pool and provides control of both vertical and azimuthal position. The DAISY's hydrophone element was positioned at a depth of 1 m, and a calibrated acoustic source (F41 transducer) was positioned 3.17 m away at a depth of 1 m.

Transmission loss as a function of frequency was measured for three configurations, each of which represent of a portion of possible paths by which sound could reach the hydrophone. These were compared to the unshielded frequency response of the hydrophone, measured in-situ to account for its own directional sensitivity. The configurations evaluated transmission loss associated with (1) the fabric shield, (2) the metal rods used to tension the fabric, and (3) the PVC guard. Sweeps consisted of three pings at each frequency from 10 to 150 kHz in 1 kHz steps.

Finally, a measurement was conducted to directly observe directional dependency. Transmission loss at 100 kHz was measured as a function of azimuth angle for both a shielded and an unshielded hydrophone. Because the flow shield contains six metal rods positioned around the central axis at 60° intervals, the sweep was conducted over a range of 60°.

The effect of the PVC guard bar that will be used to protect the hydrophone in wave environments is shown in Figure 97. The bar causes little effect below 50 kHz, then causes substantial attenuation at higher frequencies. At 50 kHz, the acoustic wavelengths is ~ 3 cm, which is in agreement with the expectation that reflection becomes significant when an obstructing object's size is on the order of 1/10 of the wavelength.

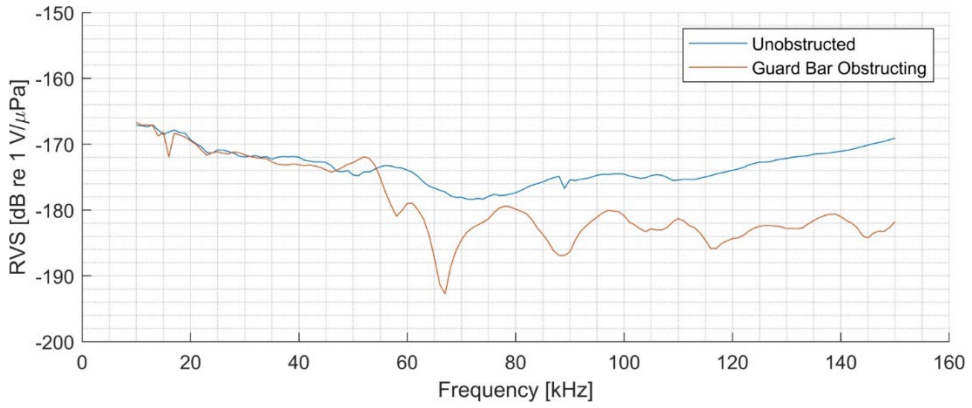

Figure 97: Receive voltage sensitivity for unobstructed hydrophone and hydrophone obstructed by PVC guard bar

As shown in Figure 98, the metal spring steel causes attenuation of 4-6 dB at frequencies down to the lowest characterized (i.e., 10 kHz). However, as shown in Figure 99, the effect of the fabric flow-shield is, in net terms, relatively limited. However, the receive voltage sensitivity has significant "structure", which is indicative of interference patterns generated by scattering of the transducer ping by the support structure. This is also apparent in the directional sensitivity at 100 kHz, shown in Figure 100. Based on this, we expect that some scattering may also occur for sound sources originating off-axis from the PVC guard bar (Figure 97).

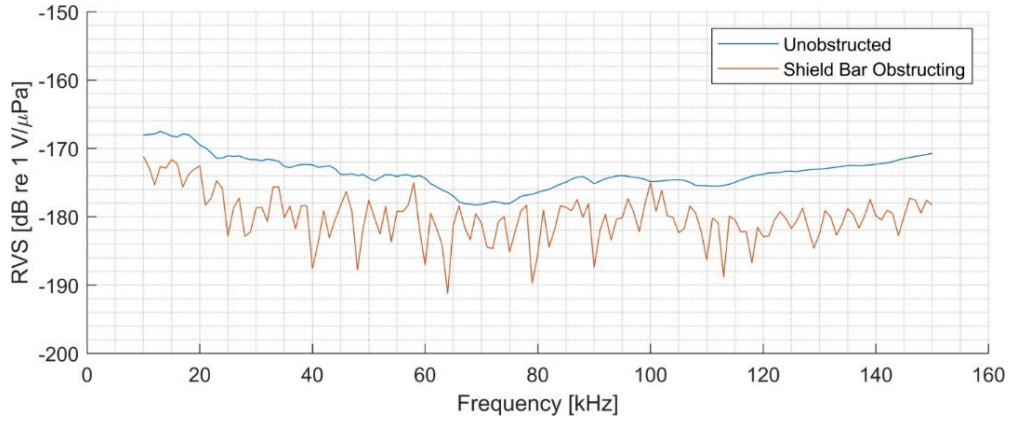

Figure 98: Receive voltage sensitivity for unobstructed hydrophone and hydrophone obstructed by the spring steel support bar and flow-shield

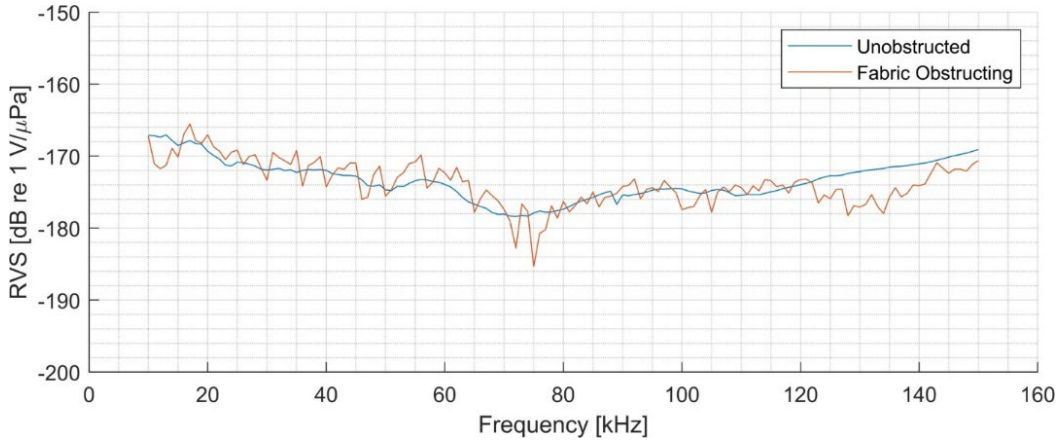

Figure 99: Receive voltage sensitivity for unobstructed hydrophone and hydrophone obstructed by nylon flow-shield.

While it would be preferable for protective shielding to not affect received levels, in our opinion, these performance characteristics are acceptable. First, the scattering from a directional source of sound at close range is likely to represent a worst case scenario for the effect of the protective shielding. For the flow-shield, given that the attenuation or amplification is on the order of 2-3 dB for the frequencies characterized, this is within the range of other experimental uncertainties when characterizing current turbines in the field. Second, while the PVC guard that would be employed at wave energy sites significantly attenuates sound at frequencies greater than 50 kHz, wave converters generally produce sound at frequencies below 10 kHz. Consequently, the guard is unlikely to affect conclusions drawn from measurements of wave converters. This guard could also be removed for some measurements, though this would increase the risk of hydrophone damage.

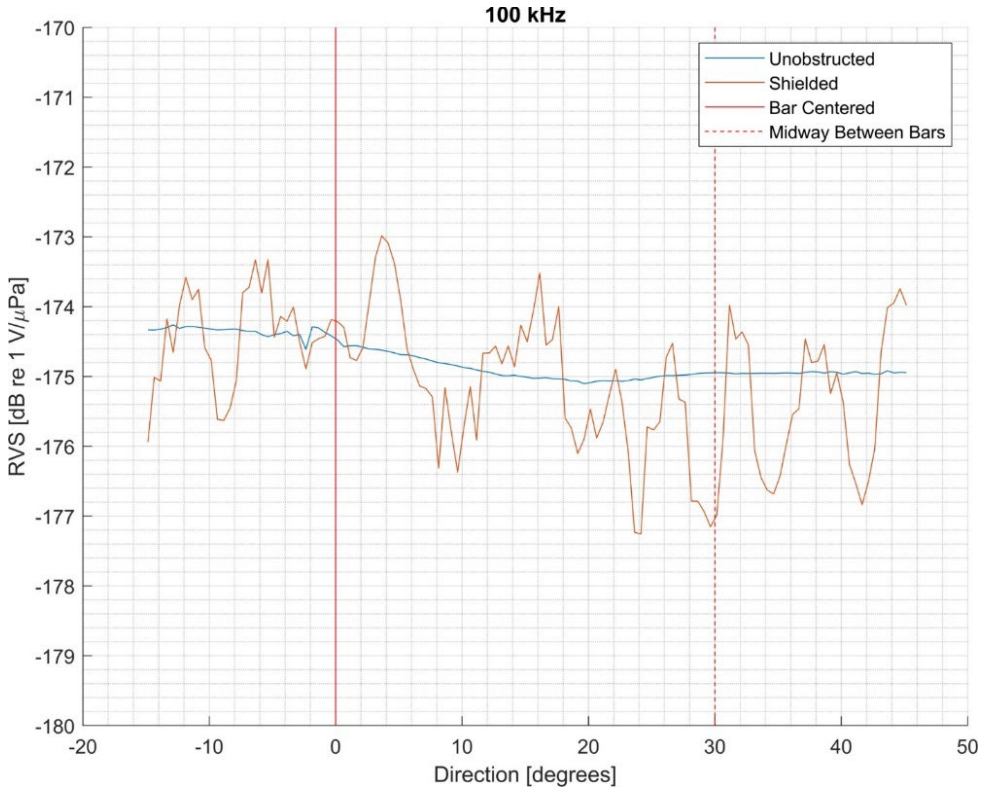

Figure 100: Directional receive voltage sensitivity at 100 kHz for unobstructed hydrophone and hydrophone equipped with a flow-shield.

Appendix 2: Hardware Bill of Materials

Part #	Component Name	Mfg. or Supplier	P/N	Qty per DAISY	Description (units)	Material Cost per Float

NOTE: Pricing based on making 5 DAISYs, includes material cost only. Labor cost for fabrication and assembly not included and are significant for some subsystems.

Sheet Materials and Supplies

Split across the subsystems below

PVC Type 2 Sheet, Th-0.25"	Professional Plastics	PVC Type 2	1	Sheet L-96", W-48", Th-0.25", waterjet 1 DAISY = approx 864 in^2, 1 sheet = 5 DAISYs	$ 64.60
PVC Type 2 Sheet, Th-0.5"	Professional Plastics	PVC Type 2	0.5	Sheet L-96", W-48", Th-0.5", waterjet 1 DAISY = approx 384 in^2, 0.5 sheet = 5 DAISYs	$ 58.94
Foam, Yellow	Friendly Foam Shop	Y20 Yoga Foam	1.5	Youngboard cross-linked PE/EVA closed cell foam, P/N Y-S-20 (Density 2 pcf) Sheet L-80", W-40", Th-4", handcut 1 DAISY = approx 768 in^2, 1.5 sheet = 5 DAISYs	$ 160.24
Rubber, EPDM, 40 durometer, Compound 040K0038	Warco-Biltrite	44222881	1	Sheet, L-48", W-12", Th-0.25", waterjet 1 DAISY = 100 in^2, 1 ft = 5 DAISYs	$ 10.48
Sheet Lead, Th-1/8"	Non-Ferrous Metals	Sheet Lead 1/8"	1	Sheet, L-48", W-20", Th-0.125", 8 lbs/SF 1 DAISY = 180 in^2, 48"x20" = 5 DAISYs	$ 39.11
Vytaflex 40 Urethane Rubber for casting	Smooth-On	Vytaflex 40	1	Vytaflex 40 Urethane Rubber for Casting (gal)	$ 31.84
Flowshield Fabric	Seattle Fabrics	FLD	3	DriFit Wicking Spandex Ripstop, 56" wide (yd)	$ 61.12
Flowshield Thread	Seattle Fabrics	DB92	1	DB92 Polyester Thread, Professional Duty (spool)	$ 8.35

Surface Expression Foam Buoy $ 1,228.47

1	Buoy Base Plate	Fabricated	n/a	1	PVC sheet, Type 2, Th-1/4", waterjet, drilled	see Matls
2	Buoy Foam, Bottom, 16" diam	Friendly Foam Shop	Y20 Yoga Foam	1	Foam, Th-4", bandsaw and handcut, Youngboard cross-linked PE/EVA closed cell foam, P/N Y-S-20 (Density 2 pcf)	see Matls
3	Buoy Foam, Middle, 15" diam	Friendly Foam Shop	Y20 Yoga Foam	1	Foam, Th-4", bandsaw and handcut, Youngboard cross-linked PE/EVA closed cell foam, P/N Y-S-20 (Density 2 pcf)	see Matls
4	Buoy Foam, Top, 14" diam	Friendly Foam Shop	Y20 Yoga Foam	1	Foam, Th-4", bandsaw and handcut, Youngboard cross-linked PE/EVA closed cell foam, P/N Y-S-20 (Density 2 pcf)	see Matls
5	Rubber Gaskets, Elec Hold	Fabricated	n/a	2	40A EPDM Rubber Sheet, Th-1/4"	see Matls
6	Grab Bar Assembly	Fabricated	n/a	1	Assembly of rolled 1" tube with support legs, welded, powder coated, SS316	$ 532.02
7	Grab Bar Screw	McMaster	91735A197	6	#8-32 Screw, Phillips, Pan, L 0.75", SS316	$ 1.83
8	Grab Bar Nut	McMaster	90715A009	6	#8-32 Nut, Nylok Hex, SS316	$ 2.07
9	Mast Assembly	Morad	custom	1	Base & Stanchion, Anodized Aluminum	$ 138.23
10	Mast Screw	McMaster	91500A338	4	1/4"-20 Screw, Phillips, Flat, L-7/8", SS316	$ 2.64
11	Mast Nut	McMaster	90715A125	4	1/4"-20 Nut, Nylok Hex, SS316	$ 6.61
12	Flag	Amazon	Orange Flag	1	Orange Flag with Grommets for Visibility	$ 7.21
13	Collar	Fabricated	n/a	1	PVC sheet, Type 2, Th-1/2", waterjet, drilled	see Matls
14	Collar Alignment Tab	Fabricated	n/a	2	PVC sheet, Type 2, Th-1/4", waterjet	see Matls

15	Collar Screw	McMaster	91735A154	4	#6-32 Screw, Phillips, Pan, L-1.0", SS316	$ 1.78
16	Collar Nut	McMaster	92891A500	4	#6-32 Nut, Square, SS316	$ 2.47
17	Spring Latch, Hinged	Protex	27-633/316SS	2	Spring Claw Toggle Latch Light Duty, SS316	$ 38.42
18	Catch Plate	Protex	02-633/316SS	2	Catch Plate for Toggle Latch, SS316	$ 11.18
19	Catch Plate Rivet	McMaster	97550A615	4	Rivet, 5/32" diam, Th-0.178"-0.255", SS316	$ 7.62
20	Buoy Tension Bar	OnlineMetal	SS316 bar	2	Bar W-1/2", Th-1/8", L-8", SS316, drilled	$ 20.92
21	Tension Bar Screw	McMaster	98164A519	2	1/4"-20 Screw, Hex Drive, Buttonhead, SS316	$ 2.64
22	Tension Bar Nut	McMaster	90715A125	2	1/4"-20 Nut, Nylok Hex, SS316	see P/N 26
23	Tension Bar Alignment Insert	Fabricated	n/a	2	PVC sheet, Type 2, Th-1/2", machined	see Matls
24	Angle Bracket, 90 degree	Garvin Industries	BA-1-4-SS	2	90 deg angle bracket, SS316, 1/4" thru holes	$ 7.43
25	Angle Bracket Screw	McMaster	91500A538	2	1/4"-20 Screw, Phillips, Flat, L-5/8", SS316	$ 1.78
26	Angle Bracket Nut	McMaster	90715A125	2	1/4"-20 Nut, Nylok Hex, SS316	see P/N 26
27	Tension Rod	McMaster	93250A125	3	1/4"-20 Threaded Rod, SS316, L-14.25"	$ 24.13
28	Acrylic Sleeve	McMaster	8532K12	3	Clear Acrylic Tube, Wall-Th-1/8", OD-1/2", 12.25"	$ 5.09
29	Flat Washer, PVC, Large	McMaster	95611A033	6	PVC Washer, OD-1.25", ID-0.562"	$ 3.00
30	Flat Washer, PVC, Small	McMaster	95611A029	6	PVC Washer, OD-0.75", ID-0.312"	$ 1.87
31	Flat Washer, SS316, 1/4"	McMaster	90107A029	6	Washer, SS316, OD-0.625", ID-0.281"	$ 1.98
32	Lock Washer, SS316, 1/4"	McMaster	92147A029	6	Washer, Lock, SS316, OD-0.487", ID-0.26"	$ 1.24
33	Tension Rod Nuts	McMaster	94819A043	12	1/4"-20 Nut, Hex, SS316	$ 1.96
34	Vinyl Cap	Tacoma Screw	089-003	6	1/4" Screw Protector, Vinyl	$ 3.33

Surface Expression Spar — Included in Foam Buoy Above

35	Spar Tube	McMaster	48925K99	1	PVC Tube, Schedule 40, 2-1/2", L-24"	$ 12.79
36	Spar Base	Fabricated	n/a	2	PVC sheet, Type 2, Th-1/2", waterjet, drilled	see Matls
37	Spar Base Screw	McMaster	92186A544	12	1/4"-20 Screw, Hex Head, Partial Thread, L-1-1/4"	$ 6.35
38	Spar Base Nut	McMaster	90715A125	12	1/4"-20 Nut, Nylok Hex, SS316	see P/N 26
39	Handle	Uxcell	A13112800-UX0234	1	Plastic Handle, Uxcell, L-6", W-1.1", H-1.65"	$ 7.20
40	Handle Screw	McMaster	91500A544	2	1/4"-20 Screw, Phillips, Flat, L-1-1/4", SS316	$ 1.17
41	Handle Nut	McMaster	90715A125	2	1/4"-20 Nut, Nylok Hex, SS316	see P/N 26
42	Spar End	McMaster	4880K852	1	PVC Pipe Cap, External Hex Drive, 6 Socket Male	$ 19.16
43	Lead Ballast	Non-Ferrous Metals	Sheet Lead 1/8"	8	Sheet Lead, Th-1/8", W-2", Approx L-7" (6.5" for inside layer, 8" for outer layer)	see Matls
44	Ballast Screw	McMaster	92186A544	4	1/4"-20 Screw, Hex Head, Partial Thread, L-1-1/4"	see P/N 41
45	Ballast Nut	McMaster	90715A125	4	1/4"-20 Nut, Nylok Hex, SS316	see P/N 26
46	Pin, 7.5"	McMaster	92186A660	1	3/8"-16 Bolt, Hex Head, L-7-1/2", SS316	$ 8.17
47	Wingnut	McMaster	93575A031	1	3/8"-16 Wingnut, SS316	$ 6.18
48	Pin Spacer, 2.25"	McMaster	92825A257	2	LDPE Unthreaded Spacers	$ 6.68

Holster for Lower Housing and Hydrophone — $ 110.88

49	Holster Cover, PVC Tube 6"	Home Depot	202564459	1	PVC Tube, Schedule 40, 6", OD-6.25", ID-5.9", L-16.25"	$ 10.78
50	Pin, 7.5"	McMaster	92186A660	1	3/8"-16 Bolt, Hex Head, L-7-1/2", SS316	see P/N 50

51	Wingnut	McMaster	93575A031	1	3/8"-16 Wingnut, SS316	see P/N 51
52	Pin Spacer, 2.25"	McMaster	92825A257	2	LDPE Unthreaded Spacers	see P/N 52
53	Buoyancy Foam	General Plastics	R-3312	2	R-3312 Foam, Density 12 lb/ft^3, Depth Rated to 300 ft Supplier Opt 1: General Plastics Supplier Opt 2: Blue Robotics	$ 45.20
54	Foam Rod	McMaster	98831A340	4	#10-24 Threaded Rod, Nylon, L-5"	$ 2.07
55	Foam Washer	McMaster	90295A455	4	#10 Washer, Flat, Nylon, OD-0.734", ID-0.281"	$ 3.23
56	Foam Nut	McMaster	94812A500	8	#10-24 Nut, Hex, Nylon	$ 1.81
57	Holster Collar	Fabricated	n/a	1	PVC sheet, Type 2, Th-1/2", waterjet, drilled	see Matls
58	Collar Screw	McMaster	91735A154	2	#6-32 Screw, Phillips, Pan, L-1", SS316	see P/N 19
59	Collar Nut	McMaster	92891A500	2	#6-32 Nut, Square, SS316	see P/N 20
60	Holster Tension Bar	OnlineMetal	SS316 bar	2	Bar W-1/2", Th-1/8", L-8.25", SS316, drilled	see P/N 24
61	Bracket, Frame Spacer	Fabricated	n/a	4	PVC sheet, Type 2, Th-1/2", waterjet, drilled	see Matls
62	Bracket Screw	McMaster	93190A541	4	1/4"-20 Screw, Hex Head, L-7/8", SS316	$ 1.21
63	Bracket Nut	McMaster	92891A100	4	1/4"-20 Nut, Square, SS316	$ 3.77
64	Spring Latch, Hinged	Protex	27-633/316SS	2	Spring Claw Toggle Latch Light Duty, SS316	see P/N 21
65	Catch Plate	Protex	02-633/316SS	2	Catch Plate for Toggle Latch, SS316	see P/N 22
66	Catch Plate Rivet	McMaster	97550A615	4	Rivet, 5/32" diam, Th-0.178"-0.255", SS316	see P/N 23
67	Holster Base	Fabricated	n/a	1	PVC sheet, Type 2, Th-1/2", waterjet, drilled	see Matls

68	Base Screw	McMaster	91735A154	2	#6-32 Screw, Phillips, Pan, L-1", SS316	see P/N 19
69	Base Nut	McMaster	92891A500	2	#6-32 Nut, Square, SS316	see P/N 20
70	Holster Ballast Lead	Non-Ferrous Metals	Sheet Lead 1/8"	6	Sheet Lead, Th-1/8", Approx W-1.6", Approx L-5", (Actual surface area 6 in^2)	see Matls
71	Ballast Screw	McMaster	92186A546	4	1/4"-20 Screw, Hex Head, Partial Thread, L-1-1/2"	$ 4.89
72	Ballast Nut	McMaster	90715A125	4	1/4"-20 Nut, Nylok Hex, SS316	see P/N 26
73	Ballast Cover	Fabricated	n/a	1	PVC sheet, Type 2, Th-1/4", waterjet, drilled	see Matls
74	Hydrophone Guard, Tall	McMaster	87025K29	1	PVC Type 2 Rod, 3/8" Diam, 30" L, bent, drilled	$ 10.82
75	Hydrophone Guard, Short	McMaster	87025K29	1	PVC Type 2 Rod, 3/8" Diam, 30" L, bent, drilled	$ 10.82
76	Guard Threaded Insert	McMaster	92398A113	4	#6-32 Threaded, Hex Press-In Insert, 18-8SS	$ 2.17
77	Guard Base Screw	McMaster	91500A148	4	#6-32 Screw, Phillips, Flat, L-1/2", SS316	$ 2.28
78	Guard Top Screw	McMaster	91735A154	1	#6-32 Screw, Phillips, Pan, L-1", SS316	see P/N 19
79	Guard Top Nut	McMaster	90715A007	1	#6-32 Nut, Nylok Hex, SS316	$ 1.90
80	Rubberbands	Office Depot	856297	4	Size 32, 3" x 1/8"	$ 0.67
81	Rubber Gaskets, Elec Hold	Fabricated	n/a	2	40A EPDM Rubber Sheet, Th-1/4"	see Matls
82	Bracket, Flow Shield	Fabricated	n/a	3	PVC sheet, Type 2, Th-1/2", waterjet, drilled	see Matls
83	Bracket Screw	McMaster	91720A255	6	#10-24 Screw, Hex Head, L-1-1/2", SS316	$ 5.42
84	Bracket Nut	McMaster	90715A011	6	#10-24 Nut, Nylok Hex, SS316	$ 2.17
85	Bracket Washer	Tacoma Screw	147-205-1	12	#10 Washer, Flat, Nylon, OD-0.437", Th-0.062"	$ 1.67

7 m rubber cord (with terminations) $ 47.30

86	3/8" Rubber Cord, L-7m	Grainger	6RRX4	1	Rubber Cord, EPDM, OD-3/8", L-25 ft to manf	$ 23.02
87	Thimble	Fisheries Supply	28565	2	Nylon Thimble, 5/8" x 1" x 3", Seadog P/N 173556	$ 5.55
88	Whipping Cord	Fisheries Supply	453178	2	Excel Racing Cord, Marlow P/N ER0112, Diam-3mm, L-1m (or similar low stretch, high strength line)	$ 2.81
89	Casted Rubber Urethane	Smooth-On	66761	2	Vytaflex 40 Urethane Rubber, Mold Casted	see Matls

2.5 m rubber cord (with terminations) $ 38.09

90	3/8" Rubber Cord, L-7m	Grainger	6RRX4	1	Rubber Cord, EPDM, OD-3/8", L-12 ft to manf	$ 13.81
91	Thimble	Fisheries Supply	28565	2	Nylon Thimble, 5/8" x 1" x 3", Seadog P/N 173556	$ 5.55
92	Whipping Cord	Fisheries Supply	453178	2	Excel Racing Cord, Marlow P/N ER0112, Diam-3mm, L-1m (or similar low stretch, high strength line)	$ 2.81
93	Casted Rubber Urethane	Smooth-On	66761	2	Vytaflex 40 Urethane Rubber, Mold Casted	see Matls

Heave Plate Assembly $ 100.41

94	Heave Plate, 60 cm	Fabricated	n/a	1	PVC sheet, Type 2, Th-1/4", waterjet	see Matls
95	Flange	Lowe's	811250	1	Sioux Chief 3" Gasketed Black ABS Inside Fit Closet Flange - Sioux Chief P/N 888-GAM	$ 18.00
96	Top Ring	Fabricated	n/a	1	PVC sheet, Type 2, Th-1/4", waterjet	see Matls
97	Flange Screw	McMaster	92186A546	4	1/4"-20 Screw, Hex Head, Partial Thread, L-1-1/2", SS316	see P/N 75

98	Flange Nut	McMaster	90715A125	4	1/4"-20 Nut, Nylok Hex, SS316	see P/N 26
99	Flange Washer, Flat	McMaster	90107A029	8	1/4" Washer, Flat, SS316, OD-0.625"	see P/N 38
100	Flange Washer, Lock	McMaster	92147A029	4	Washer, Lock, SS316, OD-0.487", ID-0.26"	see P/N 36
101	Spar Tube, ABS	Home Depot	202300519	1	ABS Pipe, 2", OD-2.375", ID-2.049", L-24"	$ 4.30
102	Spar Screws	McMaster	92186A555	2	1/4"-20 Screw, Hex, Partial Thread, L-3-1/4", SS316	$ 1.48
103	Spar Nuts	McMaster	90715A125	2	1/4"-20 Nut, Nylok Hex, SS316	see P/N 26
104	Adapter Fitting, ABS	Home Depot	100344737	1	ABS Fitting, 2", Female Socket, Female Threaded	$ 2.64
105	Plug Fitting, ABS	Home Depot	100344835	1	ABS Plug, 2", Threaded	$ 1.31
106	Adapter Safety Screw	McMaster	92186A558	1	1/4"-20 Screw, Hex, Partial Thread, L-4", SS316	$ 0.95
107	Adapter Nut	McMaster	90715A125	1	1/4"-20 Nut, Nylok Hex, SS316	see P/N 26
108	Heave Plate Ballast Lead	Non-Ferrous Metals	Sheet Lead 1/8"	1	Sheet Lead, Th-1/8", Approx 2 lb	see Matls
109	Eye-Bolt	McMaster	8891T72	2	1/4"-20 Eye Bolt, 1" thread, 3/4" eye diam	$ 28.34
110	Casted Rubber Urethane	Smooth-On	66761	2	Vytaflex 40 Urethane Rubber, Mold Casted	see Matls
111	Shackle, Wide-D	Fisheries Supply	77025	2	Shackle, Wide-D, 2-3/4" x 1-11/16", 3/8" diam pin, SS316, SeaDog P/N 147190-1	$ 43.37

Fabric Flow Shield $ 224.56

112	Fabric Shield	Seattle Fabrics	n/a	1	DriFit Wicking Spandex Ripstop, Hand-sewn	see Matls
113	Spring Rod	Industrial Steel & Wire	n/a	3	Spring Temper Wire, Diam-0.162", straightened and to L-72", SS316	$ 84.68
114	Endstop Block	McMaster	90138A140	6	Unthreaded spacer, OD-1/4", ID-0.166", SS316	$ 38.58

115	Endstop Washer	McMaster	91525A318	6	#8 Washer, Flat, OD-0.5", ID-0.172", SS316	$ 2.19
116	Collar, Top	Fabricated	n/a	1	PVC sheet, Type 2, Th-1/2", waterjet, drilled	see Matls
117	Loop Clamp	McMaster	8876T11	12	#8-32 Nylon Loop Clamp, ID-1/8"	$ 1.69
118	Loop Clamp Threaded Insert	McMaster	92398A114	12	#8-32 Threaded Insert, Hex, For Plastic	$ 9.56
119	Loop Clamp Screw	McMaster	91735A194	12	#8-32 Screw, Phillips, Pan, L-1/2", SS316	$ 2.80
120	Drawstring Cord	Fisheries Supply	444790	1	Excel Pro, Marlow P/N ES0091, Diam-3mm, L-1m (or any similar low stretch, high strength line)	$ 0.69
121	Wire Rope Clamp	McMaster	3677T51	2	Wire Rope Clamp, For Line 5/64" diam, SS316	$ 12.98
122	Collar, Middle	Fabricated	n/a	1	PVC sheet, Type 2, Th-1/2", waterjet, drilled	see Matls
123	Collar, Bottom	Fabricated	n/a	1	PVC sheet, Type 2, Th-1/2", waterjet, drilled	see Matls
124	Bracket Bolt	McMaster	92186A546	3	1/4"-20 Screw, Hex Head, Partial Thread, L-1-1/2"	see P/N 75
125	Bracket Captured Nut	McMaster	92891A100	3	1/4"-20 Nut, Square, SS316	see P/N 67
126	Clamping Bolt	McMaster	92186A550	3	1/4"-20 Screw, Hex Head, Partial Thread, L-2"	$ 1.91
127	Clamping Nut	McMaster	90715A125	3	1/4"-20 Nut, Nylok Hex, SS316	see P/N 26

Appendix 3: Electronics Bill of Materials

Lower Housing

Group	Part Name	Value	#/Housing	Cost Each	Total Cost
Battery	Battery		1	$129.00	$129.00
Housing	Watertight Enclosure - 4" x 9"		1	$54.00	$54.00
Housing	Aluminum Endcap (4" - 5 Holes)		1	$16.00	$16.00
Housing	Aluminum Endcap (4" - No Holes)		1	$16.00	$16.00
Housing	O-Ring Flange (4" Series)		2	$29.00	$58.00
Housing	Blank Penetrator		1	$4.00	$4.00
Housing	Enclosure Vent and Plug		1	$8.00	$8.00
Electronics	PocketBeagle MCU		1	$25.00	$25.00
Electronics	Bulkhead Connector (2 Pin)		1	$80.00	$80.00
Electronics	Bulkhead Plug (2 Pin)		1	$80.00	$80.00
Electronics	Bulkhead Connector (3 Pin)		1	$80.00	$80.00
Electronics	Bulkhead Plug (3 Pin)		1	$80.00	$80.00
Electronics	Dummy Plugs		3	$35.00	$105.00
Electronics	Power Switch		1	$14.00	$14.00
Electronics	Pressure Sensor		1	$85.00	$85.00
Electronics	IMU Board (9 DOF Absolute Orientation)		1	$34.95	$34.95
Electronics	Custom PCB w/ Components and Assembly		1	$95.00	$95.00
Electronics	Single-cell battery	3.3V	1	$3.00	$3.00
Electronics	Board Mount Humidity Sensors	BME280	1	$7.50	$7.50
Electronics	Unpolarized capacitor	0.0047uF	1	$0.10	$0.10
Electronics	Unpolarized capacitor, small symbol	0.01uF	4	$0.10	$0.40
Electronics	Unpolarized capacitor	0.12uF	1	$0.10	$0.10
Electronics	Unpolarized capacitor, small symbol	0.1uF	21	$0.18	$3.78
Electronics	Unpolarized capacitor	0.1uF	1	$0.10	$0.10
Electronics	Unpolarized capacitor	0.47uF	1	$0.21	$0.21

Electronics	Unpolarized capacitor, small symbol	100uF	1	$2.78	$2.78
Electronics	Polarized capacitor, small symbol	100uF	1	$2.78	$2.78
Electronics	Unpolarized capacitor, small symbol	10pF	1	$0.18	$0.18
Electronics	Unpolarized capacitor, small symbol	10uF	1	$0.15	$0.15
Electronics	Unpolarized capacitor, small symbol	10uF	7	$0.23	$1.61
Electronics	Polarized capacitor	10uF	5	$0.76	$3.80
Electronics	Unpolarized capacitor, small symbol	10uF	2	$0.86	$1.72
Electronics	Unpolarized capacitor	10uF	1	$0.21	$0.21
Electronics	Unpolarized capacitor, small symbol	150pF	2	$0.82	$1.64
Electronics	Unpolarized capacitor	15nF	1	$0.91	$0.91
Electronics	Unpolarized capacitor, small symbol	1nF	1	$0.22	$0.22
Electronics	Unpolarized capacitor, small symbol	1uF	34	$0.09	$3.06
Electronics	Unpolarized capacitor, small symbol	1uF	1	$0.09	$0.09
Electronics	Polarized capacitor, small symbol	1uF	1	$0.12	$0.12
Electronics	Unpolarized capacitor, small symbol	2.2uF	5	$0.53	$2.65
Electronics	Unpolarized capacitor, small symbol	22nF	1	$0.32	$0.32
Electronics	Unpolarized capacitor, small symbol	270pF	1	$0.96	$0.96
Electronics	Unpolarized capacitor	8.2pF	1	$0.64	$0.64
Electronics	Light emitting diode	LED	7	$0.96	$6.72
Electronics	Schottky Power Rectifier	MBRS130T3G	1	$1.42	$1.42
Electronics	ADC, DELTA-SIGMA, 24BIT, 512KSPS, TQFP32	ADS127L01IPBSR	1	$15.17	$15.17
Electronics	IC REG LIN -1.5V 150MA SOT23-5	AP1156ADS15	1	$1.30	$1.30
Electronics	DiodesZetex AP2204K-3.3TRG1, LDO Voltage Regulator, 150mA, 3.3 V, 2.3 24 Vin, 5-Pin SOT-23	AP2204K-3.3TRG1	4	$1.75	$7.00
Electronics	DiodesZetex AP7312-1830W6-7, Dual LDO Voltage Regulator, 150mA, 1.8 V, 3 V, 2% 6-Pin, SOT-26	AP7312-1830W6-7	1	$1.50	$1.50
Electronics	FDS9435A, P-channel MOSFET Transistor 5.3 A 30 V, 8-Pin SOIC	FDS9435A	3	$0.75	$2.25

Electronics	5A Fixed / Adjustable Output Linear Regulator	LM1084IS-5.0_NOPB	1	$4.25	$4.25
Electronics	Switched Capacitor Inverter	LM2776DBVR	1	$2.25	$2.25
Electronics	150-mA LOW-NOISE LOW-DROPOUT REGULATOR WITH SHUTDOWN	LP2985A-33DBVTE4	1	$1.51	$1.51
Electronics	Micropower 150-mA Low-Noise Ultra-Low-Dropout Regulator in SOT-23 packages	LP2985IM5-3.5_NOPB	1	$1.75	$1.75
Electronics	LINEAR TECHNOLOGY - LTC4007EGN#PBF - BATTERY CHARGER, SMD, SSOP24, 4007	LTC4007EGN#PBF	1	$8.50	$8.50
Electronics	Linear Technology LTC4151IMS#PBF, Dual Voltage Detector, 7 80 V, 10-Pin MSOP	LTC4151IMS#PBF	1	$3.20	$3.20
Electronics	0.25ppm Noise, Low Drift Precision Buffered Reference	LTC6655CHMS8-3PBF	1	$8.59	$8.59
Electronics	Voltage regulator,MC33269D3.3 MC33269D-3.3G, Low Dropout Voltage Regulator, 0.8A 3.3 V, 1%, 8-Pin, SOIC	MC33269D-3.3G	1	$1.50	$1.50
Electronics	IC REG LINEAR 5V 200MA SOT23-5	RT9069-50GB	1	$0.75	$0.75
Electronics	Dual-Bit Dual-Supply Bus Transceiver with Configurable Voltage Translation and 3-State Outputs	SN74AVC2T45DCUR	3	$2.35	$7.05
Electronics	IC REG LINEAR 3.3V 500MA SOT23-5	SPX3819M5-L-3-3_TR	1	$1.65	$1.65
Electronics	LDO Voltage Regulators 500mA Low0Noise LDO Voltage Regulator	SPX3819M5-L-5-0_TR	1	$2.50	$2.50
Electronics	ST3232ECTR, Line Transceiver, EIA/TIA-232, RS-232, V.24, V.28 2-TX 2-RX 2-TRX, 3.3 V, 5 V, 16-Pin TSSOP	ST3232ECTR	1	$2.75	$2.75
Electronics	Low Noise, Precision, 150MHz, Fully Differential Amplifier	THS4551IDGKT	1	$7.75	$7.75

Electronics	4-Channel USB ESD Solution with Power Clamp	TPD4S012DRYR	1	$0.30	$0.30
Electronics	Generic connector, single row, 01x02	BH_Switch	1	$0.99	$0.99
Electronics	Generic connector, single row, 01x02	Conn_01x02	3	$0.99	$2.97
Electronics	Generic connector, single row, 01x03	Conn_01x03	1	$1.09	$1.09
Electronics	Generic connector, single row, 01x04	Conn_01x04	3	$1.19	$3.57
Electronics	Generic connector, single row, 01x03	HTI Hydrophone Power/Input	1	$1.09	$1.09
Electronics	Hirose Straight 50 Surface Mount UFL Connector, Receptacle, Solder Termination	U.FL-R-SMT(01)	1	$1.75	$1.75
Electronics	USB mini/micro connector	USB_OTG	1	$4.25	$4.25
Electronics	Molding Type Power Inductor	ASPI-0630LR-100M-T15	1	$2.25	$2.25
Electronics	Ferrite bead	Ferrite_Bead	3	$0.95	$2.85
Electronics	Light emitting diode	LED1	1	$0.50	$0.50
Electronics	GPS Standalone Module, 20-pin	FGPMMOPA6H	1	$14.95	$14.95
Electronics	50V Vds, 0.22 A Id, N-channel MOSFET, SOT-23	2N7002	2	$1.65	$3.30
Electronics	N-Channel Enhancement MOSFET SOT-23 Diodes Inc BSN20-7 N-channel MOSFET Transistor, 0.5 A, 50 V, 3-Pin SOT-23	BSN20-7	1	$0.95	$0.95
Electronics	FAIRCHILD SEMICONDUCTOR - FDC645N - MOSFET, N, SUPERSOT-6	FDC645N	1	$0.75	$0.75
Electronics	SI4431BDY-T1-E3, P-channel MOSFET Transistor 5.7A 30V, 8-Pin SOIC	SI4431BDY-T1-E3	1	$0.95	$0.95

Electronics	-60V Vds, -0.18A Id, P-Channel MOSFET, SOT-23-3	TP0610T	5	$0.95	$4.75
Electronics	Resistor	0.028	1	$0.10	$0.10
Electronics	Resistor	0.05	1	$0.10	$0.10
Electronics	Resistor, small symbol	1.2k	2	$0.10	$0.20
Electronics	Resistor, small symbol	10	3	$0.10	$0.30
Electronics	Resistor	100	1	$0.10	$0.10
Electronics	Resistor, small symbol	100k	16	$0.10	$1.60
Electronics	Resistor, small symbol	10k	8	$0.10	$0.80
Electronics	Resistor, small symbol	160k	1	$0.10	$0.10
Electronics	Resistor	1k	4	$0.10	$0.40
Electronics	Resistor	20m	1	$0.10	$0.10
Electronics	Resistor	26.7K	1	$0.10	$0.10
Electronics	Resistor	3.01k	2	$0.10	$0.20
Electronics	Resistor	32.4K	1	$0.10	$0.10
Electronics	Resistor	33	4	$0.10	$0.40
Electronics	Resistor, small symbol	330	5	$0.10	$0.50
Electronics	Resistor	4.99K	1	$0.10	$0.10
Electronics	Resistor	453K	1	$0.10	$0.10
Electronics	Resistor, small symbol	5	2	$0.10	$0.20
Electronics	Resistor	6.04K	1	$0.10	$0.10
Electronics	Resistor, small symbol	60.4k	1	$0.10	$0.10
Electronics	Resistor, small symbol	660	3	$0.10	$0.30
Electronics	Resistor	68	6	$0.10	$0.60
Electronics	USB Power Distribution	TPS2051CDBVT	1	$0.10	$0.10
Electronics	Thermistor	Thermistor_NTC_10K	1	$0.10	$0.10
Electronics	IMU Header	MPU9250	2	$0.10	$0.20
Electronics	PocketBeagle Header	PocketBeagle	2	$0.10	$0.20

Electronics	TCXO Oscillators 16.384MHz LVCMOS .05ppm at -40C +85C	AST3TQ-T-16.384MHz-50-C	1	$19.95	$19.95
Electronics	Diode Zener Single 18V 5% 200mW SOD323 Diodes Inc MMSZ5248BS-7-F Zener Diode, 18V 5% 200 mW SMT 2-Pin SOD-323	MMSZ5248BS-7-F	1	$1.25	$1.25
Hydrophone	HTI-99-UHF		1	$1,710.00	$1,710.00

Upper Housing

Group	Part Name	Value	#/Housing	Cost Each	Total Cost
Battery	Battery		1	$129.00	$129.00
Housing	Watertight Enclosure - 4" x 9"		1	$54.00	$54.00
Housing	Aluminum Endcap (4" - 5 Holes)		1	$16.00	$16.00
Housing	Aluminum Endcap (4" - No Holes)		1	$16.00	$16.00
Housing	O-Ring Flange (4" Series)		2	$29.00	$58.00
Housing	Blank Penetrator		1	$4.00	$4.00
Housing	Enclosure Vent and Plug		1	$8.00	$8.00
Electronics	PocketBeagle MCU		1	$25.00	$25.00
Electronics	Bulkhead Connector (2 Pin)		1	$80.00	$80.00
Electronics	Bulkhead Plug (2 Pin)		1	$80.00	$80.00
Electronics	Bulkhead Connector (8 Pin)		1	$80.00	$80.00
Electronics	Bulkhead Plug (8 Pin)		1	$80.00	$80.00
Electronics	Dummy Plugs		3	$35.00	$105.00
Electronics	Power Switch		1	$14.00	$14.00
Electronics	Pressure Sensor		1	$85.00	$85.00
Electronics	IMU Board (9 DOF Absolute Orientation)		1	$34.95	$34.95
Electronics	Xbee Pro 900HP		1	$35.00	$35.00
Electronics	Custom PCB		1	$95.00	$95.00
Electronics	Single-cell battery	3.3V	1	$3.00	$3.00
Electronics	Board Mount Humidity Sensors	BME280	1	$7.50	$7.50

Electronics	Unpolarized capacitor	0.0047uF	1	$0.10	$0.10
Electronics	Unpolarized capacitor, small symbol	0.01uF	4	$0.10	$0.40
Electronics	Unpolarized capacitor	0.12uF	1	$0.10	$0.10
Electronics	Unpolarized capacitor, small symbol	0.1uF	21	$0.18	$3.78
Electronics	Unpolarized capacitor	0.1uF	1	$0.10	$0.10
Electronics	Unpolarized capacitor	0.47uF	1	$0.21	$0.21
Electronics	Unpolarized capacitor, small symbol	100uF	1	$2.78	$2.78
Electronics	Polarized capacitor, small symbol	100uF	1	$2.78	$2.78
Electronics	Unpolarized capacitor, small symbol	10pF	1	$0.18	$0.18
Electronics	Unpolarized capacitor, small symbol	10uF	1	$0.15	$0.15
Electronics	Unpolarized capacitor, small symbol	10uF	7	$0.23	$1.61
Electronics	Polarized capacitor	10uF	5	$0.76	$3.80
Electronics	Unpolarized capacitor, small symbol	10uF	2	$0.86	$1.72
Electronics	Unpolarized capacitor	10uF	1	$0.21	$0.21
Electronics	Unpolarized capacitor, small symbol	150pF	2	$0.82	$1.64
Electronics	Unpolarized capacitor	15nF	1	$0.91	$0.91
Electronics	Unpolarized capacitor, small symbol	1nF	1	$0.22	$0.22
Electronics	Unpolarized capacitor, small symbol	1uF	34	$0.09	$3.06
Electronics	Unpolarized capacitor, small symbol	1uF	1	$0.09	$0.09
Electronics	Polarized capacitor, small symbol	1uF	1	$0.12	$0.12
Electronics	Unpolarized capacitor, small symbol	2.2uF	5	$0.53	$2.65
Electronics	Unpolarized capacitor, small symbol	22nF	1	$0.32	$0.32
Electronics	Unpolarized capacitor, small symbol	270pF	1	$0.96	$0.96
Electronics	Unpolarized capacitor	8.2pF	1	$0.64	$0.64
Electronics	Light emitting diode	LED	7	$0.96	$6.72
Electronics	Schottky Power Rectifier	MBRS130T3G	1	$1.42	$1.42
Electronics	IC REG LIN -1.5V 150MA SOT23-5	AP1156ADS15	1	$1.30	$1.30
Electronics	DiodesZetex AP2204K-3.3TRG1, LDO Voltage Regulator, 150mA, 3.3 V, 2.3 24 Vin, 5-Pin SOT-23	AP2204K-3.3TRG1	4	$1.75	$7.00

Electronics	DiodesZetex AP7312-1830W6-7, Dual LDO Voltage Regulator, 150mA, 1.8 V, 3 V, 2% 6-Pin, SOT-26	AP7312-1830W6-7	1	$1.50	$1.50
Electronics	FDS9435A, P-channel MOSFET Transistor 5.3 A 30 V, 8-Pin SOIC	FDS9435A	3	$0.75	$2.25
Electronics	5A Fixed / Adjustable Output Linear Regulator	LM1084IS-5.0_NOPB	1	$4.25	$4.25
Electronics	Voltage regulator,MC33269D3.3 MC33269D-3.3G, Low Dropout Voltage Regulator, 0.8A 3.3 V, 1%, 8-Pin, SOIC	MC33269D-3.3G	1	$1.50	$1.50
Electronics	IC REG LINEAR 5V 200MA SOT23-5	RT9069-50GB	1	$0.75	$0.75
Electronics	Dual-Bit Dual-Supply Bus Transceiver with Configurable Voltage Translation and 3-State Outputs	SN74AVC2T45DCUR	3	$2.35	$7.05
Electronics	IC REG LINEAR 3.3V 500MA SOT23-5	SPX3819M5-L-3-3_TR	1	$1.65	$1.65
Electronics	LDO Voltage Regulators 500mA Low0Noise LDO Voltage Regulator	SPX3819M5-L-5-0_TR	1	$2.50	$2.50
Electronics	ST3232ECTR, Line Transceiver, EIA/TIA-232, RS-232, V.24, V.28 2-TX 2-RX 2-TRX, 3.3 V, 5 V, 16-Pin TSSOP	ST3232ECTR	1	$2.75	$2.75
Electronics	Low Noise, Precision, 150MHz, Fully Differential Amplifier	THS4551IDGKT	1	$7.75	$7.75
Electronics	4-Channel USB ESD Solution with Power Clamp	TPD4S012DRYR	1	$0.30	$0.30
Electronics	Xbee Header	XBP24-DMWIT-250J	1	$1.25	$1.25
Electronics	Generic connector, single row, 01x02	BH_Switch	1	$0.99	$0.99
Electronics	Generic connector, single row, 01x02	Conn_01x02	3	$0.99	$2.97
Electronics	Generic connector, single row, 01x03	Conn_01x03	1	$1.09	$1.09
Electronics	Generic connector, single row, 01x04	Conn_01x04	3	$1.19	$3.57
Electronics	Generic connector, single row, 01x03	HTI Hydrophone Power/Input	1	$1.09	$1.09

Electronics	Hirose Straight 50 Surface Mount UFL Connector, Receptacle, Solder Termination	U.FL-R-SMT(01)	1	$1.75	$1.75
Electronics	USB mini/micro connector	USB_OTG	1	$4.25	$4.25
Electronics	Molding Type Power Inductor	ASPI-0630LR-100M-T15	1	$2.25	$2.25
Electronics	Ferrite bead	Ferrite_Bead	3	$0.95	$2.85
Electronics	Light emitting diode	LED1	1	$0.50	$0.50
Electronics	GPS Standalone Module, 20-pin	FGPMMOPA6H	1	$14.95	$14.95
Electronics	50V Vds, 0.22 A Id, N-channel MOSFET, SOT-23	2N7002	2	$1.65	$3.30
Electronics	N-Channel Enhancement MOSFET SOT-23 Diodes Inc BSN20-7 N-channel MOSFET Transistor, 0.5 A, 50 V, 3-Pin SOT-23	BSN20-7	1	$0.95	$0.95
Electronics	FAIRCHILD SEMICONDUCTOR - FDC645N - MOSFET, N, SUPERSOT-6	FDC645N	1	$0.75	$0.75
Electronics	SI4431BDY-T1-E3, P-channel MOSFET Transistor 5.7A 30V, 8-Pin SOIC	SI4431BDY-T1-E3	1	$0.95	$0.95
Electronics	-60V Vds, -0.18A Id, P-Channel MOSFET, SOT-23-3	TP0610T	5	$0.95	$4.75
Electronics	Resistor	0.028	1	$0.10	$0.10
Electronics	Resistor	0.05	1	$0.10	$0.10
Electronics	Resistor, small symbol	1.2k	2	$0.10	$0.20
Electronics	Resistor, small symbol	10	3	$0.10	$0.30
Electronics	Resistor	100	1	$0.10	$0.10
Electronics	Resistor, small symbol	100k	16	$0.10	$1.60
Electronics	Resistor, small symbol	10k	8	$0.10	$0.80
Electronics	Resistor, small symbol	160k	1	$0.10	$0.10
Electronics	Resistor	1k	4	$0.10	$0.40
Electronics	Resistor	20m	1	$0.10	$0.10
Electronics	Resistor	26.7K	1	$0.10	$0.10

Electronics	Resistor	3.01k	2	$0.10	$0.20
Electronics	Resistor	32.4K	1	$0.10	$0.10
Electronics	Resistor	33	4	$0.10	$0.40
Electronics	Resistor, small symbol	330	5	$0.10	$0.50
Electronics	Resistor	4.99K	1	$0.10	$0.10
Electronics	Resistor	453K	1	$0.10	$0.10
Electronics	Resistor, small symbol	5	2	$0.10	$0.20
Electronics	Resistor	6.04K	1	$0.10	$0.10
Electronics	Resistor, small symbol	60.4k	1	$0.10	$0.10
Electronics	Resistor, small symbol	660	3	$0.10	$0.30
Electronics	Resistor	68	6	$0.10	$0.60
Electronics	USB Power Distribution	TPS2051CDBVT	1	$0.10	$0.10
Electronics	Thermistor	Thermistor_NTC_10K	1	$0.10	$0.10
Electronics	IMU Header	MPU9250	2	$0.10	$0.20
Electronics	PocketBeagle Header	PocketBeagle	2	$0.10	$0.20
Electronics	Diode Zener Single 18V 5% 200mW SOD323 Diodes Inc MMSZ5248BS-7-F Zener Diode, 18V 5% 200 mW SMT 2-Pin SOD-323	MMSZ5248BS-7-F	1	$1.25	$1.25